

Building Pathology and Rehabilitation



João M.P.Q. Delgado *Editor*

New Approaches to Building Pathology and Durability

 Springer

Building Pathology and Rehabilitation

Volume 6

Series editors

Vasco Peixoto de Freitas

Aníbal Costa

João M.P.Q. Delgado

More information about this series at <http://www.springer.com/series/10019>

João M.P.Q. Delgado
Editor

New Approaches to Building Pathology and Durability

 Springer

Editor
João M.P.Q. Delgado
Faculty of Engineering
University of Porto
Porto
Portugal

ISSN 2194-9832 ISSN 2194-9840 (electronic)
Building Pathology and Rehabilitation
ISBN 978-981-10-0647-0 ISBN 978-981-10-0648-7 (eBook)
DOI 10.1007/978-981-10-0648-7

Library of Congress Control Number: 2016932315

© Springer Science+Business Media Singapore 2016

This work is subject to copyright. All rights are reserved by the Publisher, whether the whole or part of the material is concerned, specifically the rights of translation, reprinting, reuse of illustrations, recitation, broadcasting, reproduction on microfilms or in any other physical way, and transmission or information storage and retrieval, electronic adaptation, computer software, or by similar or dissimilar methodology now known or hereafter developed.

The use of general descriptive names, registered names, trademarks, service marks, etc. in this publication does not imply, even in the absence of a specific statement, that such names are exempt from the relevant protective laws and regulations and therefore free for general use.

The publisher, the authors and the editors are safe to assume that the advice and information in this book are believed to be true and accurate at the date of publication. Neither the publisher nor the authors or the editors give a warranty, express or implied, with respect to the material contained herein or for any errors or omissions that may have been made.

Printed on acid-free paper

This Springer imprint is published by SpringerNature
The registered company is Springer Science+Business Media Singapore Pte Ltd.

Preface

Building pathology is the scientific study of the nature of building failure and its causes, processes, development and consequences. In order to provide an economic and effective remedy to building defects, it is essential to identify properly the cause to address the problem.

The main purpose of this book, *New Approaches on Building Pathology and Durability*, is to provide a collection of recent research works to produce information which will assist in the effective management of service loss, to develop and evaluate methodologies for the assessment of defects and failures and to propose methodologies for the prevention and mitigation of building defects. It includes a set of new developments in the field of building physics and hygrothermal behaviour, durability approach for historical and old buildings, building pathology versus durability, service life prediction methodologies, new approaches on biocementation applied to rehabilitation, developments on different façade solutions and a several number of pathologies associated to reinforced concrete.

The book is divided into several chapters that intend to be a resume of the current state of knowledge for benefit of professional colleagues, scientists, students, practitioners, lecturers and other interested parties to network. At the same time, these topics will encounter a variety of scientific and engineering disciplines, such as civil, materials and mechanical engineering.

João M.P.Q. Delgado

Contents

Assessment and Rehabilitation of Industrial Building for the Production of Ammonium Nitrate Low Density	1
Mara Regina Pagliuso Rodrigues, Raphael Mairal and Osny Pellegrino Ferreira	
Building Materials Capillary Rise Coefficient: Concepts, Determination and Parameters Involved	27
Nikos Karagiannis, Maria Karoglou, Asterios Bakolas and Antonia Moropoulou	
Statistical Modelling of Service Life Prediction of Exterior Painted Surfaces	45
Ana Silva, Pedro L. Gaspar and Jorge de Brito	
Corrosion Propagation Phase Studies on Finnish Reinforced Concrete Facades	75
Arto Köliö, Mari Honkanen and Jukka Lahdensivu	
Biocementation as Rehabilitation Technique of Porous Materials	99
Rafaela Cardoso, Rita Pedreira, Sofia Duarte, Gabriel Monteiro, Hugo Borges and Inês Flores-Colen	
Study of Pozzolanic Admixtures Effects in the Concretes Under Chemical Attack	121
Henrique Catuzzo, Giovanna Patricia Gava and Camila Salvi Malacarne	
Durability of ETICS and Premixed One-Coat Renders in Natural Exposure Conditions	131
Luís Silva, Inês Flores-Colen, Nuno Vieira, Ana Barros Timmons and Pedro Sequeira	

Photocatalytic TiO₂ Nano-Coating for Biofouling Prevention of Clay Façades 159
Lorenzo Graziani, Enrico Quagliarini and Marco D’Orazio

Rehabilitation of Concrete Industrial Building Facades Attacked by Acids. 177
Agnus Rogério Rosa, Antônio Neves de Carvalho Júnior, Eduardo Chahud and Luiz Antônio Melgaço Nunes Branco

Pathologies—Incompatibility of Materials and Human Intervention in a Historic Building of Elvas 193
Soheyl Sazedj, António Morais, M^a Teresa Pinheiro-Alves and Rui Silva

Assessment and Rehabilitation of Industrial Building for the Production of Ammonium Nitrate Low Density

Mara Regina Pagliuso Rodrigues, Raphael Mairal
and Osny Pellegrino Ferreira

Abstract This work consists of the structural evaluation and rehabilitation of industrial building for the manufacture of ammonium nitrate low density in the Brazilian company Vale Fertilizers. The building was designed by the German company Friedrich Uhde GmbH in 1954, currently working with ThyssenKrupp Uhde GmbH name. The aggressiveness of the products used in process to the structure of reinforced concrete, lack of adequate maintenance and protection systems, giving rise to various pathologies in the building. The activities covered in evaluation of the building comprising a number of studies such structure as-built, inspection of existing conditions, material characterization, structural numerical analysis according to current code recommendations in the country, allowing a proper diagnosis for structural rehabilitation project that tend to improve the structural performance and ensure longer life of the structure. Was adopted in this work different techniques, equipment and testing (destructive and non-destructive) for inspection and diagnosis, such as 3D laser scanning, non-destructive rebar detection, carbonation test, contamination analysis of the soil in contact with the foundation, electrical resistivity test of concrete, etc. This work highlights the importance of knowledge of the effects of chemicals agents in choosing the most suitable system protection for structures in contact with agents of extreme aggressiveness. The objective of this work is not to present specific results of tests performed, but present techniques currently available and methodology for assessment and recovery of industrial buildings.

M.R.P. Rodrigues (✉)

Instituto Federal de São Paulo (IFSP), Votuporanga, SP, Brazil
e-mail: marareginapr@gmail.com

R. Mairal

Engineering of the Mairal Engenharia, São Carlos, SP, Brazil
e-mail: raphael@mairal.com.br

O.P. Ferreira

Universidade de São Paulo (EESC-USP), São Carlos, SP, Brazil
e-mail: Osnypefe@sc.usp.br

Keywords Structural rehabilitation · Reinforcement corrosion · Structure pathology

1 Introduction

1.1 Building Description and History

The building to be recovered consists of rectangular plan building with $22 \times 16.50 \text{ m}^2$, with floors at +0.00; +4.50; +9.00; +13.50; +18.00 levels and coverage at +22.50 and +24.50 levels with stairway access to all levels according to information gathered in the area, it was designed by Friedrich Uhde GmbH in 1954, German company specialized in industrial plants, currently serving under the name of ThyssenKrupp Uhde GmbH. It is estimated that the structure is approximately 54 years old, according to the Vale Fertilizantes website “April 16th was chosen to mark the beginning of the activities of Ultrafértil because on this date in 1958, the oldest unit of the company started operating, the Cubatão Industrial Complex (CCB)”.

Figure 1 shows a current structure overview. At unspecified date, over 20 years ago the initial plant was reduced by the structural demolition, as shown in Fig. 2. In addition, also at undefined date it was performed strengthening and recovery in some structural elements as it was possible to observe during the field investigations which will be presented later.

From the remaining plant most of the construction was nearly deactivated, using only the region between the 9 and 11 axes serving as support tanks and equipment

Fig. 1 Building neutralization overview



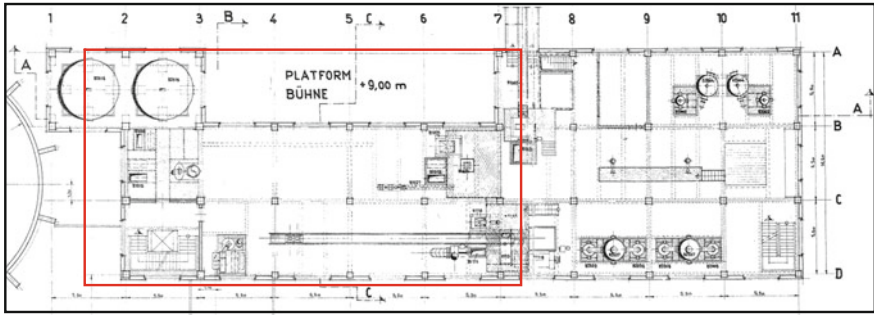
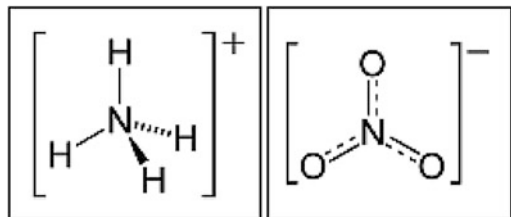
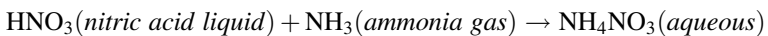


Fig. 2 Demolished part of the initial building plan

Fig. 3 Chemical bonds of ammonium nitrate



for the production of ammonium nitrate. The acid-base reaction (neutralization) using anhydrous ammonia gas and concentrated nitric acid, with an exothermic reaction (heat release) happens there. After this solution is formed, the excess water is evaporated to obtain a concentration of ammonium nitrate (salt). Figure 3 shows the chemical bonds of such salt.



On this densified form, the ammonium nitrate is mainly used as fertilizer since the low-density ammonium nitrate is primarily intended for making explosives. In CCB unit Ultraprill (low-density ammonium nitrate) is produced.

The ammonium nitrate offers a range of risks, the main ones are described below:

The most iminent hazard: Being oxidant, because it can interact with other products. When it is contaminated with organic or oxidising materials, warm, confined, and even under the action of initiators, it can detonate. There is risk of ignition or detonation by exposing the product to heat and incompatible materials.

Physical and chemical hazards: The Ammonium nitrate is a strong oxidant. The contamination can promote their decomposition, making it volatile and dangerous. The contaminants include organic matter, chlorides, fluorides and also some metals (examples: Copper, Chromium, Zinc, etc.).

Product effects in animals: Inhalation may cause respiratory tract irritation, cough, sore throat and difficulty breathing. Contact with the product can cause irritation to the skin and eyes. When exposed to high temperatures due to

decomposition, it can release toxic ammonia and nitrous gases (NO_x), capable of causing acute respiratory problems.

Environmental effects: It is very soluble in water and it can contaminate waterways, making them unsuitable for any purpose use. The combustion product of ammonium nitrate and nitrous oxide, N₂O. This compound is an aggravating to the greenhouse, and 273 times more harmful than carbon dioxide, CO₂ (Xavier, A. Agronomy/UFSM, 2008).

Effects on human health: Ammonium nitrate causes eye irritation, skin and respiratory tract. The substance can affect the blood, due to the nitrate ion, causing a condition called methemoglobinemia, or blue baby disease (IPCS ICHM, 2011). Its main effects on human health and ecosystems are the result of secondary compounds that can be formed.

Note: The effects of even touching the components of reinforced concrete structures will be described in subsequent item.

2 Surveys and Tests Performed

2.1 Architectural and Structural Survey

The only technical document found was a drawing provided by Vale Fertilizantes (UF-CB56-AQ1-0059 of Friedrich Uhde GmbH) which is presented in this part of the architectural design, although we observed several inconsistencies with the existing architecture as well as being outdated due to several changes in the building so it was not used as a reference for updating the drawings.

The architectural surveys and the structural form were executed with the help of a 3D Scanner—Leica ScanStation a Geosystem equipment, which from the cloud is possible to model all the existing elements, as shown in Fig. 4.

The benefits of using this technology are:

- Surveys Accuracy
- Increased safety and reliability of the measures (millimetric precision). Requiring no stairs, platform lifts, tape measures, etc. They can be made out of risk areas as runner-propelled machines, and no physical contact with the elements in the facility, avoiding risks for humans, as well as smaller numbers of people for surveys in the unit.
- Possibility to include AS-BUILT pipes or equipment in the future.
- Eliminated the need to return to the location to new measurements or conferences, facilitates the generation of 2D documentation (seen in plan, section, elevation, isometric, etc.).

For scanning unification it was used several fixed points called Target's (targets). In Fig. 5 we can observe the third floor of the building and cloud points obtained through the scanning.



Fig. 4 ScanStation inside the building



Fig. 5 Photographic image/3D scanner points cloud

2.2 *Steel Frame Surveying*

To survey the steel frames was used the Profoscope of Proceq Swiss parcometer, electronic locator of metal bars in concrete with digital display, the method is non-destructive and uses electromagnetic-pulse-induction technology to detect the frames (Fig. 6). The device locates the bars, estimates the diameter and thickness up to 150 mm away from the surface.

With this equipment you can:

- locate steel frames
- locate the midpoint between the frames
- determine the concrete layer
- estimate the frame diameter
- determine the frame direction

The measurements are saved in a memory device and displayed on the software.



Fig. 6 Reinforcement lifting and positioning

(concrete beam/ stirrup/ metal profile/ soldered)

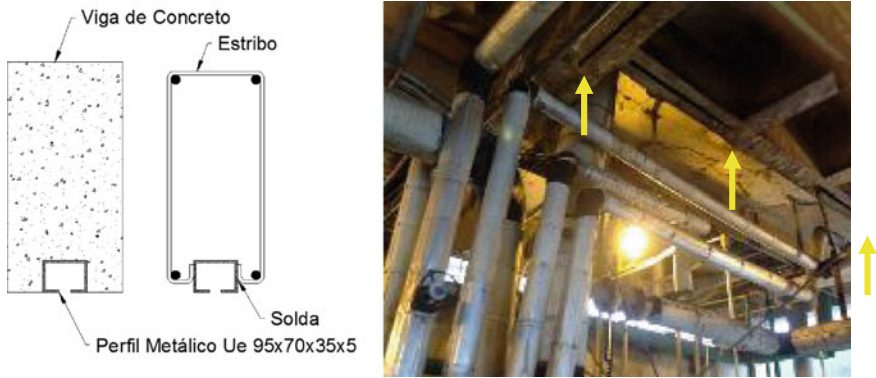


Fig. 7 Metal profiles support

Although it's a very precise equipment, it can be affected by metal objects near or frames close to each other, thereby generating inconsistent results because it uses electromagnetic pulse. Thus the results were interpreted carefully.

Many of the beams presented their lower face embedded in metal for piping and equipment support, the embedded beams had their stirrups broken and soldered as shown in Fig. 7. This greatly hindered the surveys for causing interference to equipment measurements. In some cases, where the reinforcement of the concrete cover had already calcined openings it was possible to confirm the data.

A safety device was designed to the use of these metal brackets that were in good condition for attaching the lanyard carabiners when working on stairs, it was approved by the unit's security team.

Figure 8 shows a point where the concrete was already broken around the profile enabling the observing of that constructive detail.

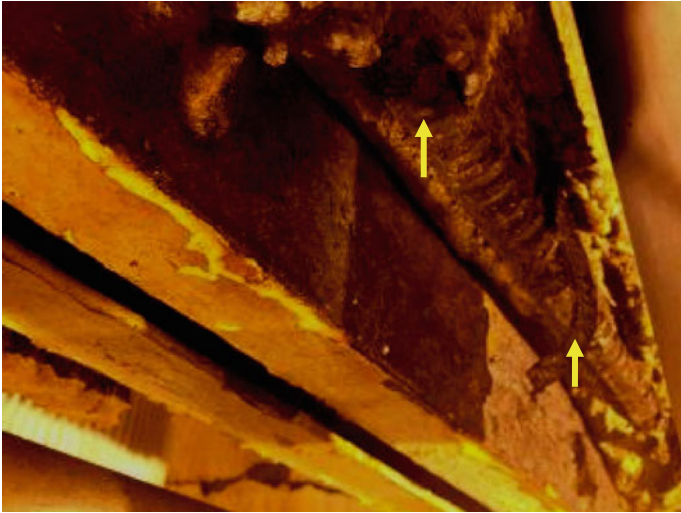


Fig. 8 Metal profiles stirrups interruption

2.3 Steel Frame Characterization

To determine the resistance and the reinforcement steel damage it was extracted 3 samples at different spots of the structure, spots where the concrete was already broken and the frames were shown, in order to be able to test as shown in Fig. 9, and they were tested at the Instron Satec Systems traction in pneumatic (see Fig. 10).

The average of the mean flow stress determination from the frame disposal was not possible due to the corrosion form presented. The first one being uniformly across the plates in different spots of the structure caused by the depassivation of the existing concrete around the surface of the bars (carbonation and/or aggressive agents) as shown in Fig. 11 and the other transgranular and transcristalin or accelerated by the action of nitric acid in bars under tension.

The transgranular corrosion phenomenon is manifested in the form of cracks, which propagates through the interior of the material grains, as in the case of stress corrosion cracking, the image as shown in Fig. 12 is amplified.

The steel structure seems fully integrated to the sufficient traction application of force to the opening of these cracks, as shown in Fig. 13. Thou has its resistance limited by the most damaged area's cross section.

For calculation purposes it was used to the mechanical characteristics of the steel CA25 (Table 1) commonly used at the time of construction of the building.

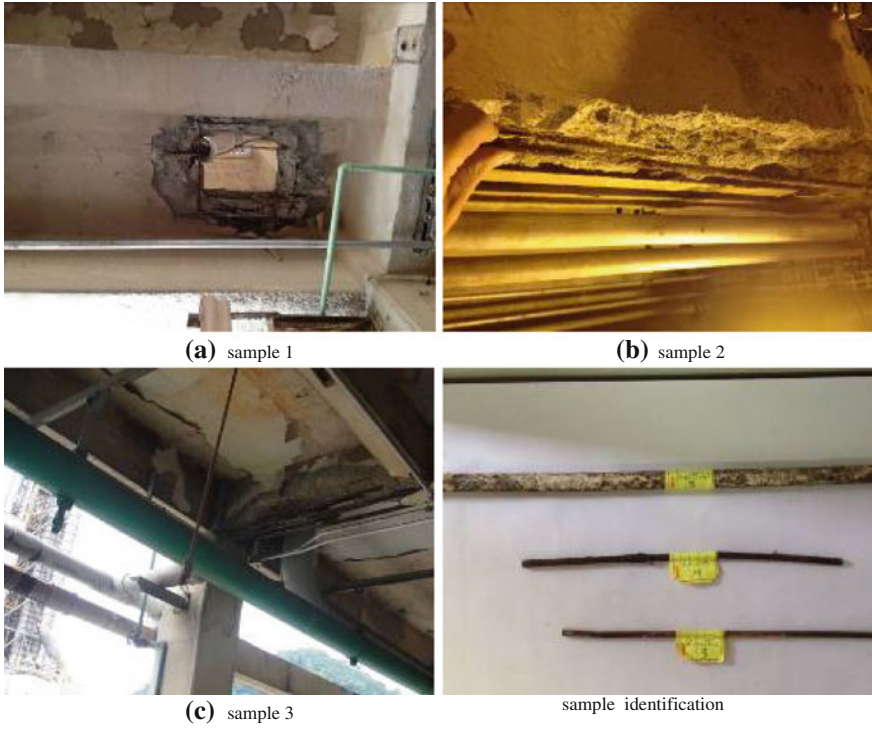


Fig. 9 Steel frames samples

Fig. 10 Frame test



Fig. 11 Plates corrosion sample



Fig. 12 Transcrystalin or transgranular corrosion



2.4 Concrete Characterization

The existing concrete is characterized by withdrawal of cylindrical bodies of the test piece called testimony and tested according to the recommendations of NBR 7680 (2007) (extraction, preparation, testing and analysis of testimonies of concrete structures). 4 witnesses were taken using electric Hilti DD120 model equipped with diamond crown drill with 4 in. in diameter, pulling bodies of the test piece with about 10 cm in diameter and 20 cm in length (Fig. 14).

Before drilling, the frame was located and positioned so that the drilling rig did not reach the frame. The testimonies were extracted from different levels to greater representativeness, they were chosen from P10 pillars (CP1) and P12 (CP4) level 0.00; P7 (CP2) level +9.00; P9 level +13.50 (CP3).

Fig. 13 Transgranular corrosion (sample 3)



Table 1 Mechanical properties of the steel considered

Steel type	f_{yk} (MPa)	f_{yd} (MPa)
CA25	250	215

During the testimony extraction in Pilar P12 (CP4) reinforcing steel was found in about 12 cm of depth from the surface where it could be seen two distinct concrete layers (Fig. 15), indicating the implementation strengthening by encapsulating about 10 cm from that area.

The test bodies were identified immediately after the removal and sent to the Department of USP Construction from São Carlos laboratory for grinding the edges and uniaxial compression test as shown in Fig. 16.

The concrete mechanical properties values of each core are shown in Table 2. For the calculations it was used the average strength of the evidence CP1, CP2 and CP3 resulting in an average compressive strength $f_{cm} = 20$ MPa.

After removing the structure evidence which was compounded with high strength grout (Supergraute of Quartzolit), following all the manufacturer's recommendations, reaching chemical and mechanical characteristics superior to the existing concrete for the application of MDF grout pipes which were properly set as shown in Fig. 17.

Samples were also taken from the L428 and L431 level +13.50 slabs for checking the thickness of counter floor (see Fig. 18). The flooring appears to have a great thickness variation from one side to the other of the structure. It was



Fig. 14 Testimonies extraction

considered the average thickness against the floor to the average thicknesses of the sample, which was 5 cm. This thickness was adopted for calculation loads and during modeling to define the thickness and height of the slab beams.

2.5 Research Foundations

An excavation was performed around the P16 column (see Fig. 19) in order to investigate the kind, position and state of foundation structures and baldrame beams, this point was chosen because it was not necessary to break any floor, it did not have pipes or equipment close by and it was way from people circulation area, having previously been approved by a technical Vale team and endowed digging certificate.

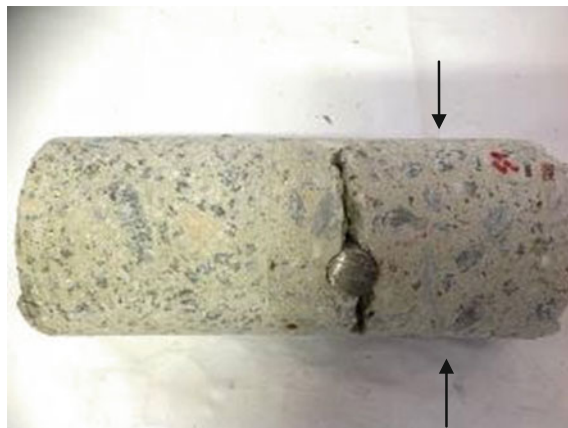


Fig. 15 CP4 image



Fig. 16 Rectification and testing of the bodies of the test piece

Table 2 Results of uniaxial compression testimony tests

Testimony/body test	Compressive strength ABNT NBR-5739: 1994 f_{cj} (MPa)	Elasticity modulus E_c (MPa) ^a
CP1	16.50	19.335
CP2	23.00	22.828
CP3	20.90	21.761
CP4 ^b	25.50	24.037

^aCalculated based on ABNT NBR 8800: 2008

^bConcrete structural reinforcement



Fig. 17 Reconstitution of testimony extraction points



Fig. 18 Floor against level samples +13.50

Through this research it was observed that a triangular three-stake block, was in a deep foundation, beneath the baldrame beams (see Figs. 20 and 21). The data was used to design and structural modelling.



Fig. 19 Excavation spot on an isolated area



Fig. 20 Type and form the foundation structure



Fig. 21 Measurement of the foundation structures dimensions

2.6 Soil Contamination Test

Verifying possible soil contaminants that can chemically attack the foundation structures, two soil samples were taken close to pillar 16 and another next to the column 20, the samples were identified, packaged (see Fig. 22) and sent to the laboratory for chemical analysis. The results are shown in Tables 3 and 4.

As shown in Table 3, the soil sample 1 showed a slightly alkaline pH, and virtually no contamination by ammonia and nitrate due to the very close results to the limit of quantification. Theoretically, any environment presenting pH less than 12.5 can be quantified as aggressive for reinforced concrete structures, in practice the aggression only manifests itself to pH below 6.5. Although the soil sample 2 showed a slightly alkaline pH, it is possible to observe a significant contamination



Fig. 22 Sample packs for soil testing

Table 3 Soil sample 1 analysis results

Parameter	Unit	L.Q. ^a	Results	Methodology
pH (1:1) ^b	–	1.00–14.00	7.18	ABNT 14339-1999
Ammonia (NH ₃)	mg/kg	0.1	<L.Q.	SMEWW 21a Ed. 2005
Nitrate	mg/kg	0.1	0.2	Manual HACH 8039

^aQuantification limit

^bAccredited Testing ISO/EC 17025 NBR

Table 4 Soil sample 2 analysis results

Parameter	Unidade	L.Q. ^a	Results	Methodology
pH (1:1) ^b	–	1.00–14.00	7.71	ABNT 14339-1999
Ammonia (NH ₃)	mg/kg	0.1	176	SMEWW 21a Ed. 2005
Nitrate	mg/kg	0.1	40	Manual HACH 8039

^aQuantification limit

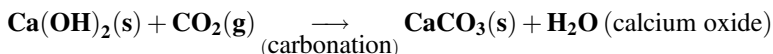
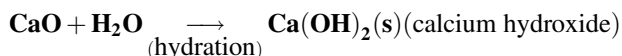
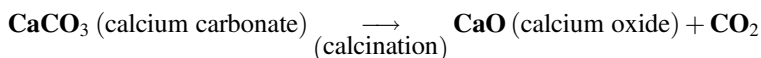
^bAccredited testing ISO/EC 17025 NBR

by ammonia and nitrate, but which was not capable of causing significant damage to the foundation structures.

2.7 Concrete Carbonation Essay

In concrete, the steel lies within a highly alkaline medium in which it would be protected from the corrosion process due to the presence of a protective film passive character. The alkalinity of the concrete comes within the liquid phase in its pores containing hydroxyl groups derived from the ionization of calcium hydroxides, sodium and potassium. Even in advanced concrete ages still providing a basic medium that protects the armor of the corrosion phenomenon. However, the presence of a sufficient quantity of chloride ions (in the atmosphere in marine and industrial or environments present in the concrete itself components) causes a decrease in the concrete alkalinity due to reactions called carbonation, but also the penetration of acidic substances and leaching, there is a loss of this film involves passive armor.

Calcium hydroxide is presented as a white powder, alkaline (pH 12.8), slightly soluble in water (solubility of 1.2 g/l of water at a temperature of 25 °C). This is a strong base obtained from the calcination (heating) of calcium carbonate, up to its transformation into calcium oxide (quicklime). With the hydration of calcium oxide which is present in the cement comes to the calcium hydroxide present in the hardened concrete and the reaction between it and the carbon dioxide leads to the formation of calcium carbonate, such reactions can be represented thus:



It's also possible to say that the passivating pellicle is "calcium ferrate" resulting from the combination of the superficial surface and calcium hydroxide.

The concrete carbonation is usually a determining factor to the reinforcement corrosion onset. Once the carbonation reaches the corresponding thickness in the steel coatings, it starts depassivation and begins to rust.

As the biggest problem is the pH fall it is applied an alcohol solution of phenolphthalein, which remains colorless when applied in carbonated concrete, and changes to pink in the concrete and does not carbonated. This test was performed at different spots of the structure, especially in the pillars near the floor at half height, making 16 mm diameter holes and deeping them from the surfasse to each 2 mm, and also applying the solution until it found concrete not carbonated. Then its depth was measured as shown in Fig. 23.



Fig. 23 Carbonation depth determination

The carbonation depth tests were compared with the average coating frames on each pillar. It is important to emphasize that a very large frame coating variation, which complicates the definition of areas susceptible to corrosion, was found. On the other hand, the microregion (position within the structure) where the component deepens the carbonation has a great variation. It's more frequently the corrosion emergence happening at the base of pillars which gradually spread into the upper regions. The relative humidity of the air near the floor can be 10–20 % higher than on the liner (WEXLER et Paulo RL Helene).

2.8 Potential Test of Reinforcement Corrosion

The aim was to use a non-destructively corrosion detection for the concrete frame through the referenced electrode, known as the Swiss equipment CANIN semi-stack+ which can detect sites that have corrosion before they become visible and causes injury, however due to the application of several layers of coating (paint) the use of the equipment has been dropped.

2.9 Electrical Resistivity Test

Tests and empirical theory show that the resistivity of concrete is directly related to both the likelihood of corrosion due to diffusion of chlorides and the corrosion rate after the steel depassivation has begun. The low resistivity of the concrete causes



Fig. 24 CP1 testimony electrical resistivity test

Table 5 Results of the testimonies electrical resistivity tests

Testimony/body test	Pilar	Average electrical resistivity (k Ω cm)
CP1	P10—level 0.00	106
CP2	P7—level +9.00	120.5
CP3	P9—level +13.50	122.4

the frames to be more susceptible to corrosion. The electrical resistivity of the concrete testimonies was measured by a Resipod equipment that applies a current to two probes at the edge and measures the potential difference between two internal probes as shown in Fig. 24.

Empirical tests reach the following limits for the measured resistivity, values that can be used to determine the likelihood of corrosion.

When $\pi \geq 150$ – 100 k Ω cm corrosion is unlikely

Where $\pi = 10$ – 50 k Ω cm corrosion is possible

When $\pi \leq 10$ k Ω cm corrosion is quite likely

The values of the average evidence resistivity of CP1, CP2 and CP3 are shown in Table 5.

Analyzing the average values of measurements we can conclude that the building concrete or at least the analyzed pillars has a low probability of corrosion, a fact that may have contributed to the good condition of the structure after 54 years in places where there was no direct contact with aggressive agents.

3 Pathologies Submitted

3.1 Reinforced Concrete Degradation

The chemical reactions that cause the concrete degradation may result from chemical interactions between aggressive agents present in the external environment and the constituents of the cement paste or may be a result from internal reactions, alkali-aggregate reaction type, or the hydration reaction delayed CaO and Crystalline MgO, if they are in excessive amounts, or even electrochemical corrosion of the concrete reinforcement.

During the corrosion process of the reinforcement formed by iron oxy-hydroxides, which occupies volumes from 3 to 10 times greater than the original reinforcing steel volume, it may cause expansion pressures greater than 15 MPa, generating tensile stresses in the concrete and as a result the appearance of cracks and peeling on the structure. The electrochemical concrete reinforcement corrosion occurs due to a natural phenomenon which can be accelerated by the presence of external or internal specific chemical agents.

Acidic solutions containing anions are often found in the industrial processes; hydrochloric acid, sulfuric acid and nitric acid are some of them. The cation exchange reactions between the alkaline and cement paste constituents generate soluble calcium salts which can be removed by leaching and degrading the concrete. The insoluble calcium salts, resulting from aggressive agents reactions contain certain anions with the cement slurry, if they are not expandable nor removed by infiltration, they do not degrade the concrete.

Prolonged attack acidic solutions can provoke the loss of some cement characteristics, as seen in some parts of the building, Fig. 25 shows a concrete sample showing these characteristics and it can easily break apart with bare hands.

The acid neutralizing by bases can be total or partial, originating salts yielding acidic, basic, neutral, or hydrated mixed. The neutral salt is characterized by the total neutralization of an acid or a base, or are free of H^+ and OH^- ions, with the consequent absence in the formula of H^+ and OH^- ions. The so-called neutral salts



Fig. 25 Concrete samples which suffered nitric acid attack

do not alter the pH of a solution, the sodium chloride is the best example of this type of salt. Other salts may raise or lower the pH of a solution, depending on their acidity or alkalinity. The chemical formula of a salt is represented using always first the cation then the anion, the salt is designated by adding the name of the anion and the cation name which constituted, in this order. The anion is named after the termination of the acid that raises them.



Dry salt crystals are electrical insulators, however salts in aqueous or fused solutions are electric current conductors. Thus the concrete subjected to a relative high humidity temperature under the presence of ions shall correspond to a reduced electrical resistivity.

Any potential difference is produced between two edges of the bar, by the difference of humidity, aeration, salt concentration, tension in the concrete and steel, it is capable of eliciting batteries or battery strings connected in series. Most often, MICROFCELLS are formed and may even change pole position, causing widespread corrosion. When the anodes are reduced and dimensions stabled, it can produce the so-called localized corrosion, intense and dangerous.

Localized corrosion is rare in reinforced concrete, it is more frequent in wires and wire ropes for prestressed concrete. In some cases it may be called stress corrosion cracking, its main characteristic is to break without warning, in other words bring about a brittle fracture in a defined section, without a prior deformation of the structure to alert, allowing the problem to be fixed in time. Figure 26 shows one of the beams of the first floor which clearly occurred stress corrosion cracking in some bars. This beam probably did not collapse completely due to the negative reinforcement and redistribution efforts.

The structural system of a building must be designed so that it is able to withstand not only the vertical loads but also the horizontal actions that may cause significant effects.



Fig. 26 Stress corrosion cracking reinforcement

The vertical loads consist of: self weight of structural elements, own weight coverings and walls, and other permanent actions, variable arising from the use, and specific actions such as equipment weight, etc.

Beams support their own weight, the reactions from the slabs, walls weight, and also actions from other elements, such as support reactions from other beams, etc. Generally the beams work to bending and shearing and transmit these actions to the pillars.

The concrete is intended to join concrete that has good compressive strength but low tensile strength to the steel that has a good tensile strength. In the case of beam subjugated to bending stress, as shown in Fig. 27, while the concrete is resistant to compressive forces (A-B long side) of the positive reinforcement resistant to traction forces (C-D pulled) so making the resistance mechanism. Furthermore, the beams are subjected to shear stress (shear) generating tensile stresses are resisted by stirrups. Figure 28 shows one of the structure beams, where you can clearly see the breakdown of this sturdy beam mechanism therefore it is an imminent ruin situation.

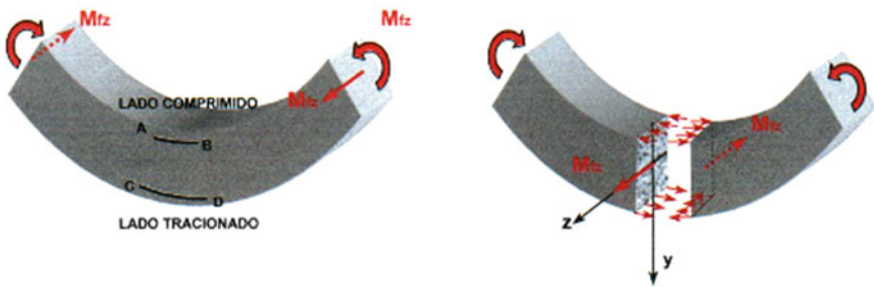


Fig. 27 Beam under bending stress

Fig. 28 Beam with virtually no frames



Fig. 29 Pilar P9—ground level



The pillars, in a simplified way are the elements that have the function of taking the loads from other structural elements in the foundation, essentially the compression work and depending on the integrity of the concrete section. Figure 29 shows P9 pillar on the ground level where you can see virtually cracks, concrete peeling, thereby decreasing its useful section.

Therefore the structure has serious pathologies, it justifies an Immediate Action Plan where temporary shoring are placed to reduce the risk of collapse until the implementation of structural recovery are defined.

3.2 Pathologies Mapping

This item seeks to identify the origins, manifestations, consequences and mechanisms of failures occurrence of degradation systems.

The conditions were mapped and classified into three levels according to the type, risk offered and difficulty of maintenance, which are: *Light* when it presents no direct structural risk, but impairs the functionality and/or aesthetic aspect (ex. floors degradation, closing masonry paints, etc.); *Average* that can compromise the structural performance over time, diagnosed admits some standardization; *Grave* causing risk of collapse, which require individual analysis, that do not follow the conventional inspection engines and do not follow the routine maintenance schedules, so the recovery will be monitored by a professional in charge and must have highly specialized knowledge. The following examples in Figs. 30, 31 and 32.

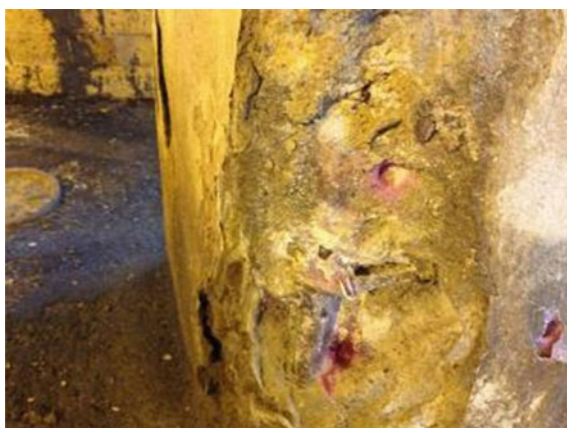
Fig. 30 Masonry detachment near the column, possible displacement of the support (L)



Fig. 31 Pilar with high carbonation depth along the floor (M)



Fig. 32 Pilar with peeling exposed and frame along the floor (G)



4 Existing Structure Verification

A three-dimensional model (Fig. 33) was prepared with the assistance of TQS software (software for calculation and design of concrete structures) as surveys and properties of the tested materials, which were introduced by all the shipments for structural analysis and evaluation of carrying capacity.

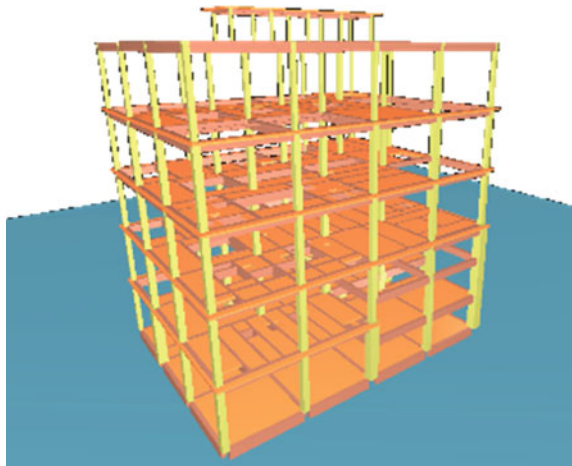
Data used:

- Wind basic speed ($v_0 = 39$ m/s)
- Overload in slabs of 500 kg/m²
- coatings/subfloor 100 kg/m²

After processing the efforts and details of the structure by software, the necessary frames were compared with the frames that were possible to be identified in the field. Although concrete coatings are incompatible with those determined by the NBR 6118 (2007), it varies greatly from one side to the other, they are compatible to the ordered efforts. Considering that the structure has a relief in carrying due to partial use, disabling much of the building.

The latest revision of ISO 6118 was published in 2003 and adopted as standard to reference for the calculation of concrete structures in Brazil. Its origin concomitant with the principle of normalization in the country when, in 1940, there was an official decree by President Getúlio Vargas for the mandatory use in public projects. And then published by the ABNT NB-1 with the acronym. In its history, there were undergone revisions in 1960 (NB-1: 1960) adopting by the European standards reference of CEB and thus consolidated in 1978. In 1980 review there was a register at the INMETRO under the identification of NBR-6118. The last review of 2003, that was valid from March 30th, 2004 on, received significant changes and had the greatest impact on the concrete specification which are related to ensure the quality, durability and service life of the structures.

Fig. 33 Structural model 3D
TQS



The building structure in question was designed according to the criteria of the European Standards which was in force at the time, using calculation procedures and details from different procedures used today. Therefore the framework for building on current standards of detail and design became a practical point of view and unviable economic.

5 Recovery and Structural Enhancement

Reinforcement of the development project and recovery structure aims prevention of pathologies and reinforcements to ensure safety and extend the life of the building. The concrete degradation and reinforcement corrosion is a phenomenon that only occurs when the protective conditions are insufficient. This failure, as seen, can be brought about by agents originating from different sources provoking the necessity to identify them, so that we can achieve an effective and lasting protection.

Because of the wide variety of types and stage of the found conditions it is not possible the standardization of recovery procedures, therefore, the procedures were listed and indicated for each pathology according to its need and form of structural recovery drawings, which were also found in the architectural recoveries (floor coatings, paints, etc.), they are essential to prevent disease and prolong the life of the structure.

Due to the degradation level, low safety and the operational part preventing a more detailed study of the conditions in some parts of the structure, it was done during the recovery process, with the temporary reinforcements and installation of switched off equipment. The inspection during the recovery project refers to the need of deepening the studies conducted and therefore fit to be complemented by the responsible company for the structural recovery.

6 Maintenance Schedule

Note that due to the nature of the pathologies (contamination of materials) and aggressive agents that come into direct contact with the structure it is not a single maintenance plan over the years, it requires annual inspection to observe the emergence of new diseases by a qualified professional to do so (leaks, cracks, spalling, deterioration of paintings, floors degradation, etc.). Following all the correct recovery procedures, it is possible that after its realization it is only necessary to maintain the exterior paint every 5 years, and finishing coat made of polyurethane every 10 years.

Since the structure has reached its life expectancy and because of the severity suffered with the chemical attacks a continuous monitoring is necessary to possible future pathologies that may occur after the recovery.

7 Final Considerations

The main cause of the disorders was due to the lack of maintenance of protection systems (coating, painting, sealing, etc.) and lack of hydraulic drainage facilities, making the water and contaminants come direct into constant contact to the structures of concrete and constructive elements.

Although the building has already reached the expected life (over 50 years) the general conditions for most of the building are reasonable considering the highly aggressive environment in which it is possible to a relatively simply recover. However in some specific points the structure suffered further degradation due to contamination by nitric acid and ammonium nitrate, jeopardizing both the concrete and the steel, so the strengthening and reconstruction of some structural elements with utmost urgency is needed in addition to provisional reinforcements immediate.

From a global point of view of building up the measures taken to recover are “extenuating” characters, since the framework of the whole structure of the building in technical standards would not be feasible from a technical and economic point of view. However it is possible that the recovery of the entire structure will enable their use and may not require the whole track, the time for additional life service.

References

- NBR 7680 (2007) Extraction, preparation, testing and analysis of concrete cores (in Portuguese)
- NBR 6118 (2007) Design of structural concrete—Procedure (in Portuguese)
- Helene Paulo RL (1986) Corrosion of concrete reinforcement, IPT, PINI

Building Materials Capillary Rise Coefficient: Concepts, Determination and Parameters Involved

Nikos Karagiannis, Maria Karoglou, Asterios Bakolas
and Antonia Moropoulou

Abstract The presence of water is one of the main decay factors in buildings. Capillary rise is the most important mechanism of water penetration into building materials in liquid phase. The free capillary water uptake experiment, used for the estimation of the capillary water absorption coefficient, a crucial materials property, is widely used for the characterization of building materials. The capillary water absorption coefficient was calculated according to three different European standards and recommendations. The three methods were compared in order to investigate which is the most appropriate for the calculation of the capillary water absorption coefficient. In addition, the effect of temperature on the estimation of the capillary water absorption coefficient of different building materials such as stones, bricks and mortars, was investigated for three different room temperatures (20, 25, 30 °C). From the results it was found a linear dependence between temperature T and the capillary water absorption coefficient.

Keywords Capillary rise coefficient · Temperature · Stones · Bricks · Mortars · Building materials

Nomenclature

ε_o Total porosity (%)
 g Gravitational constant (m/s^2)
 h Capillary moisture equilibrium height (m)
 σ Water surface tension (dyn/cm)
 T Air Temperature (°C)
 V_p Total pore volume (mm^3)
 V_b Material bulk volume (mm^3)
 V_s Material total volume (mm^3)

N. Karagiannis · M. Karoglou · A. Bakolas (✉) · A. Moropoulou
Department of Materials Science and Engineering, School of Chemical Engineering,
National Technical University of Athens, Zografou Campus, 15780 Athens, Greece
e-mail: abakolas@mail.ntua.gr

ρ_b	Material bulk density (kg/m ³)
ρ_s	Material true density (kg/m ³)
ρ	Water density (g/cm ³)
r	Material average pore radius (μm)
θ	Liquid-solid contact angle
A_w	Capillary water absorption coefficient (mg/cm ² s ^{1/2})
A	Specimen surface area (cm ²)
ΔB	Mass of the absorbed water (mg)

1 Introduction

Water can reach a building material through the material pores in several ways. It originates from e.g. driving rain, condensation of air humidity, run off from roof and facade and/or capillary rise of ground water (Arnold 1982; Karoglou et al. 2005). Building materials usually contain an amount of physically bound water without affecting their durability. But if the material's moisture content is above a certain percentage, the deterioration effect of moisture is activated causing an amount of physical, chemical and biological issues (Oliver 1997; Avoletti 1997; Moropoulou et al. 2014):

- Physical issues: Water will transport contaminants such as soluble salts. If wet, the material can become susceptible to freezing damage. In this case, major decay phenomenon is the formation of ice in low temperatures.
- Chemical issues: While water penetrates into a building material, salt crystallization may occur at the surface, or just under the surface. Some salts are hygroscopic, facilitating water vapor absorption and in many cases causing further structural damages.
- Biological issues: Moisture may also act as a substrate for the growth of bacteria, fungi, or algae with possible physical and chemical damages, but also possible health risks.

Thus, the knowledge of the water movement within a building material is of great importance to determine the degradation mechanism in question.

Main decay mechanisms are: hydrolysis, dissolution, hydration, oxidation, capillary rise, salt transfer and crystallization, hygroscopicity, cycles of wetting/drying; while main types of decay caused are: spalling, peeling, delamination, blistering, shrinkage, cracking, crazing, irreversible expansion, embrittlement, strength loss, staining discoloration, bio-decay of building materials (Connolly 1993).

Potential sources of water are: the ground, the environment (rain, sea, water vapor etc.), possible water sewage leakages, use of water for the production of building materials, interventions with the use of extensive quantities of water, salts hygroscopicity (Oxley and Gobert 1998). Best way to “fight” moisture related problems in buildings is the prevention of the entrance of moisture at the design

phase. However, the elimination of the problem in existing structures, especially historical ones, is more complicated.

1.1 Capillary Rise

Capillary rise is the main mechanism by which water penetrates into a building material. Capillary rise is, by definition, the upward vertical movement of ground water through a permeable wall structure (Alfano et al. 2006) causing the appearance of rising damp into the structure.

Building materials have pores of different shapes and different diameters, which means that they contain air voids. The main parameter of each material microstructure is the total porosity ϵ_o of the material, which is defined as the ratio of the material empty space V_p divided by the material's total volume V_s (Amoroso and Camaiti 1997):

$$\epsilon_o = \frac{V_p}{V_s} = 1 - \frac{V_b}{V_s} = 1 - \frac{\rho_b}{\rho_s} \tag{1}$$

where ρ_b, ρ_s are the bulk and the true density of the material and V_b the material bulk volume.

However, some material pores behave like closed ones (Fig. 1) and do not play a significant role in the water movement into the material. This is the reason why the estimation of the effective or open porosity is more representative. This refers to the fraction of the total volume in which fluid flow is effectively taking place and includes catenary and dead-end pores and excludes closed pores (or non-connected cavities).

The pore structure, meaning pore shape, size, distribution, and networking of pores is very difficult to define. Capillary rise takes place inside the capillary pores of a building material. The capillary pore radius is a controversial issue among researchers but, in general, its range is considered to be from about 10 nm to 10 μ m (Table 1). A very useful classification of pores based on their diameter according to researchers (Mehta 1986; Mindess et al. 2003) and IUPAC is listed in Table 1.

Fig. 1 Schematic pores classification, according to their accessibility to surroundings (*Legend* *a* closed pores, *b, f* pores open only at one end, *c, d, g* open pores, *e* open at two ends (through) pores)

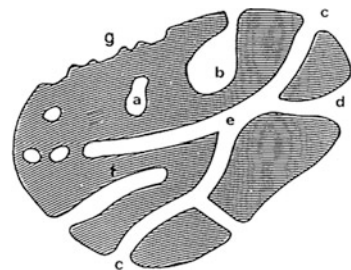


Table 1 Pore classification based on their diameter d (nm)

According to IUPAC		According to Mehta (1986)		According to Mindess et al. (2003)	
Name	Size range	Pore type	Size range	Name	Size range
Micropores	up to 2 nm	Interparticle space between C-S-H sheets	1–3 nm	Micropores “inter layer”	Up to 0.5 nm
				Micropores	0.5–2.5 nm
Mesopores	2–50 nm	Capillary pores (low w/c)	10–50 nm	Small (gel) capillaries	2.5–10 nm
		Capillary pores (high w/c)	3–5 μm	Medium capillaries	10–50 nm
Macropores	>50 nm	Entrained voids	50 μm –1 mm	Large capillaries	50 nm–10 μm
				Entrained air	0.1–1 mm

Pores can also be classified according to their accessibility to surroundings (Fig. 1). The pores communicating with the external surface are named open pores, like (b), (c), (d), (e) and (f). They are accessible for molecules or ions in the surroundings. Some are open only at one end (b, f). These are described as blind pores. Others may be open at two ends (through pores, (e)) (Zdravkov et al. 2007; IUPAC 1994).

Ground water can rise into the pore structure of a building material driven by the force of capillarity. Capillarity is greater for small capillaries and inversely proportional to the pore radius according to Jurin’s law. Jurin’s law is referred to the height h of the vertical rise in a capillary pore and is given by the following equation (Gennes et al. 2004):

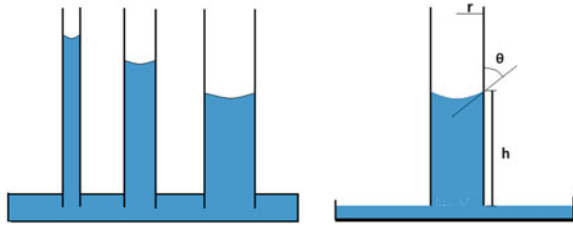
$$h = \frac{2\sigma \cos \theta}{\rho g r} \quad (2)$$

where r is the mean radius of the capillary pore, σ the surface tension of the liquid, θ the water contact angle, ρ the water density and g the gravity acceleration (Fig. 2).

1.2 Capillary Water Absorption Coefficient

Capillary water absorption coefficient, or A -coefficient, is one of the most important features of a building material because it governs the liquid moisture movement into it and expresses the rate of absorption of water due to capillary forces for building materials. Thus, it must be taken into consideration when determining the hydrometric properties of the material.

Fig. 2 Capillary action depends on the radius of a capillary tube. The smaller the tube, the greater the height reached



1.3 Estimation of the Capillary Water Absorption Coefficient

There are many European and international standards and recommendations by which researchers estimate the capillary water absorption coefficient of building materials. The majority of these standards are related to building materials and materials used in cultural heritage protection. European standard EN 1925 (2000) refers to natural stones, while EN 1015-18 (2002) refers to hardened mortars. European standard EN 13057 (2002) describes the measurement of the capillary water absorption of hardened concrete. Normal 11/85 (1985) refers to materials and conservation interventions of cultural heritage and it was replaced by the UNI 10859 (2000) standard, which refers to natural and artificial stones. Finally, EN 15801 (2009) refers to porous inorganic materials used for and constituting cultural property and the European standard EN 480-5 (2005), describes the determination of the water capillary absorption coefficient of concrete, mortars and grouts.

The experimental setup for a water absorption experiment as described in the EN standards and recommendations is quite common (Hall 1989). After drying each sample at 60 °C to constant mass in a hot-air oven, its dry mass is measured. Each sample is cooled to room temperature and is putted on a tray of distilled water. The position of the waterfront is gradually approaching the opposite side of the sample and the water intake is governed by capillary and viscous forces. The quantity of the absorbed water is measured at standard time intervals by weighing the specimen. Each weighing should be completed as quickly as possible (typically within 30 s). The capillary water absorption coefficient is determined with three different ways.

According to EN 1925 and EN 1015-18, the capillary water absorption coefficient is the gradient of the straight line obtained by plotting the cumulative mass of water absorbed per unit area against the square root of time t obtained from this first stage according to the following equation:

$$A_w = \frac{\Delta B}{A\sqrt{t}} \quad (3)$$

where A_w ($\text{mg}/\text{cm}^2 \text{ s}^{1/2}$) is the water absorption coefficient, A (cm^2) is the surface area of the cross section of the specimen and ΔB (mg) is the mass of the absorbed water. This estimation way is known as the one tangent method.

The Italian UNI 10859 standard refers to natural and artificial stones and indicates that the capillary water absorption coefficient should be calculated according to the following equation:

$$A_w = \frac{Q_{30} - Q_0}{\sqrt{t_{30}}} \quad (4)$$

where, Q_{30} is the cumulative mass of water at 30 min, Q_0 is the cumulative mass of water at the beginning of the experiment and t_{30} is the time of 30 min. This estimation method is known as the 30 min method.

Finally, in Italian Normal 11/85 the two tangents method is described. According to this method, the capillary water absorption coefficient should be determined according to the following equation:

$$A_w = \frac{M^*}{\sqrt{t^*}} \quad (5)$$

where A_w ($\text{mg}/\text{cm}^2 \text{ s}^{1/2}$) is the capillary water absorption coefficient, M^* (g/cm^2) is the asymptotic value of the absorbed water per unit area of the sample and t^* (s) is the abscissa of the point of intersection between the straight line passing through the asymptote and the tangent to the straight portion of the curve measured in seconds.

Many researchers have investigated the capillary water absorption coefficient as a part of their research works, however using each time one of the precedent standards.

Plagge et al. (2005) described an experimental method of an automated water uptake test. Moreover, they used this method to determine the capillary water uptake coefficient A_w according to EN 15148. Candanedo and Derome (2005) conducted capillary absorption tests to measure the water absorption coefficient in the longitudinal, radial and tangential directions and the capillary moisture content for one softwood species, Jack Pine, according to the one tangent method. Fronteau et al. (2010) studied the sedimentological and petrophysical properties of some Lutetian limestones of the Paris Basin. In this study, the building stones were characterized and their petrophysical characterizations were carried out using normalized tests recommended for building stones. They also determined the water uptake coefficient by capillary according to EN 1925. Juhász et al. (2014) analyzed the migration characteristics of *Bacillus cereus* in porous limestone, as well as the capillary absorption and elevation properties of porous limestone and they measured the water absorption coefficient according to EN 1925. Sengun et al. (2014) determined the capillary water absorption coefficients of 118 different natural stone types having different structural and textural features in accordance with the EN 1925 standard and related these coefficients with other rock properties such as bulk density, apparent porosity, total porosity, seismic velocity, etc.

Calcaterra et al. (2000) studied Piperno, a Late Quaternary magmatic rock, from different points of view, namely mineralogy, petrography and engineering geology and they measured the capillary water absorption coefficient of this rock according

to the Normal 11/85. Stefanidou and Papayianni (2005) examined the role of aggregates on the structure and behaviour of lime mortars by studying the influence of the aggregate content and the grain size on strength, porosity and volume stability of the mortars. They also measured capillary water penetration by suction according to the Normal 11/85. Karoglou et al. (2005) developed a first-order capillary rise kinetic model for predicting the water capillary rise of several building materials. In this work, the experimental procedure for the calculation of the moisture content of the materials followed the instructions of Normal 11/85. Karoglou et al. (2013) also studied the water vapor transfer rate of repair coated and uncoated plasters, used for masonries suffering by rising damp phenomena. Moreover they performed an ageing test with repeated cycles of capillary absorption of sodium sulphate solution, on brick-plaster-coating systems in accordance with Normal 11/85. Dei and Salvadori (2006) in their study, tried to evaluate the effectiveness of inorganic compatible treatments, based on nano-sized particles of calcium hydroxide (slaked lime) dispersed in alcoholic medium, as consolidants for limestones and painted surfaces. Both in situ and laboratory tests were carried out on carbonatic, low-porosity stones and on frescoes. The measurements of water absorption by capillarity in two classes of stones, both for the untreated and consolidated samples were conducted according to the Normal 11/85.

Maravelaki-Kalaitzaki et al. (2005) conducted a research with hydraulic restoration mortars for a historic masonry in Crete, Greece. They also presented the results of the physico-chemical characterization of original mortars and plasters and the evaluation of the repair ones prepared with natural hydraulic lime (NHL) as binding material and siliceous sand and crushed brick as aggregates. Water absorption measurements were carried out and the test was performed according to the methodology described in the normal UNI 10859. Vandevorde et al. (2009) proposed an alternative method, the contact sponge method, which was tested on non-treated porous stone materials in a laboratory environment. Moreover, the results of this method were compared with results obtained via the capillary rise method according to UNI 10859 in order to evaluate its accuracy. Vandevorde et al. (2013) also presented a comparison of non-destructive techniques for analysis of the water absorption behavior of seven lithotypes, in order to develop a methodology for the selection and application of method and an adequate comparison of the results. In this work capillary rise measurements were performed according to UNI 10859. Ksinopoulou et al. (2012) investigated the performance of particle modified consolidants (PMC) applied on two types of porous stones used in historical structures in Greece. In order to evaluate the consolidation effect, changes in properties of treated specimens were estimated through several methods such as SEM, mercury intrusion porosimetry, water absorption by capillarity, etc. More specifically, the water absorption coefficient was estimated through capillary rise tests according to UNI 10859.

While, the experimental procedure estimating the capillary water absorption coefficient of building materials remains unquestionable, the comparison of A-coefficient values is difficult due to different estimation methods. Indeed, as it is

often observed, a building material presents a different A -coefficient value depending on the estimation method. Thus, different materials A -coefficient cannot be compared based on different estimation methods.

2 Materials and Methods

Three main types of building materials were selected and studied (bricks, stones, and natural hydraulic mortars) with different microstructural characteristics. Bricks are symbolized with codes starting with the letter B , stones with S and mortars with M . Two different types of clay brick have also been investigated. One was a traditional handmade clay brick (BRM) and the other one was a typical solid clay brick (BRI). Two sedimentary quarry stones originated from Rethymno, Crete island (SRY) and from Rhodes island (SRH) respectively were the stones investigated. The mortars examined were prepared by using two different types of natural hydraulic lime ($NHL2$ and $NHL3.5$) in accordance to EN 459-1 (2010), in 3 different binder/aggregate ratios. The materials dimensions were $5 \times 5 \times 5 \pm 0.1 \text{ cm}^3$. The materials characteristics are summarized in Table 2.

The aim of this work was the estimation of the A -coefficient according to three different European standards and recommendations. Additionally, the dependency of the capillary water absorption coefficient with the temperature was investigated.

Among the European standards and recommendations, the regulations chosen were: EN 1925 and EN 1015-18 in which the one tangent method is described, UNI 10859 in which the two tangents method is described and Normal 11/85 recommendation in which the 30 min method is described.

A building material was chosen for examination and capillary rise experiments were conducted at $20 \text{ }^\circ\text{C}$. The choice was the BRI brick because it exhibited the most linear first and second stages among all materials examined and because of its high homogeneity. Following the experimental procedure, the capillary rise coefficient was calculated according to the three different aforementioned methods.

Table 2 Materials description

a/a	Materials	Description
1	mca25/75	25 % NHL 2 and 75 % river sand
2	mca30/70	30 % NHL 2 and 70 % river sand
3	mca20/80	20 % NHL 2 and 80 % river sand
4	mcb25/75	25 % NHL 3.5 and 75 % river sand
5	mcb30/70	30 % NHL 3.5 and 70 % river sand
6	mcb20/80	20 % NHL 3.5 and 80 % river sand
7	BRI	Typical solid clay brick
8	BRM	Traditional handmade clay brick
9	SRH	Rhodes quarry stone
10	SRY	Rethymno quarry stone

Following this, capillary rise experiments were carried out with the rest of the materials described in Table 2, at the temperature of 20 °C, as suggested in most European standards and recommendations.

In order to investigate the dependence of the capillary water absorption coefficient on the temperature, a series of capillary rise tests were carried out at three different air temperatures of 20, 25 and 30 °C for all the examined materials. All the capillary rise experiments were performed at controlled relative humidity conditions. The water temperature was determined about 2 ± 0.5 °C lower than the air temperature while the relative humidity was 45 ± 5 % during the experiments.

At least, three specimens of each material were tested for each of the selected air temperatures.

3 Results and Discussion

In Table 3 the capillary water absorption coefficient values according to the three different estimation methods, at the air temperature of 20 °C for all the examined materials are presented. In addition, the estimation of the *A*-coefficient based on the three different estimation methods for building material *BRI* is shown in Figs. 3, 4 and 5.

Bricks presented the highest capillary water absorption coefficient values (>20) whatever the calculation method was. On the contrary, *SRY* stones and *mca25/75* mortars exhibited the lowest water absorption coefficient values probably due to their different nature and different microstructural characteristics. *BRM* bricks, *SRY* stones and *mca30/70* mortars exhibit almost the same capillary water absorption coefficient values with all the estimation methods. Moreover, in many cases (*mca20/80*, *mca30/70* and *mcb20/80* mortars) the two tangents method and the

Table 3 Water absorption coefficient A_w ($\text{mg}/\text{cm}^2 \text{ s}^{1/2}$) values for building materials at 20 °C

Materials	A_w ($\text{mg}/\text{cm}^2 \text{ s}^{1/2}$) (20 °C)					
	One tangent method	SD	Two tangent method	SD	30 min method	SD
<i>mca20/80</i>	19.2	0.59	17.6	0.89	17.9	1.07
<i>mca25/75</i>	7.90	0.80	8.00	0.42	7.20	1.00
<i>mca30/70</i>	17.5	1.02	16.0	2.08	16.1	2.37
<i>mcb20/80</i>	12.3	0.70	10.6	0.45	10.0	0.05
<i>mcb25/75</i>	9.10	0.10	7.10	0.00	5.10	0.00
<i>mcb30/70</i>	9.20	0.43	6.50	0.26	3.60	0.10
<i>BRI</i>	27.0	1.18	25.2	0.69	26.1	0.83
<i>BRM</i>	20.5	0.05	20.6	1.33	20.7	0.75
<i>SRH</i>	10.1	0.00	12.3	0.25	7.00	0.00
<i>SRY</i>	8.90	0.80	8.30	0.59	9.00	1.84

Fig. 3 Determination of water absorption coefficient due to capillarity according to EN 1925

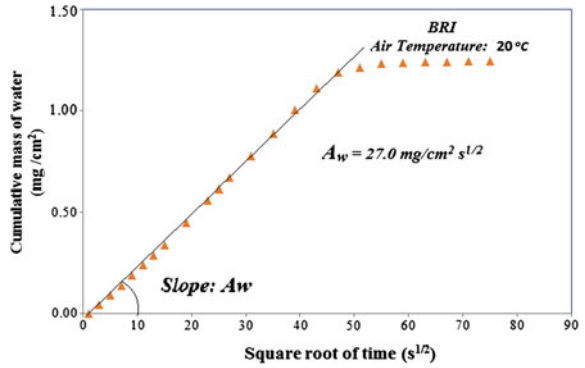


Fig. 4 Determination of water absorption coefficient due to capillarity according to normal 11/85

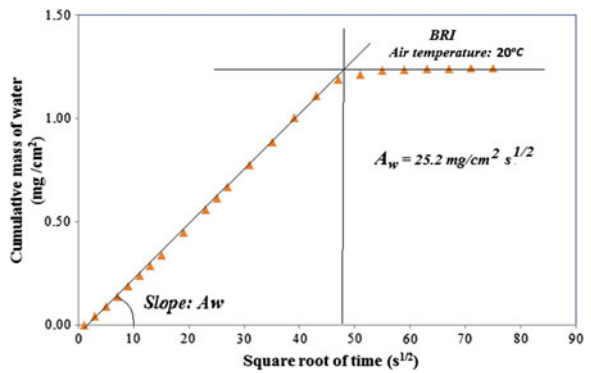
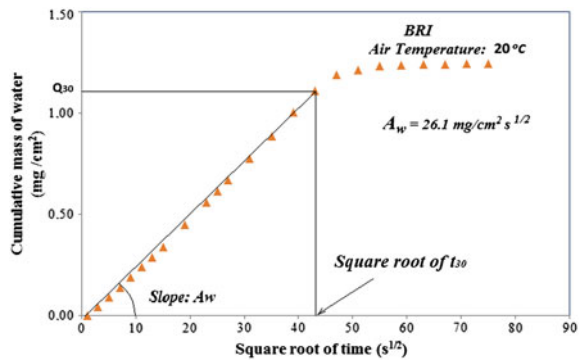


Fig. 5 Determination of water absorption coefficient due to capillarity according to UNI 10859



30 min method presented almost the same results. However, some building materials (*mcb30/70* and *mcb25/75* mortars) exhibit a slow initial water absorption rate and thus, the 30 min method estimates smaller values compared to the values given with the other two estimation methods. In Fig. 6, the capillarity rise kinetics, at 20 °C

is presented for all the examined materials. In general, *mca* mortars have higher water absorption coefficients than *mcb* mortars probably due to their different type of binder.

The main results of the capillary rise experiments for all the examined materials at the temperatures of 20, 25 and 30 °C are summarized in Fig. 6.

From the diagrams in Fig. 6, a dependence of the *A*-coefficient with the temperature is observed in all samples. More specifically, it was found that the water absorption coefficient increases with the increase of temperature. In the case of *BRI* and *BRM* bricks kinetics, the initial part is very well defined by a straight line at all the temperatures and their curve shape is the same at every temperature examined. Moreover, *BRI* brick exhibits higher capillary saturation than *BRM* brick. *SRH* stones exhibit a first stage not sufficiently defined by a straight line (see Fig. 6) and this makes the calculation of the *A*-coefficient according to the one tangent method very difficult. *SRY* stones present higher sorptivity values than *SRH* stones. Some irregularities are also observed in the curve shape of some mortars (*mca25/75*, *mcb25/75* and *mcb30/70* mortars) probably due to their different microstructure. Moreover, the two tangents method seems to be the most appropriate for the estimation of the capillary water absorption coefficient not only in the case of building materials with high homogeneity but also in the case of materials with anomalous microstructure.

Table 4 presents the results of the linear regression analyses with their R-squared values according to the two tangents method. The dependence of the water absorption coefficient values with the temperature for some of the examined building materials according the one tangent method is shown in Fig. 7.

According to the results as exhibited in Table 4 and in Fig. 7, it is evident that the capillary water absorption coefficient exhibits a linear dependence with the temperature in all the samples. In almost all the calculations standard deviation was under 10 %.

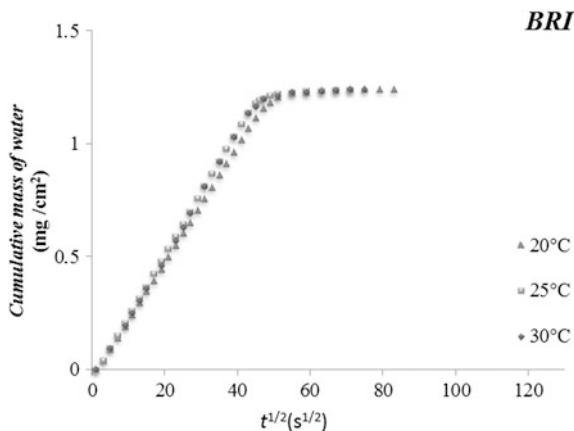


Fig. 6 Cumulative mass of capillary water uptake versus time for different building materials

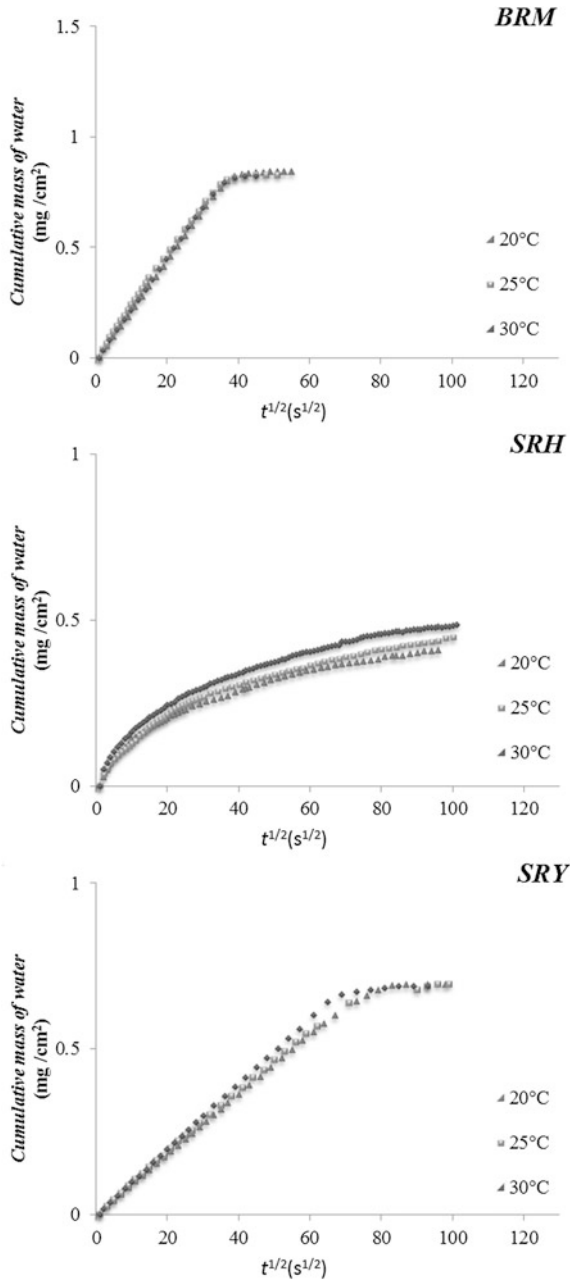


Fig. 6 (continued)

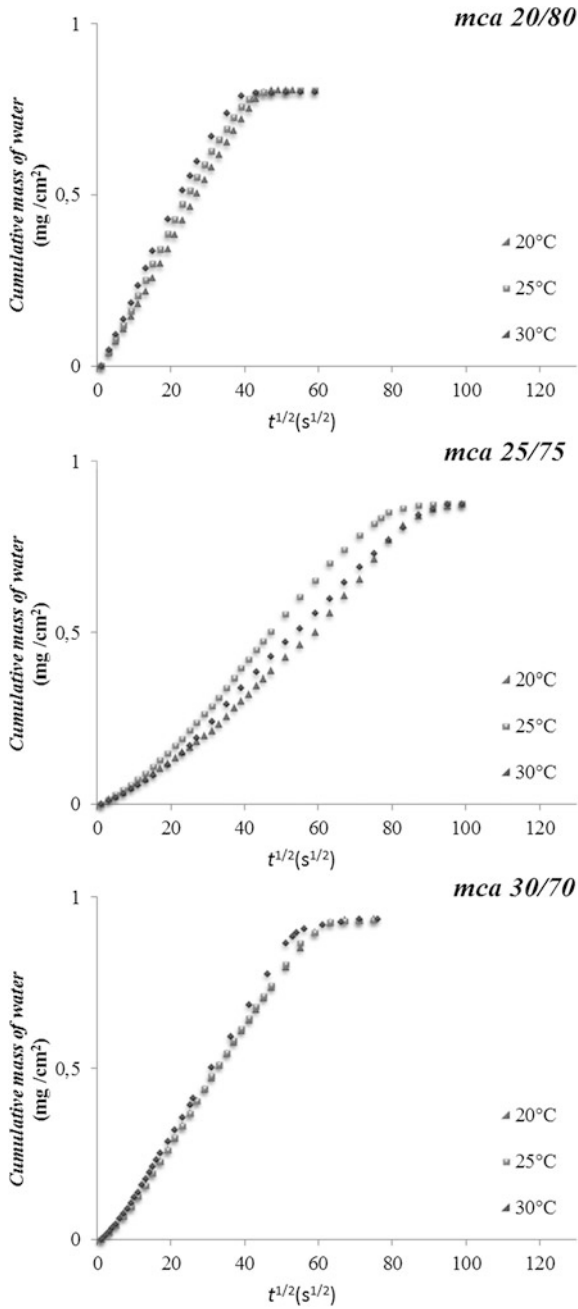


Fig. 6 (continued)

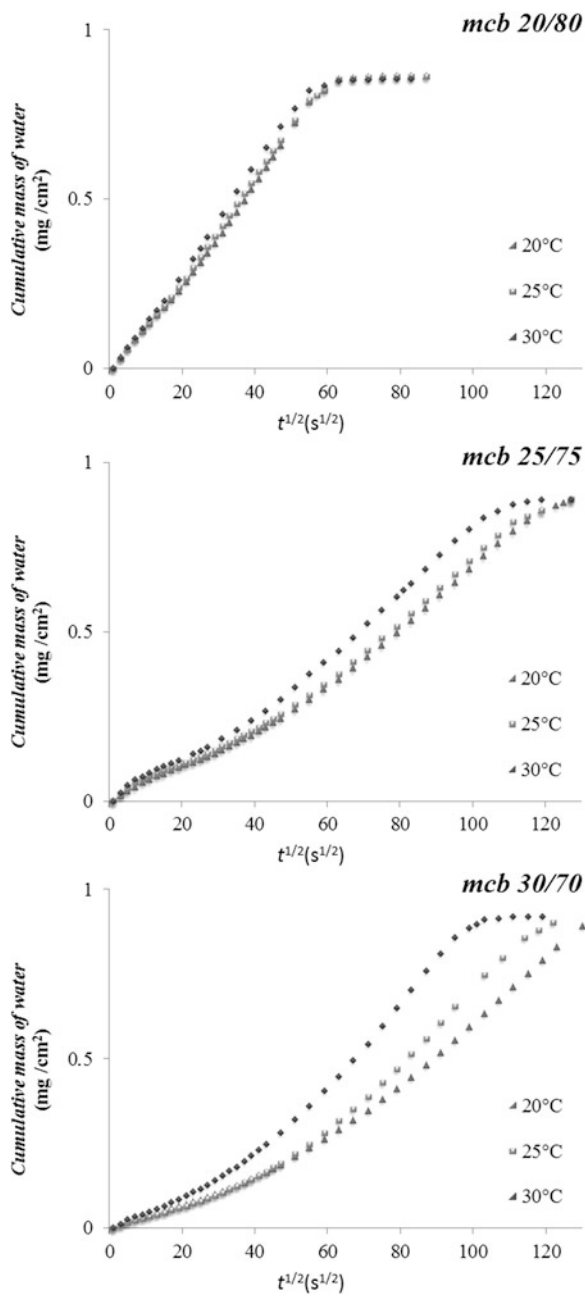


Fig. 6 (continued)

Table 4 Linear regression equations and R-squared values for the examined building materials according to the two tangents method. The A-coefficient is the slope of the linear regression equation

Materials	Two tangents method	
	Linear regression equation	R ² -value
mca25/75	$y = 0.241x + 3.030$	0.803
mca30/70	$y = 0.245x + 10.80$	0.967
mca20/80	$y = 0.171x + 14.08$	0.991
mcb25/75	$y = 0.108x + 4.87$	0.993
mcb30/70	$y = 0.049x + 5.74$	0.792
mcb20/80	$y = 0.088x + 9.11$	0.858
BRI	$y = 0.133x + 22.91$	0.914
BRM	$y = 0.146x + 17.62$	0.958
SRH	$y = 0.612x + 0.10$	0.990
SRY	$y = 0.163x + 5.20$	0.974

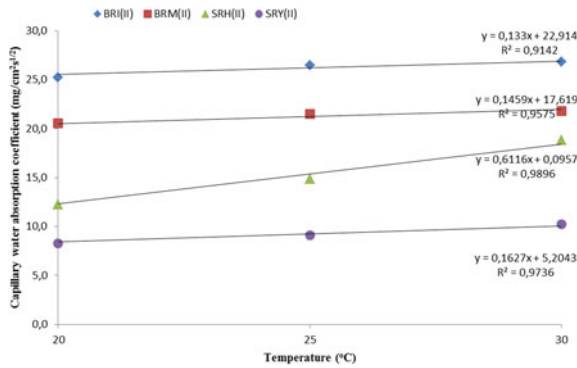


Fig. 7 Absorption coefficient values at different temperatures and use of linear regression for bricks and stones according to the two tangents method

3.1 Case Study

In order to evaluate the validity of the predicted values, the capillary water absorption coefficient of *BRI* and *BRM* bricks was measured at 15 °C. After this, a calculation of the water absorption coefficient was made, using the equations obtained from the linear regression given in Table 4 according to the two tangents method.

The results from the comparison of the experimental values with the predicted values of the capillary water absorption coefficient are shown in Table 5.

From the above reported results is evident that experimental values of the A-coefficient are in very good agreement with the predicted ones using the equations given in Table 4.

Table 5 Experimental and predicted estimation of the capillary water absorption coefficient A for bricks BRI and BRM at 15 °C

Temperature 15 °C		
Materials	Predicted A -coefficient ($\text{mg cm}^{-2} \text{s}^{-1/2}$)	Experimental A -coefficient ($\text{mg cm}^{-2} \text{s}^{-1/2}$)
BRI	24.9	25.1
BRM	19.8	19.7

4 Conclusions

In the literature, different standards and recommendations are utilized for the estimation of the capillary water absorption coefficient of building materials. Each one of them derives from a different calculation basis and gives different final results. In this paper, the capillary water absorption coefficient was estimated according to three European standards and recommendations. The two tangents method seems to be the most appropriate for the estimation of the A -coefficient especially in cases in which building materials have a first absorption stage deviating from the linearity.

The effect of air temperature on the progress of the capillary rise of various building materials was also investigated and a linear relationship between the capillary water absorption coefficient values with the temperature was observed. Moreover, a case study at a different temperature of 15 °C was performed, in order to validate the linear dependency of the A -coefficient with the temperature. Experimental A -coefficient values were found in very good agreement with the predicted ones. Hence, a prediction of the value of the water capillary rise coefficient in every air temperature using appropriate linear equations could be made.

In addition, the assumption of a constant water absorption coefficient, independent of temperature, that is often adopted, is clearly inaccurate. This dependence should be taken into account by all researchers and practitioners who use the water absorption coefficient as a mean to characterize a building material.

References

- Alfano G, Chiancarella C, Cirillo E, Fato I, Martellotta F (2006) Long-term performance of chemical damp-proof courses: twelve years of laboratory testing. *Build Environ* 41:1060–1069
- Amoroso GG, Camaiti M (1997) *Scienza dei materiali e restauro*. ALINEA, Bologna
- Arnold A (1982) Rising damp and saline minerals. In: *Fourth international congress on the deterioration and preservation of stone objects*, Louisville, pp 11–28
- Avoletti M (1997) Contro l'umidità ascendente. *Recupero Conservazione* 17:58–705
- Calcaterra D, Cappelletti P, Langella A, Morra V, Colella A, de Gennaro R (2000) The building stones of the ancient centre of Naples (Italy): Piperno from Campi Flegrei. A contribution to the knowledge of a long-time-used stone. *J Cult Heritage* 1:415–427

- Candanedo L, Derome D (2005) Numerical simulation of water absorption in softwood. In: Ninth international IBPSA conference, Montréal, Canada
- Connolly JD (1993) Humidity and building materials. In: Rose WB, Tenwolde A (eds) Bugs, mold and rot II, proceedings of a workshop by the building environment and thermal envelope council of the National Institute of Building Sciences, Washington DC, NIBS, pp 29–36
- Dei L, Salvadori B (2006) Nanotechnology in cultural heritage conservation: nanometric slaked lime saves architectonic and artistic surfaces from decay. *J Cult Heritage* 7:110–115
- EN 1015-18 (2002) Methods of test for mortar for masonry—determination of water absorption coefficient due to capillary action of hardened mortar
- EN 13057 (2002) Products and systems for the protection and repair of concrete structures—test methods. Determination of resistance of capillary absorption
- EN 15801 (2009) Conservation of cultural property—test methods. Determination of water absorption by capillarity
- EN 1925 (2000) Natural stone test methods—Determination of water absorption coefficient by capillarity
- EN 459-1 (2010) Building lime. Definitions, specifications and conformity criteria
- EN 480-5 (2005) Admixtures for concrete, mortar and grout—test methods. Determination of capillary absorption
- Fronteau G, Moreau C, Thomachot-Schneider C, Barbin V (2010) Variability of some Lutetian building stones from the Paris Basin, from characterisation to conservation. *Eng Geol* 115:158–166
- Gennes PG, Brochard-Wyart F, Quere D (2004) Capillarity and wetting phenomena: drops, bubbles, pearls, waves. Springer, New York
- Hall C (1989) Water sorptivity of mortars and concretes: a review. *Mag Concr Res* 41:51–61
- International Union of Pure and Applied Chemistry (1994) Physical chemistry division commission on colloid and surface chemistry, subcommittee on characterization of porous solids: recommendations for the characterization of porous solids (Technical Report). *Pure Appl Chem* 66(8):1739–1758
- Juhász P, Kopeckó K, Suhajda A (2014) Analysis of capillary absorption properties of porous limestone material and its relation to the migration depth of bacteria in the absorbed biomineralizing compound. *Civ Eng* 58(2):113–120
- Karoglou M, Moropoulou A, Giakoumaki A, Krokida M (2005) Capillary rise kinetics of some building materials. *J Colloid Interface Sci* 284:260–264
- Karoglou M, Bakolas A, Moropoulou A, Papapostolou A (2013) Effect of coatings on moisture and salt transfer phenomena of plasters. *Constr Build Mater* 48:35–44
- Ksinopoulou E, Bakolas A, Kartsonakis I, Charitidis C, Moropoulou A (2012) Particle consolidants in the consolidation of porous stones. In: 12th international congress on the deterioration and conservation of stone, Columbia University, New York
- Maravelaki-Kalaitzaki P, Bakolas A, Karatasios I, Kilikoglou V (2005) Hydraulic lime mortars for the restoration of historic masonry in Crete. *Cem Concr Res* 35:1577–1586
- Mehta PK (1986) Concrete: structure, properties, and materials. Prentice-Hall, Englewood Cliffs
- Mindess S, Young JF, Darwin D (2003) Concrete. Prentice Hall, New Jersey
- Moropoulou A, Karoglou M, Bakolas A, Krokida M, Maroulis ZB (2014) Moisture transfer kinetics building materials and components: modeling, experimental data, simulation. In: Drying and wetting of building materials and components. Springer International Publishing Switzerland
- Normal 11/85 (1985) Assorbimento d' acqua per capillarità – Coefficiente di assorbimento capillare, CNR-ICR
- Oliver A (1997) Dampness in buildings. In: Douglas J, Sterling JS (eds) 2nd edn. Blackwell Science, Great Britain
- Oxley TA, Gobert EG (1998) Dampness in buildings: diagnosis, treatment, instruments, 2nd edn. Biddles Ltd Guilford and King's Lynn, Great Britain

- Plagge R, Scheffler G, Grunewald J (2005) Automatic measurement of water uptake coefficient of building materials. In: Proceedings of 7th conference of building physics in Northern Countries, pp 15–22
- Sengun N, Demirdag S, Akbay D, Ugur I, Altindag R, Akbulut A (2014) Investigation of the relationships between capillary water absorption coefficients and other rock properties of some natural stones. V. Dünya Doğaltaş Kongresi (Globalstone 2014), Antalya–Türkiye, pp 22–25
- Stefanidou M, Papayianni I (2005) The role of aggregates on the structure and properties of lime mortars. *Cement Concr Compos* 27:914–919
- UNI 10859 (2000) Cultural heritage—natural and artificial stones—determination of water absorption by capillarity
- Vandevoorde D, Pamplona M, Schalm O, Vanhellefont Y, Cnudde V, Verhaeven E (2009) Contact sponge method: performance of a promising tool for measuring the initial water absorption. *J Cult Heritage* 10:41–47
- Vandevoorde D, Cnudde V, Dewanckele J, Brabant L, de Bouw M, Meynen V, Verhaeven E (2013) Validation of in situ applicable measuring techniques for analysis of the water adsorption by stone. *Procedia Chem* 8:317–327
- Zdravkov BD, Cermak JJ, Sefara M, Janku J (2007) Pore classification in the characterization of porous materials: a perspective. *Cent Eur J Chem* 5(2):385–395

Statistical Modelling of Service Life Prediction of Exterior Painted Surfaces

Ana Silva, Pedro L. Gaspar and Jorge de Brito

Abstract The degradation of building materials is a complex phenomenon, which starts as soon as construction is concluded, evolves over time, and contributes to end the service life of buildings. In fact, even for identical sets of initial conditions, degradation mechanisms and performance requirements, there are many possible outcomes with different levels of probability. Because of their great exposure to external actions and their role in the protection of masonry, wall coatings on façades are one the elements most subjected to degradation. Painting plays an important role as external coating finishing, nationally and internationally, and is the most frequently used coating in Portugal. In this study an approach to evaluate the service life of exterior surface of painted walls is proposed, based on the evaluation of the degradation state of 220 façades surveyed in the Lisbon area, in Portugal. The influence of the various characteristics of the painted surfaces and of their surroundings on their durability is also analysed. For that purpose, four methodologies are used: (i) deterministic methods; (ii) factorial methods; (iii) stochastic methods; and (iv) computational models. These mathematical models are established to estimate the degradation level of this type of coating and their service life. The predictive ability of the models is examined and some recommendations are made, concerning the advantages and limitations of the models proposed.

Keywords Degradation · Service life · Painted surfaces · Durability · Statistical tools

A. Silva (✉)

ICIST, DECivil, Instituto Superior Técnico, Universidade de Lisboa, Lisbon, Portugal
e-mail: anasilva931@msn.com

P.L. Gaspar

Faculty of Architecture, Universidade de Lisboa, Lisbon, Portugal
e-mail: pmgaspar@fa.utl.pt

J. de Brito

ICIST, Instituto Superior Técnico, Universidade de Lisboa, Lisbon, Portugal
e-mail: jb@civil.ist.utl.pt

© Springer Science+Business Media Singapore 2016

J.M.P.Q. Delgado (ed.), *New Approaches to Building Pathology and Durability*,
Building Pathology and Rehabilitation 6, DOI 10.1007/978-981-10-0648-7_3

1 Introduction

The degradation of buildings and their elements begins as soon as constructions are put into use, increasing over time until it reaches unacceptable levels (marking the end of the service life of buildings). The Portuguese building stock shows clear signs of degradation (Lanzinha et al. 2006) due to the ageing of the materials associated with an incipient culture of building maintenance. The cost of maintaining façades represents a significant percentage of the cost of intervening in buildings (Teo et al. 2005). For these reasons, it is necessary to have tools for service life prediction, providing information related to the instant to intervene, and allowing a more rational assessment of the construction elements through the definition of maintenance plans (Zhang and Gao 2012).

Predicting the service life of a building or of its components can be a complex and time-consuming process with which a number of factors are associated, including the quality of materials, the level of design and execution, the interior and external environmental conditions, the use conditions, and the maintenance level (ISO 15686: 2000). In fact, degradation phenomena are extremely complex since, even for identical sets of initial conditions, degradation mechanisms and performance requirements, there are many possible outcomes with different levels of probability. The degradation process represents the sequence of changes to which the façades are subjected during their service life, which leads to a deterioration of their physical, chemical or mechanical properties.

In the last decades, several service life prediction methods have been put forward; the majority of these are based on simple regression analysis, evaluating the loss of performance of the building component analysed (Flourentzou et al. 1999; Shohet and Paciuk 2004; Gaspar and de Brito 2008). To overcome some of the limitations of these empirical methods, some authors proposed the application of statistical and computational tools for service life prediction. Multiple linear regression and artificial neural networks have been successfully used to estimate the service life of stone claddings (Silva et al. 2011) and have been proven to be an efficient tool to solve civil engineering and construction problems (Garrett 1994; Wang and Gibson 2010; Mata 2011).

This study evaluates the service life of 220 painted surfaces (surveyed in the Lisbon area) using three statistical methods: (i) simple regression analysis; (ii) multiple linear regression analysis; (iii) and artificial neural networks. These methods allow identifying the influence of the various characteristics of the painted surfaces and their surroundings on the durability of paintings.

2 Degradation of Painted Surfaces

Coatings act like the building's skin and are one the elements most subjected to degradation due to their great exposure to external actions. Painted surfaces are the most common type of coatings used in Portugal and worldwide. The degradation of

these coatings affects the perception of urban space with direct consequences on users. In this study, the physical and visual degradation of painted surfaces are characterized by a scale ranging from level 0 (no visible degradation) to 4 (generalized degradation); in this characterization, four main defects that affect painted surfaces are considered (NP EN ISO 4628-1: 2005a; NP EN ISO 4628-2: 2005b; NP EN ISO 4628-4: 2005c; NP EN ISO 4628-5: 2005d; NP EN ISO 4628-7: 2005e; Chai et al. 2014a): (i) staining and colour change (that mostly affect the visual quality of a façade and generally arise in the very early years of the service life of paint coatings); (ii) chalking (typically causes wear, detachment and loss of material); (iii) cracking; (iv) loss of adherence (due to the combined effect of various defects and degradation agents).

To evaluate the global degradation of painted surfaces a numerical index is used, initially proposed by Gaspar and de Brito (2008) and Gaspar (2009), given by the ratio between the degraded area—weighted as a function of its state of repair—and a reference area, equivalent to the whole area of the façade with the maximum degree of degradation. This numerical index, called degradation severity S_w , is given by Eq. (1).

$$S_w = \frac{\sum(A_n \times k_n \times k_{a,n})}{A \times k} \quad (1)$$

where S_w represents the degradation severity, expressed as a percentage, k_n the multiplying factor of defects n , as a function of their degradation level, within the range $K = \{0, 1, 2, 3, 4\}$, $k_{a,n}$ the weighting factor corresponding to the relative weight of the defect detected ($k_{a,n} \in \mathbb{R}^+$) according to the cost of repair, A_n the area of coating affected by a defect n , in m^2 , A the façade area, in m^2 , and k the multiplying factor corresponding to the highest degradation level of a coating, as defined in K above, of area A .

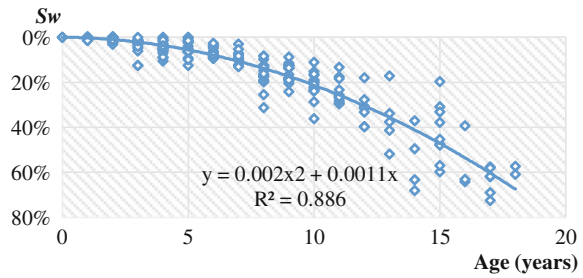
3 Deterministic Models

3.1 Simple Regression Analysis

It is possible to translate the deterioration of painted surfaces through a continuous function called “degradation curve” obtained by a simple regression analysis.

According to Shohet and Paciuk (2004), these analytical methods are able to identify wear and tear mechanisms, model and simulate them, in order to determine the service life of building components, using a performance limit criterion. This function can be graphically represented by a curve that illustrates the continuous degradation process over time (i.e. the loss of performance of painted surfaces). The age of the paintings is given in the x-axis (i.e. the time elapsed since the building is put to use or since the latest major intervention in the façade and the time of inspection) and in the ordinate axis the index that expresses the global degradation

Fig. 1 Average degradation curves (linear and polynomial) obtained from the 220 cases analysed in the fieldwork



of painted surfaces (S_w) is represented. Figure 1 shows the scatter of points obtained through an extensive field work, over which a polynomial curve is presented. This regression line represents the average degradation path of the sample. The analysis of the square of the Pearson product correlation coefficient (R^2) reveals that the regression curve has a relatively high value (R^2 of 0.89). The results obtained show that 89 % of the variability of y (degradation) is explained by x (age of the painting) and 11 % is due to other factors.

To estimate the service life of painted surfaces it is necessary to define the limit that establishes the end of their service life. However, this is a concept that varies according to acceptance criteria, related with the perception of what is acceptable or not. The maximum degradation acceptable is a relative concept that depends on the context around the decision-making, the performance expectations at a given moment or the meaning of functionality of a construction element (Chai et al. 2014a). From the analysis of the sample, a maximum degradation level of 20 % is adopted, beyond which the façades are no longer capable of meeting the requirements for which they were designed. Once this limit is defined, it is possible to estimate the service life of painted surfaces through the intersection of the degradation curve with the horizontal line that represents the minimum acceptable performance level. In this study an average service life of 9.75 years is obtained for the 220 painted surfaces, i.e. around 10 years.

Figure 1 only relates the age of the façades to their degradation. It seems relevant to analyse the influence of the characteristics of paintings in their degradation process. In this study the variables related with materials' characteristics (type of product, surface preparation, paint colour and paint finishing), environmental conditions (exposure to damp, distance from the sea, wind-rain action, façade orientation) and age of the coatings are analysed. Table 1 shows the predicted service life of paintings according to their characteristics. The results obtained are coherent from a physical point of view; concerning the façades orientation, in North-facing façades the most common defects correspond to staining problems, in façades facing South and West the most common defects are related with loss of brightness, cracking and chalking (which were the most significant anomalies in the sample, subjected to a warm temperate climate, with hot and dry summers).

Table 1 Predicted service life according to the degradation factors considered

Characteristics		Estimated service life (years)	Ratio between estimated service life and reference service life
Type of product	Plain paint	9.9	1.02
	Textured paint	9.9	1.02
	Elastic membranes	9.4	0.97
Surface preparation	Paint over render	9.7	0.99
	Repainting over existing paint	9.7	1.02
Paint colour	White	9.7	1.00
	Light colours	9.7	1.00
	Dark colours	4.7	0.49
Paint finishing	Rough	9.8	1.01
	Smooth	9.7	1.00
Exposure to damp	Unfavourable	9.4	0.97
	Current	9.9	1.02
Distance from the sea	Less than 5 km	9.4	0.97
	More than 5 km	9.8	1.01
Wind-rain action	Severe	9.5	0.98
	Moderate	9.7	1.00
	Mild	10.0	1.03
Façade orientation	North	9.9	1.02
	East	9.9	1.02
	West	9.4	0.97
	South	9.0	0.93

3.2 Multiple Linear Regression Analysis

Multiple linear regression analysis is one of the most widely used techniques to model the relationship between a dependent variable and one or more independent variables (predictors) (Mata 2011). When the regression analysis is used in prediction models, the main objective is to explain a given reality and try to anticipate the role of a dependent variable as a function of the independent variables. Multiple linear regression allows improving the first analysis; in fact, more than identifying the characteristics that influence the durability of paintings, multiple linear regression allows establishing a hierarchical distinction between the different characteristics, evaluating which variables are more relevant to the degradation of painted surfaces.

To perform a multiple regression analysis it is necessary to quantify the qualitative variables. In this study, each category was associated with a value that represents the ratio between the estimated service life as a function of each coating characteristic and the reference service life of 9.75 years (values presented in Table 1). Equation (2) presents the mathematical formula to estimate the degradation of painted surfaces as a function of the explanatory variables. A stepwise

technique from SPSS software was used to identify the explanatory variables. The simple linear regression model presented in Fig. 1, which includes only the age as explanatory variable, leads to a R^2 of 0.74; the introduction of two more variables increases the statistical significance of the model. It is important to notice that the R^2 obtained by MLR is lower than the R^2 obtained by polynomial regression (Fig. 1). The model presents a very strong correlation between variables, deemed appropriate to model the durability of painted surfaces. To apply Eq. (2), the variables must be replaced by the values presented in Table 1.

$$S_w = 0.4734 + 0.0353 \text{ Age} - 0.2618 \text{ Sea} - 0.3175 \text{ Orientation} \quad (2)$$

Using this equation it is possible to calculate the estimated service life (ESL) for each case study within the sample, assuming a maximum degradation severity of 20 %, as shown in expression (3).

$$ESL = \frac{(0.20 - 0.4734 + 0.2818 \text{ Distance from the sea} + 0.3175 \text{ Façade orientation})}{0.0353} \quad (3)$$

Using this method an average estimated service life of 8.5 years is obtained, lower than the value obtained by the graphical method (9.75 years) but still consistent with the empirical knowledge related with the durability of painted surfaces. Figure 2 shows the histogram of estimated service life obtained by the multiple linear regression model.

3.3 Multiple Nonlinear Regression Analysis

Multiple nonlinear regression analysis is similar to linear regression analysis, assuming the same assumptions in the model’s validation. Unlike linear regression, in nonlinear regression analysis the regression model is a nonlinear function of the

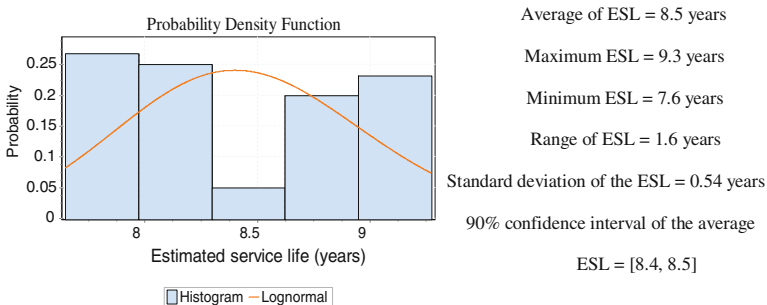


Fig. 2 Histogram of estimated service life obtained by the multiple linear regression model

parameters (Montgomery et al. 2012). In nonlinear regression models, the mathematical equation that best describes the dataset behaviour is unknown and the researcher must know a priori the variables that should be included in the model. Nonlinear regression models are more complex than simple or multiple linear regression analysis, since the model’s definition requires an iteration process to estimate the parameters to include in the mathematical equation.

This study comprises the application of nine nonlinear regression models to the service life prediction of painted surfaces: polynomial model (Eq. (4)); Gompertz curve (Eq. (5)); von Bertalanffy curve (Eq. (6)); Richards curve (Eq. (7)); Morgan-Mercer-Flodin curve (Eq. (8)); Weibull curve (Eq. (9)); Brody curve (Eq. (10)); exponential model (Eq. (11)); potential model (Eq. (12)).

$$S_w = 1.567 + 0.002A^2 - 0.166O^2 - 0.022C^2 - 0.177S^2 - 0.959TF^2 - 0.248WR^2 \tag{4}$$

$$S_w = 1.598e^{-0.151e^{-0.108A + 1.156O + 0.077C + 0.669S + 1.788WR}} \tag{5}$$

$$S_w = 5.302(1 - 0.275e^{-0.036A + 0.379O + 0.03C + 0.23S + 0.597WR})^3 \tag{6}$$

$$S_w = (1 + 0.007e^{-0.201A + 2.201O + 0.11C + 1.201S + 3.399WR})^{-2.343} \tag{7}$$

$$S_w = \frac{-361.049 + 26.825(A^{1.927} + O^{-33.364} + C^{-3.186} + S^{-68.031} + WR^{-75.914})}{10029.150 + A^{1.927} + O^{-33.364} + C^{-3.186} + S^{-68.031} + WR^{-75.914}} \tag{8}$$

$$S_w = 668.745 - 668.781e^{-4.205^{-06}(A^{1.903} + O^{-32.68} + C^{-3.097} + S^{-66.185} + WR^{-74.097})} \tag{9}$$

$$S_w = 1694.514 \left(1 - 0.999e^{-2.081^{-05}A + 2.927^{-04}O + 8.177^{-05}C + 2.88^{-04}S + 4.638^{-05}WR} \right) \tag{10}$$

$$S_w = 13.941e^{0.185A - 1.178O - 0.173C + 0.632S - 5.436WR} \tag{11}$$

$$S_w = 0.002(A^{2.108} + O^{-36.38} + C^{-3.26} + S^{-47.581} + WR^{-67.986}) \tag{12}$$

where S_w is the degradation severity, A the age of painted surfaces, O the façades orientation, C the paint’s colour, S the distance from the sea, TF the type of finishing, and WR the wind-rain action. For the application of the mathematical equation it is necessary to replace the variables by their numerical value, presented in Table 1.

Table 2 presents the statistical indicators used to evaluate the statistical significance of the various nonlinear multiple regression models proposed. The proposed models lead to a coefficient of determination greater than 0.8, revealing a high correlation between the dataset (regarding the degradation of painted surfaces) and the values predicted by the models. The Gompertz, Richards and von Bertalanffy curves, with a R^2 of 0.9, are the models with greater statistical significance. The

Table 2 Statistical indicators of predictive ability of the models proposed applied to painted surfaces

Model	R ²	Average ESL (years)	Standard deviation of ESL (years)
Polynomial model	0.898	9.724	0.502
Gompertz curve	0.900	9.659	0.579
von Bertalanffy curve	0.900	9.620	0.574
Richards curve	0.900	9.712	0.588
Morgan-Mercer-Flodin curve	0.895	9.558	0.399
Weibull curve	0.895	9.553	0.404
Brody's model	0.839	8.454	0.685
Exponential model	0.872	10.236	0.611
Potential model	0.890	9.746	0.237

Brody and exponential models are the models with the lowest explanatory power, despite showing a coefficient of determination higher than 0.8, which indicates models with high explanatory power. The average estimated service life predicted by the models varies between 8.5 and 10 years. These values are consistent with the values in the literature (Keoleian et al. 2001; Fay et al. 2000; Chai et al. 2014a, b) and with the results obtained using the previous models applied in this study.

4 Factorial Models

4.1 Classic Approach

The factor method, initially proposed by the Architectural Institute of Japan (AIJ 1993), allows taking into account all the variables that can influence the service life of the building elements. This method consists of obtaining an estimated service life from a reference service life multiplied by a series of “modifying” factors related to the specific conditions of each case (Lair 2003; Silva et al. 2012), as indicated in Eq. (13). Currently, factorial models are seen as a general framework to the service life prediction of materials and building components, allowing integrating different forms of quantification of the durability factors, ranging from absolute values to statistical distributions. These models combine flexibility and simplicity, becoming one of the main methodologies recommended for service life prediction, established in the international standard for durability (ISO 15686-1: 2000). However, these models present some disadvantages, as pointed by a number of authors (Moser and Edvardsen 2002; Hovde 2005; Emídio et al. 2014): (i) the number of durability factors or their quantification are not specified; (ii) in its simplest form, the method does not take into account the uncertainty associated with the reference service life or the durability factors; (iii) likewise it does not take into account the variability of

the aging process and does not contemplate the degradation condition of the elements under analysis; (iv) the method is highly sensitive, i.e. small variations in the quantification of the durability factors can lead to high variations of the estimated service life values; (v) it does not take into account the hierarchical relevance of the different variables, which may affect the element's service life in different ways.

$$ESL = RSL \cdot A \cdot B \cdot C \cdot D \cdot E \cdot F \cdot G \quad (13)$$

where *ESL* is the estimated service life, *RSL* the reference service life, *A* the factor related to the quality of the materials, *B* the factor related to the design level, *C* the factor related to the execution level, *D* the factor related to the interior environmental conditions, *E* the factor related to the external environmental conditions, *F* the factor related to the in-use conditions, and *G* the factor related to the level of maintenance.

Based on the generic model defined in ISO 15686-1 (2000), it is possible to establish a new model to predict the service life of painted surfaces, taking into account the factors that contribute to their degradation—Eq. (14).

$$ESL = RSL \times A1 \times B1 \times B2 \times B3 \times E1 \times E2 \times E3 \times E4 \times E5 \times F1 \times G1 \quad (14)$$

where *ESL* represents the estimated service life, *RSL* the reference service life, *A1* the type of product, *B1* the colour of the painted surfaces, *B2* the type of finishing, *B3* the building's geometry, *E1* the façades' orientation, *E2* exposure to wind driven rain, *E3* the distance from the sea, *E4* exposure to damp, *E5* the distance from pollution sources, *F1* the type of use, and *G1* the ease of inspection of the façade.

To apply this model, it is necessary to estimate the service life of each case study. For this purpose, an individual degradation path (similar to the average degradation curve, presented in Fig. 1) is defined, determining the age (*x*), which represents the estimated service life for each case study, at which the maximum degradation level (*y* = 20 %) is reached.

Based on the literature, it is assumed that the minimum estimated service life for a painted surface is 3 years (in aggressive environments) (BS 7543: 1992) and at most may have an estimated service life of 25 years (when subjected to a set of favourable conditions) (ISO 15686: 2000). It is assumed that the case studies with an expected service life with values outside this range are outliers, usually corresponding to situations of recent buildings (with less than 5 years) in which the degradation state in inspection time is inferior to 0.5 %. These case studies are removed from the initial sample to apply this model. The final sample comprises 177 case studies, with a maximum estimated service life of 25 years and with a minimum estimated service life of 4 years, and an average *ESL* of 10.4 years.

In this study, to obtain the reference service life for painted surfaces three methods are applied (Galbusera et al. 2015): (i) in the first one, the reference service life is obtained by the intersection of the average degradation curve and the maximum acceptable level of degradation; (ii) in the second one, the method of the average exposure conditions for each single case, it is assumed that the sub-factors

of the factor method assume the values 0.8 (very aggressive level), 0.9 (aggressive), 0.95 (averagely aggressive), 1.0 (slightly aggressive), 1.1 (slightly favourable) and 1.2 (clearly favourable), adapted from the work of Mc Duling (2006), and the factor method was inversely applied to each case study to evaluate the reference service life (RSL), as indicated in Eq. (15); (iii) the third method is the one of the average conditions for the whole sample, and it evaluates the ratio between the predicted service life (by the graphical method) and the service life according to the factor method, using as reference service life the average of the case studies with deviations lower than 2 % in this ratio.

$$\begin{aligned} \text{ESL} = \text{RSL} \cdot A \cdot B \cdot C \cdot D \cdot E \cdot F \cdot G &\Leftrightarrow \text{RSL} = \frac{\text{ESL}}{A \cdot B \cdot C \cdot D \cdot E \cdot F \cdot G} \Leftrightarrow \text{RSL} \\ &= \frac{\text{ESL}}{(0.8^v \cdot 0.9^w \cdot 0.95^x \cdot 1.1^y \cdot 1.2^z)} \end{aligned} \quad (15)$$

These three models lead to a reference service life of 9.7, 9.6 and 9.8 years, respectively. Therefore, the value adopted corresponds to an average of these three values—9.7 years. This value is consistent with the literature (Adalberth 1997; Hed 1999), which suggests 10 years as average service life of painted surfaces.

The last step in the application of the factor method is the determination of the durability factors. These factors are obtained through an iterative process in order to minimize the deviations between the ESL values obtained by factorial method and the values obtained by the graphical method (which represents the real degradation condition of the painted surfaces analysed during fieldwork). Table 3 presents the results of the quantification of the durability factors.

Figure 3 shows the histogram of the estimated service life for the painted surfaces determined using the factor model. An average estimated service life of 10.4 years is obtained, with a standard deviation of 3.3 years. Using the factor method an average ESL of 10.4 years is obtained, a result consistent with the literature and with the values obtained through the application of other service life prediction models.

4.2 Stochastic Approach

To overcome some of the limitations of the factor method, in this study the application of a stochastic approach of the factor method is proposed, in which the durability factors are translated into probability distributions. Using this approach, the estimated service life of every painted surface analysed is also represented by a probability distribution. In order to associate to each durability factor a probability distribution, the following procedure is applied:

Table 3 Quantification of the durability factors

Characteristics			% of case studies (number of case studies)	Durability factors value
A1	Type of product	Plain paint	34 % (61)	1.025
		Textured paint	25 % (44)	1.025
		Silicates and silicones	5 % (9)	1.0
		Elastic membranes	36 % (63)	1.015
B1	Paint colour	White	32 % (57)	1.075
		Light colours	63 % (112)	1.0
		Dark colours	5 % (8)	0.975
B2	Type of finishing	Smooth	56 % (100)	1.0
		Rough	44 % (77)	1.15
B3	Building geometry	Compact	86 % (152)	1.0
		Irregular	14 % (25)	0.975
E1	Façade orientation	East	32 % (57)	1.0
		North	18 % (32)	1.05
		West	29 % (51)	0.95
		South	21 % (37)	0.925
E2	Wind-rain action	Severe	33 % (58)	0.95
		Moderate	40 % (70)	0.975
		Mild	28 % (49)	1.0
E3	Distance from the sea	Less than 5 km	45 % (80)	0.925
		More than 5 km	55 % (97)	1.0
E4	Exposure to damp	Unfavourable	45 % (80)	1.0
		Current	55 % (97)	1.05
E5	Distance from pollution sources	Unfavourable	23 % (41)	0.95
		Current	77 % (136)	1.0
F1	Type of use	Commerce and services	66 % (116)	1.0
		Housing	34 % (61)	1.0
G1	Ease of inspection	Unfavourable	27 % (48)	0.985
		Current	73 % (129)	1.0

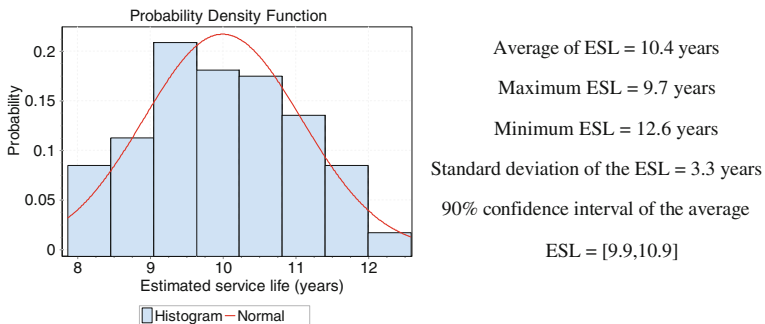


Fig. 3 Histogram of estimated service life obtained by the factor method

- First it is necessary to determine the first durability factor (factor A), through Eq. (16):

$$A = \frac{ESL}{RSL \times A1 \times B1 \times B2 \times B3 \times E1 \times E2 \times E3 \times E4 \times E5 \times F1 \times G1} \quad (16)$$

where *ESL* represents the estimated service life obtained by the graphical method; the values of the product of all other sub factors in the denominator correspond to those presented in Eq. (14), from the application of the factor method, replacing the durability factors by the values presented in Table 3 (depending on the specific conditions of each case study).

- After determining factor A, the values obtained are normalized to ensure that the average value of the probability distribution for each category is equal to the value in Table 3; the values in Table 3 minimize the errors between the values obtained by the factor method and the values obtained by the graphical method (that supposedly portray reality);
- Using the same procedure used to calculate the sub-factor A, the remaining durability factors are sequentially determined.

In this study, six continuous distributions are analysed: (i) Normal; (ii) Lognormal; (iii) Gamma; (iv) Weibull; (v) Gumbel; (vi) Logistic. To determine a ranking of the fit of the data to each distribution three statistical tests are applied (van Nunen 2010): (i) the Anderson-Darling test (A-D test); (ii) the Kolmogorov-Smirnov test (KS test); (iii) the Chi-square test. The probability distributions associated to the durability factors along with some statistical indicators are presented in Table 4.

5 Stochastic Models

Because of the substantial dependence of time and uncertainty associated with the buildings performance, it is often necessary to use probabilistic models to predict the service life of the construction elements (Ross 1996). These models allow assessing and predicting the performance and the failure probability of the elements under analysis (Lounis et al. 1998). In this study, two stochastic models are applied to the service life prediction of painted surfaces: (i) logistic regression; and (ii) Markov chain models.

5.1 Logistic Regression

Logistic multiple regression, as multiple linear regression, is used to describe the relationship between the dependent variable and one or more explanatory variables.

Table 4 Quantification of the durability factors

Characteristics			Distribution	Average	Standard deviation	Value of the factor with a probability higher than 95 % to be exceeded
A1	Type of product	Plain paint	Lognormal	1.025	0.322	0.635
		Textured paint	Lognormal	1.025	0.200	0.780
		Silicates and silicones	Gumbel	1.0	0.258	0.519
		Elastic membranes	Lognormal	1.015	0.297	0.654
B1	Paint colour	White	Lognormal	1.075	0.324	0.684
		Light colours	Lognormal	1.0	0.275	0.639
		Dark colours	Normal	0.975	0.281	0.607
B2	Type of finishing	Smooth	Lognormal	1.0	0.330	0.580
		Rough	Lognormal	1.15	0.238	0.826
B3	Building geometry	Compact	Lognormal	1.0	0.300	0.618
		Irregular	Gumbel	0.975	0.216	0.693
E1	Façade orientation	East	Gumbel	1.0	0.207	0.730
		North	Gama	1.05	0.278	0.638
		West	Lognormal	0.95	0.369	0.590
		South	Lognormal	0.925	0.233	0.585
E2	Wind-rain action	Severe	Lognormal	0.95	0.284	0.596
		Moderate	Lognormal	0.975	0.328	0.560
		Mild	Lognormal	1.0	0.188	0.754
E3	Distance from the sea	Less than 5 km	Lognormal	0.925	0.275	0.557
		More than 5 km	Lognormal	1.0	0.278	0.657
E4	Exposure to damp	Unfavourable	Lognormal	1.0	0.295	0.605
		Current	Lognormal	1.05	0.295	0.687
E5	Distance from pollution sources	Unfavourable	Lognormal	0.95	0.253	0.632
		Current	Lognormal	1.0	0.294	0.620
F1	Type of use	Commerce and services	Lognormal	1.0	0.283	0.584
		Housing	Lognormal	1.0	0.280	0.660
G1	Ease of inspection	Unfavourable	Lognormal	0.985	0.259	0.632
		Current	Lognormal	1.0	0.297	0.623

In logistic regression, the outcome variable is binary or dichotomous (with only two mutually exclusive events, usually characterized by the presence or absence of a given characteristic) (Hosmer and Lemeshow 2000). Logistic regression can be expanded to multinomial logistic regression in which the dependent variable has

more than two mutually exclusive features (Wang 2005). In this study, a logistic regression is used to evaluate the probability of a painted surface reaching the end of its service life. In this analysis, the dependent variable is represented by the question “Has the cladding reached the end of its service life?”, with two mutually exclusive classes: “yes” and “no”. Once more, it is assumed that the end of the service life occurs when a façade meets or exceeds a degradation severity of 20 %. In the sample analysed, 24.1 % of the case studies had already reached the end of their service life. For further explanations, Silva et al. (2014) clarify all the assumptions concerning the application of this methodology to the service life prediction of rendered façades. This model reveals a satisfactory adjustment between the model and the sample and correctly classifies 91.4 % of the case studies. Equation (17) presents the probability of a painted surface reaching the end of its service life based on their age.

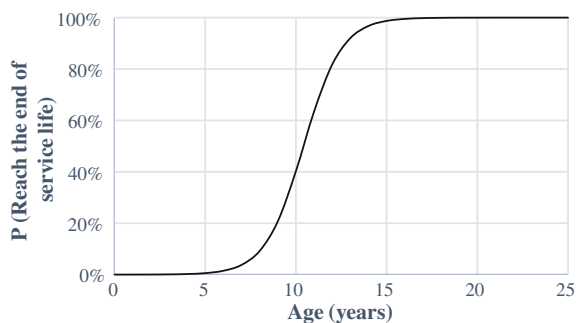
$$P(Y = \text{“End of service life”}) = 1 - \frac{1}{1 + e^{-9.865 + 0.947Age}} \quad (17)$$

Figure 4 presents the probabilistic distribution of painted surfaces reaching the end of their service life according to their age. The results reveal that after 10 years the probability of a painted surface reaching the end of its service life is higher than 50 % and, after 12 years, this probability is greater than 90 %.

5.2 Markov Chains Models

Markov chains are one of the probabilistic methods most widely used in the study of the deterioration of buildings. Markov chains are based on a set of discrete states which characterize the buildings performance. These models can be used to emulate the evolution of the degradation state of constructions, defining the probability of a future state based only on the present condition, independently of previous deterioration history (Neves et al. 2006; Silva et al. 2015). According to Garavaglia et al. (2004), the degradation phenomena can be defined as a transition process

Fig. 4 Probabilistic distribution of painted surfaces reaching the end of their service life according to their age



through different condition states. Table 5 reveals the qualitative and quantitative deterioration conditions associated to painted surfaces, ranging from the best possible condition (Condition A—no visible degradation) to the highest degradation level (Condition E—loss of functionality).

The intensity matrix Q obtained for the Markov chain model applied to painted surfaces is presented in Eq. (18) and the probabilistic distribution of the degradation condition of painted surfaces over time, based on the Markov chain model proposed, is presented in Fig. 5. The probability of belonging to condition A decreases from the outset and is lower than 5 % after 7 years. The maximum probability of

Table 5 Classification of degradation condition of painted surfaces






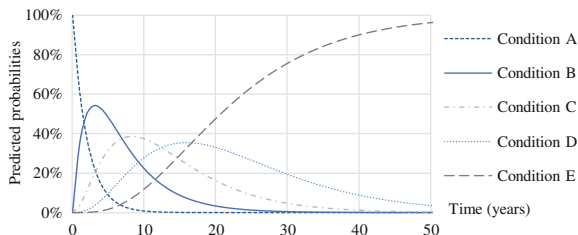
Condition level	Example	Physical and visual assessment	Severity of degradation (%)
Level A		Complete painted surface with no deterioration. No perceptible changes. No visible cracks	<1
Level B		Slight or little perceptible changes. Uniform surface dirt. Change in colour or brightness. Small number of cracks	1–10
Level C		Moderate or quite perceptible changes. Quite perceptible changes in colour or brightness. Localized surface dirt, humidity stains, efflorescence. Moderate width or number of cracks. Small amount of blistering and size up to 3 cm	10–20
Level D		Moderate to high perceptible changes. Humidity stains, efflorescence, biological growth. Localized surface dirt. Very perceptible change in colour (discolouration). Considerable number of cracks. Small amount of blistering with size between 3 and 5 cm or moderate of blistering amount and smaller than 3 cm. Small amount of peeling (area affected up to 1 %) e size up to 3 cm	20–40
Level E		High or very perceptible changes. Biological growth. High number or density of cracks. Blistering larger than 5 cm, regardless of the amount; or dense pattern of blistering regardless of the size; or moderate amount of blistering with dimension between 3 and 5 cm. Dense and moderate pattern of peeling (affected area more than 1 %) regardless of the size or small amount, but larger than 5 cm	>40

Fig. 5 Probabilistic distribution of the degradation condition of painted surfaces according to the age of the case studies



belonging to condition B is reached at 3 years ($P = 54.1\%$). The probability of belonging to conditions C and D reaches a peak after 8 years ($P = 38.5\%$) and 16 years ($P = 35.4\%$) respectively. The probability of belonging to condition E is practically residual (less than 5%) until year 7, but exceeds 90% after year 41. The transition between conditions C and D establishes the instant of the maximum probability of the façades reaching the end of their service life. For painted surfaces, this threshold occurs between year 12 and 13.

$$Q = \begin{bmatrix} q_{A,B} \\ q_{B,C} \\ q_{C,D} \\ q_{D,E} \end{bmatrix} = \begin{bmatrix} 0.4868 \\ 0.1962 \\ 0.1524 \\ 0.1062 \end{bmatrix}. \quad (18)$$

6 Computational Models

6.1 Artificial Neural Networks

Artificial neural networks (ANNs) are emulations of biological neural systems. In these models, empirical knowledge can be acquired from a learning data set relative to a given problem (Silva et al. 2012; Chai et al. 2014c). These methods are thus capable of learning and generalizing based on experience and examples, adapting to new situations. This adaptive capability is extremely important since it means that complex problems can be solved, even though they are difficult to solve either analytically or numerically (Rafiq et al. 2001). The most common type of ANN is the multilayer perceptron (MLP). An MLP is a network with three or more neuron layers consisting of: an input layer, one or more hidden layers and an output layer. MLPs are fully connected “feed-forward” networks.

In this study, MLPs were used to develop a model to estimate the degradation severity of painted surfaces, using 220 case studies analysed during the field work. A NeuroSolutions software was used for this purpose. In the model proposed the activation functions were the hyperbolic tangent for the intermediate layer neurons,

and the linear function for the output layer neurons. All channels (the inputs and the output) were normalised so that all corresponding values would be within the range $[-0.9, 0.9]$. Various architectures were tested for the networks and three runs were performed per architecture. In all runs the global set of patterns was divided into two groups: training (85 %) and cross-validation (15 %). The samples used in cross-validation were also used to test the networks. In each run, the cross-validation error was evaluated after each 50 epochs and training was concluded as soon as this error ceased to decrease or when a maximum of 65,000 epochs was reached. A sensitivity analysis was performed to determine the variables (degradation factors) that best describe the degradation severity of painted surfaces.

The network with the best results includes three variables (the same as in the multiple linear regression): (i) age of the painted surfaces; (ii) distance from the sea; and (iii) buildings' orientation. After the conclusion of the procedures described above, the explicit formulation of the degradation severity was obtained directly from the selected MLP, using its activation functions, parameters (weights and biases) and normalisation factors. The formula is simply a closed-form expression of the MLP. The degradation severity (S_w) is a function of the three variables included in the model, as seen in Eqs. (19) and (20). The coefficients h_0 to h_4 and c_{0i} a c_{8i} are presented in Table 6.

$$S_w = h_0 + \sum_{i=1}^4 h_i H_i \tag{19}$$

$$H_i = \tanh \left(c_{0i} + \sum_{n=1}^8 c_{ni} V_n \right) \tag{20}$$

Where the pattern $V_1 = 1, V_2 = 0, V_3 = 0, V_4 = 0$ represents a facade facing North, the pattern $V_1 = 0, V_2 = 1, V_3 = 0, V_4 = 0$ a facade facing East, the pattern $V_1 = 0, V_2 = 0, V_3 = 1, V_4 = 0$ a facade facing South, the pattern $V_1 = 0, V_2 = 0, V_3 = 0, V_4 = 1$ a facade facing West, the pattern $V_5 = 1, V_6 = 0, V_7 = 0$ a building located less than 1 km from the sea, the pattern $V_5 = 0, V_6 = 1, V_7 = 0$ a building located more than 1 km and less than 5 km from the sea, the pattern $V_5 = 0, V_6 = 0, V_7 = 1$ a building located more than 5 km from the sea, and V_8 the age of the painted surfaces (the age of the painted façades ranges between 0 and 18 years).

The errors obtained are relatively small (the mean percentage error normalised with respect to the maximum ($\bar{\epsilon}$) is 5.3 % and the maximum normalised percentage error (ϵ_{\max}) is 15.8 %) and the Pearson correlation coefficient (r) for the 35 case tests is 0.979, showing a strong correlation between predicted and actual values.

The formulae proposed are valid only for values of the independent variables within the limits of the input variables of the patterns used to train the MLP.

Figure 6 shows the histogram of the estimated service life for the painted surfaces determined using the ANNs model. The average estimated service life was

Table 6 Coefficients for the ANIN model

i	h_i (-)	c_{0i} (-)	c_{1i} (-)	c_{2i} (-)	c_{3i} (-)	c_{4i} (-)	c_{5i} (-)	c_{6i} (-)	c_{7i} (-)	c_{8i} (year ⁻¹)
0	3.87E-01									
1	-3.84E-02	4.29E-01	7.64E-02	7.48E-01	-6.74E-01	5.90E-01	-1.01E-01	-1.33E-01	-4.63E-01	-5.09E-02
2	1.58E-01	-1.59E+00	-5.08E-01	4.30E-01	-1.72E-01	9.88E-02	-1.07E-01	2.21E-01	-4.60E-01	1.47E-01
3	9.31E-02	-2.39E+00	1.06E+00	-4.67E-01	3.69E-01	8.44E-01	5.63E-01	3.73E-01	4.37E-01	9.34E-02
4	1.67E-01	-3.08E+00	6.35E-01	7.34E-01	1.12E+00	7.14E-01	2.19E-01	-6.87E-01	8.87E-02	1.73E-01

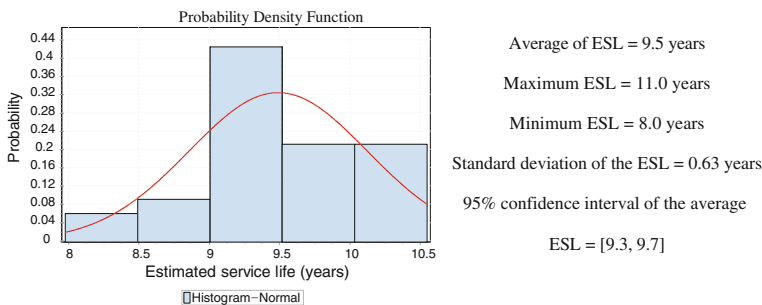


Fig. 6 Histogram of estimated service life obtained by the ANNs model

9.49 years, with a standard deviation of 0.63 years. These values are coherent with the results obtained by the previous methods.

6.2 Fuzzy Systems

Fuzzy logic models, like neural networks, are known to be able to function as universal approximators (Kosko 1994) even when there is no prior knowledge about the phenomenon under analysis. These models have been successfully applied in the construction area, especially when the problem modelled is subject to uncertainties. Fuzzy models describe the relationship between the output variable and the predictors by means of if-then rules. In computational terms, fuzzy models are flexible mathematical structures, being a combination of a linguistic modelling and mathematical regression analysis, with a better performance and accuracy than classical linear models (Vieira et al. 2015). In this study, a Takagi-Sugeno (TS) fuzzy model (Takagi and Sugeno 1985) is used to predict the service life of painted surfaces. The output of the model (S_w) (the degradation severity of painted surfaces) is obtained by adding the individual contribution of rules, represented by the Eq. (21).

$$S_w = \frac{\sum_{i=1}^C \beta_i f_i(x)}{\sum_{i=1}^C \beta_i} \tag{21}$$

where β_i is the degree of activation of the i th rule, obtained as a function of the degree of membership of each fuzzy set associated with each of the variables included in the model, and $f_i(x)$ is the discriminant function given by Eq. (22).

$$f_i(x) = a_i x + b_i, \quad i = 1, 2, \dots, C \tag{22}$$

Given N available input–output data pairs (x_k, y_k) , the n -dimensional pattern matrix $X = [x_1, \dots, x_n]^T$, and the corresponding output vector $y = [y_1, \dots, y_N]^T$ are constructed. The number of rules C , the antecedent fuzzy sets A_{ij} , and the consequent parameters a_i and b_i are determined in this step, by means of fuzzy clustering in the product space of the input and output variables (Sousa and Kaymak 2002).

In this model the whole sample is used, 220 cases of study, where 85 % of the sample (187 studies) are used as a training sample and 15 % as test sample. This test sample is the same sample used as test sample in the ANNs model.

After a sensitivity analysis, age, façades' orientation and exposure to wind-rain action are included in the model as explanatory variables. The fuzzy rules describing the local input-output relation are presented in Eqs. (23) and (24).

Rule 1: If u_1 is A_{11} and u_2 is A_{12} and u_3 is A_{13} and u_4 is A_{14} then:

$$y_1(k) = -1.43 \times 10^{-2}u_1 - 2.63 \times 10^{-2}u_2 + 4.25 \times 10^{-2}u_3 - 8.54 \times 10^{-2} \quad (23)$$

Rule 2: If u_1 is A_{21} and u_2 is A_{22} and u_3 is A_{23} and u_4 is A_{24} then:

$$y_2(k) = -4.31 \times 10^{-3}u_1 - 3.15 \times 10^{-3}u_2 + 2.30 \times 10^{-2}u_3 - 2.35 \times 10^{-2} \quad (24)$$

where u_1 represents façades' orientation, u_2 distance from the sea, and u_3 age of the buildings.

Figure 7 shows the membership functions for each of the four input variables included in fuzzy model applied to painted surfaces. The continuous lines (green) represent the membership functions obtained from cluster 1, and the dashed lines (blue) represent the membership functions obtained from cluster 2.

The analysis of the membership functions reveals that the sample is clearly divided into two clusters for the variable age. In the remaining variables, distance

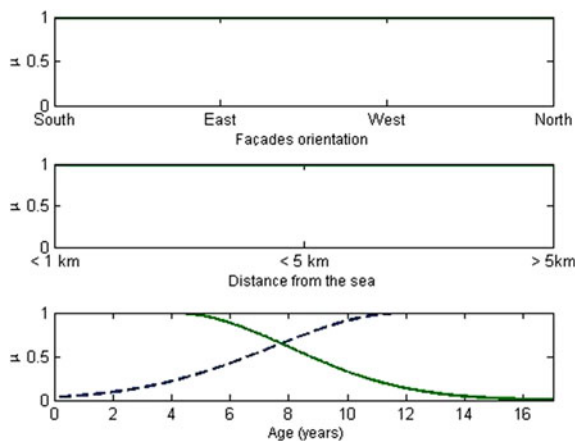


Fig. 7 Membership functions for the fuzzy model proposed

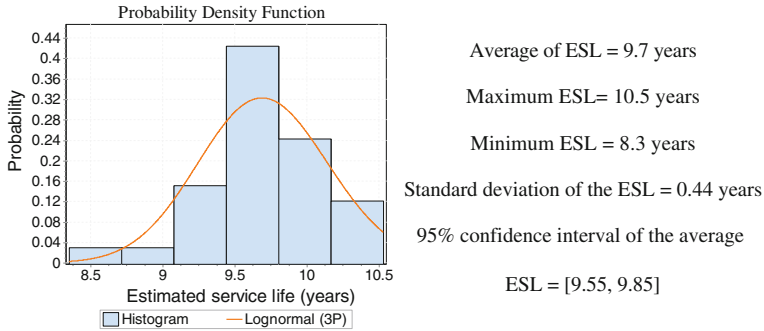


Fig. 8 Histogram of estimated service life obtained by the fuzzy model

from the sea and façades’ orientation, all the categories give the same contribution to the output of the rules number one and two.

This model leads to relatively small errors, with a mean absolute percentage error equal to 5.1 % and a maximum absolute percentage error equal to 22.1 %. Also, this model presents a Pearson correlation coefficient (r) of 0.98, revealing a very strong correlation between values predicted by the model and the observed values.

Figure 8 presents the histogram of the estimated service life for first order Takagi-Sugeno model applied to painted surfaces. This model allows obtaining an average estimated service life of 9.7 years with a standard deviation of 0.4 years.

7 Comparative Analyses

This chapter compares the different approaches to the service life prediction of painted surfaces. The proposed methods were grouped into methodological families, concerning the assumptions adopted in model’s definition. Table 7 presents the estimated service life (ESL) obtained using the various models proposed.

The results reveal that all the models are able to estimate with accuracy the service life of painted surfaces, translating with accuracy the loss of performance of this type of coating over time. The models proposed present a coefficient of determination higher than 0.8, revealing a high correlation between the observed values and the values predicted by the models. The multiple nonlinear regression models lead to better results when compared to single or multiple linear regression models; all the multiple nonlinear regression models proposed for painted surfaces have a high predictive ability with values of the coefficient of determination higher than 0.9. In the majority of the models, the values predicted are greater than the observed values (i.e. the degradation severity estimated by the models is higher than the values observed during field work), thus revealing that the models obtained for painted surfaces are conservative. Computational models lead to better results than

Table 7 Estimated service life according to the different models analysed

Model	R ²	Average ESL (years)	Maximum ESL (years)	Minimum ESL (years)	Standard deviation (years)	Value of the ESL with a probability higher than 95 % to be exceeded*	Value of the ESL with a probability higher than 5 % to be exceeded*
Simple nonlinear regression	0.874	9.664	–	–	–	–	–
Multiple linear regression	0.833	8.487	9.389	6.009	0.701	7.334	9.640
Multiple nonlinear regression—polynomial	0.889	9.724	10.772	8.596	0.502	8.899	10.549
Gompertz curve	0.875	9.659	10.697	8.481	0.579	8.707	10.611
Von Bertalanffy curve	0.890	9.620	10.655	8.403	0.574	8.676	10.565
Richards curve	0.891	9.712	10.761	8.589	0.588	8.746	10.679
Morgan-Mercer-Flodin curve	0.885	9.558	10.131	8.564	0.399	8.903	10.214
Weibull curve	0.885	9.553	10.136	8.551	0.404	8.889	10.218
Brody curve	0.833	8.454	9.381	5.999	0.685	7.328	9.582
Multiple nonlinear regression— exponential	0.867	10.236	11.417	8.765	0.611	9.232	11.241
Multiple nonlinear regression—potential	0.881	9.746	10.032	8.993	0.237	9.357	10.136
Artificial neural networks	0.959	9.491	10.548	7.977	0.623	8.451	10.533
Fuzzy systems model	0.953	9.698	10.528	8.349	0.445	8.956	10.442
Factor method	–	9.998	12.583	7.869	1.083	8.220	11.781
Graphical method	–	10.389	25.395	3.936	3.250	5.045	15.735

the other methods, with an increase on their statistically significant of 10 %, with lower deviations. The various models lead to an average estimated service life ranging between 8.5 and 10.4 years. Concerning the stochastic models, the following results are obtained: (i) in the logistic regression model, after 10 years the probability of a painted surface reaching the end of its service life is higher than 50 % and at age 12 this probability is higher than 90 %; (ii) in the Markov chain model, the transition between conditions C and D (corresponding to the end of service life of painted surfaces) reaches its peak between year 12 and 13. These results are coherent with the empirical perception concerning the durability of painted coatings and with the literature about this topic.

To perform a comparative analysis of the different service life prediction methods, it is necessary to take into account different criteria. In this study, six criteria were considered: (i) ease of learning, which evaluates the time required to acquire the theoretical knowledge necessary to implement the model; (ii) time required to create the model; (iii) software required; (iv) number and subjectivity of the variables included in the model; (v) interpretability and utility of the information produced by the model; (vi) accuracy of the model, which includes the prediction errors and deviations between predicted and observed values. Based on this analysis, it is possible to draw the following conclusions: (i) computational methods are the most complex of all the proposed methods; in particular fuzzy systems are extremely complex models, with a time-consuming learning process, and whose theoretical assumptions are intricate; stochastic models are also difficult to learn and apply, requiring specific software; deterministic models are very simple models, with an increasing level of complexity from simple regression analysis to multiple nonlinear regression models (whose model's definition is more complex and time consuming); (ii) the factor method (deterministic), simple regression, multiple linear and nonlinear regression models are those whose mathematical expressions are simpler; Markov chains and the factorial method (with a stochastic approach) provide information in the form of a probability distribution, the post-treatment of the results is more complex, but the information produced is more relevant, providing data concerning the risks associated with the degradation process, i.e. the user knows the probability of coating failure as a function of its age and characteristics; computational models are those whose interpretation is more complex; fuzzy systems lead to complex equations, which requires the use of a Matlab toolbox or graphical reading of the membership functions of the model to obtain the degree of activation necessary to apply the fuzzy rules. The application of these service life prediction models to painted surfaces reveals that the fuzzy logic model is the one with worse overall performance, as a function of criteria analysed (since it is a very complex model, with a higher cost, requiring specific software to be implemented). On the other hand, simple nonlinear regression model is the model with the best overall performance (i.e. with the largest area occupied in the diagram), followed by the logistic regression model (which allies a relative simplicity with a higher richness regarding the results produced) and the multiple linear regression.

8 Service Life Prediction Methods Applied to a Case Study

It seems now relevant to demonstrate the application of the models proposed to a case study, helping researchers unfamiliar with these models to understand the application of these methodologies to a specific case study. Figure 9 shows the description of the case study analysed. Since the acceptable performance threshold of this case study has been largely surpassed ($S_w = 57.3\%$), the methods are applied to calculate the age of the sample when the end of service life has been reached.

The application of simple regression analysis is not possible for a single case study. However, as described before, it is possible to apply the graphical method, which is similar to a simple regression analysis and involves adjusting a simple regression line—similar to the curve adapted to the scatter of points of the sample—to each case study within the sample. Using the graphical method, the estimated service life of the case study is 10.5 years.

Equation (25) illustrates the determination of the estimated service life using the multiple linear regression model. Table 8 presents the estimated service life obtained for the multiple nonlinear regression models produced (described in Eqs. (4) to (12), in which is necessary to estimate the age in which the painted surfaces reached a degradation severity (S_w) of 20 %).

$$ESL = \frac{(0.20 - 0.4734 + 0.2818 \times 1.01 + 0.3175 \times 1.02)}{0.0353} \approx 9.5 \text{ years} \quad (25)$$

Replacing the values of the sub-factors in Eq. (14), it is possible to obtain the estimated service life for the case study analysed through the application of the classical factor method, as presented in Eq. (26).

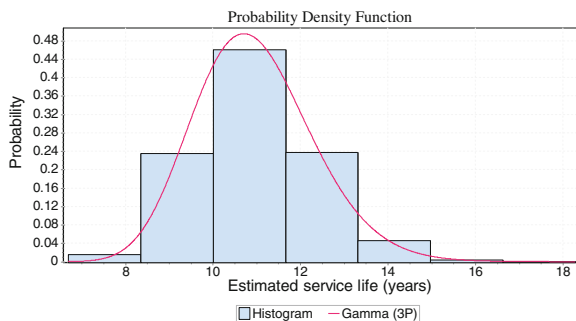
Fig. 9 Description of the case study analysed



Table 8 Estimated service life of the case study using the multiple nonlinear regression models

Model	Polynomial model	Gompertz curve	von Bertalanffy curve	Richards curve	MMF curve	Weibull curve	Brody's model	Exponential model	Potential model
ESL (years)	10.8	10.7	10.7	10.8	10.1	10.1	9.4	11.3	10.0

Fig. 10 Probability distribution of the estimated service life of the case study analysed



$$ESL = 9.7 \times 1.025 \times 1.0 \times 1.15 \times 1.0 \times 1.0 \times 1.0 \times 1.0 \times 1.05 \times 0.95 \times 1.0 \times 1.0 = 11.4 \text{ years} \quad (26)$$

Applying the stochastic approach to the factor method, the estimated service life of this case study is given by a probability distribution, as shown is Fig. 10. This method leads to an average estimated service life of 11 years, with a standard deviation of 1.4 years. The probability distribution with better adjustment is the Gamma distribution (with three parameters). The analysis of the probability distribution associated with the estimated service life of this case study reveals that an average service life of 8.8 years has a probability higher than 95 % of being exceeded; on the other hand, the case study analysed has a probability lower than 5 % of having a service life higher than 13.3 years.

The application of the artificial neural networks model is demonstrated in Eqs. (27)–(31). Due to the complexity of the equation, to obtain the estimated service life it is necessary to use a calculation sheet, using an iterative process to find the age in which the degradation severity of the case study analysed reached 20 % (defined as the maximum acceptable degradation level). Using this model, service life of 10.2 years is obtained for the case study analysed.

$$H_1 = \tanh(0.429 + 0.748 \cdot 1 - 0.463 \cdot 1 - 0.051 \cdot 10.2) \approx 0.191 \quad (27)$$

$$H_2 = \tanh(-1.588 + 0.429 \cdot 1 - 0.495 \cdot 1 - 0.147 \cdot 10.2) \approx -0.117 \quad (28)$$

$$H_3 = \tanh(-2.393 - 0.467 \cdot 1 + 0.437 \cdot 1 + 0.093 \cdot 10.2) \approx -0.899 \quad (29)$$

$$H_4 = \tanh(-3.084 + 0.734 \cdot 1 + 0.089 \cdot 1 + 0.173 \cdot 10.2) \approx -0.461 \quad (30)$$

$$S_w = 0.387 - 0.038 \cdot 0.191 - 0.117 \cdot 0.158 - 0.093 \cdot 0.899 - 0.167 \cdot 0.461 \approx 0.20 \approx 20\% \quad (31)$$

To apply the fuzzy model it is also necessary to use an iterative process to identify the age in which a degradation index of 20 % was reached. For this model, the estimated service life of the case study under analysis is 9.2 years. The degrees of

activation of the model for the case study are $\beta_1 = 1.0000$; $\beta_2 = 0.0022$, obtained through “Fuzzy Identification Toolbox for Matlab”. Equations (32)–(34) illustrate the application of the fuzzy model to the service life prediction of the case study analysed.

$$y_1(k) = -1.43 \times 10^{-2} \cdot 2 - 2.63 \times 10^{-2} \cdot 3 + 4.25 \times 10^{-2} \cdot 9.2 - 8.54 \times 10^{-2} \approx 0.200 \quad (32)$$

$$y_2(k) = -4.31 \times 10^{-3} \cdot 2 - 3.15 \times 10^{-3} \cdot 3 + 2.30 \times 10^{-2} \cdot 9.2 - 2.35 \times 10^{-2} \approx 0.171 \quad (33)$$

$$S_w = \frac{\sum_{i=1}^C \beta_i f_i(x)}{\sum_{i=1}^C \beta_i} = \frac{1 \times 0.200 + 0.0022 \times 0.171}{1 + 0.0022} = 0.1999 \approx 20\% \quad (34)$$

9 Conclusions

In this study, 220 painted façades are analysed through an extensive field work performed in Lisbon region. As in any other service life prediction method, the models are influenced by data used in the modelling. The sample analysed seeks to represent the population and the models proposed can be adapted to new data.

Four groups of methodologies are proposed for the service life prediction of painted surfaces (the most common type of coatings in Portugal, whose degradation has serious implications on the built environment). The proposed methods have different levels of accuracy and complexity. Simple regression provides the estimated service life of painted surfaces as an average value, not allowing the identification of the degradation factors with more influence on the service life of painted surfaces. This method can be described as too simplistic in the way it deals with complex phenomena such as the degradation of building elements. However, it is a simple method that can be easily applied by any stakeholder in the construction sector. Multiple linear and nonlinear regressions are an extension of simple regression, which allows the identification of the variables with more relevance in the explanation of the degradation phenomena. These models can be more complex and need software and expert knowledge to be implemented. Factorial methods, in a classical approach, are easy to understand and implement, allowing obtaining directly the estimated service life of painted surfaces. The stochastic approach of the factor method is more complex but it yields a richer output, since it presents a considerably better performance in dealing with the uncertainty associated to the degradation of painted surfaces. Computational methods are the most complex and time-consuming approaches as well as the more precise and accurate, but they can

be unintelligible to users not familiar with this technique. All methods are based on the statistical treatment of the façades analysed.

All the methods proposed can be used in building stock's management, maintenance, market and insurance policies. Maintenance has significant economic repercussions on the life cycle of constructions and their elements and tools as those proposed in this study are increasingly relevant in the definition of maintenance strategies, reducing the high costs associated with unnecessary or emergency interventions on the building stock.

Acknowledgments The authors gratefully acknowledge the support of the ICIST Research Institute, IST, Technical University of Lisbon and the FCT (Foundation for Science and Technology).

References

- Adalberth K (1997) Energy use during the life cycle of buildings: a method. *Build Environ* 32 (4):317–320
- AII (1993) The English edition of the principal guide for service life planning of buildings. Tokyo: Architectural Institute of Japan
- BSI 7543 (1992) Guide to durability of buildings and building elements, products and components. BS 7543. United Kingdom: British Standards Institution, London
- Chai C, de Brito J, Gaspar PL, Silva A (2014a) Service life prediction of external wall paintings: economic analysis of alternative maintenance strategies. *J Constr Eng Manag* 140(3):04013057
- Chai C, de Brito J, Gaspar PL, Silva A (2014b) Statistical modeling of service life prediction of painted surfaces. *Int J Strategic Property Manag* (accepted for publication)
- Chai C, de Brito J, Gaspar PL, Silva A (2014c) Neural networks applied to service life prediction of exterior painted surfaces. *Build Res Inf* 42(3):371–380
- Emídio F, de Brito J, Gaspar PL, Silva A (2014) Application of the factor method to the estimation of the service life of natural stone cladding. *Constr Build Mater* 66:484–493
- Fay R, Treloar G, Iyer-Raniga U (2000) Life-cycle energy analysis of buildings: a case study. *Build Res Inf* 28(1):31–41
- Flourentzou F, Brandt E, Wetzel C (1999) MEDIC—A method for predicting residual service life and refurbishment investment budgets. In: 8th international conference on the durability of building materials and components (DBMC), Ottawa, Canada, pp 1280–1288
- Galbusera MM, de Brito J, Silva A (2015) Application of the factor method to the prediction of the service life of ceramic external wall claddings. *J Build Perform Constr Facilities* 29 (3):04014086
- Garavaglia E, Gianni A, Molina C (2004) Reliability of porous materials: two stochastic approaches. *J Mater Civ Eng* 16(5):419–426
- Garrett JH (1994) Where and why artificial neural networks are applicable in civil engineering. *J Comput Civ Eng* [special issue] 8(2):129–130
- Gaspar PL, de Brito J (2008) Quantifying environment effects on cement-rendered facades: a comparison between different degradation indicators. *Build Environ* 43(11):1818–1828
- Gaspar P (2009) Service life of constructions. Development of a methodology to estimate the durability of construction elements, Application to renders in current buildings (in Portuguese), PhD Thesis in Engineering Sciences at Instituto Superior Técnico, Lisbon, Portugal
- Hed G (1999) Service life planning of building components. In: 8th international conference on durability of building materials and components, Vancouver, Canada, pp 1543–1551
- Hosmer DW, Lemeshow S (2000) Applied logistic regression, 2nd edn. Wiley, New York, USA

- Hovde PJ (2005) The factor method—A simple tool to service life estimation. In: 10th DBMC international conference on durability of building materials and components, Lyon, France, pp 522–529
- ISO 15686-1 (2000) Building and constructed assets: service life planning—Part 1: General principles. International Standard Organization 2000, Geneva
- Keoleian GA, Blanchard S, Reppe P (2001) Life-cycle energy, costs, and strategies for improving a single-family house. *J Ind Ecol* 4(2):135–156
- Kosko B (1994) Fuzzy systems as universal approximators. *IEEE Trans Comput* 43 (11):1329–1333
- Lair J (2003) Failure modes and effect analysis and service life prediction. Intermediary report (D4- C2-ji-01 Draft 2), IEA Task 27 (Project C2: Failure Mode Analysis), CSTB, France, pp 166–212
- Lanzinha J, Freitas V, Gomes J (2006) Exploring a performance-based diagnosis method to back housing buildings rehabilitation (in Portuguese). In: PATORREB 2006—2nd meeting on pathology and rehabilitation of buildings, FEUP, Porto, Portugal, pp 589–596
- Lounis Z, Vanier DJ, Lacasse MA (1998) A discrete stochastic model for performance prediction of roofing systems. In: CIB World Building Congress on Sustainable Construction, Sweden, pp 315–324
- Mata J (2011) Interpretation of concrete dam behaviour with artificial neural network and multiple linear regression models. *Eng Struct* 33:903–910
- Mc Duling JJ (2006) Towards the development of transition probability matrices in the Markovian model for the predicted service life of buildings, PhD Thesis in Civil Engineering, Faculty of Engineering, Built Environment and Information Technology, University of Pretoria, Pretoria
- Montgomery DC, Peck EA, Vining GC (2012) Introduction to linear regression analyses, 5th edn. Wiley, New Jersey, USA
- Moser K, Edvardsen C (2002) Engineering design method for service life prediction. In: 9th international conference on the durability of building materials and components, Brisbane, Australia, paper 222
- Neves LC, Frangopol DM, Cruz PJS (2006) Lifetime multi-objective optimization of maintenance of existing steel structures. In: 6th international symposium steel bridges, european convention for construction steelwork, Prague, Czech Republic, pp 206–215
- NP EN ISO 4628-1 (2005a) Paints and varnishes—Evaluation of degradation of coatings—Designation of quantity and size of defects, and of intensity of uniform changes in appearance—Part 1: General introduction and designation system, Portuguese Quality Institute, Lisbon, Portugal, 8 p
- NP EN ISO 4628-2 (2005b) Paints and varnishes—Evaluation of degradation of paint coatings—Designation of intensity, quantity and size of common types of defect—Part 2: Designation of degree of blistering, Portuguese Quality Institute, Lisbon, Portugal, 16 p
- NP EN ISO 4628-4 (2005c) Paints and varnishes—Evaluation of degradation of coatings—Designation of quantity and size of defects, and of intensity of uniform changes in appearance—Part 4: Assessment of degree of cracking, Portuguese Quality Institute, Lisbon, Portugal, 20 p
- NP EN ISO 4628-5 (2005d) Paints and varnishes—Evaluation of degradation of coatings—Designation of quantity and size of defects, and of intensity of uniform changes in appearance—Part 5: Assessment of degree of flaking, Portuguese Quality Institute, Lisbon, Portugal, 11 p
- NP EN ISO 4628-7 (2005e) Paints and varnishes—Evaluation of degradation of coatings—Designation of quantity and size of defects, and of intensity of uniform changes in appearance—Part 7: Assessment of degree of chalking by velvet method, Portuguese Quality Institute, Lisbon, Portugal, 8 p
- Rafiq MY, Bugmann G, Easterbrook DJ (2001) Neural network design for engineering applications. *Comput Struct* 79(17):1541–1552
- Ross SM (1996) Stochastic processes, 2nd edn. Wiley, New York, USA
- Shohet I, Paciuk M (2004) Service life prediction of exterior cladding components under standard conditions. *Constr Manag Econ* 22(10):1081–1090

- Silva A, Dias JL, Gaspar PL, de Brito J (2011) Service life prediction models for exterior stone cladding. *Build Res Inf* 39(6):637–653
- Silva A, Gaspar PL, de Brito J (2012) Application of the factor method to maintenance decision support for stone cladding. *Autom Constr* 22:165–174
- Silva A, Gaspar PL, de Brito J (2014) Durability of current renderings: a probabilistic analysis. *Autom Const* 44:92–102
- Silva A, Neves LC, Gaspar PL, de Brito J (2015) Probabilistic transition of condition: render facades. *Build Res Inf*. doi: [10.1080/09613218.2015.1023645](https://doi.org/10.1080/09613218.2015.1023645)
- Sousa JMC, Kaymak U (2002) Fuzzy decision making in modeling and control. In: *World scientific series in robotics and intelligent systems*. World Scientific Publishing Co., Singapore
- Takagi T, Sugeno M (1985) Fuzzy identification of systems and its applications to modelling and control. *IEEE Trans Syst Man Cybern* 15(1):116–132
- Teo E, Chew M, Harikrishna N (2005) An assessment of factors affecting the service life of external paint finish on plastered facades. In: *10th international conference on durability of buildings materials and components (DBMC)*, Lyon, France, pp 570–582
- van Nunen H (2010) Assessment of the sustainability of flexible building. In: *The improved factor method: service life prediction of buildings in the Netherlands, applied to life cycle assessment*, 1st edn. Aeneas, Netherlands
- Vieira SM, Silva A, Sousa JMC, de Brito J, Gaspar PL (2015) Modelling the service life of rendered façades using fuzzy systems. *Autom Constr* 51:1–7
- Wang Y (2005) A multinomial logistic regression modeling approach for anomaly intrusion detection. *Comput Security* 24(8):662–674
- Wang Y-R, Gibson GE Jr (2010) A study of reproject planning and project success using ANNs and regression models. *Autom Constr* 3:341–346
- Zhang X, Gao H (2012) Determining an optimal maintenance period for infrastructure systems. *Comput Aided Civ Infrastruct Eng* 27(7):543–554

Corrosion Propagation Phase Studies on Finnish Reinforced Concrete Facades

Arto Köliö, Mari Honkanen and Jukka Lahdensivu

Abstract This work discusses a research project on active corrosion as a part of the service life of concrete facade panels in Nordic climate. The objective of the studies was to contribute to the knowledge on the corrosion propagation phase in these structures under actual long term weather exposure and to generate data for its modelling purposes. The project combined statistical analysis of a large database of condition investigation data to the more in-depth analysis of twelve case buildings and field measurement data on reinforcement corrosion. Corrosion rate was tied to long term weather data representing the geographical location of the buildings. As one of the results it was shown that, although carbonation resistance remains as the primary factor in ensuring proper service life, the modelling of active corrosion may provide a considerable extension to it.

Keywords Concrete · Corrosion · Carbonation · Propagation phase · Condition assessment

1 Introduction

Corrosion of reinforcement affects concrete structures basically either by cracking of concrete cover caused by corrosion products or by reduction of effective steel cross-section. The functionality of reinforcement (structural/non-structural) and the corrosion mechanism are decisive for which effect is dominating service life. However, cracking is typically the first sign of corrosion damage visible to the

A. Köliö (✉) · J. Lahdensivu
Department of Civil Engineering, Tampere University of Technology, Tampere, Finland
e-mail: arto.kolio@tut.fi

J. Lahdensivu
e-mail: jukka.lahdensivu@tut.fi

M. Honkanen
Department of Materials Science, Tampere University of Technology, Tampere, Finland
e-mail: mari.honkanen@tut.fi

structure's surface. Before visible cracking occurs on the structure surface the structure has gone through an initiation phase and a propagation phase until crack formation. The both phases can be analysed as separate entities or combined to form a holistic view of the structure's lifetime for the service life design purposes.

Private and public buildings built of concrete make up 34 % of the whole building stock in Finland, of which almost 40 % is now 30–50 years old. This is in common for most European countries with notable mass housing stock (Huuhka et al. 2015). The majority of the existing concrete facades in Finland (Fig. 1) have been built in time when service life design practice was not yet established. Whereas today, a service life requirement of 50 years is commonly set. The reinforcement service life is in Finnish guidelines (by 50 Concrete code after 2004) defined as only corrosion initiation. This means that the target service life should be achieved by carbonation resistance alone. This strategy withholds additional safety since no damage at all has happened yet at the chosen end of service life. In addition in new construction carbonation can be fairly easily accounted for by engineering concrete composition and reinforcement cover depths accordingly. Concerning existing buildings a problem is formed since these properties are already fixed.

There is a rising national concern on increasing maintenance needs of the existing building stock. In existing structures, the concrete quality has been weaker and therefore the initiation phase is in many cases already passed. This makes the assessment of the residual service life of these structures problematic in two ways: (i) the residual service life is, by the definition, zero even though no damage at all has happened, (ii) there is no methods available to evaluate the residual service life. This research entity focuses on the service life design and maintenance strategies of



Fig. 1 Typical Finnish concrete facade made of prefabricated concrete panels (*right*) from 1960 to 1979

existing concrete facades in Finland. Service life extension is gained by defining the end of service life in a new way and reliably modelling the corrosion propagation phase. It is a practical issue since many of these concrete buildings have poor quality and ongoing degradation due to freeze-thaw and corrosion. The residual service life of these facades cannot be estimated by carbonation resistance since this phase has already passed. The motivation is to find a way to compare renovation projects and to manage the ever growing renovation needs. The aim is to be able to combine a carbonation model and an active corrosion phase model to form a larger picture of the service life of these structures.

The propagation of corrosion on concrete facades in Finnish environmental conditions was studied by a series of field and laboratory studies conducted on twelve residential concrete buildings located in different parts of southern Finland. The studies were conducted in connection to the normal condition assessment practice of these buildings. In addition, corrosion rates in concrete facades were evaluated by long term (25 months) field measurements on concrete facades under natural conditions. The experimental results were contrasted to statistical information on 947 case buildings. This information was used in determining critical corrosion depths (in regard of cracking) and corrosion propagation rate both critical in service life modelling.

2 Background

A widely accepted description of the corrosion process of steel in concrete withholds the phases of initiation and propagation (Tuutti 1982). The assessment of the residual service life of corroding concrete reinforcement requires detailed information on the corrosion mechanism, initiation, corrosion rate and conditions which are regarded as the end of service life. The diameter and cover depth of the corroding reinforcement as well as the type of products (rust) formed in the corrosion process have been found to have significant impact on the formation of corrosion cracking. These factors are critical in modelling of the residual service life of structures in active corrosion state.

2.1 Reinforcement Corrosion Mechanism

2.1.1 Initiation Phase

Carbonation of concrete cover is behind the corrosion phenomenon in many outdoor concrete structures, such as facades and balconies. Carbonation of concrete is a chemical reaction between the alkaline hydrates of concrete and carbon dioxide gas, both of which are dissolved in concrete pore water.

The carbonation rate of concrete is influenced mainly by factors that affect the diffusion resistance of the material between outdoor air and the carbonation zone and the amount of substances taking part in the carbonation reaction of the carbonating material. Factors that limit carbonation are (i) moisture content of concrete, (ii) reserve of calcium hydroxide in cement, (iii) impermeability of concrete, (iv) low CO₂ concentrations in air, and (v) outward diffusion of OH⁻ in water saturated concrete (Tuutti 1982).

Because carbonation is mainly controlled by the diffusion of carbon dioxide within concrete, it is commonly modelled using the square root of time relationship, derived from Fick's diffusion law, in Eq. (1).

$$x = k * \sqrt{t} \quad (1)$$

where, x = carbonation depth; t = time in years and k = carbonation coefficient taking into account both internal and external factors influencing carbonation rate.

Many models have been proposed for depicting carbonation, all of which make use of the square root of time relationship (Parrott 1987). However, empirical measurements have indicated it to overestimate carbonation especially in cases where the concrete is exposed to rain (Tuutti 1982; Huopainen 1997). Therefore, the square root equation should be regarded as an upper limit for carbonation in such cases. The carbonation coefficient k is used to adjust the model to describe the carbonation of different concretes in different environments (Monteiro et al. 2012; Tuutti 1982).

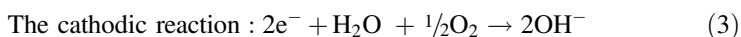
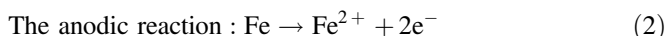
Another approach has been to incorporate the effect of different environments by modifying the exponent of time (Parrott 1987). A number of studies e.g. (Thiery et al. 2007; Hyvert et al. 2010) have been concentrated on the reaction kinetics of carbonation by utilizing physical models. The square root equation has also been improved to distinguish between the influences of different individual internal and external factors affecting carbonation (Neves et al. 2012), and to isolate the influences of specific factors (Fib 2006) opposed to the one parameter in Eq. (1). A statistical analysis of a carbonation coefficient based on field measurements has been recently presented in Portugal (Monteiro et al. 2012) and in Finland (Lahdensivu 2012). Lollini et al. (2012) have brought to light issues concerning the reliability of statistical service life estimates using the fib model for carbonation.

The main difference between the carbonation model proposed in fib model code (Fib 2006) and the one and two parameter models by Tuutti (1982) and Neves et al. (2012) is the requirement for a specific accelerated carbonation test performed in a laboratory environment to determine the carbonation resistance parameter. The latter models, on the other hand, are applicable in practice based on natural carbonation measurements conducted on site. A proposal to bridge this gap by a linear relationship between natural and accelerated carbonation has been presented in Neves et al. (2013) based on extensive carbonation field studies on 21 viaducts 4–32 years old in inland Portugal.

2.1.2 Propagation Phase

Corrosion of steel embedded in concrete is an electrochemical reaction where anode and cathode areas are formed on the steel surface as a result of differences in pH and moisture. Steel is dissolved in the pore solution in the anodic reaction and electrons are released. The electrical equilibrium is preserved by consuming of these electrons in the cathodic reaction elsewhere on the steel surface. The released ferrous ions react with chemical substances in the pore water i.e. in the electrolyte to form rust. Corrosion, especially with shallow cover depths, leads to cracking or spalling of surrounding concrete as the reinforcing bar starts to rust forming residue greater in volume than the original bar (Broomfield 2007).

Reinforcement corrosion is often described by simplified reaction Eqs. (2) and (3). The simplification is related to e.g. the consideration of plain Fe of reinforcing steel while it usually is composed of mainly Fe, C and Cr.



To happen, electrochemical corrosion requires a reactive metal where anodic oxidation can take place, a reducible substance which acts as a cathodic reactant, electrolyte allowing the migration and movement of ions and an electron conduction between anodic and cathodic areas (Page 1988). The corrosion process is influenced by the availability of oxygen (affects the cathodic reaction) and moisture (reduces the electrical resistivity of concrete). The factors affecting reinforcement corrosion have been classified as internal and external factors (Ahmad 2003).

The corrosion of reinforcing steel in carbonated concrete produces a multi-layer system, which consists of (i) mild steel rebar, (ii) porous conductive oxide layer, (iii) non-conductive iron oxide layer, (iv) carbonated concrete cover and (v) the atmosphere (Huet et al. 2007). The main conclusion is that the corrosion products form layers of different composition and characteristics around the reinforcement.

2.2 Measurement of the Extent of Corrosion

There are several ways of measuring the propagation of corrosion all connected to the properties of the corrosion process. Characteristics of a number of widely used techniques have been summarized by Rodriguez et al. (1994).

Gravimetric measurements are based on the dissolving of steel while it corrodes, i.e., the cross-section of the steel rebar is decreased. The extent of corrosion can be measured as a loss of mass by weighing a corroded steel sample which has been cleaned in acid immersion, ultrasonic cleaner or by precision sand blasting. The gravimetric measurements require uncorroded reference samples of the same

reinforcing steel to determine the initial unit weight of the steel for the extent of corrosion evaluation (Tuutti 1982).

Electrical measurements utilize the electrochemical nature of the corrosion process. The measurements provide information of the corrosion probability and/or corrosion rate by three main parameters: half-cell potential, concrete resistivity and corrosion current density (Ahmad 2003).

Visual inspection can provide general observations of the reinforcement corrosion such as rust color and form for roughly identifying corrosion products. The extent of corrosion can be assessed by measuring the surface area of the reinforcing bar covered with rust. The measurement can be performed by wrapping the sample in a film and drawing on it the corroded area. The area can then be calculated from the surface of the unrolled film. Visual inspection is not a precise method but can quickly provide general information on the corrosion case at hand (Tuutti 1982).

Optical microscopy or electron microscopy can be used to visualize the extent of corrosion (Jaffer and Hansson 2009). The main advantage is the possibility to illustrate the thickness and different layers of the corrosion products. Microscopy requires a high level of preparation of the samples.

Element analysis can be performed to identify corrosion products (Raman Spectroscopy and/or X-ray Diffractometry, XRD) or the elements in them (Energy Dispersive X-ray Spectroscopy, EDS). The identifying of corrosion products is essential in providing initial data for corrosion modelling because of the different specific volume of different corrosion products (Jaffer and Hansson 2009).

2.3 Corrosion Monitoring

Many studies to monitor the response of concrete reinforcement to either simulated atmospheric conditions or natural environment have been conducted over the years (Parrott 1987).

Andrade and Castillo (Andrade and Castillo 2003) subjected concrete specimen to both laboratory induced environments and natural environment in Madrid during a time period of five years. The authors monitored temperature, RH and precipitation as well as corrosion potential, current density and resistivity of the samples. The main influencing factors were temperature and rain events and their cyclical variation daily and seasonally. Cold climates were hypothesized to pose greater risk for corrosion due to lesser ability of the concrete to dry. It was also observed that the natural environment imposes fluctuations in the reinforcement corrosion behaviour that cannot be fully predicted by laboratory experiments. Al-Neshawy (2013) presented an automated system for monitoring temperature and relative humidity in concrete facades (RHT-MAPS-system) composed of a set of T and RH sensors, network components and analysis software. The system was utilized in predicting seasons/months with high corrosion risk. It was stated that more parameters such as wind driven rain and solar radiation would increase the reliability of the predictions.

The ability to use linear polarization resistance (LPR) technique (Stern and Geary 1957) to monitor instantaneous corrosion rate was tested over gravimetric measurements by Law et al. (2004). The authors monitored carbonation and chloride induced corrosion in reinforced concrete samples under cycles of wetting and drying in the laboratory over a period of approximately three years. LPR method was found to overestimate weight loss regardless of the way of corrosion initiation (carbonation or chloride ingress). However, in carbonation induced uniform corrosion the method was found to give more reliable measurement of corrosion rate than for localized chloride induced corrosion. Karthick et al. (2014) evaluated the functionality of both embedded potential sensors and corrosion rate monitoring probe sensors (LPR) as well as surface mounted systems. The embedded systems were found to be the most reliable in the test period of 24 months. Corrosion current densities were related to the corrosion rate of steel by Andrade and Alonso (2001).

In his research Mattila (2003) measured the corrosion current in measurement devices embedded in existing concrete facades using the LPR technique. High corrosion current was observed during a year when annual precipitation was exceptionally high. Vice versa, when annual precipitation was low also very low corrosion currents were observed.

2.4 Corrosion Propagation Modelling

Corrosion propagation can be modelled by (i) empirical, (ii) numerical or (iii) analytical approaches (Otieno et al. 2011). Empirical models are sub-divided into three types i.e.: expert Delphic oracle models, fuzzy logic models and models based on electrical resistivity and/or oxygen diffusion resistance of concrete. Empirical models are based on experimentally achieved relationship between corrosion and controlling parameters (e.g. DuraCrete 2000). Three different approaches can be used to develop numerical models: finite element method (FEM), boundary element method (BEM) and resistor networks and transmission line method. Numerical models rely on computational solving of larger entities by dividing them into small elements connected to each other by boundary conditions (FEM, BEM) (e.g. Gulikers and Raupach 2006). Analytical models apply usually thick-walled cylinder approach. Division into cracked inner cylinder and an uncracked outer have also been developed. Analytical models are based on the closed-form solving of mathematical equations derived from the geometry of the problem such as concrete cracking (e.g. Goltermann 1994).

A traditional way of modelling corrosion propagation is by the corrosion rate modified by the diameter of reinforcement and the concrete cover (Siemes et al. 1985). The corrosion rate itself is related to the wetness and temperature of the structure and is modelled e.g. by the potential electrolytical resistivity of concrete

(DuraCrete 2000). A way of finding information on the corrosion propagation phase by statistically calculating backwards the age and initiation time on existing concrete structures subjected to condition assessments has been proposed by Köliö et al. (2014).

3 Research Materials and Methods

Studies on the rate and extent of reinforcement corrosion in concrete facade panels were conducted combining statistical data gathered from standardized condition investigation reports, analysis of specific experimental research material gathered from 12 visually corrosion damaged concrete buildings, long term corrosion rate measurements on two locations and quantitative weather data from the Finnish Meteorological Institution.

3.1 Condition Investigation Database and Statistical Analysis

Concrete facades of buildings in Finland have been subjected to condition assessments since late 1980s and data measured by standardised procedures (Concrete association 2002) has been produced in majority of these assessments. The condition assessments consist of preliminary desk top studies, visual observation and rating in situ, measurements and sampling in situ and laboratory tests (Lahdensivu et al. 2013). Thus, the data includes information on both the durability properties of structures and the actual observed degradation in real outdoor environment conditions.

A database has been collected from condition assessments conducted by various professional engineers during 1992–2006. The database includes the condition assessment information of 947 buildings built 1965–1995 (Lahdensivu 2012). The assessments have been conducted in connection to renovation or systematic maintenance of the building. Typically the same building has not yet been subjected to assessment more than once. This means that each building in the database represents an individual case. The practice has been similar due to uniform guidelines used by all condition assessment practitioners. The database can thereby be argued to be very well suitable for statistical analyses.

The specified concrete grade used in facade panels was C20/25 from 1965 until 1989. The cement type used in these precast panels is mostly CEM I ordinary Portland cement. The concrete composition realized during construction has not been analysed in connection with the condition assessments and is therefore not known precisely. Therefore, the specified values should be considered when the results are evaluated.

Table 1 Research material for the statistical analysis based on condition assessment database

	Brushed painted concrete facades	Exposed aggregate concrete facades	Concrete balcony slab
Age of the structure (a)	9–43	7–37	7–52
Visual ratings (number of observations)	250	193	331
Carbonation coefficient (number of samples)	1285	849	884
Reinforcement cover depth (number of measurements)	60,640	104,958	12,957

In regard of reinforcement corrosion, the investigated structures have been subjected to thorough cover depth mapping, carbonation depth and chloride content measurements and visual inspection during the condition assessment (see Table 1).

The inspected structures have during the assessment been given a visual damage rating. This rating is (1) no visual damage, (2) local damage and (3) wide spread damage. The rating is based on visual observations by the engineer conducting the assessment. In these condition assessments the facade has been inspected for damage as one unit. Therefore, e.g. differences in signs of damage on facades facing different directions have not been recorded. Differences between the degradation of northern and southern facades are common due to the characteristics of driving rain in Finnish climate (Lahdensivu 2012). This is not however represented by the database.

Carbonation depth has been measured from core samples taken during the field investigation by spraying freshly cut surface with phenolphthalein pH indicator. By average 12 samples have been taken from one building. Reinforcement cover depths have been measured as sweep measurements on large areas of concrete surfaces using electronic cover meter and directly from concrete cover samples containing reinforcing bars. The latter measurements have been used in validating the cover meter results.

3.2 *Experimental Research on Case Buildings*

The type and critical amount of corrosion products were studied by electron microscopy and X-ray diffractometry on concrete and reinforcement samples from existing concrete facades on visually damaged locations. This information was utilized in creating a service life limit for concrete facade panels in regard of visual corrosion damage occurrence.

The research material for this study was gathered in the period of April–August 2013 in the facade condition assessment of 12 buildings chosen deliberately for this study. The buildings were located in the southern parts of Finland and their construction years ranged from 1971 to 1984. The facades were constructed using

prefabricated sandwich panels. Of the studied facades seven were of painted concrete, four of exposed aggregate and one of untreated form surfaced concrete. In all 27 sample cores of the diameter of 50 mm were drilled from the outer layer of the facade panels directly on visually observable corrosion cracks or spalls. The samples contained the corroded rebar and its surrounding concrete.

Carbonation depth measurements were used to investigate the time of corrosion initiation in these samples and thereby calculate the length of the active corrosion phase by subtracting from the total age of the samples the time of initiation.

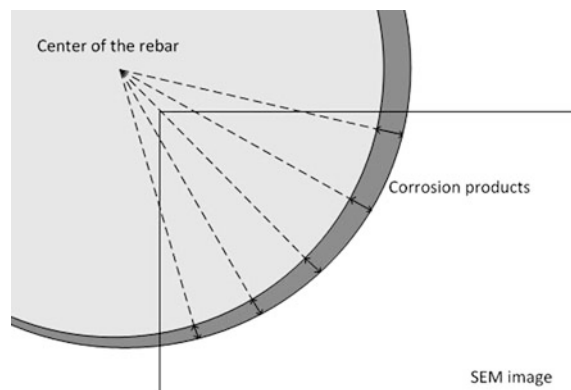
The concrete core samples were broken in laboratory and the reinforcing bars trapped inside the carbonated layer of concrete were extracted from the core samples. The diameter of reinforcing steel samples varied from 3 to 10 mm. The total number of steel samples was 35 of which 16, ranging from different diameter and corroded surface, were chosen for electron microscopic studies.

Cross sections of the reinforcing steel samples were prepared with conventional metallographic sample preparation method: molding into resin followed by mechanical grinding and polishing. Grinding, polishing, and cleaning of the cross-sectional samples were performed without water to avoid dissolution of rust. The cross-sectional samples were characterized with a scanning electron microscope (SEM, ULTRApplus, Zeiss) equipped with an energy dispersive spectrometer (EDS, INCA Energy 350 analyzer with INCAX-act detector, Oxford Instruments).

The overall thickness of corrosion products was measured from the SEM images of the samples by utilizing an image analysis software imageJ. Thicknesses were measured in evenly spaced lines perpendicular to the circumference of the reinforcing steel, see Fig. 2, and averaged over the outward and inward semicircle of the reinforcement circumference. The orientation of the reinforcing steel was identified using photographs taken for this purpose during sample preparation.

EDS analyses were performed on the samples to study the elemental composition of the rust layer. Further on scraped rust powder from 12 samples was studied with X-ray diffractometer (XRD, Empyrean, PANanalytical) to analyze compounds of the corrosion products.

Fig. 2 Statistical model for the evolution of corrosion damage



Scraped rust powder was also studied by transmission electron microscope (JEM 2010, Jeol) equipped with EDS (Noran Vantage with Si(Li) detector, Thermo Scientific). Samples for TEM studies were prepared by crushing the scraped rust powder between two laboratory glass slides and dispersing the powder with ethanol onto a copper grid with a holey carbon film.

3.3 Methods of the Corrosion Rate Studies

The research material was composed of a long term corrosion current density measurement data on concrete facades and long term weather observation data corresponding to the time span of the measurement. The corrosion current density data had been measured from the facades and balconies of two residential buildings in Finland: inland location at Fysiikanpolku 5, Tampere, built in 1978 and coastal area at Joupinrinne 4, Espoo, built in 1978. The measurements were arranged on one facade. The instrumented structures were in both measurement sites facing southern directions: at Fysiikanpolku southeast (154° north, clockwise) and at Joupinrinne 4 southwest (223° from north, clockwise).

The weather observation data was collected for this study by Finnish Meteorological Institute (FMI) and it was then further refined to form four weather parameters: Temperature (T , [$^\circ\text{C}$]), relative humidity (RH , [%]), amount of wind-driven rain on the measured wall surface (I_{WA} , [mm]), amount of direct and diffuse solar radiation on the measured wall surface (RAD , [kJ/m^2]) for evaluating their correlation to corrosion. The data was obtained from observation stations nearest to the case buildings with a time resolution of three hours (Fig. 3).

Multi linear regression (MLR) was finally used to determine the partial influence of single or a sequence of weather parameters to the observed corrosion current density. The regression was fitted by the least squares method and evaluated by the coefficient of determination.

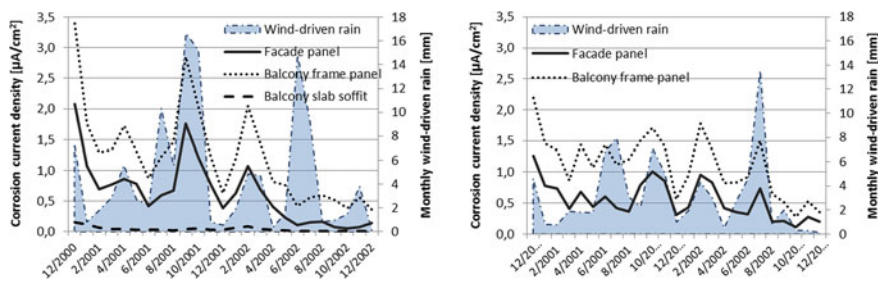


Fig. 3 An example of the monthly corrosion rates contrasted to the levels of wind-driven rain. *Left* Inland, Tampere, *Right* Coastal area, Espoo

4 Reinforcement Corrosion in Concrete Facades

This chapter discusses the service life of concrete facades in Nordic climate including the initiation of corrosion and corrosion propagation until visual corrosion cracking occurs. The discussion is based on studies described in chapter three.

During initiation phase the concrete cover is carbonated as a barrier and finally reaching the steel initiating the actual corrosion process. Until this point, no actual damage has occurred at all. In the propagation phase, as the corrosion proceeds it will eventually induce visual damage to the concrete structure's surface as cracks or spalls. The rate of this process depends on many things, such as cover depth, diameter of the reinforcing steel as well as temperature and the availability of moisture.

4.1 *Initiation of Reinforcement Corrosion in Concrete Facades*

To a large extent the service life of reinforced concrete is based on the initiation phase. The square root model is widely used to predict the initiation of reinforcement corrosion due to carbonation of the concrete cover in service life considerations of reinforced concrete structures. The model is based on diffusion laws and its validity is therefore arguable. A recent study (Köliö et al. 2015a) showed that the square root equation is capable of predicting the propagation of carbonation in actual exposed outdoor structures with a high reliability (Fig. 4). Especially, when the model is applied on already aged existing concrete structures where the carbonation rate has already stabilized.

Consecutive carbonation depth measurements on 21 existing concrete facades were compared to the square root model for predicting progress of carbonation (Eq. 1). The data from consecutive condition assessments was used to evaluate the model's representativeness of actual observed natural carbonation.

In general, the square root equation provided a good fit for the propagation of carbonation in the studied concrete structures, indicated by the overlapping of the 1st and 2nd assessment curves in Fig. 4. The predictions made based on the first measurements to the age of 50 years differed from the latter measurements by 0.8–2.4 % in brushed and painted facades and by 1.5–15.8 % in the case of exposed aggregate concrete. The prediction accuracy was greatly increased when the sample count is high ($n > 20$ per case).

Carbonation coefficients for Finnish concrete facade panels have been reported in (Lahdensivu 2012). Judging by the values for carbonation aggressiveness (Table 2) a typical time period for the facade concrete to carbonate to the level of reinforcement is 10–30 years. However, a large scatter is also associated with realized concrete cover depths which can cause high spatial difference to the initiation time.

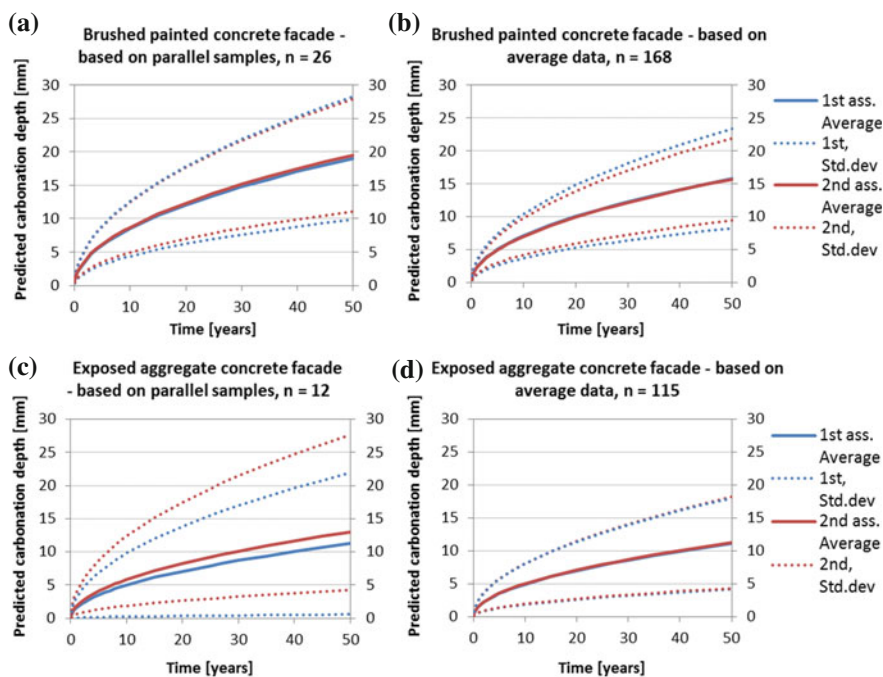


Fig. 4 Carbonation of brushed and painted and exposed aggregate concrete facades modelled by parallel samples or by average data

Table 2 Carbonation coefficients, k , for common concrete facade surfaces in Finland (Lahdensivu 2012)

Surface finish	Average	Standard deviation	Number of measurements
Brushed painted concrete facade	2.71	1.23	1285
Exposed aggregate concrete surface	1.96	1.28	849

The type and amount of cement have been found to influence carbonation resistance and, thus, the carbonation rate of concrete. The cement type used in the structures of this study has been mostly Portland cement, but the amounts used have not been determined during the condition assessments. The type and amount of cement used are considered to have only a minor effect on the conclusions made on the basis of consecutive measurements on the same structures since they are over time remained unchanged. Variation in the amount of cement along with variation in porosity and concrete composition, mixing, placing and curing have influence on the overall scatter of carbonation depth. Changes in these factors related to construction usually negate the initial presumption of homogeneity of concrete in field

studies on existing concrete structures. Therefore, the carbonation rate can differ also within a very limited area on the concrete surface. Thus, it is recommended to ensure a proper sample size in carbonation depth studies.

In the studied samples capillary porosity, which affects both the permeability and wetting of concrete, varied between 4.9 and 8.4 wt% in all samples, while average value was 6.7 wt%. The concrete of the samples was not homogenous. Capillary porosity of concrete varies a lot in existing concrete facades and balconies made in 1960s to 1980s. According to Lahdensivu (2012) small carbonation coefficients ($k < 1.0$) are associated with low capillary porosity (<5 wt%) and vice versa carbonation coefficients higher than 3.0 associated with capillary porosities above 7.0 wt%.

The micro climate around a structure influences carbonation causing different carbonation rates for structures sheltered from rain (balcony slab soffits) and structures exposed to rain (facades) as was observed in the case of different structures in this study. According to the standard EN-206, sheltered from rain structures e.g. balcony slab soffits fall into exposure class XC3 and rain exposed facades to XC4. In design it should be recognized that the exposure of XC3 class can be much more severe regarding carbonation than the following class XC4. If the scope of the service life is widened to withhold corrosion propagation, the conditions of the exposure class XC4 favour more corrosion propagation than the conditions of XC3. This means that in the design of structure service life based on carbonation resistance, the XC3 class requires higher attention than the preceding class. It is the defining the target service life that finally decides how these classes should be treated and related to each other.

4.2 Propagation of Reinforcement Corrosion in Concrete Facades

4.2.1 Statistical Modelling of the Extent of Service Life

The condition assessment database was used in studying statistically the realized service life of concrete facades in regard of visual damage caused by reinforcement corrosion (Köliö et al. 2014). The age at which visual corrosion damage is generally observed in concrete facades was studied using visual damage ratings given in condition assessments. This damage rating was used together with the age of buildings to study the time it takes for corrosion damage to propagate. A distribution over time was produced for the formation of visual damage (Fig. 5). Because the information about the age of the building is linked to the time of condition assessment these examinations do not take into account the fact that visual cracks or damage have, in fact, emerged some time before the assessment date. This time before the condition assessment is in this study unknown. Thus, the visual damage is likely to be formed even earlier than the results indicate, and the results of this study should be treated accordingly.

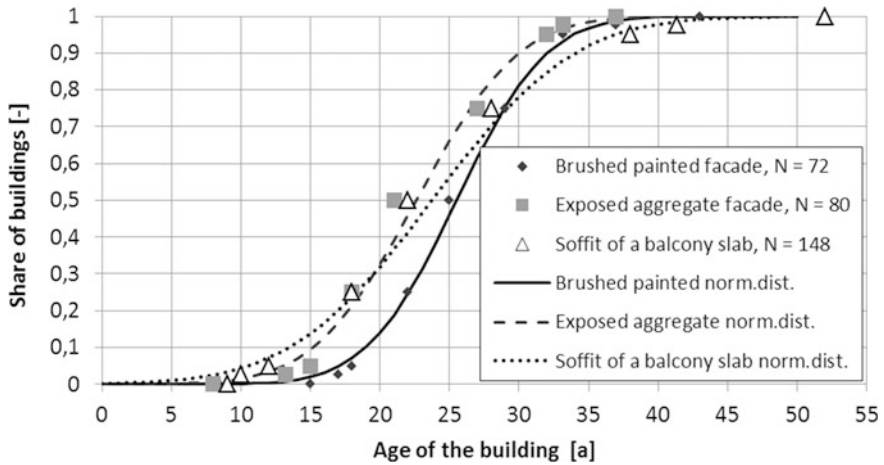


Fig. 5 Statistical model for the evolution of corrosion damage

The first visual damage had occurred after 15 years from construction in brushed and painted concrete facades and after 8 years in exposed aggregate facades. In balcony slabs first damage was observed after 9 years. By median, visual corrosion damage has formed on concrete facades after 21–25 years from construction (exposed aggregate and brushed painted respectively). The exposed aggregate surface is thereby damaged slightly faster than the brushed concrete facade. It is also illustrated that visual corrosion damage is in majority a problem with the small concrete cover depth cases where both initiation and active corrosion is fast.

The total service life is divided into an initiation phase (Fig. 6, brushed painted surface) and a propagation phase (Fig. 7). If a proper concrete cover is ensured the achieved service life by the initiation phase alone will easily exceed 50 years. However, with shallow cover depths below 15 mm the extension provided by the propagation phase is needed.

According to the calculation, the active corrosion period is 0.6–1.4 years when adopting a commonly used 5 % safety level. It relates to corrosion of reinforcement with extremely small cover depth or in very capillary concrete. However, this safety level may be too strict compared to empirical knowledge.

4.2.2 Determining the End of Service Life for Concrete Facade Panels

Material characterization and microscopy studies were used (Köliö et al. 2015b) to determine in more detail the extent of corrosion needed to cause visual damage on concrete facade surfaces (Table 3).

The studied concrete structures were on average 38.8 years old. The average time under active corrosion was for the cracked locations 26.0 years and for spalled locations 33.1 years. It should also be noted that for all of the samples corrosion has

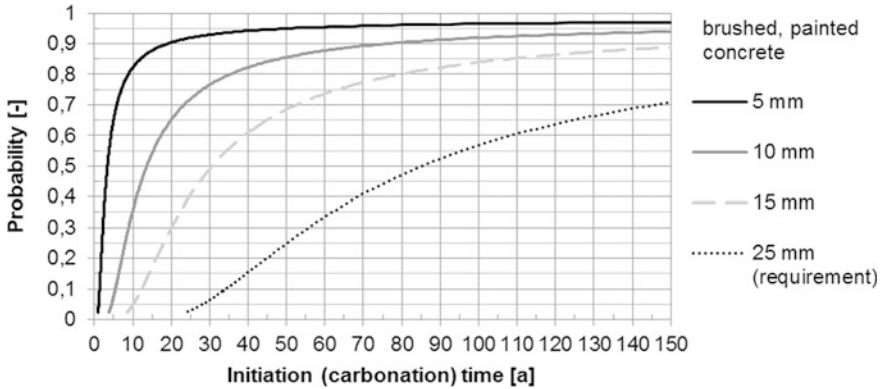


Fig. 6 The distribution of initiation time by carbonation to different depths of cover of reinforcement in brushed and painted concrete facades

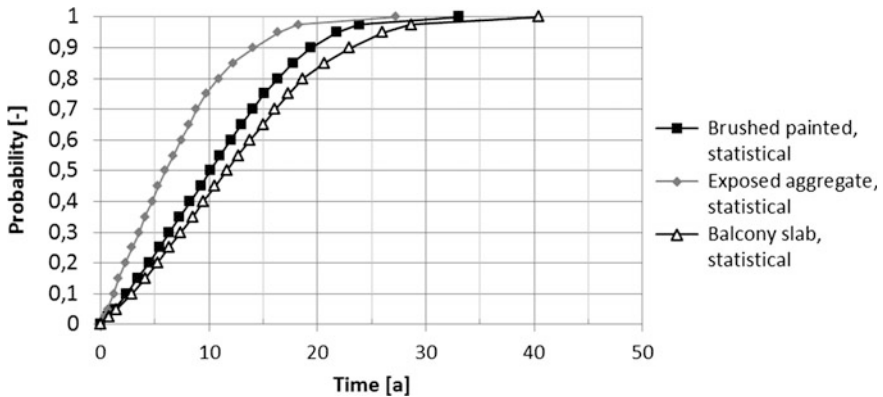


Fig. 7 Propagation time to form visual damage observed in different facade structures by statistical simulation

been initiated quite fast (by average 12.6 years) which indicates that both concrete resistance against carbonation has been poor and the environmental conditions favourable to carbonation. The SEM analysis confirmed that corrosion products form layers of different composition around the steel. Based on the EDS analysis the rust formed on rebars was divided into inner and outer rust layer (Fig. 8). The corrosion products also contained veins of highly dense rust and veins of presumably residue of concrete pore water. Also particles that were trapped inside the rust were observed.

The outer rust layer contained typically less iron and on the other hand more oxygen and various other elements than inner and single layers (Fig. 8). In the inner rust layer the amount of iron was higher and the layer was composed more strictly of pure iron oxides. Particles that were entrapped in the rust were mainly composed

Table 3 Research material for the statistical analysis based on condition assessment database

Sample id (diameter, mm)	Rust layer thickness, outward semicircle		Rust layer thickness, inward semicircle		Cover depth/steel diameter (-)
	Average (μm)	Std.dev (μm)	Average (μm)	Std.dev (μm)	
Vi 16.1 (3)	178.1	130.1	105.8	71.2	3.3
Vi 6.1 (3)	170.7	103.1	67.8	43.5	4.7
Pi 17D.1 (4)	–*	–*	–*	–*	2.8
RU 6.2 (4)	80.5	49.8	45.4	27.0	3.3
KA 9.1(5)	34.8	31.9	14.9	14.1	1.8
RU 6.1 (6)	131.9	107.4	44.7	42.1	1.8
Vi 7.2 (6)	44.8	37.2	35.8	26.5	3.5
KU 14.2 (8)	42.0	37.0	6.6	5.8	1.6
Pi 17B.2 (8)	182.3	174.9	62.3	38.4	3.0
Pi 17C.2 (8)	109.5	94.6	40.6	35.1	2.9
PU 1.2 (8)	186.1	98.0	158.4	158.2	3.8

*Steel orientation not detectable

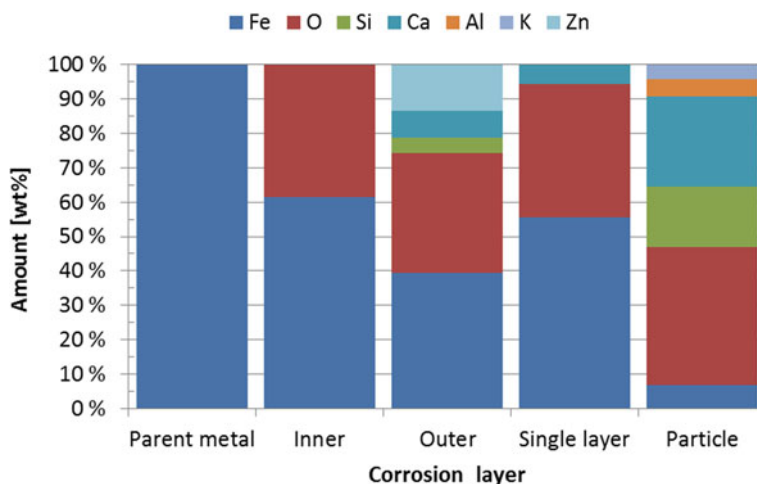


Fig. 8 The element composition (wt%) of different rust layers on corroded reinforcing steel samples (only elements >5 wt%)

of calcium, silicon, and oxygen. These constituents originate from the calcium-silicate-hydrate (CSH) and the pore water of concrete. The study suggests that the more porous corrosion products responsible for the most volume increase are located on the outer circumference near the concrete interface.

XRD patterns of the rust scraped from the samples OH 12.1 and VI 7.2 (Figs. 9 and 10) illustrate the typical rust composition in the studied samples. Mainly Goethite, Ferroxhyte and Lepidocrocite corrosion products were identified in

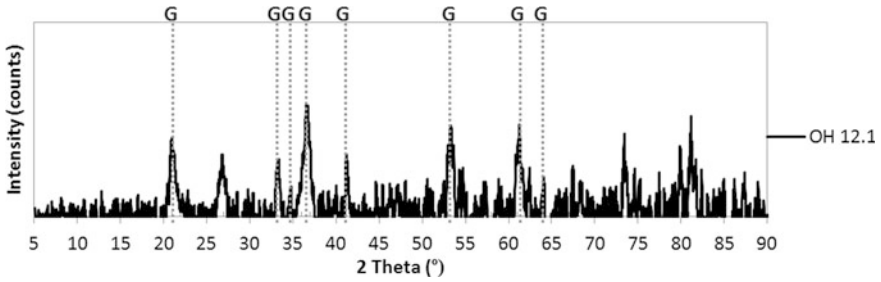


Fig. 9 XRD pattern of the rust scraped from the sample OH 12.1, *dotted lines* correspond to goethite (G)

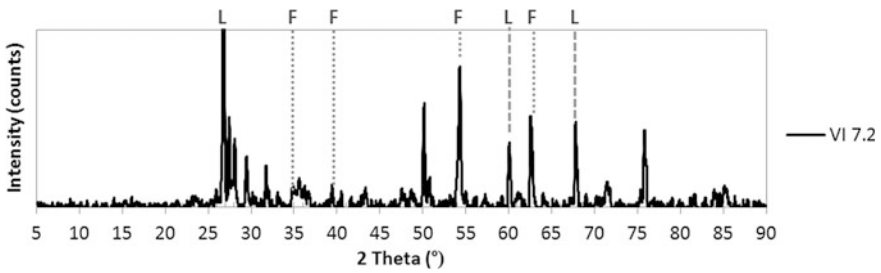


Fig. 10 XRD pattern of the rust scraped from the sample VI 7.2, *dotted lines* correspond to ferroxihite (F) and *dashed lines* to lepidocrocite (L)

majority of the samples by comparing the diffraction patterns to literature and powder diffraction files (Legodi and Waal 2006; Drits et al. 1993, PDF 00-060-0344, PDF 01-079-1971). Some of the non-rust peaks could also be identified to originate from the CSH of concrete. However, more sophisticated methods could be used to study the heterogeneity of the rust in more detail.

TEM image with selected area electron diffraction (SAED) patterns agreed with XRD results. In addition, the TEM-EDS analyses of the rust powders were similar to the cross-sectional SEM-EDS results.

In the studied structures the main reason for the damage to emerge in the studied time span as cracking or spalling was the concrete cover depth in relation to the rebar diameter, i.e. the cover/diameter ratio. Corrosion products associated with carbonation initiated corrosion on the studied concrete facade panels were mostly hydroxide type of rusts with a unit volume of roughly 3 times the volume of iron. Taking the determined relative volume of the rust layer into account the required corrosion penetration to initiate visually observable cracks in the studied facade panels was by average 38.7 μm with a corresponding rust thickness of 116.1 μm . Design values that take into account the scatter in rust thickness were produced by adding one standard deviation to the average. These values can be utilized in service life calculations of similar structures in regard of visual damage emergence. It is also well in line with earlier literature (Table 4).

Table 4 Estimates for the critical corrosion depth regarding corrosion induced concrete cracking

Source	Critical corrosion depth in regard of concrete cracking (μm)		
	Min	Average	Max
Alonso et al. (1998)	15		50
Siemes et al. (1985)			80
Broomfield (2007)			100
Köliö et al. (2015b)	22.2	67.5	119.1

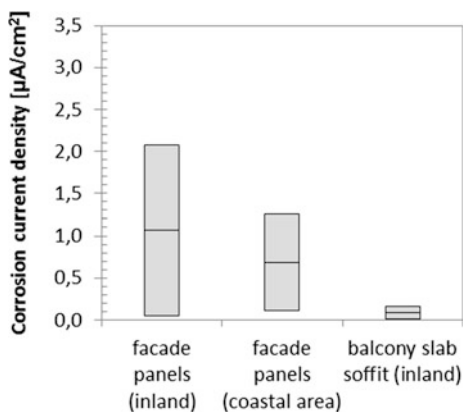
4.2.3 The Corrosion Rate in Outdoor Environment Exposed Concrete Facade Panels

Corrosion rate was determined as a combined effect of weather parameters on already carbonated concrete structures exposed to natural outdoor environment. A long term corrosion rate measurement data was combined with weather data from the location of the measurements from the same time period.

The corrosion rate monitoring data visualizes that the consecutive years have been different regarding the corrosive environmental conditions. Measured corrosion current densities show high scatter but are in general rather high (Fig. 11).

An initial presumption that corrosion rates will be higher on sites located in coastal regions was not clearly visible in the research data. Actually, the overall corrosion level has been lower in the coastal area site. The wind-driven rain amounts on the structures have during the monitoring period been 47 % higher inland than in the coastal region. Inherently, the corrosion rates have been 11–18 % higher inland than in the coastal region. This observation stresses the importance of the micro climate around the building along with the geographical location in regard of degradation rate. Current densities measured as a reference from the bottom surface of a balcony slab (sheltered from rain) were very low. In the bottom surface of the slab the shelter from wetting is shown clearly as negligible corrosion rates.

Fig. 11 Monthly averaged corrosion current densities recorded in field measurements in inland and in coastal area of Finland



In a regression analysis between corrosion rate and weather parameters all seasons showed high correlation between wind-driven rain and corrosion rate. However, correlation is low in summer season at Fysiikanpolku 5 site (Fig. 12) due to the rain event at 6–7/2002 and in spring at Joupinrinne 4 site (Fig. 13) due to a non-captured rise in corrosion rate at 4/2001.

The effect of solar radiation is high during spring but its representativeness in other seasons is low. The correlation between RH and corrosion rate is also high during spring. The correlation between temperature and corrosion rate is remarkable in winter for two reasons: first, temperature drop below 0 °C greatly hinders the corrosion process and, secondly, precipitation able to penetrate concrete (liquid form) requires a temperature of over 0 °C. As a result from this behaviour in winter the effect of temperature on corrosion rate (in this statistical model) is positive on the contrary to other seasons, where the effect is negative (due to the increased drying capability of the structure).

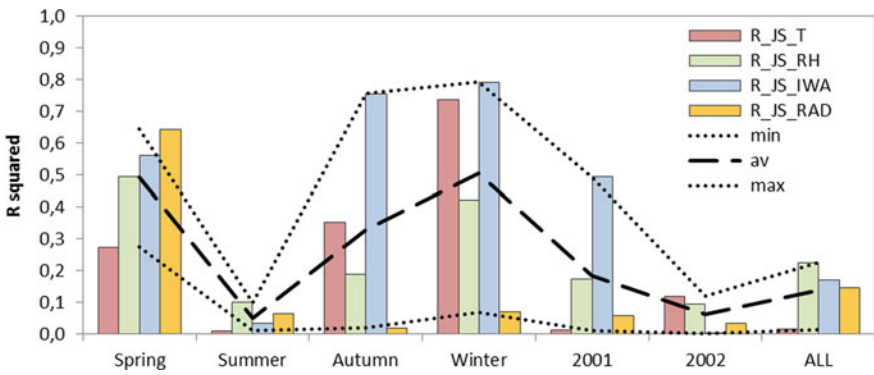


Fig. 12 The coefficients of determination of the predictions of corrosion rate based on single weather parameters. Inland, Fysiikanpolku 5 site

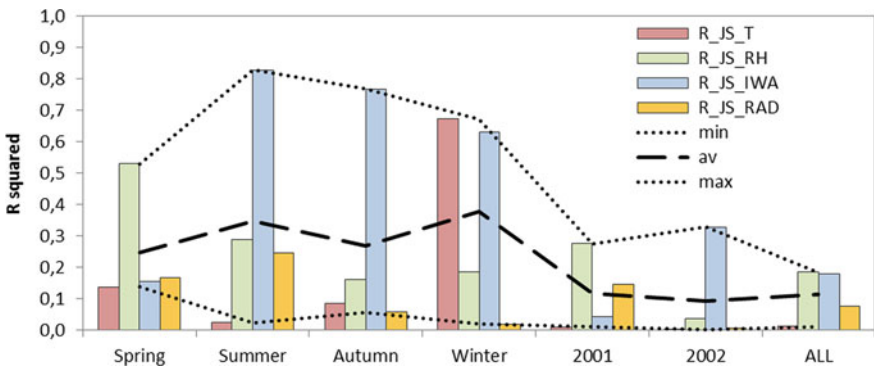


Fig. 13 The coefficients of determination of the predictions of corrosion rate based on single weather parameters. Coastal area, Joupinrinne 4 site

A multi-linear regression model for corrosion rate was created based on the correlation results of single weather parameters. The model was composed of linear relationship equations (Eq. 4) for every season utilizing monthly averaged weather parameters of temperature (T , °C), relative humidity (RH , %), wind-driven rain (I_{WA} , mm) and solar radiation (RAD , kJ/m²). The choice of parameters to the equation was made by optimizing the parameter composition in regard of the total correlation to corrosion rate (coefficient of determination) as well as choosing a composition of parameters where the effect of single weather parameters is of the suitable form (negative/positive). Table 5 shows the parameters and coefficients that can be applied in modelling reinforcement corrosion rate in concrete facades together with monthly weather data.

$$y = \beta_0 + \beta_1 \cdot x_1 + (\beta_2 \cdot x_2 + \beta_3 \cdot x_3 + \beta_4 \cdot x_4) + v \quad (4)$$

with parameters presented in Table 5. Parameters not mentioned in the table should be treated as zero for the specific season.

Corrosion rates during the lifetime of the concrete structures at Fysiikanpolku 5 and Joupinrinne 4 were estimated using the model with a record of 30-year weather data from 1979 to 2009. The weather data was available for Joupinrinne 4 site from Helsinki-Vantaa airport (distance to site 15 km) and for Fysiikanpolku 5 from Jokioinen observatory (distance to site 79 km). On a long time scale the corrosion rate on concrete facades were relatively steady at the both locations.

The long term corrosion current densities in Facades at Joupinrinne 4 (coastal area) were by average 0.5 $\mu\text{A}/\text{cm}^2$ higher than at Fysiikanpolku 5 (inland). The overall average level is 1.2 $\mu\text{A}/\text{cm}^2$ at Fysiikanpolku 5 and 1.7 $\mu\text{A}/\text{cm}^2$ at Joupinrinne 4 site. These corrosion rates correspond to a steel loss of 14.6 $\mu\text{m}/\text{year}$ and 19.6 $\mu\text{m}/\text{year}$, respectively, derived from the Faraday's law. These corrosion levels can be considered high (Andrade and Alonso 2001) in carbonation initiated outdoor concrete structures. In the studied 30-year period corrosion propagates,

Table 5 Regression models for reinforcement in facade panels

Season	R squared	Comment	Parameter	Coefficient
Spring	0.45	FYS5	β_3 , (I_{WA})	0.035
			β_4 , (RAD)	-0.0008
			β_0 (intercept)	1.913
Summer	0.95	JOU4	β_2 , (RH)	0.011
			β_3 , (I_{WA})	0.037
			β_4 , (RAD)	-0.0006
			β_0 (intercept)	0.562
Autumn	0.69	FYS5	β_3 , (I_{WA})	0.084
			β_0 (intercept)	0.112
Winter	0.79	FYS5	β_1 , (T)	0.068
			β_3 , (I_{WA})	0.134
			β_0 (intercept)	0.857

once initiated, in the coastal location 34 % faster than in inland. In this study, both of the facades were facing southern direction, but were not situated exactly the same which may cause some of the difference.

The time of corrosion initiation by carbonation of these structures is estimated to be 10–30 years in facade panels (painted brush finished concrete) according to square root relationship utilizing carbonation coefficients measured from 947 concrete buildings similar to the ones in the present study (Table 2). After initiation corrosion will propagate at rates which are greatly dependent on the surrounding weather conditions as discussed in this work. The metal loss due to reinforcement corrosion after initiation can be derived from the long term corrosion rates.

5 Summary

The studies presented in this chapter strive to enhance the knowledge on the active corrosion phase in reinforced concrete facades as a part of their service life. The research project confirmed that the active corrosion phase can provide a considerable extension to the service life of concrete facade panels in Nordic climate. This extension can be from ten to even 30 years. It was also observed that current models for active corrosion, which mostly concern chloride induced corrosion, cannot be used in this application.

The ability to model or forecast corrosion rates on concrete facades will enhance the capability of realtors to react on upcoming repair needs. This kind of model would be able to predict the residual service life of a certain structure, but it could also be used in creating renovation strategies for a larger building stock by revealing the order of importance or the urgency of single renovation projects. Such a tool could be used also in moving towards a predictive upkeep of realty and the confidence of making long term contracts between realty owners, renovation engineers and contractors.

The occurrence of visual damage is a natural way of judging the service life of these structures since all of the renovation and maintenance decisions are made based on investigations usually commissioned based on these visual signs. Corrosion induced damage occurred on the studied structures commonly on the lap splicing locations of rebars, in the edges and window openings of the panels and in locations with pronounced moisture load due to poorly functioning flashings and rain water runoff control. If the ratio of concrete cover to reinforcement diameter was small (below 1.5) corrosion related damage had emerged as spalling. If the ratio was well over 1.5 the damage more probably emerged as cracking.

One of the objectives was to determine critical parameters that can be used in service life design concerning the active corrosion phase especially. These factors included critical corrosion penetration in regard of visual damage and the corrosion rate. The general corrosion rate for these structures can be regarded high after initiation. Thus, the average extension to service life during the active corrosion phase can be approximately 1–6 years in the most severe cases. This extension to

service life is considered relatively minor. However, these structures, which are facing southern directions, are subjected to the most severe weather. In structures more sheltered from wind-driven rain due to location, orientation or obstruction factors the extension in service life can be remarkably higher.

The statistical analysis of the condition investigation data of 947 buildings was used to confirm the representativeness of the more in-depth studies of 12 case buildings. A simple linear active corrosion phase model until visual damage on concrete surface was proposed defined by the onset by carbonation, an angle coefficient of corrosion rate and a defined limit state. A limit state for corrosion until visual damage i.e. critical corrosion penetration of 15–90 μm (depending greatly on reinforcement cover/diameter-ratio and the corrosion environment) was proposed for thin concrete facade panels.

References

- Ahmad S (2003) Reinforcement corrosion in concrete structures, its monitoring and service life prediction—a review. *Cem Concr Compos* 25(4–5 SPEC):459–471
- Al-Neshawy F (2013) Computerised prediction of the deterioration of concrete building facades caused by moisture and changes in temperature. Aalto University, Doctoral dissertations 96/2013, Helsinki
- Alonso C, Andrade C, Rodriguez J, Diez JM (1998) Factors controlling cracking of concrete affected by reinforcement corrosion. *Mater Struct* 31:435–441
- Andrade C, Alonso C (2001) On-site measurements of corrosion rate of reinforcements. *Constr Build Mater* 15:141–145
- Andrade C, Castillo A (2003) Evolution of reinforcement corrosion due to climatic variations. *Mater Struct* 54:379–386
- Broomfield J (2007) *Corrosion of Steel in Concrete*, 2nd edn. Taylor and Francis, Oxon, p. 277
- Concrete Association of Finland (2002) BY 42, condition assessment manual of concrete facades and balconies. The Concrete Association of Finland, Helsinki (in Finnish)
- Drits VA, Sakharov BA, Manceau A (1993) Structure of ferroxylite as determined by simulation of X-ray diffraction curves. *Clay Miner* 28(1993):209–222
- DuraCrete (2000) Probabilistic performance based durability design of concrete structures. The European Union—Brite EuRam III, DuraCrete. Final technical report of duracrete project, document BE95-1347/R17. CUR, Gouda, Nederland
- Fib Bulletin No. 34 (2006) Model code for service life design. International Federation for Structural Concrete, Lausanne
- Goltermann P (1994) Mechanical predictions on concrete deterioration part 1: Eigen stresses in concrete. *ACI Mater J* 91(6):543–550
- Gulikers J, Raupach M (2006) Numerical models for the propagation period of reinforcement corrosion: comparison of a case study calculated by different researchers. *Mater Corros* 57(8):618–627
- Huet B, L'hostis V, Santarini G, Feron D, Idrissi H (2007) Steel corrosion in concrete: determinist modeling of cathodic reaction as a function of water saturation degree. *Corros Sci* 49(4): 1918–1932
- Huopainen J (1997) Carbonation of concrete facades—a field study. MSc thesis, Tampere University of Technology (in Finnish)
- Huuhka S, Kaasalainen T, Hakanen JH, Lahdensivu J (2015) Reusing concrete panels from buildings for building: potential in Finnish 1970s mass housing. *Resour Conserv Recycl* 101:105–121

- Hyvert N, Sellier A, Duprat F, Rougeau P, Francisco P (2010) Dependency of C-S-H carbonation rate on CO₂ pressure to explain transition from accelerated test to natural carbonation. *Cem Concr Res* 40:1582–1589
- Jaffer SJ, Hansson CM (2009) Chloride-induced corrosion products of steel in cracked. Concrete subjected to different loading conditions. *Cem Concr Res* 39(2009):116–125
- Karthick S, Muralidharan S, Saraswathy V, Thangavel K (2014) Long-term relative performance of embedded sensor and surface mounted electrode for corrosion monitoring of steel in concrete structures. *Sens Actuators B* 192:303–309
- Köliö A, Pakkala TA, Annala PJ, Lahdensivu J, Pentti M (2014) Possibilities to validate design models for corrosion in carbonated concrete using condition assessment data. *Eng Struct* 75 (2014):539–549
- Köliö A, Niemelä P, Lahdensivu J (2015a) Evaluation of a carbonation model for existing concrete facades and balconies by consecutive field measurements. *Cem Concr Compos*. Available online 22 Oct 2015
- Köliö A, Honkanen M, Lahdensivu J, Vippola M, Pentti M (2015b) Corrosion products of carbonation induced corrosion in existing reinforced concrete facades. *Cem Concr Res* 78 (2015):200–207
- Lahdensivu J (2012) Durability properties and actual degradation of Finnish concrete facades and balconies. TUT Publ, Tampere University of Technology, p 1028
- Lahdensivu J, Varjonen S, Pakkala T, Köliö A (2013) Systematic condition assessment of concrete facades and balconies exposed to outdoor climate. *Int J Sustain Build Technol Urban Dev* 4 (3):199–209
- Law D, Claims J, Millard S, Bungey J (2004) Measurement of loss of steel from reinforcing bars in concrete using linear polarization resistance measurements. *NDT&E Int* 37:381–388
- Legodi MA, de Waal D (2006) The preparation of magnetite, goethite, hematite and maghemite of pigment quality from mill scale iron waste. *Dyes Pigm* 74(2007):161–168
- Lollini F, Redaelli E, Bertolini L (2012) Analysis of the parameters affecting probabilistic predictions of initiation time for carbonation-induced corrosion of reinforced concrete structures. *Mater Corros* 63:1059–1068
- Mattila J (2003) On the durability of cement-based patch repairs on Finnish concrete facades and balconies. TUT Publ., Tampere University of technology p 111, 450
- Monteiro I, Branco FA, de Brito J, Neves R (2012) Statistical analysis of the carbonation coefficient in open air concrete structures. *Constr Build Mater* 29:263–269
- Neves R, Branco FA, de Brito J (2012) A method for the use of accelerated carbonation tests in durability design. *Constr Build Mater* 2012(36):585–591
- Neves R, Branco FA, de Brito J (2013) Field assessment of the relationship between natural and accelerated concrete carbonation resistance. *Cement Concr Compos* 2013(41):9–15
- Otieno M, Beushausen H, Alexander M (2011) Modelling corrosion propagation in reinforced concrete structures—a critical review. *Cem Concr Compos* 33(2011):240–245
- Page CL (1988) Basic principles of corrosion. In: Schiessl P (ed) *Corrosion of steel in concrete*. Chapman and Hall, London, pp 3–21
- Parrott LJ (1987) A review of carbonation in reinforced concrete. *Cem Concr Assoc*, Slough
- Rodriguez P, Ramirez E, Gonzalez JA (1994) Methods for studying corrosion in reinforced concrete. *Mag Concr Res* 46(167):81–90
- Siemes AJM, Vrouwenvelder ACWM, van den Beukel A (1985) Durability of buildings: a reliability analysis. *Heron* 30(3):3–48
- Stern M, Geary A (1957) Electrochemical polarization, I. A theoretical analysis of the shape of polarization curves. *J Electrochem Soc*, pp 56–63
- Thiery M, Villain G, Dangla P, Platret G (2007) Investigation of the carbonation front shape on cementitious materials: effects of the chemical kinetics. *Cem Concr Res* 37:1047–1058
- Tuutti K (1982) Corrosion of steel in concrete. CBI research, Stockholm. Swedish Cement and Concrete Research Institute 4, 82:304

Biocementation as Rehabilitation Technique of Porous Materials

Rafaela Cardoso, Rita Pedreira, Sofia Duarte, Gabriel Monteiro,
Hugo Borges and Inês Flores-Colen

Abstract The main findings when using microbially induced calcite precipitation, MICP, in two case-studies, a sandy soil and a mortar surface, are presented. The first case is focused on studying biocementation in sands to improve their mechanical properties. Tests were carried out with the aim to check the biological activity and understand MICP effects on a porous medium. By visual inspection it was possible to see the presence of calcite in the top of the specimens confirming that this type of treatment is mainly superficial and must be improved to be more uniform in depth. In the second case, biodeposition was tested in order to understand how it would affect the main properties of porous cement mortar such as elastic stiffness, capillarity coefficient, water vapour permeability, roughness and open porosity. These properties are relevant mainly for walls. Treatment was applied in mortar specimens by submersion in the treatment solutions during the first 28 days of curing. The results were compared with those found in similar tests performed in samples which were not subjected to treatment, which were submerged in tap water or cured in wet environment. These different porous media are

R. Cardoso (✉) · I. Flores-Colen
CERIS/ICIST, Instituto Superior Técnico, Lisbon, Portugal
e-mail: rafaela@civil.ist.utl.pt

I. Flores-Colen
e-mail: ines.flores.colen@ist.utl.pt

R. Pedreira · H. Borges
Instituto Superior Técnico, Lisbon, Portugal
e-mail: rita_pedreira@hotmail.com

H. Borges
e-mail: hugooborges@hotmail.com

S. Duarte · G. Monteiro
IBB, Instituto Superior Técnico, Lisbon, Portugal
e-mail: sofia.duarte@ist.utl.pt

G. Monteiro
e-mail: gabmonteiro@ist.utl.pt

used as example of the improvement that can be achieved using this technique to treat volume or area. Considerations are done concerning the extrapolation of the results for other porous materials used for Civil engineering applications in the context of rehabilitation and how this technique could be implemented in the construction sites.

Keywords Biocement · Bacteria · Rehabilitation · Protection · Porous media

1 Introduction

Biocement is a mineral produced by biological activity, which precipitates in the porous medium changing its properties. The most common mineral is calcium carbonate (CaCO_3) and is precipitated during the hydrolysis of urea made by microorganisms (mainly bacteria). This process is called microbially induced calcite precipitation, MICP. Several species of bacteria can be used for this purpose, being their choice dependent mainly on the result intended and if the conditions necessary for the occurrence of precipitation are ensured for that particular case.

Firstly some applications of MICP in Civil engineering applications are described, followed by a brief overview on the principles of biocementation. Then, the main findings when using MICP in two case-studies, a sand and a mortar surface, are presented. These different porous media are used as example of the improvement that can be achieved using this technique to treat volume or area of materials. Considerations are done concerning the extrapolation of the results for other porous materials used for Civil engineering applications in the context of rehabilitation.

2 MICP in Civil Engineering Applications

The first studies on biocementation started at the end of last century and several bacteria were investigated for different applications. The studies were focused mainly in the conditions necessary to promote and control their activity for different purposes. In the scope of Civil engineering, MICP has been used mainly for treating construction materials such as stones and concrete, for cementation of soils or for environmental purposes (Inanov et al. 2015; DeJong et al. 2013).

The deposition of the biocement on surfaces (calcite layers with few micrometers thick) is called biodeposition, while when it reaches depth for consolidation it is called biocementation. In the first case a protective homogenous surface with reduced permeability and providing strength to weathering is created, eventually sealing joints. In the second case particles are bonded and therefore stiffness and strength of the porous medium increase and water vapour permeability decreases.

The effects on the engineering properties of the medium due to porosity reduction are proportional to the thickness and homogeneity of the layer of calcite precipitated (Phillips et al. 2013).

In case of superficial treatment, biocementation is being used in mortars, in concrete (Ramachandran et al. 2001; De Muynck et al. 2008a, b, 2010; Achal et al. 2013; Pacheco-Torgal and Labrincha 2013; Vempada et al. 2011; Dhami et al. 2012a; Ghosh et al. 2005, 2006, 2009; Emmons and Sordyl 2006; Abo-El-Enein et al. 2013) and in porous stones such as limestone, calcarenites and marble (Jimenez-Lopez et al. 2007, 2008; Fernandes 2006; Dick et al. 2006; Tiano et al. 2006; Rodriguez-Navarro et al. 2003; Le Metayer-Levrel et al. 1999). Besides providing impervious coating or coating against weathering (Li and Qu 2012; Achal et al. 2010, 2011; Siddique and Chahal 2011), in case of concrete this technique can also delay steel corrosion and be used to seal cracks and fractures caused by aging and weathering (De Belie and De Muynck 2008; Van Tittelboom et al. 2010). Studies had also been done on using this technique for brick production (Raut et al. 2014; Dhami et al. 2012b). The use of bacteria in fresh concrete to create self healing materials is a quite recent and promising investigation topic (Jonkers 2007; Jonkers et al. 2010; Wang et al. 2012). Most of the studies from the literature concern laboratorial tests, however there are already some cases when MICP technique was tested in structures. Such is the case described by Wiktor and Jonkers (2011), where this technique showed good results sealing the joints of a concrete slab in a parking, or by Cuthbert et al. (2013) in fractured rock.

Calcite precipitation in soils has been widely investigated by several authors aiming to study the most adequate ways to perform the treatment based in its effects on the engineering properties of the soils (Al Qabany and Soga 2013; Al Qabany et al. 2012). Biocementation can be used for soil reinforcement for foundations, or to prevent internal erosion in earth dams (piping) and the destruction of dikes in the occurrence of natural disasters such as floods and storms at sea (Chu et al. 2013; Ivanov et al. 2014; Stabnikov et al. 2011; Van Paassen et al. 2010a). It also can be a good solution to treat soils with a high potential for liquefaction (DeJong et al. 2006; Montoya et al. 2013). There are also other applications mentioned in the literature, such as soil strengthening during tunnels excavation in sands or for drilling sands in the ocean for oil and natural gas extraction (Latil et al. 2008). As far as the authors know, two large scale tests were performed in sands showing still some limitations (Van Paassen et al. 2010b; Gomez et al. 2015).

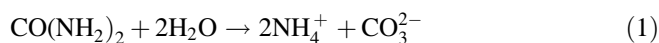
The studies mentioned show that this technique is able to consolidate materials with a wide range of pore sizes. Apparently the treatment can be applied along surfaces, resulting in homogeneous layers, or can be locally applied, for example for sealing joints. Such versatility is necessary in the rehabilitation of porous materials. However some other aspects must be considered, such as the compatibility between the biomaterial and the material to be treated, and the final mechanical and physical properties of the treated material. The work presented is focused mainly on investigating the conditions for treatment application and how it affects the engineering properties of two different porous materials relevant for their specific uses.

3 Principles of Biocementation

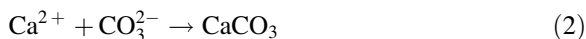
Several species of bacteria can be used for this purpose (for example *Bacillus cereus*, *Bacillus sphaericus*, *Bacillus pasteurii* or *Sporosarcina pasteurii*, *Myxococcus xanthus* and *Shewanella*). The choice depends mainly on the result intended and if the conditions necessary for the occurrence of precipitation are ensured for that particular case. In fact, it is necessary to control pH and temperature, as well as the type and chemical concentrations of nutrients supplied, retention times and input rates (Al Qabany and Soga 2013).

The bacterial species used in the present investigation is *Bacillus pasteurii* acquired from ATCC (American Type Culture Collection, strain #11859). This microorganism is non-pathogenic and exists naturally in soils and in all environments where urea can be found (bathrooms, for example) because it is quite resistant to external chemical and physical actions. Optimum conditions for growing are pH between 8 and 9 and temperature closer to 36 °C in the growing medium.

The precipitation of calcium carbonate results from the hydrolysis of urea ($\text{CO}(\text{NH}_2)_2$), which is catalysed by the enzyme urease. The equation for this chemical reaction is Eq. 1:



The ammonium (NH_4^+) released from urea hydrolysis results in pH rise and promotes the precipitation of calcium carbonate (CaCO_3). This is calcite and results from the combination of carbonate ions (CO_3^{2-}) from the hydrolysis of urea and the calcium ion (Ca^{2+}) supplied in the feeding solution, as described by Eq. 2.



The process of growth of *B. pasteurii* was performed in liquid medium composed by 20 g yeast extract (YE), 10 g of ammonium sulphate ($(\text{NH}_4)_2\text{SO}_4$), 0.13 M Tris buffer with pH 9.0. The bacteria were grown to an optimal density at 600 nm (OD_{600}) = 1 on this NH_4 -YE medium at 37 °C under aerobic condition. This corresponds to the concentration of 10^9 cells/ml. The feeding solution was prepared with 0.5 M of urea, 0.5 M of calcium chloride CaCl_2 to provide calcium ions, and 1:10 diluted culture medium, 2 g/l of YE, 1 g/l of ammonium sulphate $(\text{NH}_4)_2\text{SO}_4$, 10 g of ammonium chloride NH_4Cl and 2.12 g of sodium bicarbonate NaHCO_3 . It is worth to note that the reagents of the feeding solution can form calcium carbonate independently from the presence of the microorganisms; however in their presence the reaction is much faster and for this reason MICP is more efficient than just add the reagents.

4 Case Study 1—Biocementation in Sands

The first case presented is focused on studying biocementation in sands to improve their mechanical properties. Tests were carried out with the aim to check the biological activity and understand MICP effects on the porous medium. Specimens of non-plastic sand were prepared and treated with *B. pasteurii*. By visual inspection it was possible to see the presence of calcite in the top of the specimens confirming that this type of treatment is mainly superficial and must be improved to be more uniform in depth.

4.1 Experimental Setup

The MICP treatment performed in sands consisted of mixing the soil with bacteria and, after compacting it in a mould, feeding was done once a day for 10 days. The soil was not sterilized before the bacteria inoculation to mimic natural conditions.

The soil studied is a non-plastic sand with pH 7.0 and particle density $G_s = 2.64$. Samples were prepared with a dry volumetric weight of 17.9 kN/m^3 , a value found in situ for this type of soil. The corresponding void ratio is 0.475 (relationship between volume of voids and volume of solids), being total porosity equal to 32.2 % (found using the definition of porosity). To understand if grading size distribution has influence in MICP, two different grading size distributions, G1 and G2, were studied: G1 is an almost uniform grading size distribution, with diameters between 0.425 and 0.075 mm; G2 is a well graded sand having particles larger than 4.75 mm and 12 % of fines (material with diameter smaller than 0.075 mm). The total porosity is the same for both being the only difference the pore size distribution.

Three types of specimens were investigated for each grading size distribution considered: specimens with bacteria, prepared with soil and culture medium with known quantity of bacteria; specimens for control, prepared with soil and culture medium without bacteria; and soil specimens, prepared with soil and water. The control samples are necessary to understand if the biocement found in the treated soil results from bacterial activity, or only from chemical reaction between the reagents in the feeding solution. Soil samples were prepared only for comparison purposes, as they represent the absence of calcium carbonate independently from its origin.

All specimens were compacted in PVC cylindrical moulds (3.24 cm diameter and 12.72 cm height). The soil was compacted to have final height of 6.5 cm. The upper 3 cm of the mould worked as a reservoir for the feeding fluid. The bottom of the mould included a drainage system made of a collector chamber with 3 cm high and a silicon drain tube with 6 mm diameter, connected to a container where the volume extracted from the soil was measured. A filter made of a metallic grid and



Fig. 1 Moulds and drainage system inside the incubator

filter paper was placed in the bottom of the sample separating it from the drainage system. Metallic tweezers were used to regulate the output of the purging fluid.

Each sample was prepared with 95.87 g of soil mixed with 20 ml of medium with bacteria or of culture medium or of tap water. The specimens prepared with bacteria and for control were fed daily, by introducing 20 ml of liquid with nutrient in the top of the mould. Fluid circulation was ensured by purging 20 ml of liquid from the bottom. For the cases when *B. pasteurii* were used, and also for the control samples, the moulds were kept at constant temperature of 30 °C, as shown in Fig. 1. The relative humidity of the air was not important because the treated volume was submerged in the feeding solution.

The tests carried out were the following: durability tests, scanning electron microscopy (SEM), tests to quantify calcium carbonate (calcite) in the samples and mercury intrusion porosimetry tests. They will be described next.

4.2 Effects of Biocementation in the Porous Medium

From visual inspection it was possible to see the presence of calcite in the top of the specimens prepared with bacteria because there was the formation of a whitish zone with approximately 3 cm height, stiffer than the bottom part of the sample. This result confirms that this type of treatment is mainly superficial and must be improved to be more uniform in depth. For soils this can be achieved by improving the feeding system, maybe by injection in depth.

The upper part of these specimens was observed in SEM microscope in order to detect bacterial activity. The photographs in Fig. 2 from a sample air dried for more than 24 h show the presence of a biofilm, which indicates biological activity. This layer acts as a protective hydrated barrier between bacterial cells and the

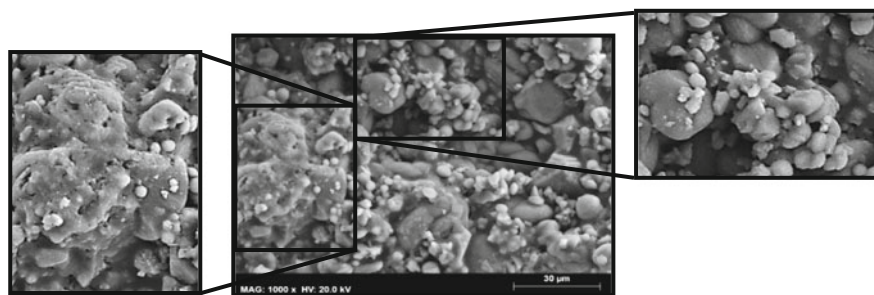


Fig. 2 SEM photographs showing the biofilm (*left*) and spheres of calcite (*right*)

environment. Spherical crystals were also observed, which are typical of calcite produced by *B. pasteurii* (Stocks-Fischer et al. 1999), and therefore it can be concluded that bioceMENT was produced. The presence of calcium in these minerals was confirmed by Energy-dispersive X-ray spectroscopy (EDS) analysis performed in other samples also observed in SEM microscope.

No biofilm was detected in the photographs taken to the samples for control, but the presence of calcite minerals was also observed both in the formation of a stiffer layer and at SEM. The presence of calcium carbonate was quantified at the end of the treatment in specimens prepared with bacteria and in control specimens to understand if biological activity was more effective than the chemical reaction of the reagents of the feeding solution.

A leaching test was performed (1:10 proportion in 5 % hydrochloric acid medium, during 24 h with continuous shaking). The analysis was performed in similar volumes taken from the top of the specimens after being dried for 24 h under 100 °C. The results found for the two grading size distributions studied are shown in Table 1 in terms of mass of calcite in total mass of treated soil and mass of calcite in total volume of soil (bioceMENT dosage). The presence of calcite can be seen in all cases. However it is much larger for the cases where bacteria were introduced. The results confirm the chemical reaction naturally occurring in the feeding solution but the presence of bacteria triples the amount of bioceMENT (3.18 times larger for G1 and 3.53 times for G2) and therefore the treatment can be considered to be efficient. The dosages found are within the ranges found by other authors (Al Qabany and Soga 2013).

Simple tests were performed to check the durability of the bioceMENT formed in the process. The samples, taken from the top 5 cm of the specimens, were submerged in water during more than one month (Fig. 3). The base of the samples was

Table 1 Results of chemical analysis for measuring CaCO₃

	G1		G2	
	Bacteria	Control	Bacteria	Control
g/kg	35.0	11.0	46.0	13.0
kg/m ³	62.7	19.7	82.3	23.3

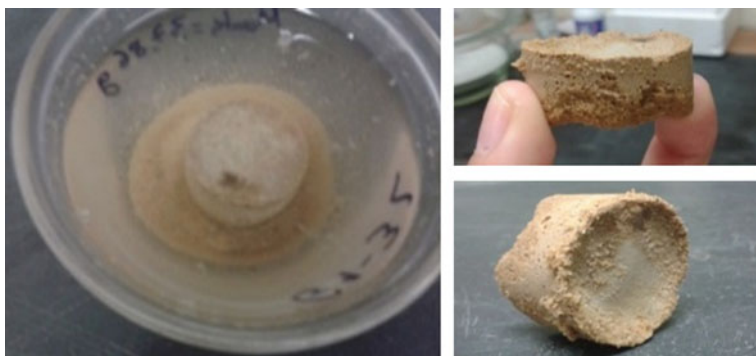


Fig. 3 Submersion test and the stiff aspect of the specimens after one month (G2)

crumbling over submersion time, as it occurs for un-cemented sand, but the upper 2–1.5 cm height part remained intact and stiff at the end of this period, even saturated. A hand crushing test revealed high strength and it was not easy to detach material with the finger nails. Similar results were found for both grading size distributions studied and when calcite was detected.

Strength and stiffness increase because the calcite formed binds the grains (see Fig. 2) and creates bonds when it accumulates forming continuous layers. This mechanism is schematically presented in Fig. 4. This figure also includes a SEM photograph taken to a G1 specimen where the calcite spheres and their contribution to cohesion between the grains due to the presence of bonds is evident.

Calcite fills the empty pores, and for this reason it is expected the reduction of porosity, and consequently permeability and water absorption reduction. The percolation of the food fluid stopped at the end of few days of test and confirms this mechanism. Figure 5 presents the results of mercury intrusion porosimetry (MIP) tests for grading size distribution G1 performed to confirm the changes in pore size distribution due to calcite formation.

The plot for the natural soil was estimated considering its grading size distribution. For the soil without treatment the dominant diameter (highest peak) is

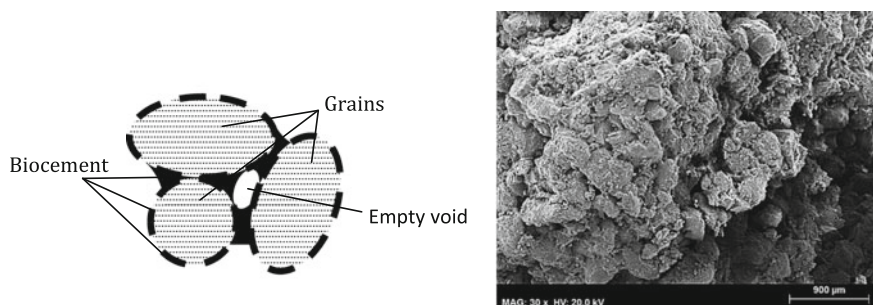
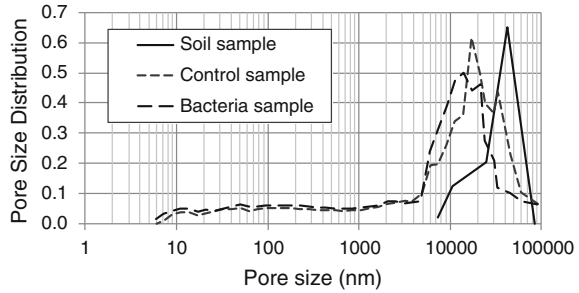


Fig. 4 Biocement binding and bonding the grains: schema (*left*) and SEM photograph (*right*)

Fig. 5 MIP results for G1 specimens



around 42.0 μm . This diameter decreases to 19.0 μm for the control samples and to 14.5 μm for the sample treated with *B. pasteurii*. This result is in accordance with data from Table 1, as the pores become filled with calcite and their size reduce while the amount of this mineral increases.

4.3 Laterally Confined Compressibility Tests

Two laterally confined compressibility tests were performed in an oedometric cell with 5 cm diameter and 2 cm high in order to quantify stiffness earned due to biocementation. The tests were performed on one specimen of sand treated with bacteria (voids ratio of 0.319 after the treatment) and on another specimen untreated (initial voids ratio of 0.310 to be similar to that of the treated specimens). The dry density of the sample before treatment was around 0.47, which is similar to that of the samples previously presented. It was reduced due to the presence of calcite filling the voids between the grains of sand. After the treatment the voids ratio was computed assuming identical solid density for the sand grains and calcite. Only the grading size distribution G1 was studied in this preliminary test.

The dosage of bacteria used was identical to those adopted for the other tests. Treatment period in this case was 40 days, keeping the specimens inside the oedometric rings. The feeding solution was in contact with the soil by the top and bottom porous stones. After this period this solution was exchanged by distilled water. The untreated specimen was tested full saturated with distilled water.

Identical stress paths were applied in the two tests. They included one unloading-reloading cycle in order to evaluate possible changes in elastic stiffness. Stress increment in each step doubled that of the previous until reaching 1200 kPa. Unloading cycles were applied under 100 and 400 kPa (minimum stress 12.5 kPa), followed by final unloading at 1200 kPa. Both compressibility curves are presented in Fig. 6. The compressibility index C_c and recompressibility index C_s measured in all unloading cycles are presented in Table 2 for the two tests.

It can be seen in Fig. 6 and in Table 2 that the compressibility index is very similar for both cases. This can be explained by the similar voids ratio of the samples preparation. For the untreated sample the values of the recompressibility

Fig. 6 Compressibility curves (G1)

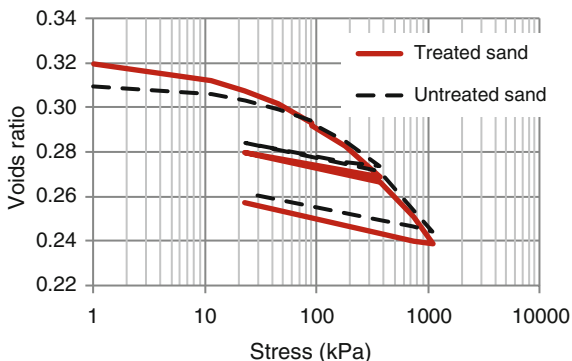


Table 2 C_c and C_s measured for the two tests

		Untreated sand	Treated sand
C_s	1st cycle	0.009	0.009
	2nd cycle	0.009	0.013
C_c		0.057	0.058

index is constant, while it increases with vertical stress at unloading. It is expected constant values because elastic stiffness remains unchanged in soils as long as there is no grain crushing. Such is the case expected for the sand studied and maximum vertical stresses applied during the test. However for structured materials, or when damage occurs such as cracks in concrete, it is well known that elastic stiffness decreases and this is observed for the treated material, even if slightly.

This result confirms that biocementation has effects on the material mechanical properties. The presence of the biocement connecting the grains was not evident during compression because the connections are punctual (see Fig. 4). However some of these connections were broken during loading and for this reason there were irreversible changes that have affected the elastic behaviour of the material (observed only at unloading). However these effects are not very evident because the treatment was performed in the absence of vertical stress, and for this reason bond breakage on stress release was not as evident as it should be expected.

To conclude, the treatment appeared to be homogeneous in the entire sample volume at the end of the test.

4.4 Main Conclusions from Case-Study 1

The main conclusions from this case-study are the following:

- MICP treatment was effective for the two sands studied because total porosity decreased and the formation of biocement providing stiffness and strength was evident, even by visual analysis of the samples extracted from the PVC tubes.

- In these samples the biocement was concentrated mainly at the top of the treated samples. It was very difficult to achieve homogeneous treatment in the entire volume because the injection solution was not percolating through the sample.
- The changes in elastic compressibility observed in the oedometer tests also had shown the formation of biocement, even considering the differences in the treatment conditions applied in these tests and in the PVC molds.
- In the oedometer rings it appears that the treatment was homogeneous in the entire volume, maybe due to the small length of the samples and hydraulic boundary conditions of the test.

Comparing the results found using the PVC moulds and the oedometer rings it can be concluded that it is difficult to have a homogeneous treatment in the entire volume of soil. Other authors have found similar results (Van Paassen et al. 2010b). This result leads to the next case study, in which the treatment was applied in area instead of in volume.

5 Case-Study 2: Biodeposition in Mortar Surfaces

In this case-study, biocementation technique was tested on a porous surface of mortar. A novelty was introduced, which is the use of enzyme urease instead of bacterial cells. This idea intends to simplify logistics when applying bacteria in a construction site, since the schedules are not directly dependent on living beings and bacteria require environmental conditions and feeding schedules that may introduce delays and complexity to this treatment.

5.1 Experimental Setup

Biocementation treatment was tested in order to understand how it would affect the main properties of porous cement mortar such as elastic stiffness, capillarity coefficient, water vapour permeability, roughness and open porosity. Bacteria, enzyme urease and the feeding solution (control test) were used as treatment media of the naturally porous surface. Treatment was applied by submersion in these solutions during the first 28 days of curing. The results were compared with those found in similar tests performed in samples which were not subjected to treatment, which were submerged in tap water or cured in wet environment. The mechanical, physical and surface laboratory tests necessary for the characterization of the improvements achieved were performed after these 28 days.

During the treatment the samples were submersed in the curing solutions after being unmolded, at the end of the third day. The containers were kept in a room with controlled temperature of 30 °C. They were turned everyday and the containers were

Table 3 Dimensions and tests performed on mortar specimens

Tests	Dimensions (cm ³)	Euro standard
Ultrasonic waves propagation velocity	2 × 2 × 8	EN-12504-4
Dynamic modulus of elasticity	2 × 2 × 8	ASTM E1876
Capillary water absorption	2 × 2 × 8	EN-1015-18
Water vapour permeability	4 × 4 × 1	EN-1015-19
Surface roughness meter	2 × 2 × 8	–
Observation using optical microscope	2 × 2 × 8	–
Scanning electron microscope photographs	Fragment	–
MIP	Cylinder h = 1 cm Diameter = 1 cm	–

oscillated continuously at low speed to mix the feeding solution and allow calcite deposition in all faces of the specimens.

Mortar specimens were produced following the European standard EN 1015-2, with distinct dimensions defined in accordance with the type of laboratory tests to be performed. Volumetric ratio cement: sand adopted was 1:4, with water-cement ratio of 1:1. Average density in fresh state was about 1623.24 and 1613.30 kg/m³ when producing the mortar for the treated and untreated specimens, respectively. Cement Portland CEM II/B-L 32.5 N was used. The dimensions adopted for the samples for each test and the respective standard are in Table 3.

Visual inspection using microscope and porosity through mercury intrusion porosimetry (MIP) tests were performed aiming to check how treatment would affect the surface of the specimens, which dimensions are also in Table 3. Three samples of each type of cure were investigated.

Table 4 presents the average values found for the bulk densities in hardened state for each geometry and for all cases (respectively ρ and ρ_{all}). They are not very different and may be explained by the different productions of mortar for the treated and untreated specimens.

Table 4 Bulk densities for the different geometries of the samples in the hardened state after 28 days of curing

Geometry	Treated samples		Untreated samples	
	ρ (kg/m ³)	ρ_{all} (kg/m ³)	ρ (kg/m ³)	ρ_{all} (kg/m ³)
2 × 2 × 8	1893.1 ± 27.9	1881.5 ± 35.4	1840.1 ± 27.7	1839.1 ± 15.7
4 × 4 × 1	1909.7 ± 42.7		1854.2 ± 20.4	
4 × 4 × 4	1841.8 ± 14.9		1822.9 ± 26.9	

5.2 Curing Fluid Effect on Mortar

Scanning electron microscopy (SEM) photographs were taken to the samples after treatment. The fragment pieces analyzed were taken from the surface. This analysis aimed to see if there would be calcite at the surface and also to understand if the different solutions used in submerged cure, including their pH 9 for the treated samples, would significantly affect the hydration of cement minerals. The photographs are shown in Fig. 7.

Spherical structures characteristic of biological activity are observed in Fig. 7a–c similar configurations were observed by others in soils (De Belie and De Muynck 2008). These shapes contrast with crystals having hexagonal shapes visible in Fig. 7d, e. These structures are crystals of calcium hydroxide from the hydration of cement. Such crystals are covered by a homogeneous layer when cure is done by submersion in water (see Fig. 7d).

All samples, independently from being treated or not, show the presence of other structures similar to spider webs. They correspond to calcium aluminium silicates (C-S-H), crystals typical of Portland cement hydration. Possibly the nail shapes observed for the treated specimens in Fig. 7a is explained by the high pH during curing (Van Tittelboom et al. 2010). This last observation confirms that the different curing conditions may not have significant effect on mortar and for this reason the treatment effects are not expected to affect volumetric behaviour but only surface. The remaining results can be compared considering mainly the creation of artificial minerals from calcite.

The elastic stiffness of the different samples was evaluated using two non-destructive techniques: (i) by measuring ultrasonic wave velocity and (ii) by using an apparatus which measures the vibration frequency of a material and

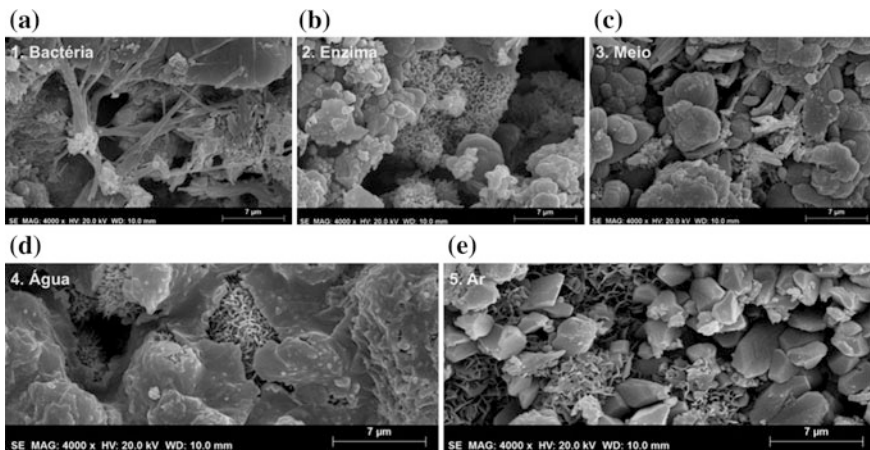
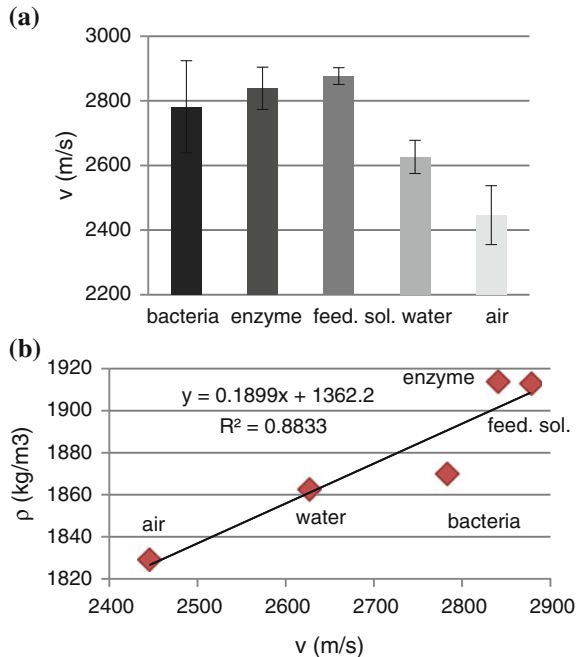


Fig. 7 Scanning electron microscopy photographs: **a** bacteria; **b** enzyme; **c** feeding solution; **d** water and **e** dry chamber

Fig. 8 Results of the ultrasonic waves propagation velocity test: **a** error bars show the standard deviation; **b** relationship between density ρ and velocity v



provides its elastic parameters such as Young modulus E, shear modulus G and Poisson coefficient.

The velocity of elastic wave propagation was computed following the standard procedure. The average values for the velocities are presented in Fig. 8a for each type of cure. The values found for the treated specimens are larger than those found for the untreated ones. However, because the treatment is superficial, these differences may be explained by the different densities of the specimens due to the fact that the mortars came from different productions. Such relationship is presented in Fig. 8b and confirms that the highest stiffness found are related with the higher densities found for these specimens. Nevertheless, for all productions similar results were found in the tests performed in fresh state and therefore it is possible that the different porosities might have been cause by the curing conditions.

The results found for each type of cure are presented in Table 5 when the other equipment was used for measuring the elastic properties of the material (ASTM E18769). The average and standard deviation of the results are included in this table, as well as Poisson coefficient ν .

Accordingly, with Table 5, higher values of E were registered on samples subjected to cure with treatment, in particular for the treatment with enzyme. It becomes difficult to draw absolute conclusions about G because there is certain dispersion. These results are in accordance with those found when analyzing ultrasonic waves velocity presented in Fig. 8. Indeed, this treatment is expected to be a surface treatment and the mechanical properties evaluated reflect the entire volume.

Table 5 Results of the dynamic module of elasticity test. E—young modulus, G—shear modulus of elasticity, σ —standard deviation, ν —Poisson coefficient

	E (GPa)	G (GPa)	ν
Bacteria	11.9 ± 0.3	2.7 ± 0.1	0.2
Enzyme	13.2 ± 0.3	4.4 ± 1.3	0.3
Feeding solution	11.8 ± 0.2	3.6 ± 1.3	0.2
Water	10.5 ± 0.2	2.3 ± 0.2	0.2
Air	8.7 ± 0.8	3.0 ± 0.8	0.2

5.3 Treatment Effect on Water Absorption Characteristics

The coefficient of water absorption by capillarity and the resistance coefficient to water vapour diffusion were measured to evaluate how treatment would affect these basic properties of mortars. The curves for the water absorption by capillarity are presented in Fig. 9. These correspond to the average values obtained considering the three specimens of each type of cure.

The absorption curve of the specimens subjected to cure on dry chamber present sharp slope of the initial straight when compared with other samples. The average values of the coefficients of water absorption by capillarity measured, C (slope at the origin), as well as standard deviation, σ , are presented in Fig. 10a.

It can be observed that all the treated samples present coefficients of capillarity lower than those measured for the reference samples. However, for the treated samples those subjected cured with bacteria have the highest coefficient of capillarity. This fact can be explained by water absorption by the bacteria in the initial moments. This can occur when bacteria are exposed to high temperatures (60 °C in this case, during drying before the test) because water is removed from them during drying but they reabsorb it when in contact with this fluid. This test provides an acceptable degree of reliability due to the reduced values of standard deviation found.

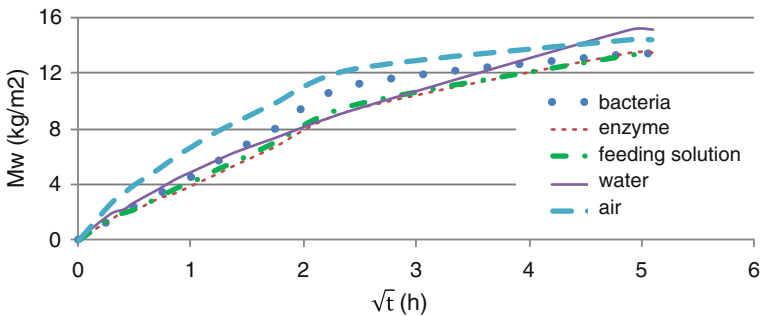
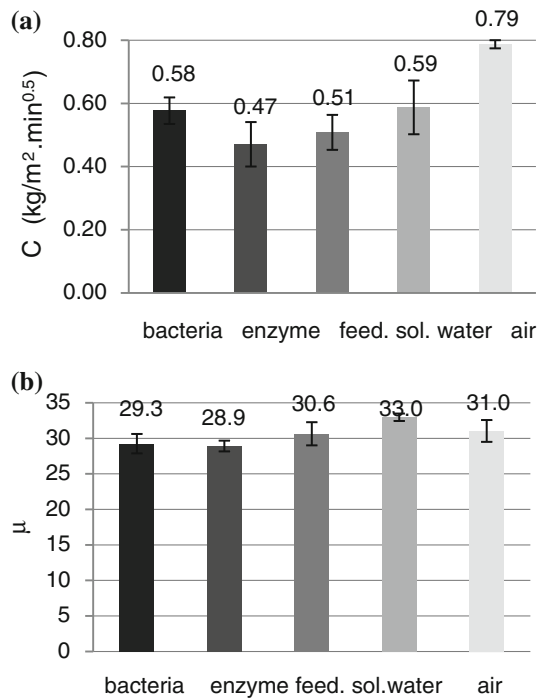


Fig. 9 Water absorption by capillarity curves

Fig. 10 Results of the tests: **a** water absorption by capillarity; **b** water vapour permeability test



The coefficient of resistance to water vapour diffusion (μ) is a dimensionless parameter that best evaluates the ability of a porous material to allow diffusion of water vapour. The values found for each type of cure (average value) are shown in Fig. 10b.

In Fig. 10b it is possible to observe that the coefficient of resistance to water vapour diffusion has the same order of magnitude in all samples. This means that upon the application of biodeposition on a coating mortar the material will not affect drying. Although the resistance values of coefficient of water vapour diffusion are identical. Those found for the samples treated with enzyme are lower. This may mean that the specimens subjected to this treatment allow better natural drying in the mortar.

5.4 Pore Size Distribution

Mercury intrusion porosimetry tests confirmed the appearance a material with larger pores superimposed to the pores already existing. The curves are presented in Fig. 11a.

For the untreated sample studied the largest number of pores has a diameter of 2480 nm, whereas for the treated samples the largest number of pores have diameter

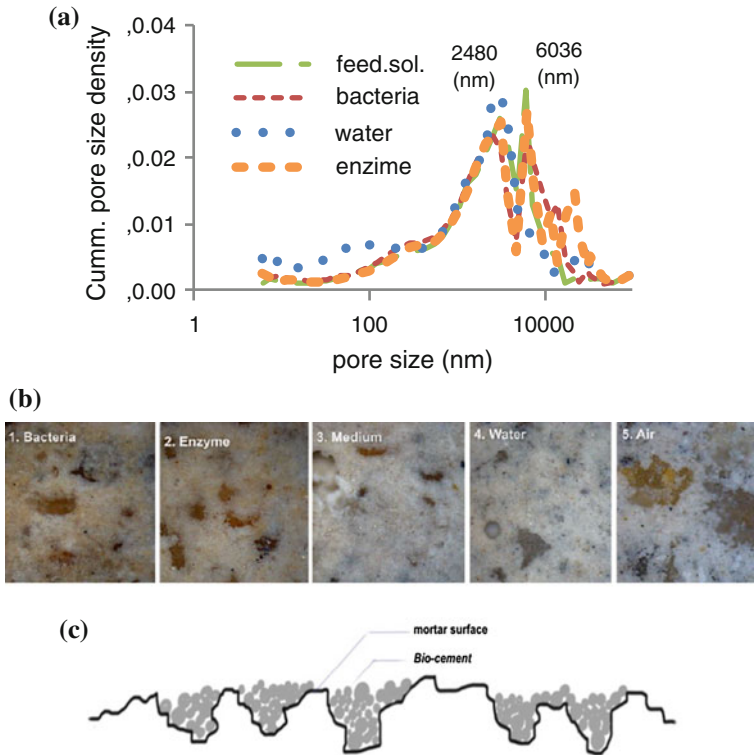


Fig. 11 Evidence of formation of a porous coating: **a** pore size distribution; **b** photographs of the different surfaces; **c** scheme of deposition of calcite above the surface

around 6030 nm. Some of the pores with diameter 2480 nm have lost importance in all existing pores in the sample; however a new pore diameter corresponding to 6030 nm earned importance. These results are consistent with the presence of a coating resulting from the treatment, being a rough layer which does not clogs the large pores but eventually can create new pores, larger than those existing in the mortar.

It is believed that the coating from the treatment is a rough layer which does not clogs the large pores but eventually can create new. Evidence of this coating is found when the different specimens are observed using optical microscope. Some photographs are shown in Fig. 11b. It can be noted that the grains of sand are covered with smaller grains for the treated samples, showing a slightly yellowish colour, while the boundaries of the grains of sand are perfectly marked in the untreated specimens and the general colour is grey. This result indicates that the biocement coats the mortar but this coating is porous and not homogeneous in the surfaces. Figure 11c presents a scheme illustrating this effect.

5.5 Conclusions from Case-Study 2

The results from the research presented confirm that biodeposition occurred and had some effects on mortar surfaces. The main conclusions are highlighted as follows:

- The procedures adopted did not affect much the hydration of cement minerals and therefore the mechanical properties of the mortar were not different for the treated and untreated cases.
- The biotreatment appears to reduce the coefficient of water absorption by capillarity on current mortars. Thus, it is expected that a mortar treated with bacteria or with enzyme, in service, absorbs less amount of water in liquid phase than a current cement mortar.
- There was a decrease in the coefficient to resistance to water vapour diffusion (drying is easier) for the treated specimens, in particular when using enzyme.
- The changes observed in the physical properties investigated can be explained by the precipitation of calcite, or biocement, which may have clogged some voids on the mortar surface. This corresponds to the formation of a porous coat, confirmed by MIP tests.
- From the observations in optical microscope it could be seen that calcite precipitates essentially on existing voids on the surface of the mortar, and for this reason this coating layer is not continuous. This result shows that biodeposition is more adequate to be applied in localized flaws instead of in surfaces.

To conclude, the presence of the calcite coat, by one hand, increases the rate of water vapour diffusion, but by the other hand reduces the absorption of liquid water. For coating materials it is desired to have balance between absorption and drying speed rates, and for this reason calcite may be a suitable coating material. Moreover, because it is not an waterproofing coating, it will not introduce undesired hydraulic gradients in the contacts with original surface. For this reason, biodeposition may be adequate for consolidating old materials and very porous surfaces.

6 Rehabilitation Using MICP

The studies performed allowed learning about the rehabilitation of porous surfaces using MICP technique. In order to implement this technique in field applications, the first step for the application on an industrial scale of this repair procedure is to conduct both laboratory and in situ applications studies. The use of the enzyme as treatment may be better than using bacteria, because enzyme is easy to be produced at a large-scale and stored with activity and it was proved that this type of treatment has even better efficiency than the direct use of bacteria.

Similar to the difficulty to get a homogeneous treatment in the volume of treated soil, for the surfaces the layer of biocement must be continuous and have controlled thickness in the entire area to ensure its effective protection. For the particular case

of porous surfaces with flaws, the treatment must be superficial but also should penetrate in depth and close the flaws. The process of adding the bacteria and feeding solution are fundamental for this purpose. Both bacteria and feeding solution can be spread in liquid phase along the area as long as the thickness of the liquid film is controlled during the process and the entire area becomes soaked to ensure some penetration in depth. The alternative to spray, followed by some authors, is to submerge the elements to be treated in the liquid containing bacteria and feeding solution, but this is not possible for facades.

The optimal conditions for the activity of the microorganisms must be ensured because the survival of the bacteria depends on keeping pH and temperature constants and within specific intervals. This may not be very important for soils because this media naturally favour the development of such kind of bacteria and therefore feeding is what is important. However, for the surfaces the biofilm must be protected from atmospheric agents and external actions (animal and human action, among others) and therefore it is desirable to protect it with plastic layers, clay or mortar during the treatment. Adding to this, the biofilm must also have conditions to get attached to the surface, which is generally ensured by natural roughness.

Concerning the monitoring of the process, it is expected to be easier in case of surfaces because they are more accessible than the interior of the soil (unless excavation is made). This can be a disadvantage as well because accessibility can lead to interaction with living organisms and call the attention of the public, eventually raising concerns about toxicity and if there are pathogenic effects.

Finally, in opposition with the case of MICP in soils, for the surfaces the nature of the biomineral produced is important because its colour may contrast with that of the existing surface. Chemical reactions with the materials from the surfaces or corrosion due to significant changes in pH must also be avoided, in particular in the rehabilitation of historical constructions. For this reason, the feeding solution and pH under which the bacteria operate are fundamental.

7 Concluding Remarks

MICP is a sustainable and environmentally friendly technique that is being used in laboratory studies and already at some field cases for the treatment of several kinds of porous media. This technique must be optimized to find the best conditions (pH, soil, temperature, nutrient concentration, etc.) for bacterial activity, and also to get homogeneous distribution in the medium treated, independently if it is soil to be cemented or a porous surface to be rehabilitated. The use of the enzyme as treatment may be better than using bacteria and must be tested as well.

To conclude, the design of biocement solutions must be done experimentally and several situations must be tested in which the organisms used, their feeding, their maintenance during the treatment and the effects for each case must be determined. Several cases from the literature can be used as starting point. The amount of

biocement produced must be predicted and for this reason the number of bacteria and concentration of the feeding solution must be defined. Feeding frequency and the duration of the treatment eventually can be fixed during the treatment based in monitoring data.

Acknowledgements The authors acknowledge Leonor Lopes for helping preparing the enzyme and the bacteria used in this study, as well as INESC-MN for lending the optical microscope. Acknowledgement is also due to CERIS for the support to this investigation. This work was financed by national funds through FCT—Foundation for Science and Technology, under the project UID/BIO/04565/2013.

References

- Abo-El-Enein SA, Ali AH, Talkhan Fatma N, Abdel-Gawwad HA (2013) Application of microbial biocementation to improve the physico-mechanical properties of cement mortar. *HBRC J* 9:36–40
- Achal V, Mukherjee A, Reddy MS (2010) Microbial concrete: away to enhance the durability of building structures. *J Mater Civ Eng* 23:730–734
- Achal V, Mukherjee A, Reddy MS (2011) Effect of calcifying bacteria on permeation properties of concrete structures. *J Ind Microbiol Biotechnol* 38:1229–1234
- Achal V, Mukerjee A, Reddy MS (2013) Biogenic treatment improves the durability and remediates the cracks of concrete structures. *Constr Build Mater* 48:1–5
- Al Qabany A, Soga K (2013) Effect of chemical treatment used in MICP on engineering properties of cemented soils. *Geotechnique* 63:331–339
- Al Qabany A, Soga K, Santamarina C (2012) Factors affecting efficiency of microbially induced calcite precipitation. *J Geotech Geoenviron Eng* 138: 992–1001
- Chu J, Ivanov V, Stabnikov V (2013) Microbial method for construction of aquaculture pond in sand. *Géotechnique* 63:871–875
- Cuthbert MO, McMillan LA, Handley-Sidhu S, Riley MS, Tobler DJ, Phoenix VR (2013) A field and modeling study of fractured rock permeability reduction using microbially induced calcite precipitation. *Environ Sci Technol* 47:13637–13643
- De Belie N, De Muynck W (2008) Crack repair in concrete using biodeposition. In: *Proceedings of ICCRR, Cape Town, South Africa*
- De Muynck W, Debrouwer D, De Belie N, Verstraete W (2008a) Bacterial carbonate precipitation improves the durability of cementitious materials. *Cem Concr Res* 38:1005–1014
- De Muynck W, Cox K, De Belie N, Verstraete W (2008b) Bacterial carbonate precipitation as an alternative surface treatment for concrete. *Constr Build Mater* 22:875–885
- De Muynck W, De Belie N, Verstraete W (2010) Microbial carbonate precipitation in construction materials: a review. *Ecol Eng* 36:118–136
- DeJong JT, Fritzges MB, Nusslein K (2006) Microbially induced cementation to control sand response to undrained shear. *J Geotech Geoenviron Eng* 132:1381–1392
- DeJong JT, Soga K, Kavazanjian E, Burns S, Van Paassen L, Al Qabany A, Aydilek A, Bang SS, Burbank M, Caslake LF, Chen CY, Cheng X, Chu J, Ciurli S, Esnault-Filet A, Fauriel S, Hamdan N, Hata T, Inagaki Y, Jefferis S, Kuo M, Laloui L, Larrahondo J, Manning DAC, Martinez B, Montoya BM, Nelson DC, Palomino A, Renforth P, Santamarina JC, Seagren EA, Tanyu B, Tsesarsky M, Weaver T (2013) Biogeochemical processes and geotechnical applications: progress, opportunities and challenges. *Geotechnique* 63:287–301
- Dhami NK, Reddy SM, Mukherjee A (2012a) Biofilm and microbial applications in biomineralized concrete. In: Seto J (ed) *Advanced topics in biomineralization*. In Tech, Rijeka, pp 137–164

- Dhami NK, Reddy MS, Mukherjee A (2012b) Improvement in strength properties of ash bricks by bacterial calcite. *Ecol Eng* 39:31–35
- Dick J, De Windt W, De Graef B, Saveyn H, Van der Meeren P, De Belie N, Verstraete W (2006) Bio-deposition of a calcium carbonate layer on degraded limestone by *Bacillus* species. *Biodegradation* 17:357–367
- Emmons PH, Sordyl DJ (2006) The state of the concrete repair industry, and a vision for its future. *Concr Repair Bull* 6:7–14
- Fernandes P (2006) Applied microbiology and biotechnology in the conservation of stone culture heritage materials. *Appl Microbiol Biotechnol* 73:291–296
- Ghosh P, Mandal S, Chattopadhyay BD, Pal S (2005) Use of microorganism to improve the strength of cement mortar. *Cem Concr Res* 35(10):1980–1983
- Ghosh P, Mandal S, Pal S, Bandyopadhyaya G, Chattopadhyay BD (2006) Development of biocement material using an enrichment culture of novel thermophilic anaerobic bacteria. *Indian J Exp Biol* 44:336–339
- Ghosh S, Biswas M, Chattopadhyay BD, Mandal S (2009) Microbial activity on the microstructure of bacteria modified mortar. *Cem Concr Compos* 31:93–98
- Gomez M, Martinez M, DeJong JT, Hunt C, de Vlaming L, Major D, Dworatzek S (2015) Field-scale bio-cementation tests to improve sands. In: *Proceedings of the institution of civil engineers, ICE, ground improvement*, vol 168, no 3, pp 206–216
- Inanov V, Chu J, Stabnikov V (2015) Chapter 2: Basics of construction microbial biotechnology. In: Pacheco Torgal et al F (eds) *Biotechnologies and biomimetics for civil engineering*. Springer International Publishing Switzerland
- Ivanov V, Chu J, Stabnikov V, Li B (2014) Strengthening of soft marine clay using biocementation. *Mar Georesour Geotechnol* 33(4):325–329
- Jimenez-Lopez C, Rodriguez-Navarro C, Pinar G, Carrillo-Rosúa FJ, Rodriguez-Gallego M, González-Munoz MT (2007) Consolidation of degraded ornamental porous limestone by calcium carbonate precipitation induced by microbiota inhabiting the stone. *Chemosphere* 68:1929–1936
- Jimenez-Lopez C, Jroundi F, Pascolini C, Rodriguez-Navarro C, Piñar-Larubia G, Rodriguez-Gallego M, González-Munoz MT (2008) Consolidation of quarry calcarenite by calcium carbonate precipitation induced by bacteria activated among the microbiota inhabiting the stone. *Int Biodeterior Biodegrad* 62:352–363
- Jonkers HM (2007) Self healing concrete: a biological approach. In: van der Zwaag S (ed) *Self healing materials: an alternative approach to 20 centuries of materials science*. Springer, Berlin, pp 195–204
- Jonkers HM, Thijssen A, Muyzer G, Copuroglu O, Schlangen E (2010) Application of bacteria as self-healing agent for the development of sustainable concrete. *Ecol Eng* 36:230–235
- Latil M-N, Van der Zon W, Lehnen C, Ineke E, Marcelis F, Van Eijden J, Baaijens T, Baaijens T, Bol G (2008) Environmental friendly technology for biological sand-consolidation of oil and gas wellbore. In: *Proceedings of the 1st bio-geo engineering conference, Deltares*, pp 82–89
- Le Metayer-Levrel G, Castanier S, Oriol G, Loubiere JF, Perthuisot JP (1999) Applications of bacterial carbonatogenesis to the protection and regeneration of limestones in buildings and historic patrimony. *Sediment Geol* 126(1–4):25–34
- Li P, Qu W (2012) Microbial carbonate mineralization as an improvement method for durability of concrete structures. *Adv Mater Res* 365:280–286
- Montoya BM, DeJong J, Boulanger R (2013) Dynamic response of liquefiable sand improved by microbial-induced calcite precipitation. *Geotechnique* 63(4):302–312
- Pacheco-Torgal F, Labrincha JA (2013) Biotech cementitious materials: some aspects of an innovative approach for concrete with enhanced durability. *Constr Build Mater* 40:1136–1141
- Phillips A, Gerlach R, Lauchnor E, Mitchell A, Cunningham A, Spangler L (2013) Engineered applications of ureolytic biomineralization: a review. *Biofouling J Bioadhesion Biofilm Res* 29:715–733
- Ramachandran SK, Ramakrishnan V, Bang SS (2001) Remediation of concrete using micro-organisms. *ACI Mater J* 98:3–9

- Raut SH, Sarode DD, Lele SS (2014) Biocalcification using *B. pasteurii* for strengthening brick masonry civil engineering structures. *World J Microbiol Biotechnol* 30:191–200
- Rodriguez-Navarro C, Rodriguez-Gallego M, BenChekroun K, Gonzalez-Munoz MT (2003) Conservation of ornamental stone by *myxococcus xanthus*-induced carbonate biomineralization. *Appl Environ Microbiol* 69:2182–2193
- Siddique R, Chahal NK (2011) Effect of ureolytic bacteria on concrete properties. *Construct Build Mater* 25:3791–3801
- Stabnikov V, Chu J, Naeimi M, Ivanov V (2011) Formation of water-impermeable crust on sand surface using biocement. *Cem Concr Res* 41:1143–1149
- Stocks-Fischer S, Galinat JK, Bang SS (1999) Microbiological precipitation of CaCO_3 . *Soil Biol Biochem* 31:1563–1571
- Tiano P, Cantisani E, Sutherland I, Paget JM (2006) Biomediated reinforcement of weathered calcareous stones. *J Cult Heritage* 7:49–55
- Van Paassen LA, Daza CM, Staal M, Sorokin DY, van der Zon W, van Loosdrecht MCM (2010a) Potential soil reinforcement by biological denitrification. *Ecol Eng* 36:68–75
- Van Paassen L, Ghose R, van der Linden T, van der Star W, Van Loosdrecht M (2010b) Quantifying biomediated ground improvement by ureolysis: large-scale biogROUT experiment. *J Geotech Geoenviron Eng* 136:1721–1728
- Van Tittelboom K, De Belie N, De Muynck W, Verstraete W (2010) Use of bacteria to repair cracks in concrete. *Cem Concr Res* 40:157–166
- Vempada SR, Reddy SSP, Rao MVS, Sasikala C (2011) Strength enhancement of cement mortar using microorganisms-an experimental study. *Int J Earth Sci Eng* 4:933–936
- Wang J, Tittelboom K, De Belie N, Verstraete W (2012) Use of silica gel or polyurethane immobilized bacteria for self-healing concrete. *Constr Build Mater* 26(1):532–540
- Wiktor V, Jonkers H (2011) Quantification of crack-healing in novel bacteria-based self-healing concrete. *Cem Concr Compos* 33:763–770

Study of Pozzolanic Admixtures Effects in the Concretes Under Chemical Attack

Henrique Catuzzo, Giovanna Patricia Gava
and Camila Salvi Malacarne

Abstract The alkaline nature of concrete makes it highly vulnerable to acidic attack. The chemical attack occurs due to the decomposition of hydration products, forming soluble products that can be leached, or insoluble products than can expand in their formation site. The use of cements with pozzolan and blast furnace slag in concrete mixtures reduces their permeability, as well as their porosity, besides consuming part of the calcium hydroxide. These characteristics are signs of benefits for the reduction of the effects of corrosion caused by acid in the concretes. In this study, the effect of the presence of pozzolanic materials on the resistance of concrete against acidic attack had been investigated by considering two different acids. The concretes studied were inserted in lactic and formic acid solutions, thus simulating environments commonly found in the dairy, paper and cellulose industries, respectively. The tests were made with concretes with two water/cementitious materials ratios and two different content of replacement of cement by silica fume, 8 and 15 %, apart from pozzolanic cement. Test specimens with 100 mm × 200 mm cylindrical dimensions were immersed in acid solutions after the curing process, and then subjected to cycles of wetting and drying. Mass loss and compressive strength tests were carried out between cycles of exposure to the acids. At each water/cementitious materials ratio, the mass loss and compressive strength loss of concrete with silica fume were less than the concrete without pozzolan. The presence of pozzolan decreased the detrimental effect of both acids in concrete. And besides, it was verified that formic acid is more aggressive for all concrete mixtures.

Keywords Chemical Attack · Concrete · Acidic attack · Lactic acid · Formic acid · Silica fume · Mass loss

H. Catuzzo · G.P. Gava (✉) · C.S. Malacarne
Western Parana State University, Cascavel, Brazil
e-mail: gpgava@gmail.com

H. Catuzzo
e-mail: henriquecatuzzo@hotmail.com

C.S. Malacarne
e-mail: camila.malacarne@hotmail.com

1 Introduction

Concrete is an alkaline material that presents low resistance to the attack of strong acids, such as: lactic, formic and acetic acids, commonly found in industrial environments. In most times, the acids attack calcium hydroxide and some hydration products of the cement matrix, forming compounds that, when soluble, can be leached or causing decomposition of these products and consequent degradation of the mechanical properties of concrete (Goyal et al. 2009).

The resistance of the cement matrix to acid corrosion depends primarily on its pore structure characteristics, the ability of matrix components to neutralize acid and also on the products of acid corrosion (Shi and Stegemann 2000).

The use of pozzolanic materials such as fly ash and silica fume is believed to increase the durability of concrete through pore refinement and the reduction of calcium hydroxide content of the cement paste matrix. However, the beneficial effect of these materials on acidic attack is still under review (Goyal et al. 2009). While some research works point towards improvement through the use of silica fume or fly ash (Kim et al. 2007; Roy et al. 2001) other works report that pozzolanic materials have only little or no effect on the durability of concrete under acid attack (Pavlik 1996; Pavlik and Uncik 1997).

In this study, the effect of the water/cementitious materials ratio and the presence of pozzolanic materials on the resistance of concrete against acidic attack had been investigated by considering two different acids: lactic and formic acids. It was investigated the mass loss and the compressive strength loss of concretes.

2 Experimental Program

The experimental program, including test solution and measurements, to carry out the chemical attack process was based on researches performed by Dal Molin (1996) and Kulakowski (1997), which resistance of concrete under acidic attack were evaluated by mass loss and compressive strength tests.

2.1 Materials

2.1.1 Aggregates

Crushed basalt with a maximum nominal size of 19 mm was used as coarse aggregate, natural river sand with a fineness modulus of 1.95 and a crushed basalt with a fineness modulus of 3.15 were used as fine aggregates. The properties of the aggregates are listed in Table 1.

Table 1 Properties of aggregates

Property	Natural sand	Fine crushed basalt	Coarse aggregate
Maximum characteristic dimension (mm)	2.36	4.75	19.50
Minimum characteristic dimension (mm)	0.15	<0.15	6.30
Fineness modulus	1.98	3.15	6.81
Material finer than 75 μm (n° 200 sieve) (%)	0.30	18.20	0.50
Specific gravity (g/cm^3)	2.65	2.94	2.96
Absorption (%)	1.33	1.10	1.10

2.1.2 Cementitious Materials

Two types of cement were used throughout the investigation, CP IV—Portland Pozzolan Cement and CP V ARI RS—Portland Cement with High Early Strength and Sulfates Resistance, whereas only in the latter silica fume was added. The silica fume used as a pozzolanic addition presented a pozzolanic activity index of 79 %, features of amorphous material. The most important characteristics of all cementitious materials are presented in Table 2. Figure 1 shows the X-ray diffractogram of the silica fume.

2.1.3 Additive

The additive used was Muraplast FK 110, produced by MC-Bauchemie Brasil, which acts as a dispersal agent to the cement particles, preventing its agglomeration and reducing the superficial tension of the mixing water. It has a density of $1.20 \text{ g}/\text{cm}^3$.

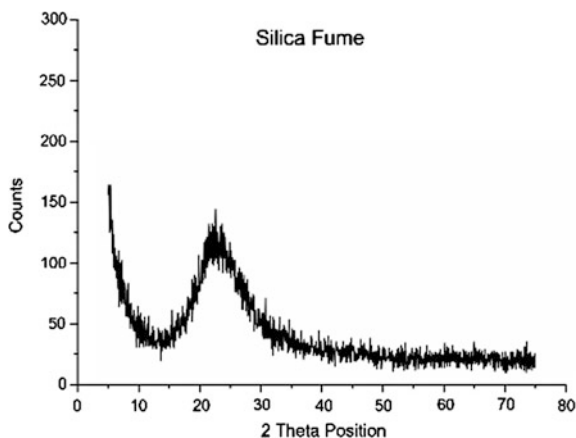
2.1.4 Acids

The acids used were lactic acid, found in dairy industries, and formic acid, present in the paper and cellulose industries, with densities of 1.21 and $1.20 \text{ g}/\text{cm}^3$, respectively.

Table 2 Characteristics of cementitious materials used in this study

Cement	Loss on ignition (%)	Insoluble residue (%)	Specific gravity (g/cm^3)	Alkali content $\text{Na}_2\text{O}_{\text{eq}}$ (%)
CP IV	2.90	24.27	2.73	0.65
CP V ARI RS	2.71	8.58	2.94	0.70
Silica fume (SF)	–	–	2.22	0.74

Fig. 1 X-ray diffraction analysis of silica fume



2.2 Preparation of Test Especimens

A total of eight concrete mixtures were prepared through a combination of two different types of cement (CP IV—Portland Pozzolan Cement and CP V ARI RS—Portland Cement with High Early Strength and Sulfates Resistance), two water/cementitious materials ratios (0.45 and 0.55) and silica fume as cement replacement, used in two different content levels (8 and 15 %). The concrete mixtures were attacked separately by two different acid solutions, one with lactic acid and other with formic acid, both with 6 % concentration.

The consumption of materials per cubic meter of fabricated concrete is presented in Table 3.

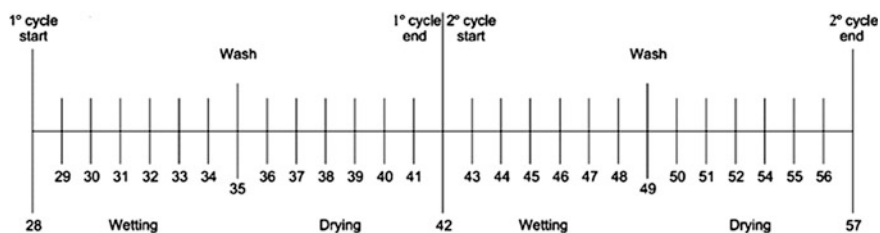
2.3 Test Methods

100 mm × 200 mm test specimens were cast for all mixtures, for the performance of mass loss and compressive strength tests. The specimens were cured for 21 days, immersed in a water and lime solution. After that period, 12 test specimens were exposed to air curing in the lab environmental for 7 days, and in the end of that period, they were immersed in acid solution. Before the immersion in acid, the specimens were coated with colored paraffin in their upper and lower surfaces to guarantee that the attack would happen only in its side and also help in its identification, then the specimens were weighed and placed in groups of 6 in each type of acid.

The acid attack test consisted of two immersion cycles in lactic or formic acid solution, where the solution presented a pH equal to 1.73. Each cycle of immersion in acid lasted 7 days, in the seventh day the specimens were removed from the acid solution for washing with a polypropylene bristle brush. After the wash, the specimens were kept out of the solution for air drying, in the lab environmental, for 7 days.

Table 3 Consumption of material per cubic meter of fabricated concrete

Concrete (water/cementitious materials ratio)	Cement (kg)	Silica fume (kg)	Natural sand aggregate (kg)	Fine crushed basalt aggregate (kg)	Coarse aggregate (kg)	Water (l)	Additive (l)
CP V (0.45)	438	–	556	258	1064	197.2	0.39
CP V–8 % SF (0.45)	403	25.8	556	258	1064	197.2	1.42
CP V–15 % SF (0.45)	372	48.3	556	258	1064	197.2	1.43
CP V (0.55)	357	–	604	286	1065	196.6	0.00
CP V–8 % SF (0.55)	328	21.0	604	286	1065	196.6	0.31
CP V–15 % SF (0.55)	303	39.4	604	286	1065	196.6	0.67
CP IV (0.45)	433	–	550	255	1052	195.0	0.91
CP IV (0.55)	354	–	598	283	1055	195.0	0.00

**Fig. 2** Exposure cycles with time scales in days

Once the drying period was over, the specimens were weighed to determine the amount of mass loss, and compressive strength tests were carried out in 2 specimens. At the end of this first process, 3 specimens were returned to the recipient containing acid to start the second cycle. Figure 2 exemplifies the process of aggression.

The compressive strength tests were carried out in accordance with recommendations from ABNT NBR 5739 (2007), and the absorption and void ratio tests according to ABNT NBR 9778 (2009) recommendations.

3 Results

The compressive strength test and absorption test results of the concretes at 7 and 28 days, before immersion in acids solution, were presented in Table 4.

Figures 3 and 4 present the percentage of mass loss of the concretes when exposed to 6 % latic acid or formic acid in relation to the voids ratios in the concretes, for the mixtures with water/cementitious materials ratios of 0.45 and 0.55, respectively.

Table 4 Compressive strength and absorption test results

Concrete (water/cementitious materials ratio)	Compressive strength at 7 days (MPa)	Compressive strength at 28 days (MPa)	Absorption (%)	Void ratio (%)
CP V (0.45)	47.0	56.8	5.35	12.85
CP V-8 % SF (0.45)	48.5	69.4	4.57	10.96
CP V-15 % SF (0.45)	42.3	59.3	4.57	10.83
CP V (0.55)	36.2	41.8	6.32	15.16
CP V-8 % SF (0.55)	35.0	53.1	5.64	13.39
CP V-15 % SF (0.55)	33.1	54.9	4.96	11.94
CP IV (0.45)	37.1	48.0	4.05	9.80
CP IV (0.55)	24.1	34.3	4.53	11.01

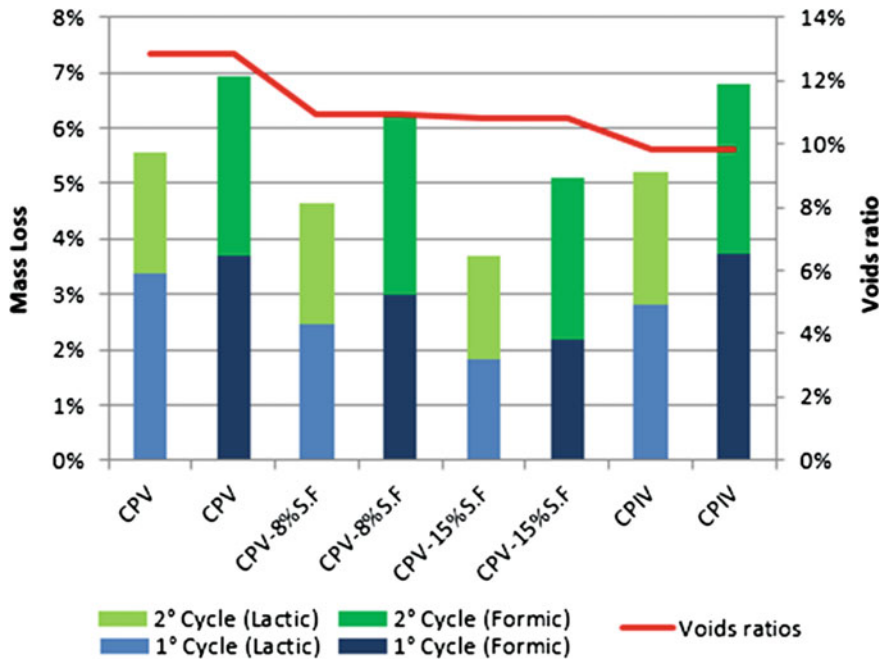


Fig. 3 Mass loss of concretes with water/cementitious materials ratio of 0.45

Figures 5 and 6 present the results of the compressive strength loss of the concretes when exposed to 6 % latic acid or formic acid in relation to the mass loss of concretes with water/cementitious materials ratios of 0.45 and 0.55, respectively.

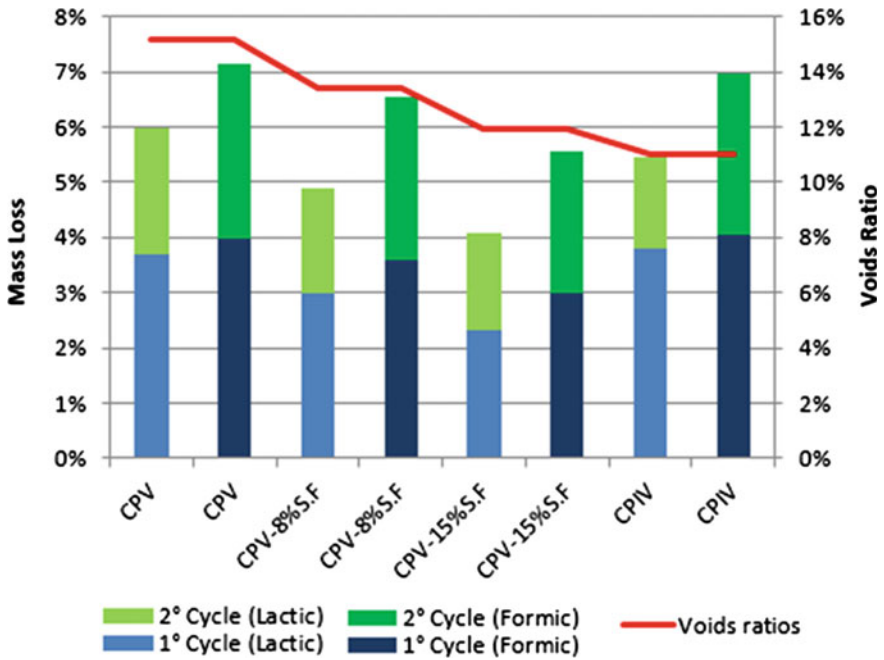


Fig. 4 Mass loss of concretes with water/cementitious materials ratio of 0.55

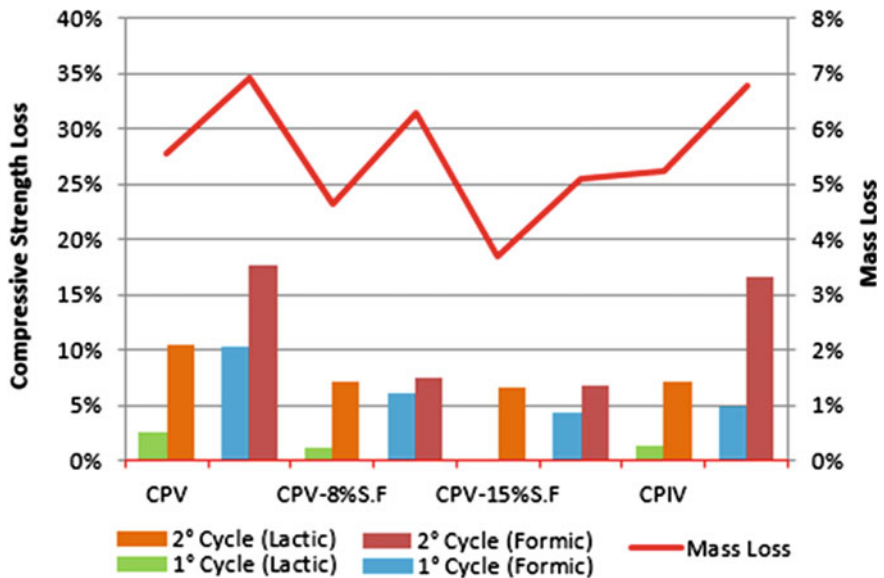


Fig. 5 Compressive strength loss of concretes with water/cementitious materials ratio of 0.45

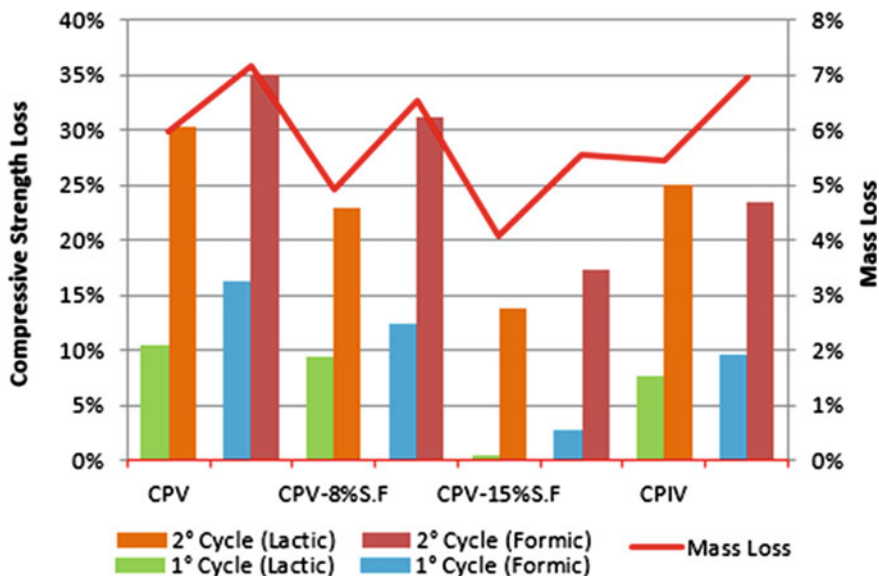


Fig. 6 Compressive strength loss of concretes with water/cementitious materials ratio of 0.55

3.1 Results and Discussion

The additions of silica fume decreased the mass loss of concretes. It was observed that as the silica fume content increased, the mass loss of concretes decreased, as well as the absorption values and the void ratios decreased. The effect of silica fume in decreased mass loss of concrete can be seen in Fig. 7.

Concretes with Portland Pozzolan Cement (CP IV) presented mass loss values intermediary between concretes with Portland Cement with High Early Strength and Sulfates Resistance (CP V ARI RS) without addition and with replacement of 8 % silica fume, however, with the smallest void ratios found. These results show that the silica fume is more efficient than pozzolan present in Portland Pozzolan Cement, in that case fly ashes, to reduce the detrimental effect of the acids over concrete.

The mass loss caused by the second cycle of aggression was smaller compared to the first cycle. That can be explained by the fact that from the first process of degradation, some aggregates are already exposed, thus decreasing the attack's area of influence (cement paste). It is important to emphasize that acids react directly with the cement paste compounds such as calcium hydroxide.

There was a great contribution of silica fume to improve the acid resistance of concrete. For both acids analyzed, lactic and formic, the concretes with 15 % of cement replaced by silica fume, even after two cycles of exposure to acid, practically did not present compressive strength loss (values of compressive strength loss inferior to 7 %).

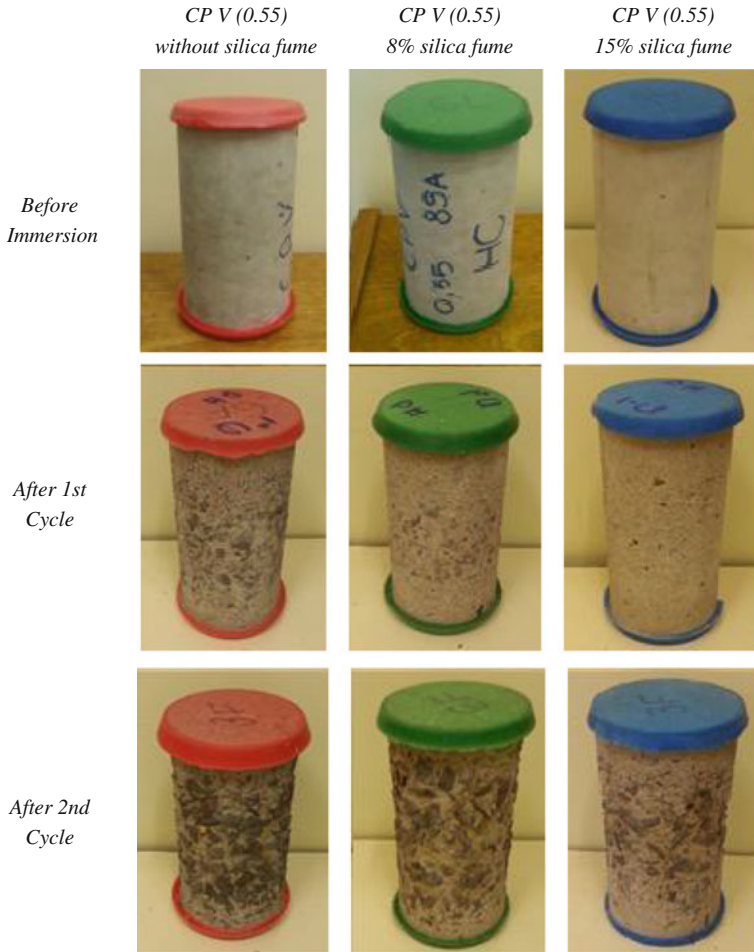


Fig. 7 The effect of silica fume in the specimens

It was observed that with increased in water/cementitious materials ratio, mass loss increased and compressive strength loss increased. It occurs because concretes with water/cementitious materials ratio of 0.55 are more porous and consequently the acid effects are less superficial than in the concretes with water/cementitious materials ratio of 0.45.

Formic acid, commonly found in industrial paper and cellulose installations, dye houses and food industries, was more aggressive to concrete than lactic acid, present in dairy products.

4 Conclusions

The accelerated test of degradation by acid, among other tests, provided results that showed that the presence of silica fume lowers the detrimental effect of lactic and formic acids on concrete and increase the durability of concrete. With the addition of silica fume, due to the pozzolanic reaction, voids ratios were reduced, contributing with to the decrease of particles leaching and decreasing the compressive strength loss. The silica fume is more efficient than pozzolan present in Portland Pozzolan Cement, in that case fly ashes, to reduce the detrimental effect of the acids over concrete.

The water/cementitious materials ratio also proved itself as an important asset in the control of acid attack. Among the eight mixtures tested, it was noticed that the most efficient combination for the control of the effects of degradation by acid was concrete that used CP V ARI RS with 15 % of cement replaced by silica fume and water/cementitious materials ratio equal to 0.45, considerably reducing the mass loss and almost inhibiting the compressive strength loss.

References

- ABNT NBR 5739 (2007) Concrete—compression test of cylindrical specimens—method of test. Rio de Janeiro
- ABNT NBR 9778 (2009) Hardened mortar and concrete—determination of absorption, voids and specific gravity. Rio de Janeiro
- Dal Molin D (1996) Study of concrete with addition of silica fume under attack aggressive agents in flooring specials. In: 1st International congress in high-performance concrete structures. Proceedings. Florianopolis
- Goyal S, Kumar M, Sidhu DS, Bhattacharjee B (2009) Resistance of mineral admixtures concrete to acid attack. *J Adv Concr Technol* 7(2):273–283
- Kim HS, Lee SH, Moon HY (2007) Strength properties and durability aspects of high strength concrete using Korean metakaoline. *Constr Build Mater* 21(6):1229–1237
- Kulakowski MP (1997) Study of action of formic acid in concrete with silica fume with addition of views on employment in industrial environment. Proceedings of 39^a REIBRAC—meeting of IBRACON, São Paulo (SP)
- Pavlik V (1996) Corrosion of hardened cement paste by acetic and nitric acids: Part III. Influence of water cement/ratio. *Cem Concr Res* 26(3):475–490
- Pavlik V, Uncik S (1997) The ratio of corrosion of hardened cement pastes and mortars with additive of silica fume in acids. *Cem Concr Res* 27(11):1731–1745
- Roy DM, Arjunan P, Silsbee MR (2001) Effects of silica fume, metakaolin and low-calcium fly ash on chemical resistance of concrete. *Cem Concr Res* 31(12):1809–1813
- Shi C, Stegemann JA (2000) Acid corrosion resistance of different cementing materials. *Cem Concr Res* 30(5):803–808

Durability of ETICS and Premixed One-Coat Renders in Natural Exposure Conditions

Luís Silva, Inês Flores-Colen, Nuno Vieira, Ana Barros Timmons and Pedro Sequeira

Abstract In situ testing is a precious auxiliary mean to reduce the subjectivity of visual inspections, leading to a more accurate characterization of existing degradation mechanisms of buildings systems. Inspections under natural conditions over time can increase the knowledge of in-service behaviour and can contribute also to a better correlation between accelerated and natural ageing tests. The knowledge of performance during time of façades' cladding allows maintenance planning and adequate interventions during the life cycle of these systems. This work presents data collected from field experimental campaigns carried out over 10 years after construction using several premixed one-coat rendered walls and during 4 and 6 years after construction in the case of External Thermal Insulation Composite Systems (ETICS), in order to study the water resistance of cladding systems under real service conditions. This analysis was focused on the study of the influence of the hydrophobic agent (salts of fatty acids and waxes or silanes for organic renders in ETICS) on the performance in terms of surface condition and water penetration. In addition, adhesion results, concerning premixed one-coat render, were also collected. The quantitative results obtained were correlated with visual inspection data in order to define potential relationships between common anomalies in such façade solutions and the main causes. This information will contribute to the

L. Silva (✉) · N. Vieira · P. Sequeira
Saint Gobain Weber Portugal, Aveiro, Portugal
e-mail: luis.silva@saint-gobain.com

N. Vieira
e-mail: nuno.vieira@saint-gobain.com

P. Sequeira
e-mail: pedro.sequeira@saint-gobain.com

I. Flores-Colen
IST, Department of Civil Engineering and Architecture,
University of Lisbon, Lisbon, Portugal
e-mail: ines.flores.colen@ist.utl.pt

A.B. Timmons
CICECO, Department of Chemistry, University of Aveiro, Aveiro, Portugal
e-mail: anabarro@ua.pt

development of solutions to prevent early ageing and adequate maintenance methodologies to delay their effect. Indeed, the results obtained showed that rendering solutions ageing, especially after 5 or 6 years in service, is a consequence of their loss in resistance to liquid water absorption, especially at the surface. Considering the ageing and water penetration processes are stronger for South and West orientations, additional mechanisms such as leaching of hydrophobic agents from the mortars and photochemical degradation are thought to be involved. Finally, the Karsten pipe testing proved to be the most reliable methodology to determine the loss of water penetration resistance of render solutions and predict the ageing of façade solutions.

Keywords Natural ageing tests · Façade solutions · Water resistance · Hydrophobic agents · Adhesion

1 Façades in General

Façade are an important element of a building and it influences its comfort, safety and aesthetics. The technology used on façades can be divided into two categories (Hendriks and Hens 2000; Svendsen and Rudbeck 2000): (1) façades with traditional solutions, such as brick wall with mineral renders; (2) façades with non-traditional or innovative al solutions that can improve performance, such as ventilated systems or walls with ETICS. In Europe, the Construction Products Regulation (CPR, N° 305/2011) lays down certain periodic requirements for construction works (buildings as a whole and in their separate parts, e.g. the façade) under seven current requirements when subject to maintenance an in an economically reasonable working life: (i) mechanical resistance and stability (ER1); (ii) safety in case of fire (ER2); (iii) hygiene, health and the environment (ER3); (iv) safety and accessibility in use (ER4); (v) protection against noise (ER5), (vi) energy economy and heat retention (ER6); and (vii) sustainable use of natural resources (ER7).

In this context, façades shall fulfil several performance characteristics in order to meet users' requirements. Usually, characteristics are presented on specific standards according to materials type presentation. For instance, mineral renders follow EN 998:1 (CEN 2010) and ETICS follow ETAG 004 (EOTA 2008).

Claddings must allow the fulfilment of the main function of the façade, i.e. to serve as a barrier between the indoor and outdoor environments (resistance to heat, moisture, air and other flows within acceptable limits). Their adequate choice, application and maintenance are important aspects to the healthiness, comfort, durability, and aesthetic appearance. Aesthetics, waterproofing and, nowadays, thermal insulation can be considered the main functions that a facade's cladding must fulfil during its service life. For façade cladding, the performance-based methodology includes the definition and quantification (by the designers, backed by the manufacturers) of the cladding properties relevant to a proper in-service performance.

Condition assessment, based on technical in-service assessment, must define the problem, collect the available data, characterize the existing anomalies and their probable causes, evaluate the in-service performance (fulfillment of the functions established at design phase), check whether the users' demands are being fulfilled and, finally, define the corrective, preventive or monitoring in service actions.

2 Façade Pathology (Typical Degradation Agents) and in Service Performance

Façades are constantly affected by climatic effects and atmospheric pollution that can lead to an increase of the degradation rate, with probable serious implications in safety and users' comfort. A degraded façade is currently a source of problems of non-functionality within the building, due to dampness and water leakage and also unsafe conditions (such as stone plates or ceramic tiles falling off).

The degradation agents can be classified according to their nature (ASTM 1996; BSI 2003), namely: mechanical, electromechanical, thermal, chemical and biological.

The façade's global performance depends on the performance of its systems during the life cycle of the building: separation, support and facilities (Hermans 1995), which deteriorate at different rates when subjected to degradation agents. Each system deteriorates to a limit state at which maintenance is no longer practical or possible and replacement is required (Lacasse 2003). Therefore, the assessment of a façade includes the study of each system and its interaction with other systems within the building.

A consistent knowledge of design solutions durability (long-term performance) is crucial to assure the reliability of any maintenance strategy. Different means may be used to assess the performance over time (service life) (CSA 2001)—based on demonstrated performance (experience components and assemblies currently in use); performance testing; or the analysis of results from modelling (both in new components and assemblies, whose long term behaviour has not yet been characterized). However, results from tests and modelling should be interpreted in combination with information gained from in-service performance (Lacasse 2003).

The observation of facades over time exposure to environmental conditions suggests that aesthetic is strongly conditioned by the performance that a cladding system has in the presence of water and its effective capacity to prevent the penetration and thus to overcome this degradation mechanism (ANFAPA and ITeC 2008; CEN 2010; EOTA 2008).

Water, under different physical forms and different mechanisms is one of the main factors causing building deterioration, including façade solutions, no matter the origin come (precipitation, condensation, construction moisture, water leaks or rising damp) (Addleson 1992; Freitas et al. 2008; Mathivat 1983).

Other climate exposure factors than water can be considered as solar radiation, ambient infrared heat radiation, high and low temperatures, temperature gradients,

physical strains, wind, erosion, pollutions, microorganisms, oxygen and others. Often, materials are exposed to a combination of several of these factors, and the total climate strain may be substantially larger than the added sum of the single exposure factors. Nevertheless, it is widely recognised that water is the hardest climate factor to materials. Several studies correlate long term durability of wood structures with the effect of permanent water. The time of wet conditions is considered as a useful indicator for development of mould growth on surfaces. Hygrothermal conditions are particularly important, high humidity or condensation along with raised temperatures, favouring microorganisms' growth on the paint surfaces. According to ETAG 004 (EOTA 2008), ETICS durability is linked to stability to air temperature, air humidity, moisture and shrinkage (Viitanen et al. 2010; Foliente et al. 2002; Gaylarde et al. 2011; Allsop et al. 2004; Jelle 2012; Garrido et al. 2012).

The ability that a pre-mixed one-coat render has to resist the penetration of water is usually expressed by the coefficient of water absorption by capillarity, which measures the rate at which the material absorbs water by this mechanism. The requirements for resistance to water penetration are classified in three classes, EN 998-1 (CEN 2010), namely, W0 when not specified; W1 when the value is between 0.2 and 0.4 kg/m² min^{1/2}; and W2 when the value appears less than 0.2 kg/m² min^{1/2}. For durability testing, the same standard covers this issue in the case of one-coat renders, recommending, beyond the study of adhesion, resistance to water permeability after exposure to climate cycles with a maximum requirement of 1 ml/cm², after 48 h of testing (CEN 2010). However, as mentioned by Quintela (2006) these tests may not correspond to significant variations that can express changes in terms of real in-service performance.

As regards ETICS, the ability of these systems to confer water resistance is expressed by water absorption coefficient determined by capillarity which should be less than 1 kg/m² after 1 h. If this value is less than 0.5 kg/m² after 24 h, the performance is considered better and includes resistance to freeze-thaw. Additionally, water tightness is a major concern, including a hygrothermal behavior analysis, with heat-rain and heat-cold cycles (EOTA 2008).

ETICS and premixed one-coat rendered walls are porous materials hence contact between them and water is governed by capillary forces which in turn depend not only on the pore size and its distribution but also on the characteristics of the surface. If the surface is hydrophilic, water tends to spread and wet the solid surface, yielding a small contact angle (<90°). Conversely, on hydrophobic surfaces, the contact angle is higher and external pressure would be necessary to allow the liquid to penetrate the solid pores. In other words, the surface wettability of hydrophobic surfaces is reduced.

To ensure the minimum requirements recommended by the standards, mortars are formulated with hydrophobic agents in order to reduce their wettability. Ideally, these agents should prevent the absorption of liquid water whilst allowing the vapour diffusion in order to increase the façade durability (McGettigan 1995a, b). Yet, although it is generally accepted that higher durability are associated with low water

absorption coefficients, for longer periods other factors seem to play a role. Also, field observations of façades indicate signs such as dirt deposition, discolouration, among others which is thought to be associated with the degradation or leaching of water repellent agents after the first years. Furthermore, the delivery systems of hydrophobic agents must be adapted to the application method (dry mixes, admixtures or emulsions for post-treatment) (Lecomte 2013). Additionally, the characteristics of the substrate, of the hydration products, of the hydrophobic agent and the concentration used are also critical parameters that can affect the durability of façades as they can affect the microstructure of the materials, including the possible entrapment of air and water during application (Lazniewska-Piekarczyk 2010).

Water repellents can be classified according to the characteristics of their active ingredients as film formers or penetrants. The former include mineral gum waxes such as low molecular weight polyethylene, stearates and the latter include silanes, siloxanes and methyl siliconates (McGettigan 1995a, b). In turn, film formers can act in distinct modes, i.e. either as a coating or as a pore blocker. According to the Masonry Institute of Washington, Pocket Guide—Brick and CMU Construction (2012) another class can also be considered: the consolidants, but this is beyond the scope of this chapter. Figure 1 illustrates schematically the mechanism of action of the water repellents.

For example, waxes form a thin waxy film over the substrate reducing the wettability of the surface. Indeed, they have the ability to bridge small hairline cracks. However they reduce water vapour permeability. Nevertheless, their use on ETICS proved efficiency over four years though between the 5th and 6th year visible dark and green spots were clearly visible. This was attributed to algae and fungi possibly associated with leaching of biocides (Silva et al. 2015). Stearates, like calcium or zinc stearates, are normally incorporated in a polymeric resin, and react with free salts filling the pores prevents diffusion of liquid water.

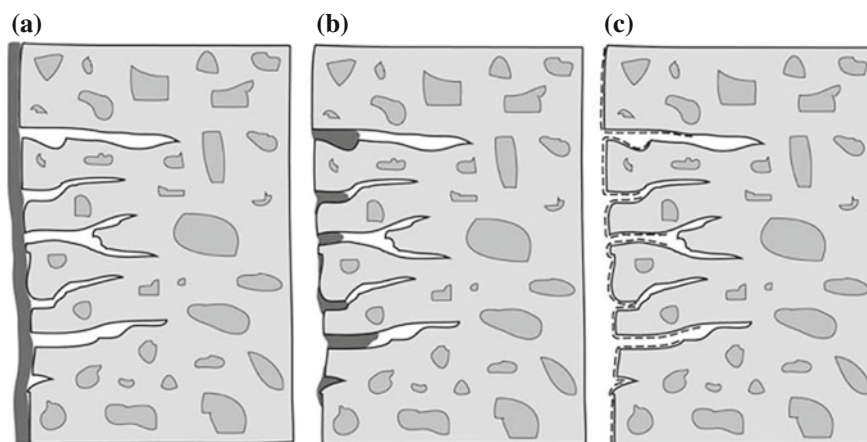


Fig. 1 Schematic representation of the mechanism of action of water repellents: **a** coating, **b** pore blocker, **c** pore liner. Adapted from Medeiros and Helene (2009)

Metallic soaps such as salts of oleic or stearic acid are commonly used to provide hydrophobicity to one-coat mineral renders due to their efficiency/cost ratio. In this context, any mortar which incorporates concentrations of 0.2–0.5 w/w% of these compounds will show coefficients of water absorption by capillarity well below the maximum levels adopted by standard requirements (CEN 2010). However, the fact that this type of water repellent blocks the pores inhibits water vapour leakage which can lead to excessive condensation as well as the appearance of efflorescence. Furthermore, a result of their surfactant characteristics, over time migration to the surface and leaching may occur, together with chemical degradation. Traditionally, the use of this type of water repellent was the main solution but nowadays a great deal of attention is given to silicon derived systems as discussed next. Nevertheless, natural ageing tests carried out to study in service performance of pre-mixed one-coat rendered walls containing salts of stearic and oleic acids over 6 and 10 years of exposure to environmental conditions showed that this system confers waterproofing properties for long periods. Interestingly, even though after 6 years degradation signs were detected, adequate resistance to water penetration was kept indicating that at surface level other degradation mechanisms such as photochemical and thermal may be involved.

As mentioned above, in the last decades silicon based water repellents have been receiving a great deal of attention. Within this so called family, there are those classified as film formers, and others as penetrants. Silicone resins form a film over the pore whilst penetrants, such as silanes and siloxanes act as pore liners penetrate concrete pores, forming a hydrophobic layer, thus inhibiting the penetration by water in liquid form but allowing water vapour to enter and exit, allowing the material to “breathe” freely. As a result of this, they have a better resistance to superficial condensation and to efflorescence. Notice should be made that in what regards the classification of silicone resins, care should be taken as they were classified as film formers by Edward McGettigan and as penetrants by the Masonry Institute of Washington, Pocket Guide—Brick and CMU Construction.

Figure 2 illustrates the structure of the main types of silicon based materials used as water repellent materials (Lecomte 2013). As it can be observed, silanes are silicon based chemicals that have a hydrolytically sensitive centre which can react with inorganic substrates to form stable covalent bonds and an organic moiety that alters the surface properties of treated surfaces (Tanford 1980; Wacker 2014).

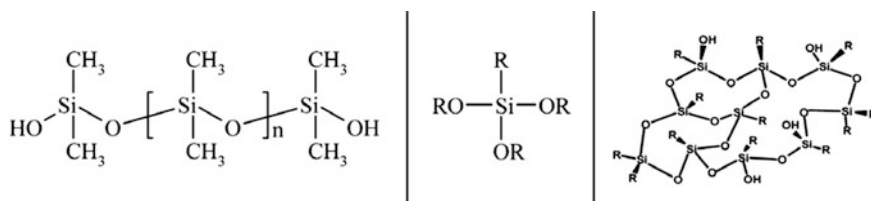


Fig. 2 Structure of polydimethylsiloxane, alkyl trialkoxysilane and schematic representation of a silicone resin, where R can be ethoxy, methoxy, methyl, phenyl or octyl groups (Lecomte 2013)

A good overview of the chemistry of this type of materials associated build building materials can be found in Torraca (2009).

Due to of their ability to form strong bonds with the substrate, silicon based water repellents confer excellent water resistance and their durability is quite good. However, they are prone to degradation via hydrolyses of the (O-Si-O) bonds especially in alkaline environments such as those found in the pores of cement based materials, or via acid rains. Additionally the organic radicals undergo oxidation reactions when exposed to air and light (Torraca 2009). Another problem that is frequently associated with the limited performance of penetrants is the fact that they do not penetrate the substrate to a significant depth (>0.1 inch). Hence, adequate quantities must be used and measurements should be made on the very same substrate to be treated (McGettigan 1995a, b). A number of studies have been reported on the performance of silicon based water repellents using laboratory tests on a variety of substrates, with particular emphasis on concrete and stone (Raupach and Wolff 2005; Lanzón and Garcia-Ruiz 2008; Maranhão and Loh 2010; Silva et al. 2011; Lecomte 2013; Muzenski et al. 2014; Esteves et al. 2014).

However, not much has been reported on long term field studies of one coat renders. Nevertheless, reference must be made to the 12 year study carried out by Schueremans et al. (2007), on the durability of reinforced concrete in marine environment. A significant contribution in this field was also the PhD dissertation of Kus (2002) which consisted in a holistic approach to the long-term study of the performance, degradation processes and ageing characteristics of rendered auto-claved aerated concrete (AAC) with and without water repellents (Kus 2002). Wacker (2014) has shown that silanes improve the hydrophobic behaviour of mortars yielding better water resistance and longer effect.

Recently, Silva et al. (2015) have reported results of semi-laboratorial tests carried out to monitor the performance of ETICS exposed to natural ageing conditions over 6 years. Up to 4 years, there is hardly any change in the water resistance capacity.

As mentioned above, a very judicious choice of the water repellent is required as its performance depends on a variety of parameters to ensure the compatibility between the substrate properties, the service conditions and application method. To address the complexity of such problem, Falchi et al. (2015a, b) have recently reported a systematic study of the effect of different water repellents in the preparation of limestone cement mortars and a detailed characterization. The same authors has also used multivariable the statistical methods to analyse the physical properties of different substrates and evaluated the relationship between the physical properties and the durability of the mortars by principal component analysis (PCA) and linear regression models. Interestingly, the use of linear regression models allowed the identification and quantification of associations between properties, composition and durability (Falchi et al. 2015a, b).

An indication of the importance of the use of water repellents and its limitations is the fact that several researchers continue to work on this field either using statistical methods as mentioned above, as well as developing complex hydrophobization modifiers as is the case for example of Tkach et al. (2015).

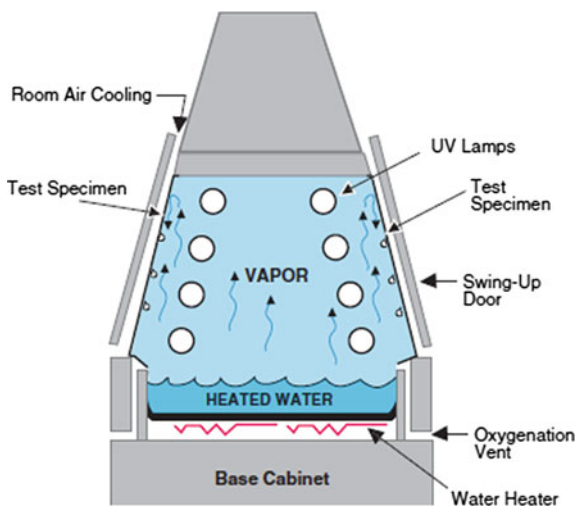
3 Durability Assessment Methodologies

Facing the needs to increment façades service life, which includes prediction of critical mechanisms when solutions start degradation and preventive or active maintenance actions, several methodologies have been studied and presented since many years. Many weathering or accelerated climate ageing methods and standards exist, that include water as a relevant parameter. Jelle (2012) point more than 20 standards on this topic. Even so, there are other methods that focus more on other parameters such as UV, temperature, intrinsic properties and compounds of the materials and construction factors. Main target of such methodologies is to correlate their results with service life prediction. Garrido et al. (2012), present several technical committees that have been worked as CIB W80, RILEM (71-PSL, 100-TSL, 175-SLM, ISO standards (ISO TC 59 SC 14) or others.

Other laboratory tests have been developed to accelerate materials weathering as close as in situ environment. Such method is known as the accelerating method QUV test and is already used for different materials namely coatings, adhesives, plastics and textile (Fig. 3). QUV accelerated weathering tester consists in a chamber able to simulate, as close as possible, outdoor conditions using a short wavelength, ultraviolet light and moisture cycles that are able to simulate in a realistically way the damaging effects of sunlight, dew, and rain. With this chamber it is possible to generate reproducible and reliable weathering data in just a few weeks or months, with good correlation to outdoor weathering test. With this technology, is possible to assess the durability of existing and new solutions for façades before being used in service conditions (ASTM G154 2006; ASTM D4329 1999; ASTM D4587 2014; ISO 4892 2013).

Silva et al. (2011) considering the need for more knowledge about the real durability of façade solutions, have focused one coat renders and ETICS in Portugal

Fig. 3 Scheme of QUV chamber, according to <http://www.q-lab.com/documents/public/>



region (between Oporto and Lisbon). The experimental methods allowed the evaluation which represents a large time span analysis, with a global time exposure to environmental conditions of up to 10 years, using several premixed one-coat rendered walls with and during 4 and 6 years after construction in the case of ETICS. Evaluation is made in terms of its ability to resist penetration of liquid water and, by extension, in terms of the waterproofing contribution of hydrophobic agents such as conventional metallic soaps. Tests were carried out always in dry conditions, usually in spring time. Finally, the study presents correlation between laboratory tests (characterization and accelerated) and in situ techniques that can characterize the slow degradation mechanisms in field conditions (natural ageing). According to Köppen climate classification, Portugal is representative of the Mediterranean climate and characterized as Csa, Csb (Peel et al. 2007).

3.1 Application and Evaluation in Rendered Walls Exposed to Natural External Conditions (Semi-laboratorial Tests)

The experimental work consisted in the application of one-coat render, with salts of stearic acid and oleic hydrophobic agents and classified as a W2 by EN 998:1 (LNEC 2004), through a machine for discontinuous projection on masonry walls (brick 11 cm), exposures to the North, South, East and West. Specifically, in the North direction, the mortar was applied and subjected to a different finish, i.e. float finish/sanded unlike all other cases where it took place a scraped finish. Table 1 shows, briefly, the relationship between the orientations of the walls and the parameters of the study.

After applying the mortar, a series of inspections for each year of service with the aim of analysing various characteristics of the one-coat renders were performed. Therefore, assessments of adherence by perpendicular tensile tests (pull-off tests) and of render inherent capacity to resist to liquid water penetration were performed. In this context, the following tests were included within inspections:

- (a) After the pull-off test, samples were collected from the rendered walls and prepared with $4 \times 4 \text{ cm}^2$ (thickness equals to mortar applied in case of adhesive tensile strength, or smaller, in the case of cohesive rupture in this test), according to Fig. 4a. In this context, it should be noted that, in any case, the thickness obtained was never less than 1 cm; absorption coefficient of

Table 1 Relation between orientations of the rendered walls and parameters of the study

Wall orientation	Color	Finishing
North	Red ("brick")	Float finish/sanded
South	Red ("brick")	Scraped
East	Red ("brick")	Scraped
West	Red ("brick")	Scraped

water by capillarity was also determined for the collected samples, according to EN 1015: 18 (CEN 2002).

- (b) Penetration tests of liquid water under pressure, known as pipe method or Karsten test, were conducted on tested-walls; this technique consists in the measurement of water volume absorbed by the mortar's surface in a given area and for an established period of time. The technical procedure uses a graduated tube, pipe-shaped, with a circular cross-section, 5.7 cm^2 along surface contact with mortar; the total height of the water column applied is 9 cm (see Fig. 4b). The results for this analysis are expressed in terms of accumulated values of absorbed water after 180 min.
- (c) Finally, the resultant samples from the adherence test were also tested for the determination of open porosity by hydrostatic weighing method with immersion in water, in order to investigate possible changes in the internal structure of mortars which may, by changing the structure of pores, contribute to possible variations of capillarity and water absorption (Flores-Colen et al. 2010).

The wettability of surfaces is normally assessed by measuring the static contact angles between the substrate and a drop of liquid. The values obtained provide information about the affinity of the surface and water and as illustrated in Fig. 5. A low contact angle corresponds to a high surface wettability as described by Young's equation (Shaw 1992). Contact angles can be measured using different techniques, being the most common the measurement of the contact angle formed in a drop of liquid placed on a horizontal surface. Figure 6 show the equipment used which is coupled to a camcorder and was developed at the University of Brno, Czech Republic.

In view of the intrinsic heterogeneities of surface, different measurements must be considered and averaged. An alternative method that is frequently used to assess the wettability of granular materials is the capillary rise method (CRM) also known as the Washburn cup method (Yuan and Lee 2013).

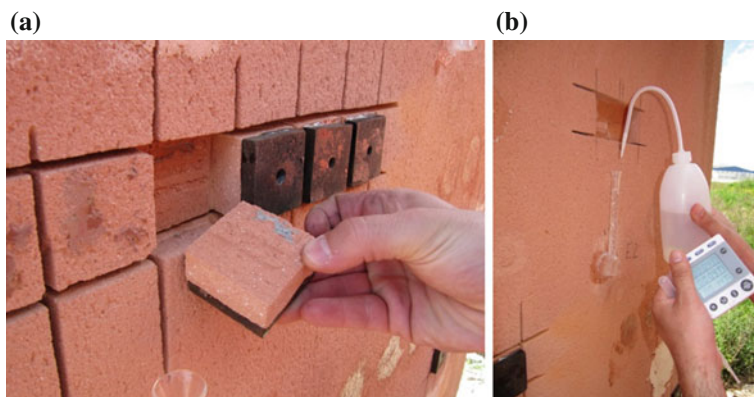


Fig. 4 **a** The perpendicular tensile adhesion test with consequent sampling for the determination of the coefficient of absorption of water by capillarity; **b** Karsten tube test

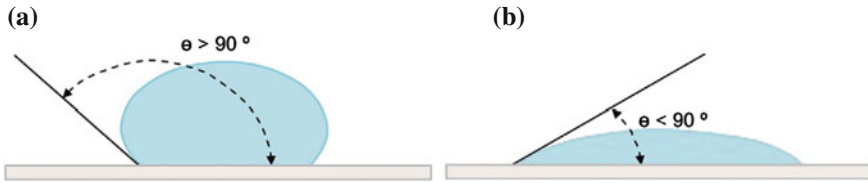


Fig. 5 Wettability of a solid surface by a liquid: **a** $\theta > 90^\circ$ and **b** $\theta < 90^\circ$, indicating non-wettability and high wettability, respectively (Klein et al. 2012)

Fig. 6 Equipment for the evaluation of contact angle



Even though this is a technique that is well established and used in different fields it is worthy of note that Klein et al. (2012) have published a comparative study on the evaluation of the wettability of mortar component granular materials through contact angle measurements. Additionally, it is also of relevance the review work published by Crick and Parkin (2010) regarding the preparation of super-hydrophobic surfaces which gives a good overview of the methods available to prepare surfaces that are super-hydrophobic to water droplets, discusses the most relevant models to describe the interaction between the surfaces and water and the effect of different parameters namely that of surface roughness.

3.2 Application and Monitoring of ETICS Exposed to Natural External Conditions (Semi-laboratorial Tests)

The experimental work consisted in the application of ETICS system using an organic render and silane agents as hydrophobic agents. Only North and South orientations for exposure have been considered (Fig. 7a). Table 2 summarizes the experimental conditions used.

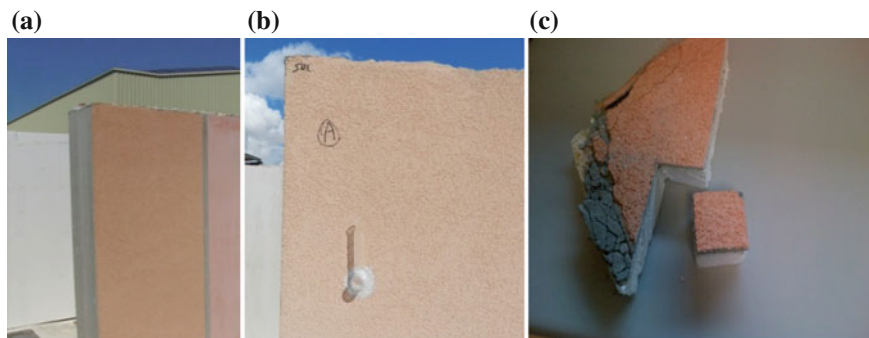


Fig. 7 **a** ETICS samples preparation; **b** Karsten tube test; **c** extracted sample for the determination of the coefficient of absorption of water by capillarity

Table 2 Relationship between orientations of the ETICS wall and parameters of the study

Wall orientation	Color
North	Red (“brick”)
South	Red (“brick”)

Upon 4 year in service the ETICS walls water resistance capacity was evaluated using the (a) Karsten pipe test method and (b) capillarity tests:

- (a) Karsten test, were conducted on tested-walls considering methodology described previously (see Fig. 7b);
- (b) Samples were collected from the rendered walls (see Fig. 5c) and prepared with $4 \times 4 \text{ cm}^2$ whose thickness corresponds to the whole system. The absorption coefficient of water was determined by capillarity absorption was according to ETAG 004 (EOTA 2008).

3.3 *In Situ Evaluation of ETICS Exposed to Natural External Conditions*

For the in situ evaluation of ETICS a system with the corresponding ETA 11/0287 (LNEC 2011) that includes a finishing render containing polyethylene waxes as hydrophobic agent was studied.

Visual inspections were carried out over time starting in 2008 up to 2014 (i.e. 6 years exposure conditions) in order to evaluate aesthetical performance in all orientations, Figs. 8 and 9.

Concerning the semi-laboratorial evaluation of the ETICS walls water resistance capacity the results presented in Table 3 show that upon 4 years there is hardly any significant effects. On the other hand, no damages in aesthetical performance were



Fig. 8 Visual inspection of in situ evaluation of ETICS at the beginning, after 4 years exposure conditions (*left* South orientation; *right* North orientation)



Fig. 9 Visual inspection of in situ evaluation of ETICS at the beginning, after 6 years exposure conditions (*left* South orientation; *right* North orientation)

Table 3 Results of the coefficient of absorption of water by capillarity and water absorption after 180 min for various one coat rendered walls' orientations, after 10 years of exposure to environmental conditions

Façade orientation	C (kg/m ² min ^{1/2})		Absorption of water under pressure ^a (ml)	
	Lab	10 years	Lab	10 years
North	<0.05	0.030	<0.5	0.20
South		0.033		5.60
East		0.019		0.80
West		0.046		8.50

^aAccumulated value over 180 min

noticed concerning in situ evaluation of ETICS exposed to natural external conditions for up to 4 years as shown in Fig. 9. However, between the 5th and 6th year, visible dark and green spots are clearly visible especially for the South orientation. This is thought to be associated with fungi and algae, as a result of water penetration on the surface of finishing thin render of the system.

3.4 Capillarity and Karsten Pipe Measurements

The capillary is water process progression in the liquid state through the capillary pores of a material and occurs when the adhesion forces between the liquid and the solid material are stronger than the cohesive forces of the liquid. Capillarity occurs when a material contacts with water in liquid phase. This phenomena result from particular properties of humidification of the solid material, generating curves interfaces between water and the retained air in the pores interior. A pressure gradient is formed on the interface liquid/gas, defined as capillary pressure, function of the interfacial tension, radius of curvature and from the humidification angle. The cohesive strength is the intermolecular attraction between similar molecules, or affinity between the molecules of the liquid, i.e., the tendency of the liquid has to remain as a group of particles. The adhesion strength is the attraction between different molecules, that is, the affinity of the liquid molecules with the solid pores molecules. If the adhesion forces between the liquid molecules and a solid that are in contact exceed the cohesion forces between the liquid molecules, the molecules of this tend to move to the solid surface and the area contact between the liquid and the solid tends to increase. The determination of water absorption by capillary action is done through the evolution of the amount of water absorbed by the solid unit surface area (kg/m^2), as a function of square root of time ($t^{0.5}$), yielding a graph where slope corresponds to the rate of water adsorption in the early stages, so the coefficient of water absorption by capillarity (C) ($\text{kg}/\text{m}^2\text{s}^{0.5}$) can be determined by Eq. 1 (Dullien 1979; Bear and Bachmat 1990).

$$C = \frac{m_{sat} - m_{dry}}{A\sqrt{t}} \times 10^3 \quad (1)$$

- m_{sat} —mass after capillary water absorption (g)
- m_{dry} —initial mass (g)
- A —area of the solid (mm^2)
- t —time (h)

According to EN 1015-18 (CEN 2002) the determination of water absorption by capillary can be determined from the difference of the gain between 10 and 90 min for samples with dimensions ($40 \times 40 \times 160$ mm). The Eq. 2 describes this method.

$$C = 0.1 \times (m_2 - m_1) \quad (2)$$

- m_1 —mass after 10 min (g)
- m_2 —mass after 90 min (g)

The Karsten tube technique registers the volume of water absorbed during chosen time-spans, usually 30, 60 or 180 min and determines the permeability, of the analyzed surface, to liquid water under low pressure, which enables the evaluation of its waterproof capacity. Individually or simultaneously, there are a vast

amount of factors that can influence this test. The existence of micro cracks, the state of the surface, the bonding process of the tube to the surface, climate conditions, number of tests, location of the tubes, different types of support and coatings, are some examples (Galvão et al. 2011; Flores-Colen et al. 2010).

Capillarity coefficient and water absorption under pressure results, from Silva et al. (2015) works, are presented on Tables 3 and 4 and in Figs. 10 and 11.

Upon application the one-coat renders were inspected regularly each year. As expected the results presented in Fig. 10 and Table 3 show differences in the absorption coefficient of water by capillarity for the various walls' orientations studied, after 10 years of exposure to environmental conditions. Interestingly, after 6 years the water absorption determined using either method show a significant increase confirming the expected result previously outlined (Silva et al. 2011).

The analysis of Fig. 11 also shows that the absorption of water, determined by Karsten tube method, is more affected over years of exposure than the coefficient of absorption of water by capillarity. In fact, this test presented a significant change after 5 years of exposure and, for two specific orientations, the values obtained raise doubts about the current capacity of mortar to resist to the penetration of water and to ensure waterproofing. It is assumed that mortar will continue to fulfil

Table 4 Results of the coefficient of absorption of water by capillarity and water absorption after 180 min for various ETICS walls' orientations, after 4 years of exposure to environmental conditions

Façade orientation	Water absorption by capillarity (kg/m ²)				Absorption of water under pressure ^a (ml)	
	After 1 h		After 24 h		Lab	4 years
	Lab	4 years	Lab	4 years		
North (A)	0.05	<0.01	0.22	<0.01	<0.5	0.10
North (B)		ND		ND		0.10
South (A)		<0.01		<0.01		0.20

^aAccumulated value over 180 min; ND—not measured

Fig. 10 Results for rendered walls after 10 years of different exposure conditions as a function of time for capillarity coefficient

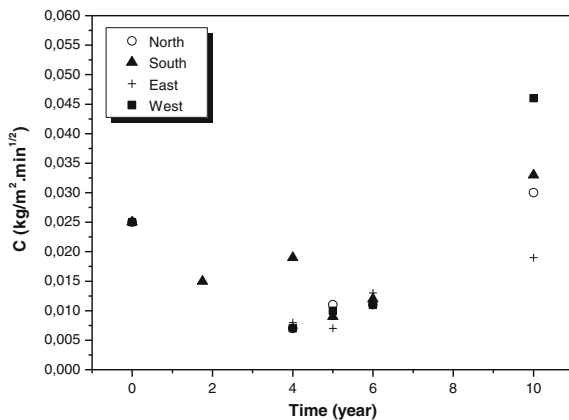
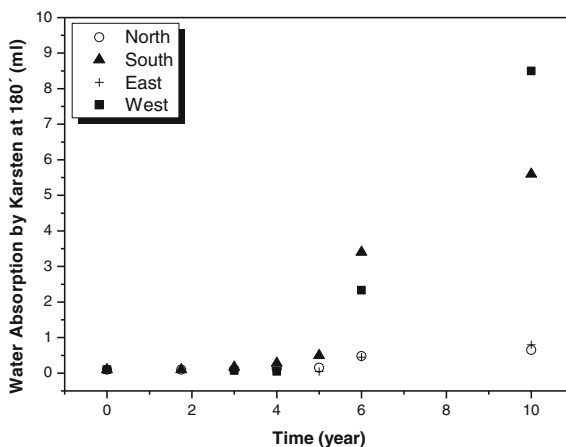


Fig. 11 Results for rendered walls after 10 years of different exposure conditions as a function of time for water absorption by Karsten tube



waterproofing function by considering that the coefficient of capillarity is not superior to standard values considered as a guarantee of efficiency at this level (water absorption with suction mechanism). On the other hand, results from Karsten tube can complement the interpretation of aesthetic variation occurred in rendered walls. With effect from 4 years it was observed higher concentration of fungi on rendered walls which can derive greater concentration of moisture on the mortar surface, clearly evidenced by the increase of water absorption values at 180 min.

Analyses of Table 3 and Figs. 10 and 11 show that South and West orientations have less resistance to water penetration as water absorption values are substantially higher for these orientations. Furthermore this difference increases with time with the “rupture point” occurring around 5–6 years suggesting that maintenance repairs should be scheduled for this period.

Also interesting was the fact that the Karsten pipe method is more sensitive than the capillarity tests as it allowed early and unequivocal identification of the effect of orientation and exposure time. Thus, this method has been used to study the impact of orientation on façade water resistance.

Concerning the semi-laboratorial evaluation of the ETICS walls water resistance capacity the results presented in Table 4 show that upon 4 years there is hardly any significant effects. On the other hand, no damages in aesthetical performance were noticed related to in situ evaluation of ETICS exposed to natural external conditions for up to 4 years as shown in Fig. 4. However, between the 5th and 6th year, visible dark and green spots are clearly visible especially for the South orientation. This is thought to be associated with fungi and algae, as a result of water penetration on the surface of finishing thin render of the system.

Although water absorption was recorded for all cases, all of them are below standard limits hence, it is more than reasonable to consider degradation as a process mainly at their surface responsible for the aesthetical ageing. On the other hand, considering that water absorption is more intense for the South and West orientations, especially when the Karsten method is used, it seems that other

degradation mechanisms, besides leaching, may be involved such as photochemical and thermal degradation. Additionally, other processes can be associated with façade ageing namely water evaporation, as water vapour resistance and dry index are complementary properties to be considered. Furthermore, leaching of other components such as biocides, also contributes to the façade ageing especially in organic renders and coatings as those used in ETICS.

3.5 *Laboratory Tests for Accelerated Ageing*

Considering hydrophobicity as the main affected mortars property, with direct impact on durability, Silva et al. (2011) developed a laboratory methodology, accelerating ageing by exploring the potential leaching of hydrophobic materials by water exposure.

The laboratory testing campaigns consisted in the assessment of hydrophobicity capacity under the following conditions:

1. Preparation of test circular pieces of one-coat render with (a) metallic soaps (0.5 %) and (b) silanes (0.5 %), with 2 cm thickness and diameter of 13 cm subject to curing conditions 22 °C, 55 % RH, for 28 days (t_0);
2. After the period mentioned in the test specimens, determination of the coefficient of absorption of water by capillarity, absorption of water under pressure from Karsten tube and contact angle of one drop applied on the surface of the samples (the last one, just in case t_0 and t_1) were performed; the static contact angle was measured with an instrument (coupled to a camcorder) that measures the surface energy according to Fig. 6.
3. Further study of the previous properties was performed after samples were subjected to leaching/drying cycles—different times of immersion in water (t_1 : 24 h, t_2 : 7 days and t_3 : 14 days) with subsequent drying to 70 °C until constant weight.

Results of such approach are presented on Figs. 12, 13, 14, 15, 16, 17, 18 and Table 5.

Laboratory tests reveal, as expected, significant differences in the behaviour of mortar when protected with metallic soaps or with silanes. As noted by Figs. 12 and 13 and Table 5, the values of absorption of water by capillarity are much lower when silanes are added. Figures 16 and 17 show a value of capillarity increment after the first cycle of leaching/drying (t_1) although the stability is reached for subsequent cycles. An attempt of correlation between the results shown in this context with the results relating in situ tests, expressed in Fig. 10, allows the consideration of a “pseudo-trend”, mentioned at the beginning of this discussion, can indeed be true, but this can only be proven with further testing with more years of evaluation.

Also, the absorption of water by Karsten tube test is significantly lower when the mortar presents the silane as hydrophobic agent, as revealed by the results show in

Fig. 12 Capillarity curves of one-coat mortar with metallic soaps, depending on curing time at normal conditions (t0) and after lixiviation/drying cycles (t1, t2 and t3)

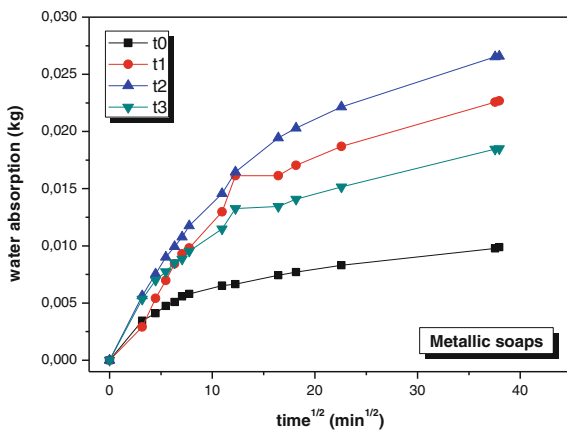


Fig. 13 Capillarity curves of one-coat mortar with silane, depending on curing time at normal conditions (t0) and after lixiviation/drying cycles (t1, t2 and t3)

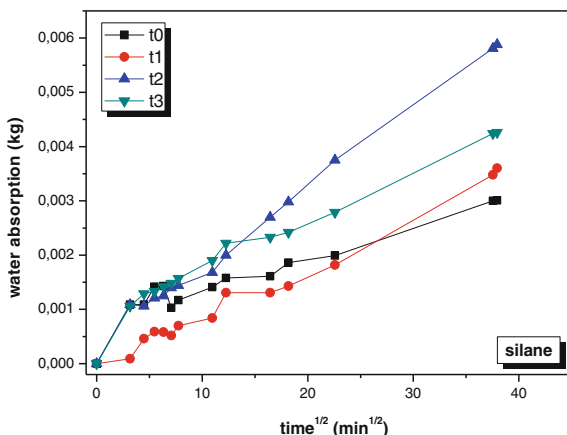


Fig. 14 Karsten pipe test graphs of one-coat mortars with metallic soaps, depending on curing time at normal conditions (t0) and after lixiviation/drying cycles (t1, t2 and t3)

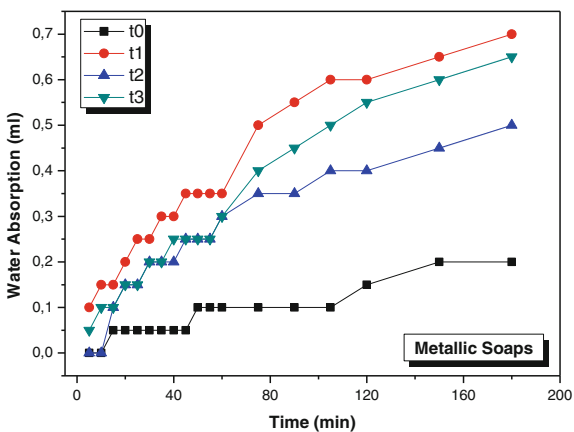


Fig. 15 Karsten pipe test graphs of one-coat mortars with silane, depending on curing time at normal conditions (t0) and after lixiviation/drying cycles (t1, t2 and t3)

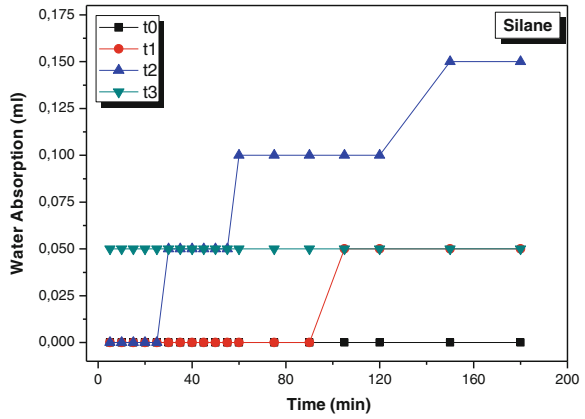


Fig. 16 Variation of coefficient of capillarity, depending on the number of leaching/drying cycles

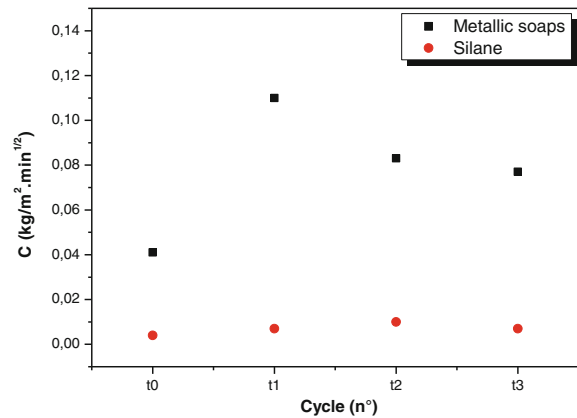
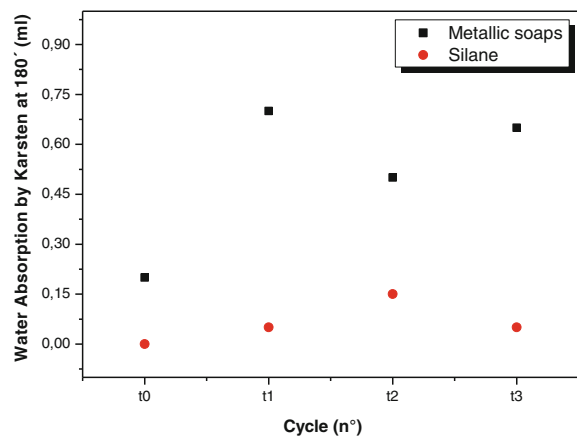


Fig. 17 Variation of water absorption by Karsten pipe method, depending on the number of leaching/drying cycles



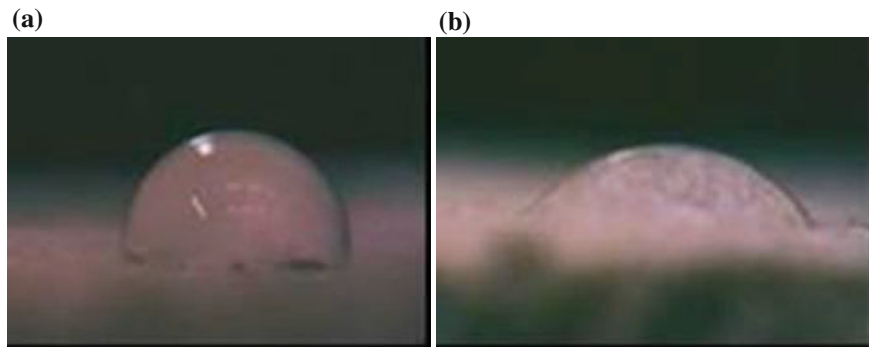


Fig. 18 Contact angle images after t0; **a** silane; **b** metallic soap

Table 5 Capillary coefficient, water absorption after 180 min (Karsten pipe) and contact angle measurements

Façade		C (kg/m ² min ^{1/2})	Absorption of water under pressure 180 min (ml)	Contact angle (°)
Silane	t0	0.004	0	89.70
	t1	0.007	0.05	–
	t2	0.010	0.15	–
	t3	0.007	0.05	84.30
Metallic soap	t0	0.041	0.2	45.96
	t1	0.11	0.7	–
	t2	0.083	0.5	–
	t3	0.077	0.65	46.94

Table 5 and Figs. 14 and 15. The data in Fig. 14 shows, especially for the mortar with metallic soaps, that its resistance to penetration of water decreases shortly after the first cycle of leaching/drying. Analysis of values obtained indicates that, although not reaching values as high, can make an interesting correlation with the values obtained by in situ tests, as shown in Fig. 11, and assume that this action of leaching/drying causes an action equivalent to a range around 5–6 years for in situ conditions assessed. For mortar with silane, the variation is not so evident, especially because it is considered that absorbance values are substantially lower. Nevertheless, the leaching action causes a change in resistance of mortar to penetration of liquid water, since it also register the increase in the value of water absorption. The analysis of Table 5 and Fig. 18, on the assessment and measurement of the angle of contact of mortars studied, reveals a peculiar behaviour, since increase for the case of metallic soaps and a decrease in case of silanes which leads to the difficulty to relate directly this property with measurements of coefficient of capillarity and absorption of water by Karsten pipe. Again, data analysis shows the biggest potential of silanes in ensuring the hydrofobicity of mortars, since these compounds have led to contact angle values significantly higher.

3.6 Pull-Off and Open Porosity

Additional properties as pull-off and open porosity are also important since contribute to evaluate mechanical stability, crack resistance and de-bonding, typical causes of water infiltration. As consequence, is recommendable to apply such techniques that evaluate adhesion and mechanical compatibility between materials since they can represent an indirect way of material mechanical characterization.

In situ evaluation of the cladding adherence must be performed periodically, for in-service conditions, allowing the timely detection of potential problems of loss of adherence and detachment. According to ASTM E2270 (ASTM 2005), a detailed inspection is recommended comprising at least three pull-off tests per coated surface

Since the technique is destructive, this allowed its use as a “probing” technique, leading to the analysis of the specimens and of their background after the pulling off had been carried through. Also, only the evaluation of the rupture mode and of the respective tension allowed pursuing complete knowledge of the causes of detachments or of deficient quality, very often associated with execution errors hugely different from one case to the other.

The number of valid tests, between five and 10, was enough in most cases for a qualitative diagnosis. However, each case must be analysed individually, taking into account the evaluation of the balance between human and economic resources available and the achievement of the established goal (with as little damage to the existing cladding as possible). These technique can be in conjunction of other non-invasive techniques application or through a systematic approach (Flores-Colen et al. 2009).

Collecting samples under in-service conditions and analysing them in the laboratory may complement the data acquired with the in situ methods since it is possible to study the material actually applied and not the one produced in the lab (under controlled conditions very different from the real ones). Measuring given in-service parameters in small samples collected during inspections may provide relevant data within a performance evaluation methodology for rendered façades, especially when there are no in situ tests to analyse certain in-service parameters.

Open porosity concerns voids that inter-communicate to allow the circulation of fluids within the mortar (the material is more or less permeable depending on the size and geometry of the pores).

Thomson et al. (2004) reports that open porosity is measured by microscopy or intrusion techniques. The most current are water immersion (sub-pressure or pressure) or mercury porosimetry. Only the latter also allows data collection on the porosimetric distribution (pore size and shape) (Veiga et al. 2004).

The hydrostatic or underwater weighing method cited above for bulk density, also allows the determination of open porosity, using Eq. 3.

$$P_{ap}(\%) = \frac{M_3 - M_1}{M_3 - M_2} * 100 \quad (3)$$

where M_1 , M_2 and M_3 represent the mass of the dry material, the mass of the immersed material and the mass of the saturated material, respectively. According to Navarro (2003), this method was established for stone by Hirschwald (1912), standardized by RILEM/PEM25 (1980), and later on extrapolated to other materials such as mortars and ceramics (ASTM 2006a, b). While the vacuum procedure is commonly used there are alternatives which vary essentially in the sample saturation method (immersion after depressurization or under pressure), the pressure levels used and the test duration.

One coat render adhesion and porosity results are presented in Figs. 19 and 20, respectively. Data of open porosity of mortar, showed in Fig. 20, suggest a slight decrease trend over the years of exposure, therefore this parameter can't contribute to the interpretation of results related to the variations of the absorption coefficient of water by capillarity and water absorption by Karsten tube method. The variation of adhesion (Fig. 19) corroborates the previous statement because the results

Fig. 19 Variation of the pull-off adhesion test, for the rendered walls orientations evaluated, according to the time of exposure to environmental conditions

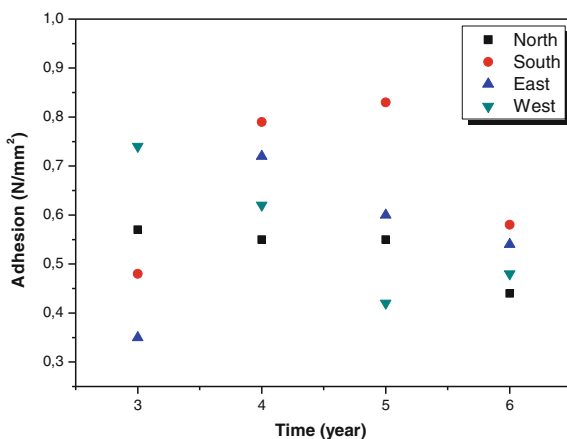
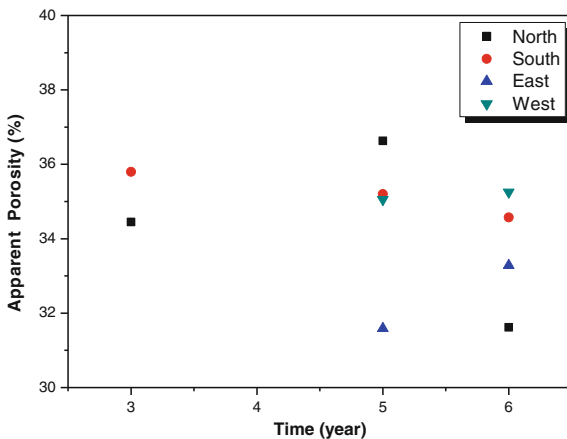


Fig. 20 Variation of open porosity, for the rendered walls orientations evaluated, according to the time of exposure to environmental conditions



haven't also shown any direct relationship with this parameter and the hydrometric properties evaluated.

As regards the role of the of internal structural changes resulting from the dynamics of hydration of cement of mortar over time on the mortars, from Figs. 19 and 20 it clear that the data are rather scattered. Even so, it may be acceptable to consider that adhesion seems to decrease over time whilst the porosity slightly increases; however, no clear trend can be established as most of the differences are within the method's error variations. These results indicate that the key parameter affecting water resistance penrance is the hydrophobicity of the render.

3.7 *Correction, Prevention and Maintenance*

Durability methods also allow to identify and to plan maintenance and prevention actions that can assure a lifetime increase of façade solutions with good performance. According to Flores-Colen et al. (2011), allow to focus the real needs of the solutions in service, the most critical items and to improve actions. This information will contribute to the development of solutions to prevent early ageing and adequate maintenance methodologies to delay their effect.

Figure 21 shows an example of a potential maintenance action plan for ETICS solution. According to this figure, a well-defined plan of inspection and maintenance of façades must always be in place which includes inspection, cleaning and then two level of intervention: (a) light intervention and (b) heavy intervention. Inspection should consider the appearance of cracks or any type of faults such as hairline cracks, gaps, patches, discoloration, biological colonization, blisters, or signs of corrosion associated with the vicinity of metallic elements. This type of inspection should be carried out every two years. However, more vulnerable areas such as those exposed to human action, near windows and drainage systems should be inspected annually. As regards cleaning, depending on the level and type of dirt, it may be limited to the use of diluted solutions of detergent and/or soft brushing. Yet, if biological colonization have developed, an aqueous solutions containing biocides is required. These procedures should be carried out every two years but areas at ground level or prone to be splashed (near sills and copings) should be cleaned on an annual basis. Additionally, rain pipes and external metallic elements must also be cleaned ever year. Maintenance to ensure façade durability requires different types of interventions over time. The so called light intervention corresponds to some repairs to be carried out, in average, every two years. Small gaps must be filled with compatible materials and some localized replacement of ETICS may be necessary. In the case of larger gaps the use of repair mortars and glass fiber mesh are necessary. Additionally, every five years, hydrophobic agents should be applied and some localized sections of the drainage system replaced such as joints, and some sections of the pipes. Heavy intervention is normally required every 25 years and those involve the replacement of the cladding of extensive areas of the façades.

Cód.	Maintenance actions list	Action Type	Scheduling of actions							
			M	S	A	B	Q	D	O	
I3	Checking for any cracks, gaps or detachments near the singular points of the system (startup profiles; angle in corners, adjustments with other elements on the facade border).	Inspection				x				
I6	Scan spots, discolorations, uniform or differential dirt, biological colonization on the coating surface on a current location and adjacent to border elements (sills, copings, etc.).					x				
I7	Check cracking coincident with the insulating boards, deficient flatness areas, located detachments or other anomalies that might indicate instability and systems deformations.				x					
I8	Check stilted areas at level of the ETICS finishing.				x					
I9	Identify critical areas of the facade (with insufficient detailing) and if there are aggressive conditions in service (exposed areas to human action).				x					
I10	Check moisture spots, stains, dirt on masonry elements in vain and trim and caulking on window frames.				x					
I11	Check the operation of roller shutters, including fittings and accessories.				x					
I12	Checking the drainage system and the proper functioning of the collection and drainage of the water (rain and domestic waters).				x					
I13	Checking for the presence of corrosion spots, buckling events in the connections with metal profiles, on adjustments areas and on the outer metallic elements.				x					
L1	Periodic cleaning of the decorative finishing to remove dirt and stains using dilute detergent solution, cold water at low pressure and/or brushing with soft brushes.		Cleaning			x				
L2	Cleaning biological colonization (algae, fungi, lichens) or biological microorganisms through organic compounds in aqueous dispersion (biocides or similar products) and applied by brush or roller with manual removal and brushing with soft brushes if necessary (dry brushing in case soluble salts).						x			
L3	Cleaning the coating surface area at the level of the ground floor, splash zone at the base of the walls and accessible areas along the ledges and copings coverage. The cleanig could be done using low pressure water, with or without a mild detergent, followed by an abundant rinse with water.					x				
L4	Cleaning copings and flashings, rainwater drainage network, gutters and other elements that contribute to the tightness of the facades.					x				
L5	Cleaning and clearing of gutters and exterior metallic elements.				x					
IL1	Punctual repair of the areas with gaps, dents or punctures due to the service impacts, with the filling of compatible material or pontual replacement of affected zones on the ETICS system.	Slight intervention			x					
IL2	Replacement of sealants and damaged joint materials.				x					
IL3	Crack repair in singular areas (close to the windows or connections) and critical point of the system (startup spots, corners and joints) with glass fiber net reinforcing.				x					
IL4	Located repair of cracks (only those that cross the first layer/finishing of the system or those that cross all the layers up to the backing) by application of finishing mortar or repair mortar with glass fiber net in the existing cracks with the greater opening in the backing.				x					
IL5	Application of water repellent or additives to improve the water resistance and the resistance of the surface dirty fixing or biological colonization developing.					x				
IL7	Replacement of decorative finishing by another compatible with adequate water vapor permeability, considering the accumulation of dirt, aging in service, and eventual stilted areas.						x			
IL8	Replacement of coating areas or ETICS insulation boards wich have anomalies, with application of new bonding material and/or mechanical fixation.							x		
IL9	Repair broken stonework and cracks treatment with resin or stone dust.					x				
IL11	Correction of the constructive arrangements in the facade areas (copings, window sills, etc.), to minimize degradation effects on the ETICS, if necessary.								x	
IL15	Located replacement of joints and water drainage pipe sections.						x			
IP1	Replacement of the coating system on large areas of the facade.	Heavy intervention							25	
IP2	Replacing the system coating mortar or system insulation boards on large areas of facade.								25	
Subtittle:										
M - Monthly; S - Semester; A - Annual; B - Biennial; Q - Five Year; D - Ten Year; O - other intervals										

Fig. 21 Example of maintenance action plan concerning an ETICS solution

4 Conclusions

Field testing, such as the determination of the coefficient of absorption of water by capillarity and Karsten tube, revealed behaviour changes in the ability of façades systems, as one coat renders or ETICS, to resist to the penetration of liquid water.

Despite of the fact that both types of systems studied have proven to yield results below the recommend standard limits, it can be inferred that exposure to climatic conditions leads to the start of degradation between 5 and 6 years of service. This degradation is revealed by the appearance of grey and green spots associated with the presence of fungi and/or algae colonies. Those spots are just sporadic in the beginning but increase over time.

Since both systems presented adequate resistance to water penetration it is considered that degradation consists in a surface process. On the other hand, considering that water absorption is more intense for the South and West orientations, especially when the Karsten method was used, it is concluded that other degradation mechanisms, besides leaching, may be involved such as photochemical and thermal degradation. Hence, future work should focus also on this hypothesis in order to improve durability of façades.

Finally, the relevance of the Karsten pipe methodology was highlighted since it reflects early changes in water resistance of façade solutions and show better correlation with aesthetical ageing as a result of exposure to real conditions.

Further tests are recommend (SEM, EDX, ...) to study the performance at different ages in order to investigate the degradation mechanisms at a molecular and structural levels.

Acknowledgements The authors acknowledge the support of the CERis/ICIST research centre from IST and of FCT (Foundation for Science and Technology). This work was also developed in the scope of the project CICECO-Aveiro Institute of Materials (Ref. FCT UID/CTM/50011/2013), financed by national funds through the FCT/MEC and when applicable co-financed by FEDER under the PT2020 Partnership Agreement.

References

- Addleson L (1992) *Building failures—a guide to diagnosis, remedy and prevention*, 3rd edn. Butterworth Architecture, Oxford, 166p
- Allsop D, Seal K, Gaylarde C (2004) Introduction to biodeterioration, Chap. 3. In: *Biodeterioration of refined and processed materials: paints*, 2nd edn. Cambridge University Press, Cambridge, pp 78–85
- ANFAPA and ITeC (2008) *Morteros Monocapa. Revestimientos de fachada*, Asociación Nacional de Fabricantes de Morteros Industriales, Servicio Editorial del ITeC, May
- ASTM (1996) *Standard practice for developing accelerated tests to aid prediction of service life of building components and materials*. ASTM E632-82. American Society for Testing Materials, Philadelphia
- ASTM D4329 (1999) *Standard practice for fluorescent UV exposure of plastics*

- ASTM (2005) Standard practice for periodic inspection of building facades for unsafe conditions. ASTM E2270. American Society for Testing Materials, Philadelphia
- ASTM (2006) C 830—Test methods for apparent porosity, liquid absorption, apparent specific gravity and bulk density of refractory shapes by vacuum pressure. ASTM Standard C830, American Society for Testing and Materials, West Conshohocken
- ASTM G154 (2006) Standard practice for operating fluorescent light apparatus for UV exposure of nonmetallic materials
- ASTM D4587 (2014) Standard practice for fluorescent UV-condensation exposures of paint and related coatings
- Bear J, Bachmat Y (1990) Introduction to modeling of transport phenomena in porous media, vol 4. Kluwer, Dordrecht
- BSI (2003) Guide to durability of buildings and building elements, products and components. BS 7543. British Standards Institute, London
- CEN, 1015:18 (2002), Methods of test for mortar for masonry—Part 18: determination of water absorption coefficient due to capillary action of hardened mortar. Committee for Standardization, Brussels
- CEN, EN 998-1 (2010) Specification for mortar for masonry. Rendering and plastering mortar. Committee for Standardization, Brussels
- Crick CR, Parkin IP (2010) Preparation and characterization of super-hydrophobic surfaces. *Chem Eur J* 16:3568–3588
- CSA (2001) Guideline on durability in buildings, CSA S478-95 (2001). Canadian Standards Association, Toronto, 112p
- Dullien F (1979) Porous media—fluid transport and pore structure, 2nd edn. Academic Press, New York. ISBN 0-12-223650-5
- EOTA, ETAG 004 2008, Guideline for European technical approval of External thermal insulation composite systems with rendering. European Organisation for Technical Approvals, Brussels
- Esteves C, Flores-Colen I, Veiga R (2014) Performance assessment of hydrophobic treatments on different substrates. 7th international conference on water repellent treatment and protective surface technology for building materials. LNEC, Lisboa, September 2014, pp 215–224
- Falchi L, Varin C, Toscano G, Zendri E (2015a) Statistical analysis of the physical properties and durability of water-repellent mortars made with limestone cement, natural hydraulic lime and pozzolana-lime. *Constr Build Mater* 78:260–270
- Falchi L, Zendri E, Müller U, Fontana P (2015b) The influence of water-repellent admixtures on the behaviour and the effectiveness of Portland limestone cement mortars. *Cement Concr Compos* 59:107–118
- Flores-Colen I, de Brito J, Branco FA (2009) In situ adherence evaluation of coating materials. *Exp Tech* 33(3):51–60
- Flores-Colen I, Silva L, de Brito J, Freitas V (2010) In-service parameters from façade rendering mortars: Bulk density and open porosity determined from samples collected in situ. *Struct Surv* 28(1):17–27
- Flores-Colen I, de Brito J, Freitas V (2011) On-site performance assessment of rendering façades for predictive maintenance. *Struct Surv* 29(2):133–146
- Foliente GC, Leicester RH, Wang C, Mackenzie C, Cole I (2002) Durability design for wood construction. *For Prod J* 52(1):10–19
- Freitas VP, Torres MI, Guimarães AS (2008) *Humidade ascensional*, 1a edn. FEUP edições, Porto
- Galvão J, Flores-Colen I, Brito J (2011) In-situ testing to evaluate the mechanical performance of rendered façades—rebound hammer and ultrasound techniques. 12th DBMC international conference on durability of building materials and components, Porto, April 2011, pp 991–999
- Garrido MA, Paulo PV, Branco FA (2012) Service life prediction of façade paint coatings in old building. *Constr Build Mater* 29:394–402
- Gaylarde CC, Morton LHC, Loh K, Shirakawa M (2011) Biodeterioration of external architectural paint films. *Int Biodeterior Biodegradation* 65:1189–1198
- Hendriks L, Hens H (2000) Building envelopes in a holistic perspective. International Energy Agency, Energy Conservation in Buildings and Community Systems, Amsterdam, vol 1, 101p

- Hermans M (1995) Deterioration characteristics of building components. A data collecting model to support performance management. Doctoral thesis. TUE University, Eindhoven, 233 p
- Hirschwald J (1912) Handbuch der Bau-technischen Gesteinpru-fung. Berntraeger, Berlin
<http://www.q-lab.com/documents/public/>
- ISO 4892-2 (2013) Plastics: methods of exposure to laboratory light sources, Part 2: Xenon-arc lamps
- Jelle BP (2012) Accelerated climate ageing of building materials, components and structures in the laboratory. *J Mater Sci* 47:6475–6496
- Klein NS, Bachmann J, Aguado A, Toralles-Carbonari B (2012) Evaluation of the wettability of mortar component granular materials through contact angle measurements. *Cem Concr Res* 42:1611–1620
- Kus H (2002) Long-term performance of water repellents on rendered autoclaved aerated concrete. PhD Dissertation, Centre For Built Environment, University of Gävle, Royal Institute of Technology, Stockholm
- Lacasse MA (2003) Durability and performance of building envelopes. NRCC-46888. National Research Council Canada, Ottawa. <http://irc.nrc-cnrc.gc.ca/fulltext/proc/nrcc46888>. Accessed in 20 July 2005
- Lanzón M, Garcia-Ruiz PA (2008) Effectiveness and durability evaluation of rendering mortars made with metallic soaps and powdered silicone. *Constr Build Mater* 22:2308–2315
- Lazniewska-Piekarczyk B (2010) Influence of anti-foaming admixture and polycarboxylic superplasticizer type on fresh and hardened properties of self-compacting mortar. *Archit Civil Eng Environ* 4:61–72
- Lecomte J-P (2013) Mortar protection, New silicone resin-based hydrophobic powder for the dry mix market. *Eur Coat J* 12:88–91
- LNEC, ETA 11/0287, 2011, European Technical Approval—weber.therm classic. Laboratório Nacional de Engenharia, Lisboa
- LNEC, Relatório 427/05 (2004) Homologação do revestimento de paredes monocamada, weber. pral classic. Lisboa
- Maranhão F, Loh K (2010) O uso de hidrofugantes em materiais de construção porosos. *Revista de Tecnologia da Construção* (São Paulo), *Techne*, vol 155, pp 4–7 (<http://techne.pini.com.br/engenharia-civil/155/artigo287730-2.aspx>)
- Masonry Institute of Washington (2012) Pocket guide—brick and CMU construction
- Mathivat J (1983) Reinforcement et réparation des structures, Raport général génie civil-Annales de l'ITBTP, n° 412
- McGettigan E (1995a) Factors affecting the selection of water-repellent treatments, *APT Bulletin*, vol 26, no 4, Preservation of Historic Masonry
- McGettigan E (1995b) Factors affecting the selection of water-repellent treatments, *APT Bulletin*, vol 26, no 4, Preservation of Historic Masonry, pp 22–26 doi:10.2307/1504446 read online http://www.jstor.org/stable/1504446?seq=5#page_scan_tab_content
- Medeiros MHF, Helene P (2009) Surface treatment of reinforced concrete in marine environment: Influence on chloride diffusion coefficient and capillary water absorption. *Constr Build Mater* 23:1476–1484
- Muzenski SW, Flores-Colen I, Sobolev K (2014) 4th international conference on the durability of concrete structures. Purdue University, West Lafayette, Indiana, 24–26 July 2014
- Navarro C (2003) Porosimetric analysis of ornamental rocks. Technical cahiers. Diagnosis and evaluation methodology of treatments for the conservation of historical buildings (in Spanish), Editor Junta de Andalusia, Granada, Spain, pp 134–153
- Peel MC, Finlayson BL, McMahon TA (2007) Updated world map of the Koppen-Geiger climate classification. *Hydrol Earth Syst Sci* 11:1633–1644
- Quintela MA (2006) Durabilidade de revestimentos exteriores de parede em reboco monocamada, MS. SC. Thesis, FEUP, Porto
- Raupach M, Wolff L (2005) Long term durability of hydrophobic treatment on concrete. Institute for Building Materials Research of the Technical University, Aachen

- RILEM (1980) Recommended tests to measure the deterioration of stone and to assess the effectiveness of treatment methods, Commission 25-PEM: Protection et Erosion des Monuments, pp 175–253
- Silva L, Flores-Colen I, Vieira N, Timmons AB (2011) Natural ageing tests to study in-service water resistance of pre-mixed one-coat rendered walls with hydrophobic agents. In: Proceedings of XII DBMC, Porto, Portugal, CD
- Silva L, Flores-Colen I, Vieira N, Timmons AB (2015) Natural ageing tests to study in-service different façade solutions—ETICS and premixed one-coat rendered walls. IPSB, Porto, Portugal, CD
- Schueremans L, Van Gemert D, Giessler S (2007) Chloride penetration in RC-structures in marine environment—Long term assessment of a preventive hydrophobic treatment. *Constr Build Mater* 21:1238–1249
- Shaw JD (1992) Introduction to colloid & surface chemistry, 4th edn. Butterworth Heinemann, Oxford
- Svensden S, Rudbeck C (2000) Development and optimisation of building envelopes for existing and new buildings. Methodology evaluation and design tools. International Energy Agency—Energy Conservation in Buildings and Community Systems, Leuven, 71p
- Tanford C (1980) The hydrophobic effect. Wiley, New York
- Thomson ML, Lindqvist JE, Elsen J, Groot C (2004) Porosity of historic mortars. In: Martens D, Vermeltfoort A, Damsma C (eds) Proceedings of 13th international brick and block masonry conference. IBMAC—13th international brick and block masonry conference. Eindhoven University of Technology, Amsterdam
- Tkach EV, Semenov VS, Tkach SA, Rozovskaya TA (2015) *Procedia Engineering* 111:763–769
- Torraca G (2009) Lectures on materials science for architectural conservation. The Getty Conservation Institute Los Angeles
- Veiga MR, Magalhães AC, NBokan-Bosilikov V (2004) Capillarity tests on historic mortar samples extracted from site. Methodology and compared results. In: Martens D, Vermeltfoort A, Damsma C (eds) Proceedings of 13th international brick and block masonry conference. IBMAC—13th international brick and block masonry conference. Eindhoven University of Technology, Amsterdam
- Viitanen H, Toratti T, Makkonen L, Peuhkuri R (2010) Towards modelling of decay risk of wooden materials. *Eur J Wood Wood Prod* 68:303–313
- WACKER 2014, The threat: what's just rain to most people is the worst enemy for coatings, www.wacker.com. Retrieve on 29 Sept 2014
- Yuan Y, Lee TR (2013) Contact Angle and wetting properties, Chapter 1. In: Bracco G, Holst B (eds) *Surface science techniques*, springer series in surface science 51. Springer, Berlin

Photocatalytic TiO₂ Nano-Coating for Biofouling Prevention of Clay Façades

Lorenzo Graziani, Enrico Quagliarini and Marco D’Orazio

Abstract Energy saving in building construction is an actual problem and it is central to the debate. In order to ensure low energy consumption of a building, the global building thermal resistance and the airtightness were enhanced until “overinsulated” buildings and air permeability of the entire building envelope (opaque surfaces and windows) was reduced. In this way, moisture loads and surface condensations are favoured and ideal conditions for the proliferation of microorganisms arise. Innovative techniques for biofouling prevention include the application of nano-coatings able to destruct bond between cells of microorganisms and substrata. The most used nano-material is TiO₂ because of its non-toxicity, photo-chemical stability and low cost. In this chapter, biofouling on brick substrata was presented, and the inhibitory effect of TiO₂ was studied as an alternative method to traditional maintenance intervention. Biofouling was measured through time by digital image analysis and colorimetric measurements. Results show TiO₂ was able to inhibit algal adhesion, and TiO₂ efficiency is strictly related to physical properties of substrata like porosity and roughness.

Keywords Nano-coating · Façade biodeterioration · Algae · Cyanobacteria · Durability

L. Graziani (✉) · E. Quagliarini · M. D’Orazio
Università Politecnica delle Marche, via Brecce Bianche, Ancona, Italy
e-mail: lorenzo_graziani@virgilio.it

E. Quagliarini
e-mail: e.quagliarini@univpm.it

M. D’Orazio
e-mail: m.dorazio@univpm.it

1 Introduction

Growth of aero-terrestrial microorganisms on man-made surfaces such as roof tiles, building façades and concrete pathways is regarded as a biofouling problem (D’Orazio 2012; Johansson 2011, 2005; Flores-Colen et al. 2008).

Biofouling occurs on building façades because they are inevitably subject to the action of weather that contributes to create a suitable combination of dampness, warmth and light, necessary for algal growth (Barberousse et al. 2006; Miller et al. 2009).

In addition, in recent years, demand for energy saving and lowering of maximum thermal transmittance, has led to a modification of building envelope used in either new buildings or energy requalification of ancient buildings (Sedlbauer and Krus 2002; Kunzel 2007; Kunzel et al. 2002; Künzel et al. 2006).

The new technologies used for building insulation lead to “overinsulated” buildings limiting outgoing heat flux from inside the building to outside (Kunzel et al. 2002; Künzel et al. 2006; Sedlbauer 2001). The very little resulting heat flow coming from the building walls is generally not sufficient to prevent a temperature drop of the finishing exterior layer, which in turn, is responsible for condensation (D’Orazio et al. 2014).

These are the main causes at the base of biofouling on building envelope that, in conjunction with bioreceptivity (Guillitte and Dreesen 1995) of the substrata, lead to the deterioration caused by the colonization of microorganisms (biodeterioration).

Biodeterioration consists in the appearance of stains in the short period and it causes the breakage of the elements if no maintenances occur. The presence of microorganisms could help also the proliferation of spores or other harmful particles for human health causing breathing problems, irritation or allergies (Verdier et al. 2014).

Beside the aesthetical and health problems, biofouling causes an increasing in costs for restoration, inevitably.

Biofouling involves also brick surfaces, indeed statistical data, from natural observations, show that about 35 % of the analysed parts of monolithic brick wall exhibits microbial growth on the surface (Flores-Colen et al. 2008; Silvestre and de Brito 2011, 2009).

Traditional methods for biofouling remediation (either mechanical, physical or chemical) need manpower, re-application over time, and they are not always adequate to be applied for biofouling remediation (e.g. chemical product in Cultural Heritage).

Actually, nanotechnologies allow coating substrata with products that weaken the link between cells of microorganisms and construction materials. The most promising nanomaterial used in building construction is titanium dioxide (TiO₂) (Graziani et al. 2013, 2014a, b).

Under ultraviolet (UV) exposure, TiO₂ becomes super hydrophilic, and so creates an uniform water film on treated surfaces, preventing contact between external dirt (including algal cells) and the substrate (Chen and Poon 2009; Fujishima et al. 2000; Fujishima and Zhang 2006).

In this chapter, the potential use of titanium dioxide for biofouling reduction on brick façades was investigated under accelerated climatic conditions.

Experimental campaign consists in three main phases. Firstly, TiO₂ efficiency was tested under weak UV radiation to simulate a non-direct solar light. Secondly, the effect of substrata was studied by treating specimens with different porosity and roughness. Finally, two doped TiO₂ sols with Ag and Cu nanoparticles were applied on specimens to understand the effect of the addition of other noble metal with bactericidal properties.

Results shown TiO₂ is able to slow down the growth of microorganisms on the specimens' surface. In favourable conditions (low porosity and roughness), treatment inhibits algal adhesion almost completely.

2 Materials and Methods

2.1 Tested Materials and Characterization

Research activities were conducted on two types of prismatic clay bricks specimens with 80 × 80 × 30 mm³ dimension. The first was a fired clay brick manufactured by extrusion and fired at about 1200 °C (labelled with M), while the second was formed by hand and then it was fired at about 700 °C (labelled with A). Table 1 resumes tested specimens with their description and treatment.

These types were chosen because they replicate brick used in modern architecture (M) and historic buildings (A).

Total porosity and porous distribution of clay brick specimens was measured by a mercury intrusion porosimeter (Micromeritics Autopore III) according to the ASTM D4404 standard (2010).

Not only total porosity was considered, but also correlation between biofouling and surface's roughness was found because these parameters showed to play a key role in the bioreceptivity of other building materials (Barberousse et al. 2006; D'Orazio et al. 2014; Miller et al. 2012; Ortega-Calvo et al. 1995; Jain et al. 2009; Tran et al. 2014).

Arithmetic average roughness (Ra) were evaluated according to European standards (UNI EN 1994; UNI EN ISO 2009) by using a Diavite DH-5 portable rugosimeter. Ten measurements were made on the surface of each specimen on a track of 15 mm with a cut-off length of 0.8 mm.

Table 1 Specimens identification and description

Sample name	Description	Treatment	Test conditions
MU	Low porous specimen with rough surface	Untreated	UV = 165 mW/cm ²
MT	Low porous specimen with rough surface	TiO ₂	UV = 165 mW/cm ²
ARU	High porous specimen with rough surface	Untreated	UV = 8 W/m ²
ART	High porous specimen with rough surface	TiO ₂	UV = 8 W/m ²
ALU	High porous specimen with smooth surface	Untreated	UV = 8 W/m ²
ALT	High porous specimen with smooth surface	TiO ₂	UV = 8 W/m ²
MRU	Low porous specimen with rough surface	Untreated	UV = 8 W/m ²
MRT	Low porous specimen with rough surface	TiO ₂	UV = 8 W/m ²
MLU	Low porous specimen with smooth surface	Untreated	UV = 8 W/m ²
MLT	Low porous specimen with smooth surface	TiO ₂	UV = 8 W/m ²
ARUn	High porous specimen with rough surface	Untreated	UV = 8 W/m ²
ARAg	High porous specimen with rough surface	TiO ₂ -Ag	UV = 8 W/m ²
ARCu	High porous specimen with rough surface	TiO ₂ -Cu	UV = 8 W/m ²
ALUn	High porous specimen with smooth surface	Untreated	UV = 8 W/m ²
ALAg	High porous specimen with smooth surface	TiO ₂ -Ag	UV = 8 W/m ²
ALCu	High porous specimen with smooth surface	TiO ₂ -Cu	UV = 8 W/m ²
MRUn	Low porous specimen with rough surface	Untreated	UV = 8 W/m ²
MRAg	Low porous specimen with rough surface	TiO ₂ -Ag	UV = 8 W/m ²
MRCu	Low porous specimen with rough surface	TiO ₂ -Cu	UV = 8 W/m ²
MLUn	Low porous specimen with smooth surface	Untreated	UV = 8 W/m ²
MLAg	Low porous specimen with smooth surface	TiO ₂ -Ag	UV = 8 W/m ²
MLCu	Low porous specimen with smooth surface	TiO ₂ -Cu	UV = 8 W/m ²

2.2 Nano-coatings Preparation and Application

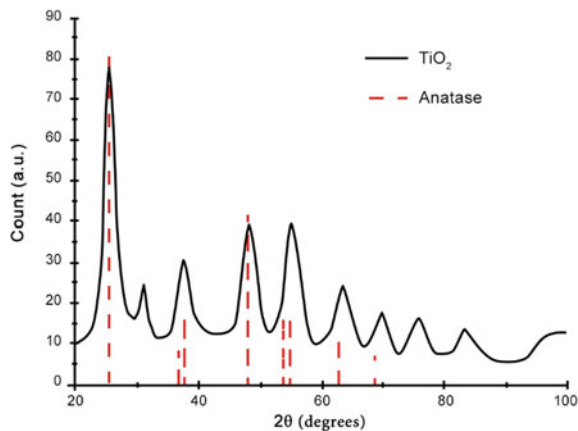
Nano-TiO₂ sols were prepared by Salentec S.r.l. from tetrapropyl orthotitanate (TPOT) from Sigma-Aldrich 97 % as TiO₂ precursor (Licciulli et al. 2011). The calculated content of TiO₂ from such a preparation is 1 wt%. A white precipitate is formed and readily dissolved by stirring and heating in about two hours.

After this process, a TiO₂ amorphous sol was obtained, and it was composed by very fine anatase crystals with an average diameter of 4 nm, as estimated by XRD patterns elaboration (Fig. 1).

The average crystal size was around 40–50 nm with a narrow grain size distribution indicating a partial aggregation of the primary crystallites.

TiO₂ sol was the base of doped solutions with Ag (TiO₂-Ag) and Cu (TiO₂-Cu). Ag nano-powders were added to TiO₂ base with concentration of noble metal equal to 1 % (molar weight/TiO₂ weight), while the concentration of TiO₂-Cu solution was equal to 1 % (weight/TiO₂ weight). Thus, 100 ml of solution contains 1 g of TiO₂ and 0.02 g of Ag and 0.01 g of Cu, respectively.

Fig. 1 XRD pattern of synthesized TiO₂ particles



The sols were deposited directly on brick specimens by spray coating. The spray coating was chosen because of its simplicity, quickness and compatibility with real applications.

The solutions were manually applied by an air spray gun with a nozzle of 0.8 mm diameter from a distance of about 250 mm.

Scanning electron microscopy (SEM) observations were carried out to study the microstructure of deposited TiO₂. By a FEI Quanta-200 instrument equipped with an energy-dispersive X-ray spectroscopy (EDS) analysis system (Oxford INCA 350).

2.3 Accelerated Biofouling Test

Two algal strains were chosen for accelerated biofouling test: *Chlorella cf. mirabilis* and *Chroococciopsis fissurarum*, both deposited at the Algotheque du Laboratoire de Cryptogamie of the Museum National d'Histoire Naturelle (MNHN) (Fig. 2). These microorganisms are common colonizers of building façades (Barberousse et al. 2007).

Each strain grown separately in Bold's Basal Medium (BBM), prepared as indicated in ASTM D5589-09 (2009), until the needed amount of broth culture was reached.

Accelerated biofouling tests on the specimens were achieved by performing water run-off tests in the laboratory-made system showed in Fig. 3.

Biofouling tests were carried out into three glass chambers (100 × 40 × 53 cm³) containing two aluminium-glass composed racks to fix up specimens. Forty litres of broth culture were inoculated into the chambers. Algal suspensions were composed by BBM and algal cells (5 %) with a final concentration of approximately 4 mg/L (dry mass determination).

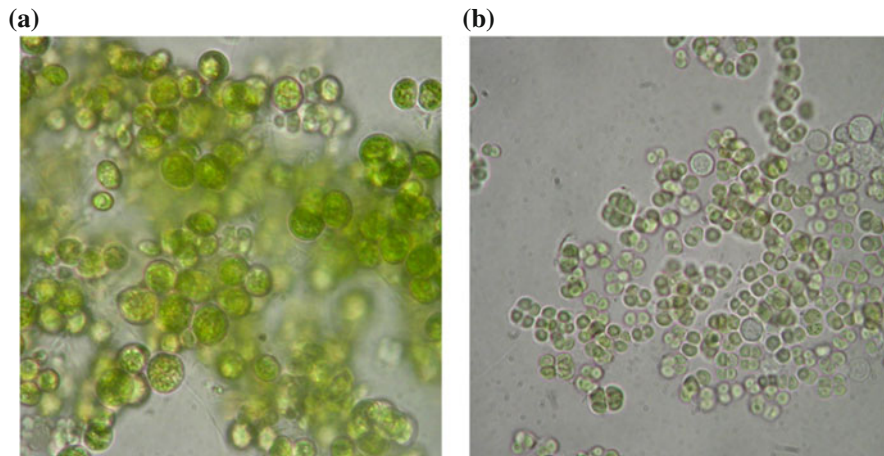


Fig. 2 Microbial culture used in the research: *Chlorella mirabilis* (a), *Chroococcidiopsis fissurarum* (b)

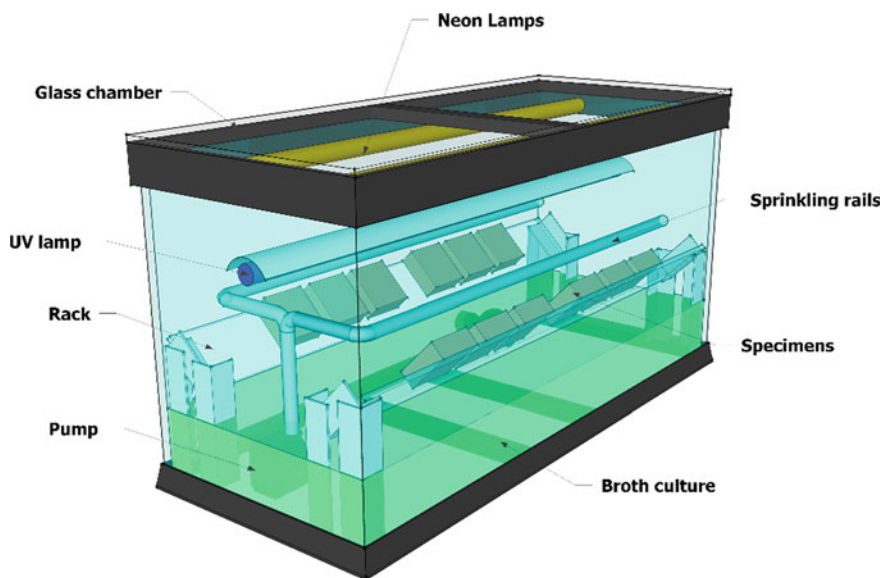


Fig. 3 Scheme of glass chamber used for accelerated growth test

Figure 4 shows climatic conditions inside the chambers. Algae broth culture were maintained at 24 °C with a heater (Heather Bluclima 150 W) and continuously agitated by two wave pumps (Hydro, model Koralia 1600/425).

Since algae are phototroph organisms, needed daylight was provided by two 39 W neon lamps with a light temperature of 5000 K. During test with low UV

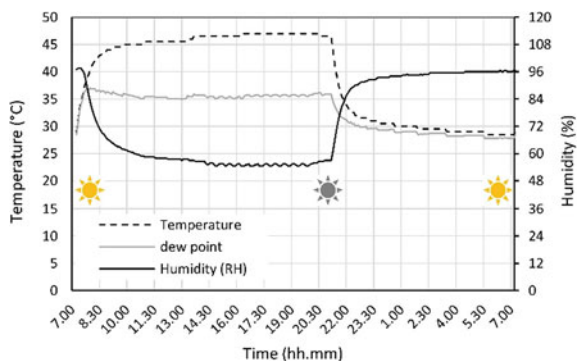


Fig. 4 Daily climatic conditions inside the glass chamber during accelerated growth test. *Yellow* symbols indicate light on, *grey* symbol indicate light off

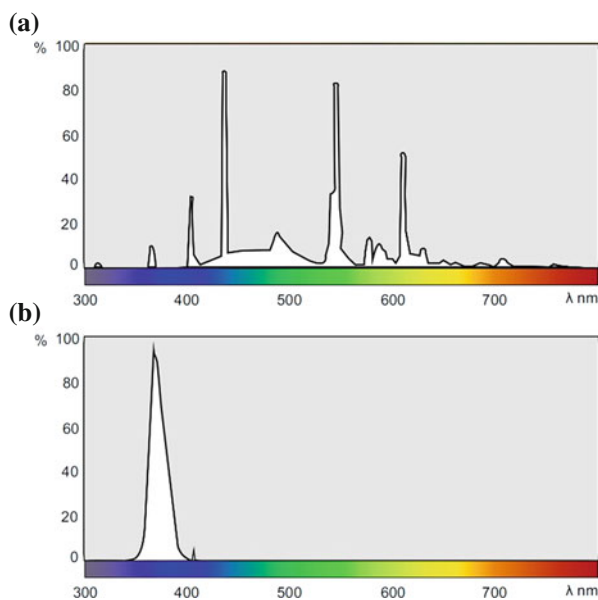


Fig. 5 Light spectrum of daylight neon lamps (a) and UV-A lamp (b) used in accelerated growth test

intensity, no neon lamp was installed and daylight lamps provided an UV intensity equal to 165 mW/cm^2 . In other cases, climatic chambers were equipped with two Black Light Blue neon to provide UV irradiation (8 W/m^2), necessary for the activation of photocatalytic power of TiO₂.

Day/night period was set as 14/10 h respectively; during day all neon were switched on, and during simulated night period they were turned off (Fig. 4).

Figure 5 shows the light spectrum of both daylight and UV lamps.

Specimens were sprinkled with broth culture (run/off cycle of 15 min for a duration of 6 h) by two PVC tubes with three 2 mm-holes drilled every 20 mm connected to a 500 L/h water pump (Blupower) submerged in the broth culture. Fifteen litres of broth culture were sprinkled every day/night period.

2.4 Biofouling Evaluation

In order to evaluate the biofouling on the specimens' surface, two techniques were adopted: colorimetric analysis and digital image analysis (DIA). Data were collected weekly by a portable spectrophotometer (Konika Minolta CM-2600D) onto nine points over the surface of each sample.

Colour changes due to the occurrence of microalgal film were determined using Eq. 1.

$$\Delta E = \sqrt{(L_0^* - L^*)^2 + (a_0^* - a^*)^2 + (b_0^* - b^*)^2} \quad (1)$$

where L_0^* , a_0^* and b_0^* are the CIELab coordinates of samples at time zero, and L^* , a^* and b^* are the CIELAB coordinates of the sample at each measuring time (once a week).

DIA was performed to measure algal coverage (as a percentage of the total specimen surface). Office scanner (Canon Scan Lide 700F) was used to acquire image at a resolution of 600 dpi. Acquired images were filtered by a threshold and ImageJ software was then used to calculate area covered by microorganisms. In this way, only contaminated pixels by algal cells were counted, and the percentage was calculated by dividing area of algae by total area.

In order to study phenomenon at a microscopic scale, specimens were observed by using a Confocal Laser Scanner Microscope (CLSM). This investigation was carried out on specimens subject to low UV radiation only.

At the end of the accelerated growth tests, specimens were manually washed with a laboratory dispenser filled with 500 ml of distilled water.

Portions of samples ($10 \times 5 \text{ mm}^2$) were observed before and after the washing process by using a Carl Zeiss Axioplan 200 M Microscope equipped with a Zeiss LSM510 module.

After the acquisition of the images, DIA was used to measure the extension of biofilm on the surfaces. Thickness of the biofilm was also assessed by COMSTAT, as previously elucidated (Heydorn et al. 2000; Irving and Allen 2011).

Area reduction and thickness reduction due to washing process (in percentage) were calculated as indicated in Eqs. 2 and 3 respectively.

$$\Delta A = \frac{A_{BW} - A_{AW}}{A_{BW}} \times 100 \quad (2)$$

$$\Delta T = \frac{T_{BW} - T_{AW}}{T_{BW}} \times 100 \tag{3}$$

where A_{BW} was the area (in μm^2) covered by microalgae before the washing process and A_{AW} indicates extend of biofilm after the washing process, while T_{BW} and T_{AW} are the average thickness (in μm) of the biofilm before and after the washing process respectively.

3 Results and Discussion

3.1 Materials and Nanocoating Characterization

Table 2 resumes results about characterization.

Total porosity of A specimens was 36.65 %, and it was higher than porosity of L specimens equal to 19.13 %.

Mercury intrusion porosimetry revealed the microstructure of A specimens was meanly composed by pores with a diameter equal to about 0.94 mm, while M specimens were mainly characterized by pores with a diameter of about 0.38 mm. Thus, diameter of the pore in high porous specimens was more than twice the diameter of the pore in low porous specimens.

Figure 6 shows microstructure of coating applied on clay brick substrate observed by SEM as described in Sect. 2.2.

The formation of titania film was evident by comparing images of treated (MT) specimens with image of untreated ones (MU). Crystals of TiO₂ are the white spots in the image.

Micro-cracks formation (visible on MT in Fig. 6) can be associated to the roughness of the surface (Lopez et al. 2013). In fact, substrate roughness promotes retention of TiO₂ sol on the surface limiting its absorption, resulting in greater deposition of anatase crystallites and greater thickness (Lopez et al. 2013). Thick film of TiO₂ was subjected to tension during the drying step that cause the formation of cracks.

Table 2 Results about substrata’s characterization

Sample group	Total porosity (%)	Roughness Ra (μm)
M	19.13 ± 1.66	2.8 ± 0.5
AR	36.65 ± 0.65	8.9 ± 0.9
AL	36.65 ± 0.65	1.1 ± 0.1
MR	19.13 ± 1.66	2.8 ± 0.5
ML	19.13 ± 1.66	2.4 ± 0.5

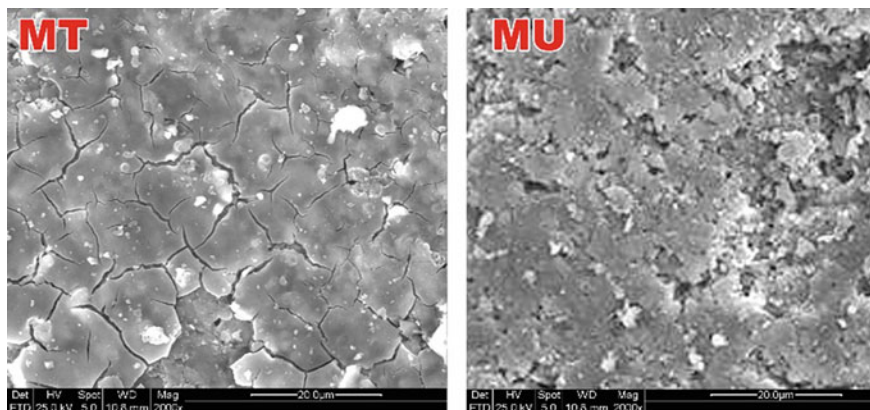


Fig. 6 SEM observation of clay brick treated with TiO_2 (MT) and control specimen (MU)

3.2 Inhibitory Effect of TiO_2 Under Low UV Radiation

In this section, the results about the anti-biofouling effect of TiO_2 , under low UV radiation were reported. In this part of the research, only MU and MT specimens were tested (see Table 1).

Figure 7 shows maximum colour variation (all CIELab coordinates) reached during the accelerated growth test corresponding to the maximum biofilm extension on the surface of the specimens.

The appearance of algal spot (green stains) caused darkening (minor L^*), greening (minor a^*), and more blu (higher b^*) specimens. The global colour variation (ΔE) was visible by naked eye in case of both untreated and treated specimens because it was higher than just noticeable difference equal to 2.3 (Sharma and Press 2002).

Fig. 7 Maximum color variation due to biofouling formation

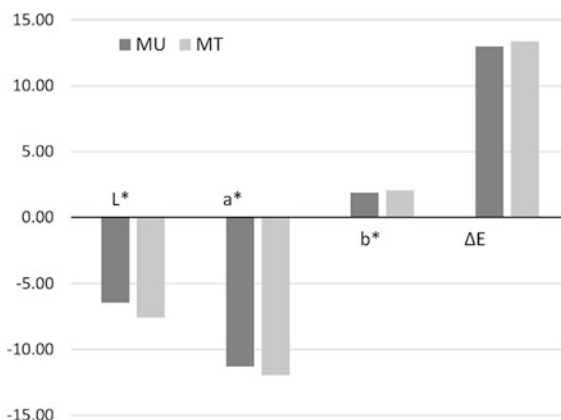
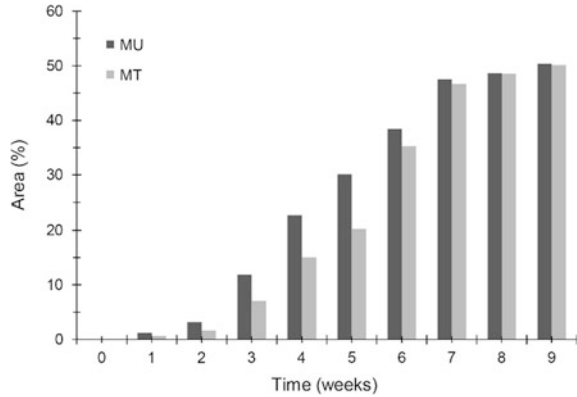


Fig. 8 Percentage of area covered by microorganisms during accelerated growth test



Conversely, no visible difference exists between treated specimens and control ones because ΔE between MU and MT was minor than 2.3. Thus, it is possible to sustain that biofouling on treated specimens was the same on control ones, and TiO₂ coating was unable to stop the superficial colonization by algae and cyanobacteria.

These evidences could be feasibly ascribed to a weak UV radiation unable to activate the TiO₂ biocide effect.

Percentages of area covered by the biofilm are given in Fig. 8. Figure 8 shows that TiO₂ did not inhibit the growth of microalgae on treated specimens; indeed area covered at the end of test was the same of control specimens. This finding confirms previous finding referred to colour variations.

Bars in Fig. 8 shows differences between MU and MT specimens from week 3 to week 6 indicating a slowing down of the microalgal colonization. In order to confirm these finding, results of micro-observation by CLSM (see Sect. 2.4) are resumed in Table 3.

CLSM observations revealed that washed area on treated specimens is about three times bigger than on control ones. Moreover, washing process cause a reduction of biofilm thickness equal to 30.47 % in case of treated specimens and to 13.67 % in case of untreated ones.

This finding might be explained by the higher wettability of specimens treated with TiO₂ and irradiated with UV light that allow the formation of a super hydrophilic film on the specimens surface, which renders the adhesion of algae and cyanobacteria more difficult, and helps the washing action of water.

Table 3 Area and thickness reduction of biofilm evaluated by CLSM

Sample	ΔA (%)	ΔT (%)
MU	9.15 ± 2.09	13.67 ± 4.69
MT	25.87 ± 2.44	30.47 ± 7.15

3.3 Relationship Between Substrata and TiO₂ Efficiency

Figure 9 shows quantitative results from DIA of both rough and smooth specimens of A and M bricks.

Trends of treated specimens (T) are always lower than curves of untreated (U) specimens, except for ART, which is overlapped to ARU from week 8 to the end of test, indicating TiO₂ was unable to inhibit algal growth on this type of specimens.

Thus, although TiO₂ has photo-induced self-sanitisation properties, it cannot inhibit the anchorage of algal cells in case of high porous substrata coupled with rough surfaces.

Table 4 reports the maximum algal coverage of each group of specimens, at the end of accelerated growth test.

The ratio between ALU and ARU was equal to 0.76, while this ratio drops to 0.34 for ART and ALT, evidencing the influence of roughness in the biofouling process, since it accelerates the biofouling on building materials by favouring the anchorage of algal cells on the substrata.

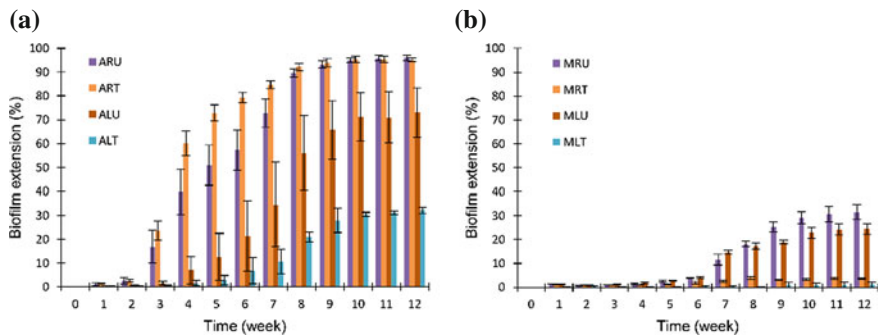


Fig. 9 Biofilm extension on A specimens (a) and M specimens (b) during accelerated growth test

Table 4 Results about substrata’s characterization

Sample	Biofouling extension (%)
ARU	96.04 ± 1.18
ART	95.12 ± 0.84
ALU	73.05 ± 1.39
ALT	32.23 ± 1.33
MRU	31.59 ± 3.21
MRT	7.67 ± 1.13
MLU	24.49 ± 2.25
MLT	3.55 ± 0.28

In addition, it is possible to conclude that TiO₂ was able to limit the adhesion offered by the asperity, in this study it allowed to reduce biofilm's extension of about 55 % in case of A specimens, and of 40 % in case of M specimens.

In case of smooth specimens, the effect of TiO₂ was less evident because a part of biofouling reduction can be attributed to a minor roughness of specimens' surface.

Another effect, due to TiO₂ treatment, was the normalization of the biofouling process as shown by standard deviations in Table 4; which in treated specimens were smaller than in untreated ones.

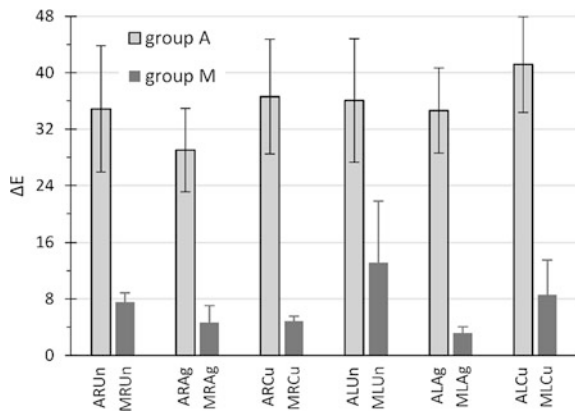
The porosity of clay bricks played a key role in the biofouling process. Indeed, the maximum algal coverage of group M (31.59 %) was lower than the minimum algal coverage of group A (32.23 %).

3.4 Ag-Doped TiO₂ and Cu-Doped TiO₂ Toward Algal Growth

In this section, results about the biocide power of doped titania with Ag and Cu nanoparticles were resumed. Biofouling was evaluated, as before, measuring colour variation and extend of algal coverage as described in Sect. 2.4.

By considering final colour variation, plots in Fig. 10 shows higher ΔE in case of A specimens. Moreover, no significant different exists between untreated specimens and treated ones of group A, except the case of low porous and smooth specimens. In case of low porous specimens and smooth surface, trends of colour variation is

Fig. 10 Colour variation ΔE at the end of accelerated growth test



quite similar, but ΔE of untreated specimens (MRUn) was about twice than ΔE of treated ones (MRAg and MRCu) at the end of accelerated test.

A noticeable difference between $TiO_2 + Ag$ and $TiO_2 + Cu$ exists in case of low porous and smooth specimens (MLAg and MLCu). In this last case, ΔE of $TiO_2 + Ag$ treatment was about 2.5 times than ΔE of $TiO_2 + Cu$. Thus, the addition of silver nanoparticles to the TiO_2 sol seems to be more efficient than the addition of copper.

By considering results about algal coverage (Figs. 11 and 12), it is possible to find the same trend of colour measurement.

In detail, the ratio between algal coverage of untreated specimens and treated ones (at the end of accelerated test) was about three in case of low porous rough specimens (LRUn), and it was equal to 1.93 in case of smoothed ones (LSUn).

Concluding, the addition of silver and copper nanoparticles to the TiO_2 sol, seemed to produce no significant benefits toward algal biofouling in high porous and high roughness conditions.

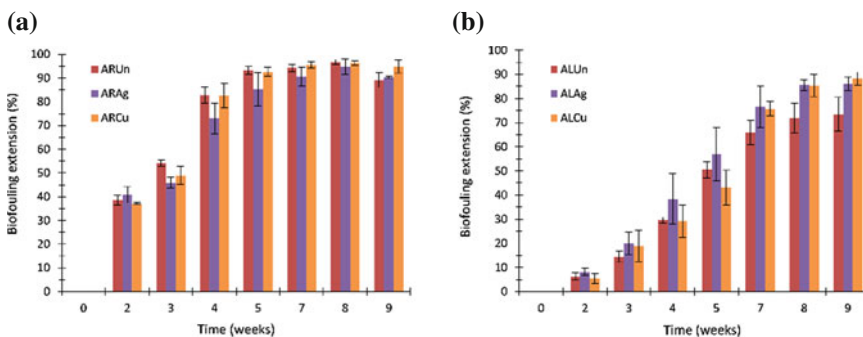


Fig. 11 Biofouling extension of treated A specimens with TiO_2 -Ag, TiO_2 -Cu, and control ones

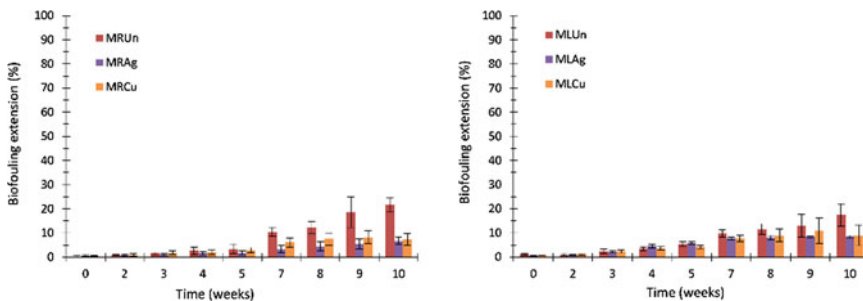


Fig. 12 Biofouling extension of treated M specimens with TiO_2 -Ag, TiO_2 -Cu, and control ones

Conversely, treatments produced noticeable benefits in case of low porous specimens (both rough and smoothed), indeed the algal coverage reach its maximum at about 10 %.

4 Conclusions

In this chapter, the inhibitory effect of TiO₂-based nano-coating against the adhesion of microalgae on clay brick façades was assessed by using an accelerated growth test under optimal conditions for multiplication of *Chlorella mirabilis* and *Chroococidiopsis fissurarum*.

Accelerated growth tests were conducted under visible VIS light conditions and under UV-A radiation. Antifouling ability of TiO₂ was monitored by colour change measurement, as well as digital image analysis. In case of VIS light, the extent of algal adhesion was also assessed from a microscopic point of view by confocal laser scanning microscopy.

Results shown TiO₂, under visible light, cannot stop biofouling due to the multiplication of microorganisms and area covered on treated specimens was about the same on control specimens.

Nevertheless, TiO₂ proved to enhance the self-cleaning ability of brick surfaces due to a washing process (i.e. rain). Thus, self-cleaning ability of TiO₂ could reduce biodeterioration of building brick façades even under VIS exposure conditions.

The accelerated laboratory growth test performed under UV-A light radiation confirmed the photocatalytic power of TiO₂, and it allowed studying the relationship between intrinsic characteristics of clay bricks and biological fouling.

It confirmed the influence of roughness and porosity on the biofouling process, whereas the nanocoating treatment with TiO₂ was proved to inhibit the biofouling of clay bricks irradiated with UV-A light.

For high porous and high rough materials, the inhibitory effect of TiO₂ was limited and no macroscopic effect was noticeable. In the case of rough specimens, the high number of superficial asperities proved to promote the adherence of microalgae to the substratum, thus increasing the colonization rate and hence leading to a rapid coverage of the nanofilm, which could no more be activate by UV light. The addition of other noble metal nanoparticles (Ag and Cu) seemed to produce no significant enhancement of anti-bacterial action of TiO₂.

Finally, TiO₂ shown to be a potential nanotechnology to prevent biofouling on modern building with clay façades limiting maintenance costs and risk for human health. In addition, this nanotechnology could be used for application in Cultural Heritage to slow down biodeterioration of monuments and historical buildings.

This study offers the opportunity to study the anti-bacterial power of TiO₂ under visible light condition for its application in indoor environment to prevent risks for human health.

References

- ASTM D4404-10 (2010) Standard test method for determination of pore volume and pore volume distribution of soil and rock by mercury intrusion porosimetry. American Society for Testing and Materials
- ASTM. ASTM D5589-09 (2009) Standard test method determine resist paint film related coatings to algal defacement
- Barberousse H, Lombardo RJ, Tell G, Coute A (2006) Factors involved in the colonisation of building facades by algae and cyanobacteria in France. *Biofouling* 22:69–77
- Barberousse H, Ruot B, Yéprémian C, Boulon G (2007) An assessment of façade coatings against colonisation by aerial algae and cyanobacteria. *Build Environ* 42:2555–2561
- Chen J, Poon C (2009) Photocatalytic construction and building materials: from fundamentals to applications. *Build Environ* 44:1899–1906
- D’Orazio M (2012) Materials prone to mould growth. In: Pacheco-Torgal F, Jalali S, Fucic A (eds) *Toxicity of building materials*. Woodhead publishing in materials, Cambridge, pp 334–350
- D’Orazio M, Cursio G, Graziani L, Aquilanti L, Osimani A, Clementi F et al (2014) Effects of water absorption and surface roughness on the bioreceptivity of ETICS compared to clay bricks. *Build Environ* 77:20–28
- Flores-Colen I, de Brito J, de Freitas VP (2008) Stains in facades’ rendering—diagnosis and maintenance techniques’ classification. *Constr Build Mater* 22:211–221
- Fujishima A, Zhang X (2006) Titanium dioxide photocatalysis: present situation and future approaches. *Comptes Rendus Chim* 9:750–760
- Fujishima A, Rao TN, Tryk DA (2000) Titanium dioxide photocatalysis. *J Photochem Photobiol C Photochem Rev* 1:1–21
- Graziani L, Quagliarini E, Osimani A, Aquilanti L, Clementi F, Yéprémian C et al (2013) Evaluation of inhibitory effect of TiO₂ nanocoatings against microalgal growth on clay brick façades under weak UV exposure conditions. *Build Environ* 64:38–45
- Graziani L, Quagliarini E, Osimani A, Aquilanti L, Clementi F, D’Orazio M (2014a) The influence of clay brick substratum on the inhibitory efficiency of TiO₂ nanocoating against biofouling. *Build Environ* 82:128–134
- Graziani L, Quagliarini E, Bondioli F, D’Orazio M (2014b) Durability of self-cleaning TiO₂ coatings on fired clay brick façades: effects of UV exposure and wet and dry cycles. *Build Environ* 71:193–203
- Guillitte O, Dreesen R (1995) Laboratory chamber studies and petrographical analysis as bioreceptivity assessment tools of building materials. *Sci Total Environ* 167:365–374
- Heydorn A, Nielsen AT, Hentzer M, Sternberg C, Givskov M, Ersbøll BK et al (2000) Quantification of biofilm structures by the novel computer program comstat. *Microbiology* 146:2395–2407
- Irving TE, Allen DG (2011) Species and material considerations in the formation and development of microalgal biofilms. *Appl Microbiol Biotechnol* 92:283–294
- Jain A, Bhadauria S, Kumar V, Chauhan RS (2009) Biodeterioration of sandstone under the influence of different humidity levels in laboratory conditions. *Build Environ* 44:1276–1284
- Johansson S (2005) Biological growth on mineral façades. Master thesis. Lund University, Lund
- Johansson S (2011) Biological growth on rendered façades. PhD thesis. Lund University, Lund
- Kunzel HM (2007) Factors determining surface moisture on external walls. In: Proceedings of the X international conference on thermal performance of the exterior envelopes of whole buildings. Clearwater Beach, ASHRAE, Florida, p 6
- Kunzel HM, Schmidt T, Holm A (2002) Exterior surface temperature of different wall constructions: comparison of numerical simulation and experiment. Symp. In Proceedings of building physics, Dresden, pp 441–419
- Künzel H, Kunzel HM, Sedlbauer K (2006) Long-term performance of external thermal insulation systems (ETICS). *ACTA Archit* 5:11–24

- Licciulli A, Calia A, Lettieri M, Diso D, Masieri M, Franza S et al (2011) Photocatalytic TiO₂ coatings on limestone. *J Sol-Gel Sci Technol* 60:437–444
- Lopez L, Daoud WA, Dutta D, Panther BC, Turney TW (2013) Effect of substrate on surface morphology and photocatalysis of large-scale TiO₂ films. *Appl Surf Sci* 265:162–168
- Miller A, Dionísio A, Laiz L, Macedo M, Saiz-Jimenez C (2009) The influence of inherent properties of building limestones on their bioreceptivity to phototrophic microorganisms. *Ann Microbiol* 59:705–713
- Miller AZ, Sanmartín P, Pereira-Pardo L, Dionísio A, Saiz-Jimenez C, Macedo MF et al (2012) Bioreceptivity of building stones: a review. *Sci Total Environ* 426:1–12
- Ortega-Calvo JJ, Ariño X, Hernandez-Marine M, Saiz-Jimenez C (1995) Factors affecting the weathering and colonization of monuments by phototrophic microorganisms. *Sci Total Environ* 167:329–341
- Sedlbauer K (2001) Mold growth prediction by computational simulation mold growth prediction by computational simulation
- Sedlbauer K, Krus M (2002) Mold growth on etics (EIFS) as a result of “bad workmanship”? *J Build Phys* 26:117–121
- Sharma G, Press CRC (2002) Digital color imaging handbook. CRC Press, USA
- Silvestre JD, de Brito J (2009) Ceramic tiling inspection system. *Constr Build Mater* 23:653–668
- Silvestre JD, de Brito J (2011) Ceramic tiling in building façades: inspection and pathological characterization using an expert system. *Constr Build Mater* 25:1560–1571
- Tran TH, Govin A, Guyonnet R, Grosseau P, Lors C, Damidot D et al (2014) Influence of the intrinsic characteristics of mortars on their biofouling by pigmented organisms: comparison between laboratory and field-scale experiments. *Int Biodeterior Biodegradation* 86:334–342
- UNI EN 623-4:1994 (2005) Advanced technical ceramics—monolithic ceramics—general and textural properties—Part 4: determination of surface roughness. Ente nazionale italiano di unificazione
- UNI EN ISO 4287:2009 (2009) Geometrical product specifications (GPS)—surface texture: profile method—terms, definitions and surface texture parameters. International Standards Organization
- Verdier T, Coutand M, Bertron A, Roques C (2014) A review of indoor microbial growth across building materials and sampling and analysis methods. *Build Environ* 80:136–149

Rehabilitation of Concrete Industrial Building Facades Attacked by Acids

Agnus Rogério Rosa, Antônio Neves de Carvalho Júnior,
Eduardo Chahud and Luiz Antônio Melgaço Nunes Branco

Abstract This case study was based on the project for rehabilitation of facade sealing, built in precast concrete in an industrial plant of steel structures galvanizing. Analysis of the Brazilian Standard NBR 6118 (design of reinforced concrete) was taken as well as review of literature on durability, in order to identify causes of pathologies and prescribe the best therapy with the most appropriate materials and techniques. The durability of reinforced and prestressed concrete structures is thus highly dependent on the resistance of concrete to chloride penetration. The physical resistance of concrete to chloride penetration is influenced by factors relating to the concrete itself, such as the porosity of concrete and interconnectivity of the pore system; and to factors relating to the concrete structure such as the stress conditions and the integrity of the cover. This galvanizing plant has been under severe attack of hydrochloric acid fumes for more than 15 years, so that, the main aggressive agents are chlorides. The combination of epoxy and polyurethane coatings will provide adequate protection for concrete structures.

Keywords Pathologies · Durability · Facades · Epoxy

A. Rogério Rosa (✉) · A.N. de Carvalho Júnior · E. Chahud · L.A.M. Nunes Branco
Escola de Engenharia, Universidade Federal de Minas Gerais (EEUFMG),
Belo Horizonte, Brazil
e-mail: engenharia@setaviso.com.br

A.N. de Carvalho Júnior
e-mail: ancj@ufmg.br

E. Chahud
e-mail: chahud@ufmg.br

L.A.M. Nunes Branco
e-mail: luizmelg@ufmg.br

1 Introduction

The recovery of structures in reinforced concrete should be performed using the most modern techniques available in an appropriate manner, following the technical specifications indicated, drawn from a careful evaluation.

Initially we shall make a detailed study of existing conditions to clearly identify their causes, then make precise diagnosis of pathologies encountered and finally set up the project for the rehabilitation of structures containing all necessary technical specifications, such as:

- Methodology of execution;
- Materials to be used;
- Equipment needed;
- Skilled labor for work execution;
- Operational and safety procedures;
- Timeline for implementation;
- Post-intervention monitoring and maintenance of the structures.

Here we describe the pathologic manifestations observed in an industrial galvanizing plant, built in 1999, using precast and prestressed, concrete panels and the methodology used for the recovery and rehabilitation of its structures (see Fig. 1).

The fence panels, in a double “T” geometry, have the following dimensions: height 14 m; width 2.5 m. Various pathologies were observed in the concrete panels and a photographic record was made for more detailed study.



Fig. 1 Overview of the galvanizing facilities. *Source* Authors, 2013

Fig. 2 Pathologies presented by fence panels. *Source* Authors, 2013



Initially, carbonation fronts, chloride ions attacks, reinforcement corrosion, spalling and leaching of concrete and several cracks were identified (see Fig. 2).

2 Identification of Pathological Agents

There are different types of galvanization; one of the oldest and most effective is hot-dip galvanizing. The galvanizing process consists of cleaning steel parts, with subsequent bathing in molten zinc. This process is a versatile and economic way to protect structures, steel parts and equipment against corrosion. It comprises seven steps (baths), important for the cleaning and soaking of parts.

The process of cleaning and galvanization generates various pathogenic agents that can cause severe damage to concrete structures. Samples from the residues were collected weekly for analysis. These agents below were identified by the company laboratories originated from samples collected during the year 2012.

2.1 *Originated from Degreasing*

- Organic solvents;
- Alkaline solvents;
- Emulsifier;
- Electrolytes in general.

2.2 *Originated from Pickling*

- Hydrochloric acid;
- Sulfuric acid;
- Nitric acid.

2.3 *Zinc Electrolytes May Be Acidic or Alkaline, of Which the Main Ones Are*

- Sulfur electrolytes;
- Chlorine electrolytes;
- Cyanide electrolytes.

According to CETESB (2012) as a general rule, the main contributors to a galvanization's final effluent are the following:

- The spillways of the metal surface's preparation and cleaning tanks (degreasing and pickling), where organic solvents are used to remove oils and greases, as well as acid and alkaline baths, for removal of slag, rust etc.;
- Residues originated from the electrolytic bath tanks, after several weeks or months of use;
- Splashes from parts removed or transferred from their electrolytic tanks, and leaks from tanks and pipes;
- The residues usually consist of solutions of sulfuric acid, hydrochloric acid, nitric acid and hydrofluoric acid, essentially acidic electrolytes from baths. The pH (hydrogen potential) of these residues is often below 2.

3 Identification of the Pathologies

Although the Company has a modern and efficient system for collection and treatment of gases and residues from its manufacturing process, it is inevitable that many of the agents mentioned above are capable of acting and damaging the concrete structures of the fence panels.

After 15 years under action of pathogenic agents, severe damage was caused to concrete structures. It is noteworthy that the facade in question is oriented from east to west, thus receiving solar heat during the entire day, making the damage worse because at night the structure is subject to hydrochloric acid fumes which are condensed on the surface.

Fig. 3 Hydrochloric acid tanks for pickling. *Source* Authors, 2013



During day there was drying and evaporation, in a continuous process of wetting and drying. Due to the industrial atmosphere, carbonation fronts could also be found acting on these structures.

According to Bakker, cited by Figueiredo (2005) the carbonation and chloride combination is the most common cause of severe corrosion problems (as seen on Fig. 3).

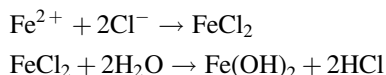
One of the mechanisms of chloride ion's penetration in the concrete is through the concrete pores' microstructure. The driving forces of these substances' transport in the concrete can be the differences in concentration, pressure, temperature, density, electric potential and capillary suction (Nepomuceno 2005).

3.1 Chloride Induced Steel Corrosion

Steel reinforcement embedded in concrete is inherently protected against corrosion by passivation of the steel surface due to the high alkalinity of the concrete. When a sufficient amount of chlorides reaches the steel reinforcement it permeates the passivation layer and increases the risk of corrosion. The resistivity of concrete can also be reduced, affecting the corrosion rate of the steel (Chloride Resistance of Concrete—Cement Concrete and Aggregates—Australia, June 2009).

According to Neville (1995), for corrosion to be initiated, the passivity layer must be penetrated. Chloride ions activate the surface of the steel to form an anode, the passivated surface being the cathode.

The reactions involved are as follow:



Thus, Cl^{-} is regenerated so that the rust contains no chloride, although iron chloride is formed at the intermediated stage.

Because the electrochemical cell requires a connection between the anode and the cathode by pore water, as well as by reinforced steel itself, the pore system in hardened cement paste is a major influencing corrosion. In electrical terms, it is the resistance of the “connection” through the concrete that controls the flow of current. The electrical resistivity of concrete is influenced by the ionic composition of the pore water, and by the continuity of the pore system in the hardened concrete.

There are two consequences of the corrosion of steel. First, the products of corrosion occupy a volume several times larger than the original steel so that their formation results in cracking (characteristically parallel to the reinforcement), spalling or delamination of concrete.

Second, the process of corrosion at anode reduces the cross sectional area of the steel, thus reducing its load-carrying capacity. In this connection, it should be pointed out that chloride induced corrosion is highly localized at a small anode, with pitting of the steel taking place (as seen on Figs. 4 and 5).

There are four basic mechanisms of transportation of aggressive fluids and ions into the concrete: permeability, capillary suction, diffusion and migration, which may act simultaneously or successively over time according to the exposure conditions that the concrete is subjected to Calçada (2004).

The chloride ion's penetration is possible only when there is water in the concrete pores. If the water is stagnant, the displacement of chloride ions takes place by diffusion. When the concrete undergoes cycles of wetting and drying, the penetration of these ions turns to capillary force of water (Guimarães 2000).

The ions penetration's depth depends on the duration of the periods of wetting and drying, as well as the permeability of the concrete surface (Bakker cited by Figueiredo 2005) and ACI 222 (1990).

Mechanisms can occur simultaneously both in real situations and in testing procedures; Nepomuceno (2005) presents some of these combinations:

- Capillary absorption, convection and diffusion: in the initial process, depending on the moisture content on concrete, the inflow of ions will occur by capillarity, and then through diffusion;
- Diffusion and migration: may occur in migration tests, where an electrical potential is applied to determine the diffusion coefficient of chlorides;
- Permeability and convection: occur when agents are contained in the fluid that penetrates the structure.

Fig. 4 Cracking and spalling, parallel to the reinforcement



Fig. 5 Corrosion with pitting of the steel taking place.
Source Authors, 2013



Corrosion of reinforcement in concrete has two important effects on the concrete: produces spalling and decreases the resistant section of the rebars (Canovas 1988).

These two problems have been identified in almost all the panels. With the corrosion of the diameter of the rebar's, there was an increase in volume of up to six times. Internal stress in the section was generated, so that there was a loss of adhesion between the concrete and the reinforcement, causing “spalling” of the concrete.

According to Thomaz (1989) the fissures and cracks are the most important anomalies due to three aspects: the acknowledgment of a serious problem in the concrete structure, the compromising of the structure's performance in service and the psychological embarrassment that a crack has on its users.

The pathogens were identified after careful inspection, and the authors experience also contributed to the diagnosis, allowing correct identification of pathogens and their effects on each of the structures.

During the inspection, a high concentration of reinforcement on the panels section was found. The covering thickness was below the NBR6118 specifications, as showed on Fig. 6.

According to Brazilian standards ABNT NBR 6118—2014 indicates the following situations to fix the coverings (item 6.4) as shown on Tables 1 and 2.

Concrete provides physical and chemical protection to the reinforcing steel from penetrating chlorides which may cause steel depassivation leading to increased risk of steel corrosion.

The chloride resistance depends on the permeability of the concrete and the thickness of cover to the reinforcement. The integrity of the concrete cover under service load, in terms of cracking and crack width, also influences the resistance to penetrating chlorides. Corrosion of steel reinforcement is an electrochemical process.

Hence electrochemical properties of concrete, such as resistivity, are important inherent properties affecting the corrosion rate of reinforcing steel.

Table 1 NBR 6118 environmental classification

Environmental classification	Aggressiveness	Project classification environment	Risk of deterioration
IV	Very strong	Industrial	High

Source ABNT (2014)

Table 2 NBR 6118 coverings specification

Structure type	Structural element	Environmental classification: IV
		Nominal coverings (mm)
Reinforced concrete	Beam/pillar	50

Source ABNT (2014)

Mehta (1988) reconfirmed from a review of case studies that it is the permeability of concrete, rather than its chemistry, which is the key to overall durability.

The causes of high permeability are not limited to poor concrete proportion but poor concreting practice, such as incomplete mixing, inadequate consolidation and curing after placement, insufficient cover to reinforcing steel, and badly constructed joints. (Chloride Resistance of Concrete—Cement Concrete and Aggregates—Australia, June 2009).

Thus the low covering thickness was also a major factor to allow penetration of chloride and accelerate the process of reinforcement corrosion.

4 Therapy Proposals for Recovering the Concrete Fence Panels

For the rehabilitation of structures of fence panels the following solution was proposed (Figs. 7, 8, 9, 10, 11, 12, 13, 14, 15 and 16) based on Cánovas (1988):

- Washing of all the structures with highly pressurized hot water;
- Demolition of all points where the concrete showed signs of deterioration;
- Washing of structures with alkaline-based anionic surfactants, alkalis, solvents and emulsifiers concentrated in detergent PH 14;
- Washing with mild biodegradable detergent and highly pressurized hot water;

Fig. 6 Reinforcement concentration, 4 rebar 20 mm diameter and low reinforcement coverings (6 mm) of concrete. The structure is already attacked by hydrochloric acid vapors. *Source* Authors, 2013



Fig. 7 Steel Corrosion Process (Source Chloride resistance of concrete–cement concrete and aggregates— Australia, June 2009)

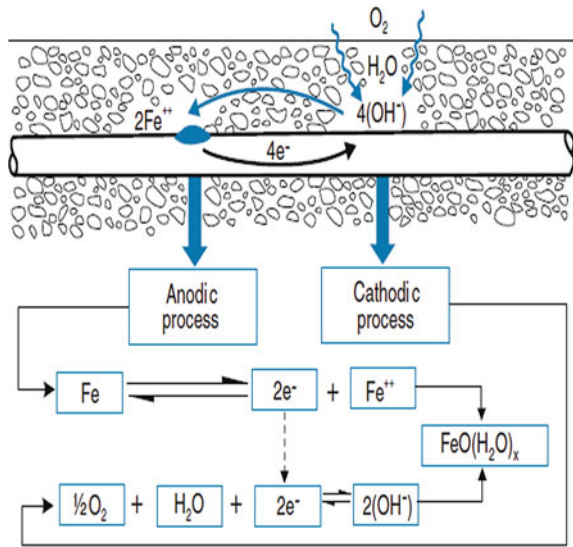


Fig. 8 First step of cleaning: washing with hot water. Source Authors, 2013



Fig. 9 Second step of cleaning: washing with pressurized water and detergent. *Source* Authors, 2013



Fig. 10 Reinforcement cleaning using needle gun. *Source* Authors, 2013



Fig. 11 Reinforcement cleaning. *Source* Authors, 2013



Fig. 12 Application of epoxy rich zinc for reinforcement protection. *Source* Authors, 2013



Fig. 13 Application of structural cementitious mortar for repairs up to 7 cm deeper.
Source Authors, 2013



- Cleaning of armor using needle guns and wire brushes to remove all corrosion points;
- Replacement of armor that had loss of greater than 5 % nominal section;
- Treatment of armor with zinc-rich epoxy two component polyamide cured to provide cathodic protection to the carbon steel;
- Application of adherence to structural thixotropic epoxy adhesive slowly picks bridge;
- Restoration of damaged and demolished structural grout areas;
- Application of Structural Polymer mortar for repairs to concrete structures with thickness 0.5–2.5 cm depth application system “dry-pack”;
- Application of cementitious mortar for structural repairs to concrete structures with thickness 3.0–7.0 cm depth application system “dry-pack”;
- Application of Grout for larger repairs, application system “dry-pack”;
- Application of the sealing epoxy varnish, polyamide cured with appropriate viscosity to allow good penetration into concrete surfaces, plaster, masonry, cement asbestos seals these surfaces prevents excessive absorption with a dry film thickness of 50 μ ;
- Application of two intermediate coats with bi cured epoxy polyamide component, high-build, fast drying, developed to protect;
- Carbon steel and concrete in industrial exposures environment, applied dry film thickness of 150 μ ;

Fig. 14 Application of epoxy varnish sealer and application of intermediate coat in epoxy two-component polyamide cured. *Source* Authors, 2013



- Apply a finish coat of acrylic aliphatic polyurethane high build, bi component with a low content of volatile organic compounds (Low VOC). Paints in acrylic aliphatic polyurethane has excellent weathering resistance, excellent flexibility and toughness to withstand the harshest working conditions, with dry film thickness of 100 μ .

All concrete structures were washed in 3 steps (Figs. 8 and 9).

The application of zinc-rich primers (ZRPs), on ferrous substrates is a very efficient method of anticorrosion protection. They are used in many aggressive media: sea water, marine and industrial environments. It is a common fact that in order to achieve a long-life coating system, a zinc primer needs to be applied as the first coat. For solvent- based zinc-rich paints it seems to be established that, at least at the beginning of immersion, zinc particles provide a cathodic protection of the steel substrate. Then, a long term protection develops due to the formation of zinc corrosion products, reinforcing the barrier effect of the paint (Hammouda et al. 2011).

Fig. 15 Application of final coat in acrylic aliphatic polyurethane low (VOC).
Source Authors, 2013



Fig. 16 Facade overview after recovering. *Source* Authors, 2013



5 Conclusions

Concrete is a very versatile construction material, it has been used in a diversified environments. The identification of service conditions that the reinforced concrete structures are subjected to is an essential factor for it to have a long and healthy life; constant maintenance and conservation allow the structures to remain in service for long periods. Hostile environments will request special concrete with appropriate protection in order to this concrete shall not be degraded.

In this case study it was found that the extreme condition in what the structures were subjected to (fronts combination of carbonation and chloride attack) and the low thickness of coverings was essential for their degradation. A special project to recovery and rehabilitation of the concrete structure had to be elaborated.

The recovery and rehabilitation of reinforced concrete structures is extremely expensive due to the need for specific treatment materials, skilled labor plus the cost of partial or total interdiction of structures.

After the structural recovery and rehabilitation of the structures, it was prescribed a protection system with the combination of epoxy and polyurethane paints. The system has an estimated useful life of 15 years and may have its life extended with specific periodic maintenance without the need for major interventions.

References

- ACI Committee 222, ACI 222R-89 (1990) Corrosion of metals in concrete. In: American Concrete Institute. Manual of Concrete Practice, Detroit: ACI Committee 222, v.1
- Associação Brasileira de Normas Técnicas. NBR 6118 (2014) Projeto e execução de obras de concreto armado. Rio de Janeiro
- Calçada LML (2004) Estudo da Eficácia do Ensaio de Migração em Condições de Fluxo Não Estacionário na Previsão da Penetração de Cloretos em Concreto. p 213 Tese (Doutorado em Engenharia Civil)—Universidade Federal de Santa Catarina, Florianópolis
- Cánovas MF (1988) Patologia e terapia do concreto armado, 1st edn. Editora PINI, São Paulo
- CETESB (2012) Companhia Tecnológica de Saneamento Ambiental de São Paulo. Apostila de Galvanoplastia, São Paulo, Julho
- Figueiredo EP (2005) Efeitos da Carbonatação e de Cloretos no Concreto. In: Isaia G (ed) Concreto: Ensino, Pesquisas e Realizações. IBRACON, São Paulo
- Guimarães ATC (2000) Vida útil de estruturas de concreto armado em ambientes marítimos. Tese (Doutorado em Engenharia Civil)—Universidade de São Paulo, São Paulo, p 267
- Hammouda N, Chadli H, Guillemot G, Belmokre K (2011) In the corrosion protection behavior of zinc rich epoxy paint in 3 % NaCl solution—advances in chemical. Eng Sci 1:51–60
- Mehta PK (1988) Durability of concrete exposed to marine environment—a fresh look. In: Proceedings in second international conference on concrete in marine environment, SP-109, St. Andrews by-the-sea, Canada
- Nepomuceno AA (2005) Mecanismo de transporte de fluidos no concreto. In: Isaia G (ed) Concreto: Ensino, Pesquisas e Realizações. IBRACON, São Paulo
- Neville A (1995) Chloride attack of reinforced concrete. Mater Struct 28:63–70
- Report (2009) Chloride resistance of concrete. Cement Concrete and Aggregates, Australia
- Thomaz E (1989) Trincas em edifícios—causas, prevenção e recuperação. Editora PINI, São Paulo

Pathologies—Incompatibility of Materials and Human Intervention in a Historic Building of Elvas

Soheyl Sazedj, António Morais, M^a Teresa Pinheiro-Alves
and Rui Silva

Abstract Preserving and safeguarding the identity and original authenticity are targets to accomplish, in an action of conservation, restoration or rehabilitation of buildings, taking into account that interventions respect the values of compatibility, adaptability and reversibility. Any intervention that takes place in a historic building, will depend on a historical survey which ideally includes the knowledge of the origin, the building design, materials and construction techniques used, building's occupants and constructive interventions realized. In a historic building, such as the military building called 'Governor's House of Square' in Elvas, after identifying the constructive anomalies and their causes, it has been found that human action was preponderant, because of vandalism and posterior constructive interventions. Some pathology identified are as, anomalies in the coating or failure in a lintel of the exterior wall. In the first case the anomalies are certainly due to incompatibility between the support material and the coating exposed to thermal amplitude. The later case shows that mechanical action involved has exceeded the capacity of flexural strength of the lintel. The posterior opening of the entrance caused changes in the distribution of vertical loads and consequently provoked the failure. In an attempt to preserve the building and the testimony of many years, it seems to be of interest to maintain the entrance and instead to replace the lintel adequately in material and dimension.

Keywords Incompatibility of intervention · Historic buildings · Rehabilitation

S. Sazedj (✉) · A. Morais · R. Silva

Faculty of Architecture, Department of Technology, University of Lisbon, R. Sá Nogueira,
1349-055 Lisbon, Portugal
e-mail: sazedj@fa.ulisboa.pt

A. Morais

e-mail: ajmorais@fa.ulisboa.pt

M.T. Pinheiro-Alves

Department of Architecture, University of Évora, Largo dos Colegiais N.2, 7004-516 Évora,
Portugal
e-mail: tpa@uevora.pt

1 Introduction

The military building of “*Governor’s House of Square*” (Fig. 1), object of this text, is located inside the bastion fortification of Elvas, a world heritage city. It is situated in the *Martim Mendes Street n° 93*, contiguous, to the Military Quarters of the Corujeira in the same street, *Quartéis da Corujeira*, near to the Castle of Elvas and the military storeroom of *Santa Bárbara*, see Fig. 2.

The building is implanted in a location of strong declivity, with the main access at the altimetry quote of 325 m. The survey of the main architectural and structural characteristics of the building, the identification of anomalies and its diagnosis, were preceded by research of historical information about the original building, its constructive alterations, interventions made and of the human occupation of it. Besides the documentary inquiry, fieldwork and contact with professionals, the availability of some relevant elements from the Department of the Heritage and Military Constraints, contributed to enrich the knowledge of the building, as military entities used the space until the last decades.

The study of this building coincided with another one carried out by the enterprise AMR, Alberto Martinez Rubio “*Levantamientos Arquitectónicos y Arqueológicos*”, requested by the City Council of Elvas, which was identified as Architectural Survey of Military Command Headquarters of Elvas (“*Levantamento Arquitectónico ao Quartel do Comando Militar—Elvas*”), Which complements this document.



Fig. 1 “Governor’s House of Square” in Elvas



Fig. 2 Aerial view of the location of the “Governor’s House of Square” in Elvas (credit of image via Michelin <http://www.viamichelin.pt> consultation in June 1, 2014)

Some of the interventions proposed, are based on values of reversibility, compatibility and adaptability, according to recommendations of the ICOMOS—International Council of Monuments and Sites.

2 Inspection Procedures and Diagnosis

In the first phase the anomalies have been identified and divided into structural and nonstructural and as coating or finishing. Environmental conditions like neighbour buildings, streets, movement of vehicles, rainwater disposal and environmental conditions were also additionally considered.

The fact of treating a historical building, obliged to deepen the research of the historical information about usage, occupancy, date and type of construction, drawings made, registry of interventions, constructive techniques applied, materials used and their sources. The City Council of Elvas has carried out several studies and analysed the characterization of materials used in military buildings of the city. The information provided by the municipality was a fundamental support to enable the analysis of the pathologies of the building.

In the civil or military historical patrimony, the use of local materials was common. Studies, effectuated by the City Council of Elvas, show that the most used materials were the massive brick, the lime as a binder, sands, as well as two forms of rammed earth called Taipa¹ and Formigões² and carved stonework for some corners.

¹Taipa—typical building technique of the Iberian Peninsula, known as rammed earth.

²Formigões—similar to concrete, in which the cement is substituted by the lime.

In parallel to the historical investigation visits and inspections of the building took place, complemented by photographic registry and measurements. The methodology of verification of the anomalies was orientated by the constructive elements of the building:

- Identification of the building;
- Evaluation of the coating;
- Evaluation of the exterior walls;
- Evaluation of the floors;
- Evaluation of the interior walls and ceilings;
- Environmental and energetically requalification;
- Thermal conditions and acoustics.

3 Documental Researches and Historical Information

The building is identified in the Portuguese System of Information for the Architectural Inheritance—SIPA, as “*Casa Brasonada na Rua dos Quartéis da Corujeira*”—Emblazoned House in the Street of the Quarters of the Corujeira, describing shortly as a XVIII century architecture of residential Manor House (SIPA–Gordalina 2008).

Documents provided by the Section of Heritage and Military Constraints, include plants of a survey carried out by Major José Santa Clara Bárbas of unknown date, probably of the beginning of the 20th century. The building is set out in documents of the Military Archive, as “*Prédio Militar n° 93*”, Military Building and PM n° 93-Elvas, which description encounters also visibly at the front of the building.

4 Identification and Characterization of the Building

In accordance with the Military Archive the building is exposed to:

- North: with the esplanade of the Castle, south of the storeroom of *Santa Bárbara*;
- South: Martim Mendes Street;
- East: São João da Corujeira Street (old “*Quartéis da Corujeira Street*”);
- West: with the wall of the esplanade of the Castle of Elvas, the spring of the public place of the old rank of the Military Radio (in another military document as neighbouring with the wall of 1st Arab Fortified Enclosure (Militar 2013)).

The Military Building n. 93 is described as consisting of 3 floors and ground attachments:

- Basement;
- Ground floor;
- 1st floor.

It presents heterogeneity in geometry, dimensions, altimetry and types of covering. The wall of the main front accompanies the declivity of the floor of the sidewalk. One of the resistant walls at the right lifted side presents a counterfort.

The building is characterized as follows. A principal facade turned to the south with a frieze on the top, which has a rectangular embroidery on the base; the east facade with heraldry as relief, a common insignia, element that tops the coat of arms, with the figure of a ceremonial helmet with visor and grills, of the XVI century, typical for the nobility and a shield divided in four sub splitting, see Fig. 3.

A rear view turned to the north, neighbouring with the wall of the castle and with the storeroom of Santa Barbara in superior altimetric quotas and ground in between, see Fig. 4.

A right side facade that faces the east, confining, with the Military Quarters of the Corujeira in lower altitude and with extensive views to the city of Badajoz in Spain, see Fig. 5.

A left facade with the wall of the esplanade of the Castle of Elvas and a half wall of another construction.

A roofing with small inclination with a ridge in the geographical directions of the building from south to north; above the right facade close to the eave, tiles of the type Marseille, contrasting with those of simple type on the opposite side; also roofing with painted wavy plates. The structure of the roofing consists of rafters and battens, see Fig. 6.

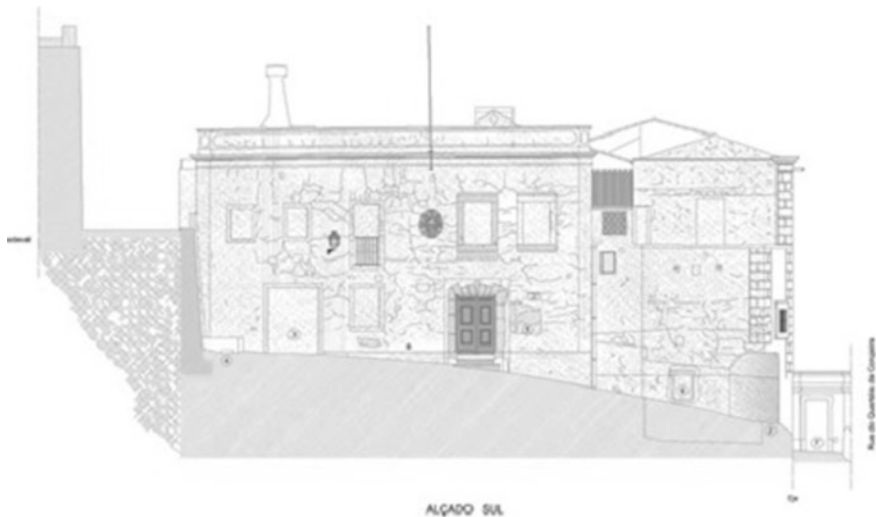


Fig. 3 Principal facade (credit of image—AMR—Alberto Martinez Rubio, “*Levantamientos Arquitectónicos*”)

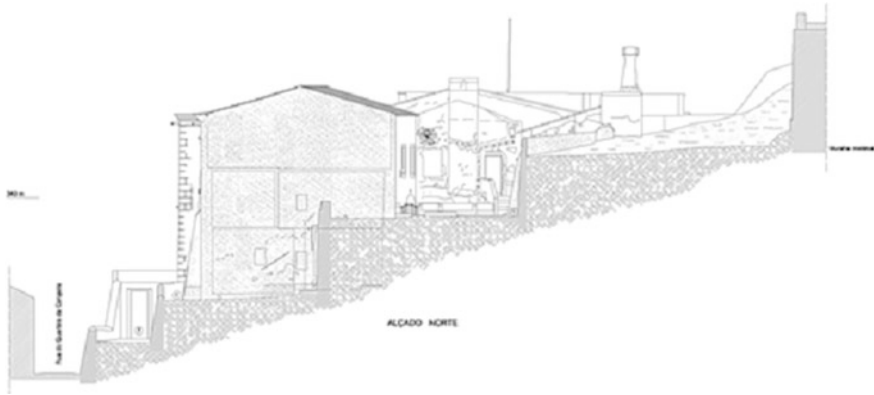


Fig. 4 Rear View (credit of image—AMR Alberto Martinez Rubio, “*Levantamientos Arquitectónicos*”)

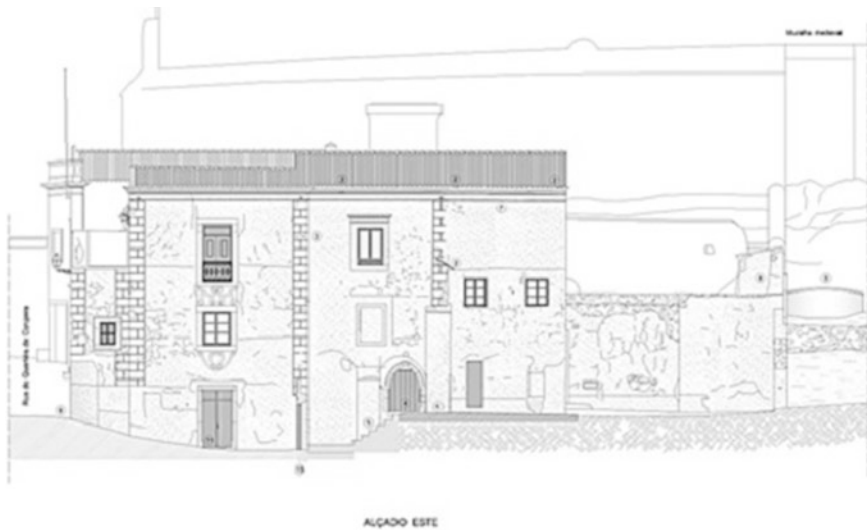


Fig. 5 Right side view (credit of image—AMR—Alberto Martinez Rubio, “*Levantamientos Arquitectónicos*”)

5 Survey and Causes of the Anomalies on the Facade

Several anomalies were found on the facade of the military building of “*Governor’s House of Square*”. Disaggregation of the mortars and extended cracks, anomalies on corners and lintel.

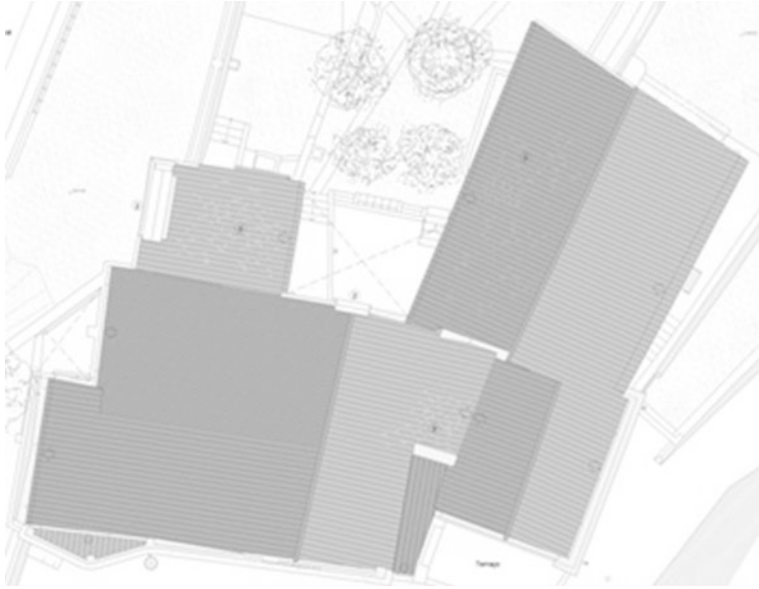


Fig. 6 Roof (credit of image—AMR—Alberto Martínez Rubio, “*Levantamientos Arquitectónicos*”)

5.1 Anomaly—Disaggregation of the Coating

In the principal facade, at the main entrance, a distinction of the revetment with similar characteristics of cement is pointed out, see Fig. 7. It exceeds the thickness of the masonry and is superimposed on the contour. This revetment is partially standing out of the support, exposing some massive bricks with Flemish pattern.

5.1.1 Causes of Disaggregation of the Revetment

The lack of cohesion, the linear delamination and the lifting off of the coating reinforces the hypothesis of an intervention with cement mortar. The incompatibility of the materials is given by the weak cohesion between them. The old coating is composed mainly of sand and lime, which has more porosity compared to a cement mortar. The old coating absorbs more humidity than cement. Cement has a higher linear thermal expansion coefficient, 0.011 mm/mK, than sand and lime, 0.0047 mm/mK. The chemical binding of these two materials with different thermal expansion behavior creates tensions that cause the cracks.

Environmental conditions, especially temperature and humidity, are relevant for this analysis. In December 2012 daily thermal variations of 4–14 °C were registered and in July and August of the same year 16–35 °C in average. The humidity in the



Fig. 7 Revetment overlaps the stone with invasive vegetation

same month and periods vary between 32 and 65 %. This data gives an idea about daily and annual thermal amplitude, as well as the moisture variations, which determine the progression of cracks in the coating. In some cases this anomaly is aggravated by the appearance of invading vegetation.

5.1.2 Solution for the Disaggregation of the Revetment

Biocide has to be applied on the invading vegetation, in order to be removed after some days without causing other damages. Considering the variety of herbaceous plants present in this building and the wide range of herbicides a chemical treatment seems adequate by applying of glyphosate for elimination and control of the weed.

“The glyphosate (N-(phosphonomethyl)glycine), C₃H₈NO₅P, CAS 1071-83-6) is a broad spectrum weed killer. It is absorbed by the leaves of the plants and it can be applied by pulverization directly on the green mass, but also in the stems and stalks by injection.” [Translation (Cutileiro et al. 2014).

To prevent any irreversible errors in interventions the following must be considered:

Issues related to the authenticity of buildings, which includes the authenticity of the materials and construction processes, and regarding the compatibility between new and old components lead to the conclusion, as a general rule, to recommend the use of traditional technologies. ... The mortars based on to the base of air lime do not pose major problems of compatibility with the old frames, to the extent that they are similar to the solutions initially used. [Translation (Freitas and Pinto 2001)].

Among several admissible interventions the following are outstanding:

- (a) Removal of the whole revetment and substitution with other compatible coating on the base of lime and sand, additives can be added to improve the mechanical property. To upgrade resistance brick powder can be used, if a high grade of any kind of chloride is expected or thermal treated kaolin, which will rise also the resistance against chlorides and sulphates (Rodrigues and Henriques 2004). The application will have to be in multilayers of small thicknesses leaving several days up to a week before application of the next layer. Each layer needs time for carbonatation to gain strength (Coelho et al. 2009). The mortar should present a decrease in the content of binder from the base layer to the final coating. The trace of the mortar of plaster should be 1:4 (lime:sand) according analysis to similar interventions in other historic buildings of the region. With the intention to compose a similar mortar as the original and trying to use original material following composition is proposed:
 - 1 portion of aerial lime hydrophobic with pozzolanic additive at the rate of 15 % of the volume of the lime
 - 4 portions of washed river sand without clay
- (b) Local application on affected areas, with application of lime mortar as already mentioned in the previous paragraph.

The finishing should also be on the basis of aerial lime. To obtain the yellow colour an ocre pigment should be added to the aerial lime.

5.2 *Anomaly—Cracking of Revetment*

In the principal facade a configuration of cracks in the revetment of the exterior wall left to the main entrance can be seen, Fig. 8. Although on the same front as the case before and probably same pathology but different solutions might be applicable.

5.2.1 Causes of Cracking

The retraction of the cement plaster causes micro cracking and the lack of cohesion between the support and the coating and the incompatibility of materials justify the appearance of cracking, which also is intensified by the thermal variation and differential behaviour of materials as mentioned before in Sect. 5.1.1. Causes of Disaggregation of the Revetment.

5.2.2 Solution for the Cracking of Revetment

Application of biocide on the invading vegetation, in the form that could be removed after some days, without causing other damages, according to indications defined in Sect. 5.1.2. Solution for the Disaggregation of the Revetment.



Fig. 8 Diffuse cracking of the coating on the main facade

Possible solutions are:

- Complete removal of the existent revetment and application of a revetment of lime mortar and sand;
- Local application of the lime mortar in 3 layers. The first one richer in lime and the last one weaker. The first layer should not have more than 0.5 cm thickness, the second 1.5 cm and the last one 0.5 cm;
- Filling the slits with compatible material, such as the injection of aerial lime;
- Ensure the success of the process, complementing with lime wash painting after cure. This procedure will inhibit the action of atmospheric agents through the fissured zones and consequently the water infiltration.

The finish will have to be equally to the base from aerial lime.

5.3 *Anomaly in the Corner of the Principal-Front*

The corner of the right side of the principal front, near the cornice, is standing out, exposing a vertical slit, which is visible in the joining with the resistant sidewall, see Fig. 9.

5.3.1 Causes of the Distinction of the Corner

There are different hypotheses that contribute to the distinction of the corner of the building, near the cornice, of which stand out the following:

- Traction of the corner caused by the electric cable;
- Loss of connection and cohesion between the stonework of corner and the transverse wall of rammed earth and stone;
- Poor locking between the stonework of corner and the transverse wall;
- Differentiated soil movement, related to the cut at the base of the wall (in longitudinal extension) or to a possible change in the soil compaction by road traffic;
- Infiltration of rainwater and invasive vegetation;
- The daily and annual thermal amplitude, as well as the moisture variations.

Fig. 9 Electric cable detail and cracking of the corner

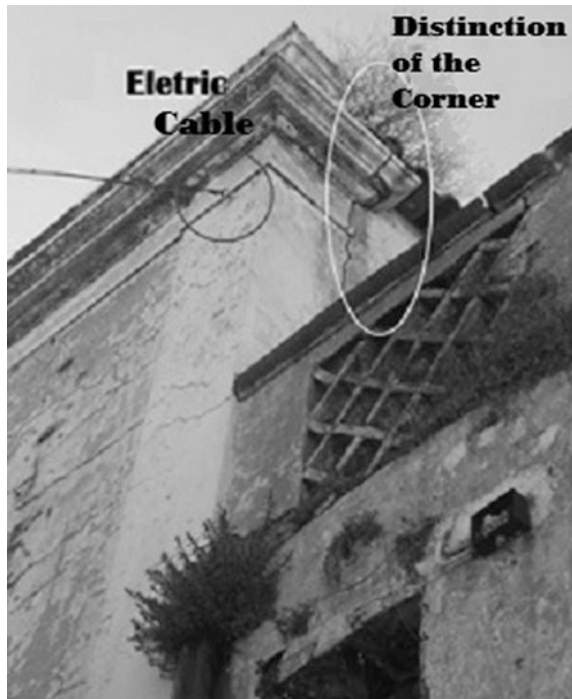




Fig. 10 Possible interventions with stapling, inserted in the wall and in the stonework

5.3.2 Solution for the Distinction of the Corner

For an efficient rehabilitation it is necessary to resolve the following causes:

- Removal of the electric cable that creates traction in the corner;
- The treatment of the invading vegetation with spraying of systemic herbicide and removal of the roots after drying shrub (as indicated in the Sect. 5.1.2. Solution for the Disaggregation of the Revetment);
- The reconnection of the corner to the wall, by stapling or by support rods making a wall anchor system (Fig. 10);
- The sealing of the fissure between the corner and the wall, by injection of hydrophobic aerial lime.

5.4 Anomaly in the Lintel and in the Wall of the Main-Front

Crack of the garage gate lintel and in the wall above between the windowsill and the lintel, see Fig. 11.

5.4.1 Causes of the Slits in the Lintel and Wall

The probable causes for the onset of cracking in the lintel, should be due to constructive changes in the building and the inability of these elements maintain



Fig. 11 Cracks under the sill of the window and in the lintel

their integrity, under the action of interventions in the presence. The garage gate, 2.16 m wide, seems to be the result of a posterior constructive change. It can be assumed that:

- constructive modification has provoked the change of discharge-resistant walls, with intercalation of lintel;
- the geometry of the lintel does not provide the “escape” of the forces to the side walls;
- the doorframe is located in an area of different morphology, in a corner of the building, not discharging properly the vertical forces.
- On the left side, next the doorframe, there is a fracture that is related to the concentration of tensions. It is the continuity, which has its origin on the left base of the windowsill. Also the fractures in the middle of the lintel show that the bending exceeds the capacity of this resistant.

5.4.2 Solutions for the Lintel and Wall

The solution for the lintel and wall will be:

- The full replacement of the frame, consisting of jambs and lintel stone.
Granite of middle quality
Resistance to compression: 100 MPa
Resistance to flexing: 160 MPa

Fig. 12 Possible solution of anchorage of the lintel



Specific weight: 26 kN/m³

Absorption of the water to the atmospheric pressure: 0.5 %

Open porosity: 3 %

Coefficient of linear dilation: 9×10^{-6} for °C (Manual da Pedra Natural para Arquitetura 2006)

- Opening of “small diameter holes, carefully located, in which are placed anchors consisting of stainless steel rods. Sealing in masonry is achieved through deformable sleeves injected” [Translation (Cóias 2007)], see Fig. 12.
- Reduction of the thickness of the coating in the cracked areas by mechanical means without percussion. See Sect. 5.2.2 for more details.

6 Conclusions

The durability of historic buildings is compromised by human intervention when:

- Structural changes are made that are not appropriate in the context of the structure of the building as in this case the opening at an unsuitable place;
- Incompatible materials are used which do not match with the original existing materials as the use of cement for revetment of walls in rammed earth;

- Inadequate accessories are installed on the building that provoke tensions, which can't be sustained by other elements, as the installation of electricity cables;
- The absence of maintenance or necessary interventions provides ideal conditions for the development and spread of invasive vegetation with particularly destructive effects.

Periodic maintenance is fundamental for the conservation of historic patrimony. Any intervention must be studied and adopted to the structural conditions and capacity of the building. Materials used for intervention must be in accordance and compatible with original materials still in use. These three points guarantee the durability of the building and the interventions, which have to be made turn not only to be beneficial for the users but also for the patrimony.

Acknowledgments This research is a result of a postgraduate course on rehabilitation of historic buildings in the world heritage city of Elvas in Portugal. By the initiative of the Faculty of Architecture—University of Lisbon and University of Évora this undertaking was accomplished with the collaboration of the University of Extremadura and the Polytechnical Institute of Portalegre. Our thanks go to the Town Hall of Elvas who supported this endeavour and research, to the Center for Investigation of Architecture, Urbanism and Design, CIAUD, of the Faculty of Architecture who supported this research and finally to Laboratory Hércules of the University of Évora.

References

- Cóias V (2007) Reabilitação Estrutural de Edifícios Antigos. GECORPA
- Coelho AZ, Torgal FP, Jalali S (2009) A Cal na Construção, Lime in Construction, TecMinho. University of Minho, Guimarães
- Cutileiro P, Sequeira S, Henriques M (2014) Fortim de São Mamede, Proposta de Intervenção. Trabalho final de Seminário de Tecnologias, Curso de Pós-graduação em “Estudos Avançados em Recuperação do Património Histórico e Regeneração Urbana e Económica”. Elvas, Portalegre, Portugal
- Fonseca LB (s.d.) Heráldica Portuguesa. <http://www.armorial.net/armorial/indice0.shtml>. Cited 10 Oct 2014
- Freitas VP, Pinto PS (2001) Rebocos à base de cal em edifícios antigos. Estudos do património, Plaster on base of Calcium Oxide in Old Buildings, Study of Heritage. Faculty of Engineering University of Porto, FEUP, Porto, pp 166–172
- Freitas VP, Torres MI, Guimarães AS (2008) Humidade Ascensional, Rising Damp. Faculty of Engineering University of Porto, FEUP, Porto
- Manual da Pedra Natural para Arquitetura (2006) Manual of natural stone for architects. Direcção Geral de Geologia e Energia, Lisboa
- Militar A (2013) PM n° 93/Elvas
- Rodrigues PF, Henriques FMA (2004) Current mortars in conservation: an overview. Int J Restor 10:692–622
- SIPA–Gordalina R (2008) SIPA. Sistema de Informação para o Património Arquitectónico, Information System for Architectural Heritage: http://www.monumentos.pt/Site/APP_PagesUser/SIPA.aspx?id=26856. Cited 30 Oct 2014